

Development of Ni-based Catalysts for Fuel Reforming with Exhaust Gas of Gasoline Engine

著者	BETCHAKU MII
学位授与機関	Tohoku University
学位授与番号	11301甲第19858号
URL	http://hdl.handle.net/10097/00135731

Doctoral Thesis

Thesis Title

Development of Ni-based Catalysts for

Fuel Reforming with Exhaust Gas of

Gasoline Engine

(ガソリンエンジンの排気ガスを改質剤とする

燃料改質用 Ni 系触媒の開発)

Department of Applied Chemistry

Graduate school of Engineering,

TOHOKU UNIVERSITY

BETCHAKU MII

指導教員	富重 圭一 教授
研究指導教員	中川 善直 准教授
審査委員 (○印は主査)	<p>○ 富重 圭一 教授</p> <p>1 村松 淳司 教授 2 吉岡 敏明 教授</p> <p>3 福島 康裕 教授 4 _____</p> <p>5 _____ 6 _____</p>

Development of Ni-based Catalysts for Fuel Reforming
with Exhaust Gas of Gasoline Engine

ABSTRACT :

Currently, there has been concern over the depletion of fossil resources and global warming, and there is a need to reduce the use of fossil resources by improving the fuel economy of automobiles. In the technique for improving fuel economy, the exhaust gas recirculation (EGR) engine is relatively inexpensive, and when combined with fuel reforming technology, it can significantly improve fuel economy. In EGR combined with fuel reforming technology (Reformed EGR), a portion of the exhaust gas is mixed with the fuel in the process of returning it to the intake side, and the H₂-rich synthesis gas obtained by passing it through the reforming catalyst is mixed with the intake gas to stabilize combustion even under lean combustion conditions. The properties required for the reforming catalyst are as follows: (i) workable at the wide range of temperature including low temperature (active at 673-773 K or less), (ii) stability (no change of performance during use), (iii) resistance to coke deposition, (iv) startability (easy activation), etc. Ni is known for its low cost and high activity in general reforming reactions, but its coke deposition resistance and structure stability are low. In this study, based on the hydrotalcite-derived Ni/Mg/Al catalyst ^[1], which has shown high catalytic performance in steam reforming, the author developed an inexpensive Ni-based catalyst with performance (i)-(v) for the reforming of toluene with model EGR gas composition (low partial pressure of steam and CO₂ coexistence) at relatively low temperature (≤ 773 K).

The catalytic performance of Ni/Mg/Al, Ni/ α -Al₂O₃, Rh/CeO₂ catalysts were evaluated in the reforming reaction at relatively low temperature (≤ 773 K), the low partial pressure of steam and in the presence of CO₂ (Chapter 2) ^[2]. In this study, toluene was used as the model compound because aromatics are the component of gasoline most likely to cause coke deposition. After the reaction, the catalyst bed was divided into three parts from the upstream side and coke deposition was measured by TG-DTA. At $W/F = 0.19$ g h mol⁻¹, the Rh/CeO₂ catalyst was kept high toluene conversion, while the toluene conversion of Ni/Mg/Al decreased from 84% to 34% in 5 hours. On the other hand, at $W/F = 0.39$ g h mol⁻¹, the toluene conversion of Ni/ α -Al₂O₃ decreased from 65% to 26% in 5 h, while that of Ni/Mg/Al was still 56% after 5 h. Ni/Mg/Al showed higher activity than Ni/ α -Al₂O₃, and the amount of coke deposition was low. The amount of coke deposition increased toward the outlet of the catalyst bed in Ni/Mg/Al, suggesting that the main coke deposition pathway was CO disproportionation. The effect of feed ratios (high and low partial pressures of steam and presence of CO₂) was evaluated using Ni/Mg/Al, and it was found that the toluene conversion decreased and coke deposition increased at low water vapor partial pressure. This indicates that low partial pressure of steam decreases the activity and coke deposition resistance of the Ni/Mg/Al catalyst.

It was reported that the addition of a second metal such as Fe or Cu to Ni/Mg/Al forms an alloy with Ni, which improves steam reforming activity and coke deposition resistance ^[3,4]. Therefore, the

Abstract

effect of alloying was evaluated in toluene reforming with model EGR gas using Ni-M/Mg/Al (M = Fe, Co, Cu) (Chapter 3). The XRD patterns and TEM-EDX of the reduced catalysts showed that all the second metals formed an alloy with Ni. The Ni-Fe/Mg/Al catalyst inhibited the decrease in toluene conversion and showed higher coke deposition resistance than Ni/Mg/Al or Ni-M/Mg/Al (M = Co, Cu) catalysts. In addition, Ni-Fe/Mg/Al showed less coke deposition in both inlet and outlet of the catalyst bed, indicating that both coke deposition due to CO disproportionation and toluene decomposition were suppressed. The XRD patterns of the catalyst after the reaction showed a low level of oxidation of the catalyst or sintering of the metal particles, suggesting that other factors were responsible for the decrease of activity. The Ni-Fe/Mg/Al catalyst maintained high coke deposition resistance even at smaller W/F or higher amount of toluene feed, although the activity decreased progressively. It has been reported in previous studies that the Ni-Fe/Mg/Al catalyst can be reused by regeneration (oxidation and re-reduction) ^[5], but re-reduction cannot be performed in Reformed EGR. Therefore, the author investigated the regeneration method and found that the activity of the reforming of toluene with model EGR gas was restored to the same level of the fresh catalyst not only by re-reduction but also by N₂ flow at 873 K or reaction at 973 K. It suggests that the adsorbed species on the catalyst surface decrease the activity. The XRD pattern of the catalyst after the reaction showed a little increase of Ni-Fe alloy peak of the outlet of catalyst bed suggesting that the Ni-M alloy was re-reduced in the outlet of the catalyst bed. On the other hand, the Ni-Fe/Mg/Al catalyst was completely deactivated by the steam flow treatment at 873 K, and the XRD pattern of the catalyst after the reaction showed that the catalyst was completely oxidized. Therefore, Ni-Fe/Mg/Al needs to be improved in its reducibility in order to obtain startability.

It has been reported that the addition of noble metals such as Pd to Ni-based catalysts improves their reducibility ^[6]. Therefore, the addition of noble metals was evaluated in toluene reforming with model EGR gas to improve the reducibility of Ni and Fe and to provide startability (Chapter 4). When the temperature of the unreduced catalysts was increased stepwise with flowing reaction gas, the Rh/CeO₂ + Ni-Fe/Mg/Al (Powder mixture) catalyst started to react at 673 K and showed higher conversion to toluene than the Rh/Ni-Fe/Mg/Al (impregnated with Rh) catalyst at all temperatures above 673 K. In addition, the toluene conversion of Rh/CeO₂ + Ni-Fe/Mg/Al and Rh/Ni-Fe/Mg/Al catalysts were higher than that Rh/CeO₂ + Mg/Al and Rh/Mg/Al catalysts, suggesting that Ni and Fe were activated by addition of Rh. On the other hand, the activity at 773 K of the Rh/CeO₂ + Ni-Fe/Mg/Al catalyst to that pretreatment was lower than that of Ni-Fe/Mg/Al catalyst after reduction at 1073 K, and no metal peaks were identified in the XRD pattern of the mixed catalyst after the reaction. Only a small amount of Ni and Fe were probably reduced to improve the activity.

This thesis describes the reforming reaction of toluene at relatively low temperature (≤ 773 K) and model EGR gas (low partial pressure of steam and CO₂ coexistence) over hydrotalcite-like-compound-derived Ni-based catalysts. The catalytic performance of Ni/Mg/Al

Abstract

which contain Ni as the active metal was superior to that of a conventional supported Ni catalyst (α -Ni/ α -Al₂O₃), although it was inferior to that of the supported Rh catalyst, the stability, coke deposition resistance and structure stability (Chapter 2). The addition of Fe to Ni/Mg/Al catalyst improved the stability and coke deposition resistance. It was found that the activity could be regenerated by a simple regeneration method, although the Ni-Fe/Mg/Al catalyst was also easily deactivated by oxidation (Chapter 3). Therefore, the Rh/CeO₂ + Ni-Fe/Mg/Al (Powder mixture) catalyst was used to improve the reducibility and to provide startability (Chapter 4). These findings will be useful for reducing the amount of noble metals in Reformed EGR catalysts and for developing Reformed catalysts for other challenging conditions.

Reference

- [1] D. Li, *et al.*, *Appl. Catal. B: Environ.*, 2011, 102, 528-538. [2] M. Betchaku, *et al.*, *Fuel Process. Technol.*, 2020, 209, 106545. [3] M. Koike, *et al.*, *ChemSusChem*, 2012, 5, 2312-2314. [4] D. Li, *et al.*, *Appl. Catal. B: Environ.*, 2016, 192, 171-181. [5] D. Li, *et al.*, *ChemSusChem*, 2014, 510-522. [6] J. Chen, *et al.*, *Appl. Catal. B: Environ.*, 2015, 179, 412-421.

Contents

Chapter 1	General introduction	1
1.1.	<i>Depletion of the fossil fuel in the world</i>	1
1.2.	<i>Fuel economy improvement for fueled automobiles</i>	2
1.2.1.	<i>Improvement of fueled automobile</i>	2
1.2.2.	<i>Exhaust Gas Recirculation (EGR) engine system</i>	3
1.3.	<i>Catalyst for reforming of fuel</i>	4
1.3.1.	<i>Reforming catalysts</i>	4
1.3.2.	<i>Coke formation</i>	7
1.4.	<i>Catalytic reforming of hydrocarbons</i>	9
1.4.1.	<i>Steam reforming</i>	9
1.4.2.	<i>Dry reforming</i>	13
1.4.3.	<i>Combined dry-steam reforming</i>	13
1.5.	<i>Hydrotalcite-like-compound-derived Ni catalyst</i>	14
1.6.	<i>Purpose of this thesis</i>	16
1.7.	<i>Outline of thesis</i>	17
Chapter 2	Reforming of toluene with simulated automobile exhaust gas over hydrotalcite-like-compound-derived Ni catalyst.....	29
2.1.	<i>Introduction</i>	29
2.2.	<i>Experimental</i>	32
2.2.1.	<i>Catalyst preparation</i>	32
2.2.2.	<i>Catalyst characterization</i>	34
2.2.3.	<i>Activity test of reforming of toluene</i>	35
2.3.	<i>Results and discussion</i>	37
2.3.1.	<i>Catalytic performance in the reforming of toluene with model EGR gas</i>	37
2.3.2.	<i>Effect of toluene feeding ratio to EGR gas</i>	41
2.3.3.	<i>Effect of reaction temperature</i>	44
2.3.4.	<i>Characterization of used catalysts and regeneration of Ni/Mg/Al</i>	45
2.3.5.	<i>Influence of feed ratio</i>	48
2.4.	<i>Conclusions</i>	51
Chapter 3	Catalytic performance of hydrotalcite-like-compound-derived Ni-metal alloy catalyst for toluene reforming with gasoline engine exhaust model gas as reforming agent	59
3.1.	<i>Introduction</i>	59
3.2.	<i>Experimental</i>	61
3.2.1.	<i>Catalyst preparation</i>	61

3.2.2.	<i>Catalyst characterization</i>	61
3.2.3.	<i>Activity test of reforming of toluene</i>	62
3.3.	<i>Results and discussion</i>	63
3.3.1.	<i>Catalyst characterization</i>	63
3.3.2.	<i>Catalytic performance of Ni-M/Mg/Al in the reforming of toluene with model EGR gas</i>	71
3.3.3.	<i>Effect of Fe/Ni ratio</i>	73
3.3.4.	<i>Effect of W/F</i>	75
3.3.5.	<i>Effect of reaction temperature</i>	78
3.3.6.	<i>Effect of feeding ratio of toluene to EGR gas</i>	81
3.3.7.	<i>Regeneration of Ni-Fe/Mg/Al catalyst with various methods</i>	83
3.4.	<i>Conclusions</i>	99
Chapter 4	Effect of addition of noble metal to hydrotalcite-derived Ni-Fe alloy catalyst for steam reforming of toluene using exhaust gas as reforming agent	109
4.1.	<i>Introduction</i>	109
4.2.	<i>Experimental</i>	110
4.2.1.	<i>Catalyst preparation</i>	110
4.2.2.	<i>Catalyst characterization</i>	111
4.2.3.	<i>Activity test of reforming of toluene</i>	111
4.3.	<i>Results and discussion</i>	112
4.3.1.	<i>Effect of the method of adding Rh to Ni-Fe/Mg/Al</i>	112
4.3.2.	<i>Noble metals screening</i>	115
4.3.3.	<i>Performance of reduced Rh/CeO₂ + Ni-Fe/Mg/Al</i>	117
4.3.4.	<i>Characterization of used or fresh catalyst of Rh/CeO₂ + Ni-Fe/Mg/Al and Rh/Ni-Fe/Mg/Al</i>	119
4.3.5.	<i>Attempt to decrease Rh amount</i>	128
4.4.	<i>Conclusions</i>	131
Chapter 5	Summary	135

Chapter 1

General introduction

1.1. Depletion of the fossil fuel in the world

The use of all primary energy sources, like fossil fuels, grows throughout every year. Although renewable energy is the world's fastest-growing form of energy, fossil fuels continue to meet much of the world's energy demand. Of primary energy consumption, petroleum and other liquids accounted for 32% in 2018 [1]. However, the available amounts of fossil fuels are limiting. Many researchers report the investigation of the results of the fossil fuel amount that we can use [1, 2, 3], and the consumption of energy in the world is listed in **Fig. 1.1**. The annual consumption of primary energy is increasing with time. Fossil fuels remain the dominant source of energy worldwide, and it is reported that the demand will increase by 80% in 2007-2030 [1, 2].

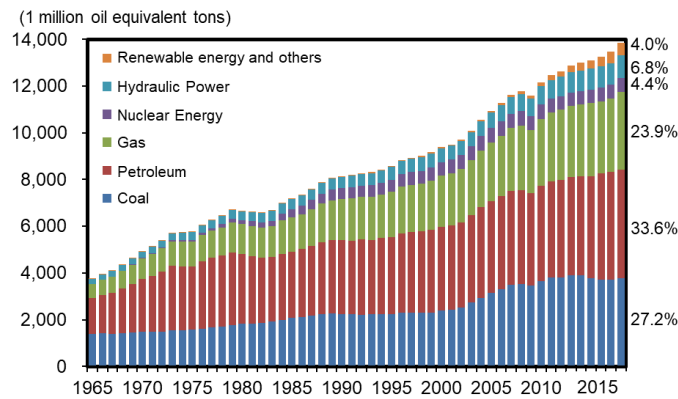


Figure 1.1 The annual consumption of energy in the world [3]

Liquid fuels, because of energy density, cost, and chemical properties, continue to be the predominant transportation fuel and an important industrial feedstock, and our life keeps receiving the benefit, but the prices are strongly affected by the demand and supply costs. On the other hand, renewable energy has been paid attention to as an environmentally harmless energy resource, and the development of the expansion of the use is actively carried out. The use is socially desirable and they will be necessary for the near future; however, the percentage is still low [3].

1.2. Fuel economy improvement for fueled automobiles

1.2.1. Improvement of fueled automobile

Also in the automobile industry, it is necessary to reduce the consumption of liquid fuels. The next-generation automobile uses alternate energy (ex. hydrogen and electricity) as a power source without gasoline [4]. However, the next-generation automobile has problems such as the limited number of the power source station, high cost of automobile, and difficult long-distance driving. On the other hand, the improved fuel economy of automobiles, which means a smaller amount of fuel as the power source, can be achieved with the relatively low additional cost of automobiles.

Technologies to improve fuel economy in automobiles include improving engine efficiency, reducing aerodynamic drag, reducing body weight, improving the drivetrain, and reducing rolling resistance, as shown in **Fig. 1.2**. There is also a technology called gasoline lean-burn engines, which reduces fuel use by increasing the air-to-fuel ratio to a lower than normal level. The lean combustion can improve fuel economy by three points; (i) reduced loss of heat transferred to cylinder wall since the burned gas temperature is decreased significantly, (ii) a reduction in the degree of dissociation in the high temperature burned gases, which allows more fuel's chemical energy to be converted to sensible energy near Top Dead Center (TDC) [5]. However, the lean-burning process requires technology to stabilize combustion.

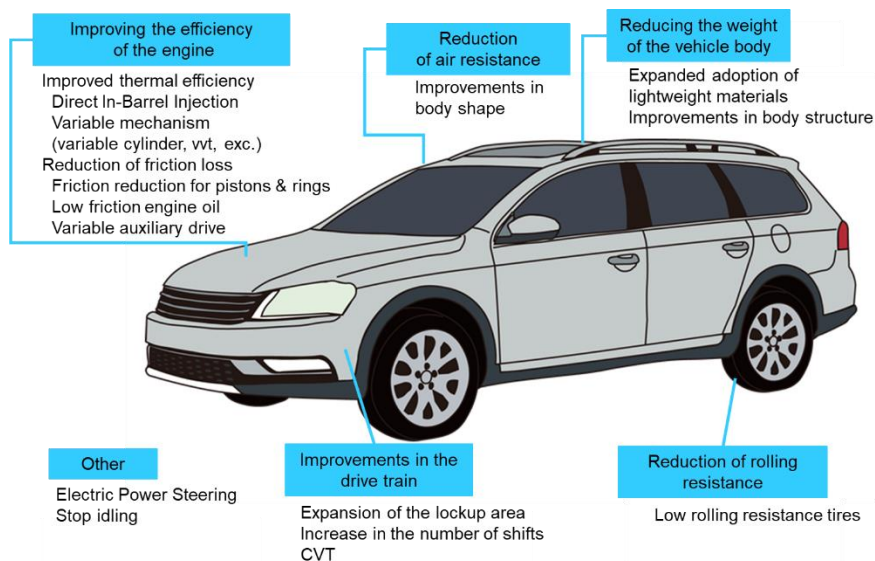


Figure 1.2 Automotive fuel economy technology

1.2.2. Exhaust Gas Recirculation (EGR) engine system

Gasoline consists of various hydrocarbons such as paraffins, olefins, aromatic compounds, etc. It also contains nitrogen compounds, which can be the source of harmful NO_x by combustion. In order to reduce NO_x emissions, an exhaust gas recirculation (EGR) engine system has been developed that can lower the temperature of the combustion chamber [6]. In this system some of the exhaust gas returns to the intake by connecting the intake pipe and exhaust pipe with a small pipe (EGR gas passage), reducing the air-fuel ratio to that the change of O₂-fuel ratio. On the other hand, the EGR engine also can improve fuel economy. The EGR engine can improve fuel economy by reduced pumping work, as can fill the cylinder with EGR gas even when the amount of air intake is reduced and hence there is no pressure difference with the outside air pressure, and by the points (i) and (ii) in the explanation for lean combustion engine described in Section 1.2.1 [5]. However, there is a problem that the combustion becomes unstable due to the increase of nonflammable gas. Therefore, a modified EGR engine was developed by applying fuel reforming technology to the EGR engine (**Fig. 1.3**). The EGR engine that uses fuel modification technology is defined as a Reformed EGR. In a Reformed EGR engine, hydrogen is produced by passing a mixture of exhaust gas and fuel through a catalyst installed in the EGR gas passage and mixed with intake gas to stabilize combustion [7-13]. In this process, the fuel hydrocarbons and the carbon dioxide and steam in the exhaust gas are used to produce hydrogen by dry reforming and steam reforming. Since these two reactions are endothermic, it is possible to recover energy from the flue gas [14]. Other reactions such as total oxidation, partial oxidation, and water-gas shift reactions also occur, but their contribution is small in the total [14]. In Reformed EGR, ignition delay and prolonged burn-up periods with reduced laminar flame velocities have been observed by stabilizing the combustion. As a result, it may be appropriate to use EGR in combination with other technologies [5]. This Reformed EGR system can be relatively simple and inexpensive since it only requires the addition of a reformer containing a reforming catalyst to a conventional EGR system.

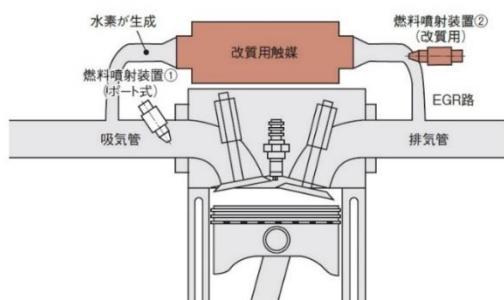


Figure 1.3 System of Exhaust Gas Recirculation (EGR) engine ^[15]

1.3. Catalyst for reforming of fuel

1.3.1. Reforming catalysts

In general, supported Rh catalysts have been investigated for modified EGR engines because of their high activity, reducibility, startability, and coke deposition resistance ^[16, 17]. CeO₂-based supports have typically been used ^[18, 19], while support modifications ^[6, 20] and Pt ^[16, 21-23] and Co as a second metal ^[24] have been applied. Some examples are shown in **Table 1.1 and 1.2**. Among them, Pt-Rh/CeO₂-ZrO₂/γ-Al₂O₃ is a prototype catalyst provided by Johnson Matthey and has been used in many studies on EGR engines ^[22, 23, 25]. However, Rh, the active center of the catalyst, is very expensive, which is a serious problem due to the high cost of the catalyst.

In general reforming catalysts, there are problems with agglomeration and oxidation of the active metal species and reduced activity due to the amount of coke deposition on the catalyst surface. There are the properties additionally required for the reforming catalyst for Reformed EGR engine because the reaction conditions in Reformed EGR are dynamically changed cost/space capacity and the for additional system is limited. The required properties for Reformed EGR can be summarized as follows ^[26].

- (i) activity at relatively low temperature (673-773 K or less)
- (ii) stability (resistance to coke deposition and aggregation of metal particles)
- (iii) reusability (no change of catalyst properties during regeneration)
- (iv) startability (easy activation)

Here, high startability means that the catalyst can exhibit activity just when the engine in a resting state starts up. Since coke deposition resistance is a critical property of the required performance, the author describes it in detail in Section 1.3.2.

Table 1.1 Example of Rh catalysts for reforming of EGR engine (reported in journal paper)

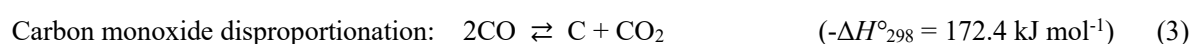
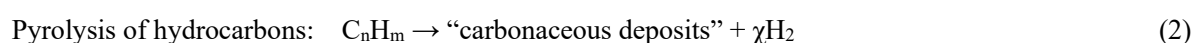
Entry	Catalyst	Flow conditions	Conversion [%]	Ref.
1	Rh/ZrO ₂ -La ₂ O ₃ -	WHSV = 137.8 h ⁻¹ , C ₈ H ₁₈ : 2.2 vol.%, CO ₂ : 13.5 vol%, H ₂ O: 12.0 vol.%, O ₂ : 1.0 vol.%, N ₂ : 71.3 vol.%, T = 853 K, total pressure = 1.3 bar	57	[27]
	Nb ₂ O ₃ -Y ₂ O ₃			
2	Blank	WHSV = 137.8 h ⁻¹ , C ₈ H ₁₈ : 2.2 vol.%, CO ₂ : 13.5 vol%, H ₂ O: 12.0 vol.%, O ₂ : 1.0 vol.%, N ₂ : 71.3 vol.%, T = 853 K, total pressure = 1.3 bar	-	[6]
	Rh/CeZrAl		57	
	Rh/Al(80)Ce(20)		53	
	Rh/Al(20)Ce(80)		54	
	Rh/CeO ₂		47	
	Rh/Al ₂ O ₃		39	
3	Pt-Rh/CeO ₂ -ZrO ₂ /γ-Al ₂ O ₃	bioethanol:H ₂ O = 1:2, liquid feed rate = 30 mL h ⁻¹ , GHSV = 25000 h ⁻¹ , T = 873 K	99	[22]
		bioethanol:H ₂ O = 1:2, liquid feed rate = 60 mL h ⁻¹ , GHSV = 25000 h ⁻¹ , T = 873 K	94	
		bioethanol:H ₂ O = 1:2, liquid feed rate = 90 mL h ⁻¹ , GHSV = 25000 h ⁻¹ , T = 873 K	99	
		CO ₂ : 15 vol%, bioethanol feed ratio = 28 mL h ⁻¹ , GHSV = 25000 h ⁻¹ , CO ₂ /Fuel = 1.0, T = 873 K	88	
		CO ₂ : 15 vol%, bioethanol feed ratio = 28 mL h ⁻¹ , GHSV = 25000 h ⁻¹ , CO ₂ /Fuel = 1.5, T = 873 K	32	
		CO ₂ : 15 vol%, bioethanol feed ratio = 28 mL h ⁻¹ , GHSV = 25000 h ⁻¹ , CO ₂ /Fuel = 2.0, T = 873 K	32	
		CO ₂ : 15 vol%, bioethanol feed ratio = 28 mL h ⁻¹ , GHSV = 25000 h ⁻¹ , CO ₂ /Fuel = 2.5, T = 873 K	38	
		O ₂ : 2 vol% + exhaust gas, exhaust gas feed ratio = 3 L min ⁻¹ , bioethanol feed ratio = 8.6 mL h ⁻¹ , O ₂ /Fuel = 0.5, GHSV = 25000 h ⁻¹ , T = 873 K	69	
4	Pt-Rh/CeO ₂ -ZrO ₂ -Al ₂ O ₃	REGR mass flow: 9.8 kg h ⁻¹ , 35 Nm/3 bar IMEP @2100 rpm (Exhaust gas; Temp. 868-878 K, CO ₂ : 14.8-15.0%, O ₂ : 0.60-0.70%, CO: 0.50-0.60%, H ₂ O: 14.3-14.4%, NO _x : 100-1200 ppm, THC: 1900-3000 ppm), gasoline injected: 0.5 mol%.	26	[23]
		REGR mass flow: 17.2 kg h ⁻¹ , 50 Nm/4 bar IMEP @3000 rpm (Exhaust gas; Temp. 868-878 K, CO ₂ : 14.8-15.0%, O ₂ : 0.60-0.70%, CO: 0.50-0.60%, H ₂ O: 14.3-14.4%, NO _x : 100-1200 ppm, THC: 1900-3000 ppm), gasoline injected: 0.5 mol%.	86	
		REGR mass flow: 24.5 kg h ⁻¹ , 50 Nm/4 bar IMEP @3000 rpm (Exhaust gas; Temp. 868-878 K, CO ₂ : 14.8-15.0%, O ₂ : 0.60-0.70%, CO: 0.50-0.60%, H ₂ O: 14.3-14.4%, NO _x : 100-1200 ppm, THC: 1900-3000 ppm), gasoline injected: 0.5 mol%.	66	

Table 1.2 Example of catalysts for reforming EGR engines (reported in patent)

Entry	Catalyst	Flow conditions	Conversion [%] (other appraisal)	Ref.
1	0.67%Rh-10%Ni-8%Ce/Al ₂ O ₃	3 vol% C ₈ H ₁₈ , 55.5 vol% air, 41.5	85	[28]
	1%Rh-10%Ni-8%Ce/Al ₂ O ₃	vol% steam, O/C = 0.46, S/C = 1.73,	92	
	2%Rh-10%Ni-8%Ce/Al ₂ O ₃	T = 723 K, SV = 150000 h ⁻¹ , reaction	82	
	1%Rh-10%Ni-8%Ce-4%Zr-4%Fe/Al ₂ O ₃	gas feed = 50 l min ⁻¹ , T = 723 K	93	
	1%Rh-10%Ni-8%Ce-4%Zr-4%Fe-4%Ca-2%Mg/Al ₂ O ₃		93	
	0.67%Rh-10%Ni-8%Ce/Al ₂ O ₃		82	
2	7 wt%SiO ₂ -1 wt%Rh/10 wt%La ₂ O ₃ -Al ₂ O ₃	W = 100 mg, F _{N₂} = 70 ml min ⁻¹ , F _{CO₂}	(Formation of H ₂ : 17 vol% (initial), 14 vol% (after endurance test))	[29]
	6 wt%SiO ₂ -1 wt%Rh/10 wt%La ₂ O ₃ - 8 wt%CeO ₂ -Al ₂ O ₃	= 40 ml min ⁻¹ , F _{gasoline} = 0.032 ml	(Formation of H ₂ : 18 vol% (initial), 16 vol% (after endurance test))	
	1 wt%Rh/10 wt%La ₂ O ₃ -Al ₂ O ₃	min ⁻¹ , O ₂ /C = 0.1, S/C = 3.3	(Formation of H ₂ : 17 vol% (initial), 10 vol% (after endurance test))	
3	4%Rh/10%La/Al ₂ O ₃ + ST-OS (2% SiO ₂)	T = 873 K, S/C = 3, LHSV = 10 ₋₁	(Performance Stability Improvement Fee: 2.0)	[30]
	4%Rh/10%La/Al ₂ O ₃ + ST-OS (4.8% SiO ₂)	(gasoline, N ₂ , H ₂ O, CO ₂ , 20 ppb SO ₂),	(Performance Stability Improvement Fee: 2.5)	
	4%Rh/10%La/Al ₂ O ₃ + ST-OS (10% SiO ₂)		(Performance Stability Improvement Fee: 1.8)	
	4%Rh/Al ₂ O ₃ + ST-OS (2% SiO ₂)		(Performance Stability Improvement Fee: 1.2)	
	4%Rh/10%La/Al ₂ O ₃ + Al ₂ O ₃ sol (2% Al ₂ O ₃)		(Performance Stability Improvement Fee: 1.0)	
	4%Rh/10%BaAlO ₃ /Al ₂ O ₃ + ST-OS (4.8% SiO ₂)		(Performance Stability Improvement Fee: 2.4)	
	4%Rh/10%SrAlO ₃ /Al ₂ O ₃ + ST-OS (4.8% SiO ₂)		(Performance Stability Improvement Fee: 2.4)	
	4%Rh/10%CaAlO ₃ /Al ₂ O ₃ + ST-OS (4.8% SiO ₂)		(Performance Stability Improvement Fee: 2.3)	
	4%Rh-2%Pt/Al ₂ O ₃ + ST-OS (4.8% SiO ₂)		(Performance Stability Improvement Fee: 1.9)	
	4%Rh-2%Pd/Al ₂ O ₃ + ST-OS (4.8% SiO ₂)		(Performance Stability Improvement Fee: 1.8)	
	4%Rh-2%Ir/Al ₂ O ₃ + ST-OS (4.8% SiO ₂)		(Performance Stability Improvement Fee: 1.7)	
	4%Rh-2%Ni/Al ₂ O ₃ + ST-OS (4.8% SiO ₂)		(Performance Stability Improvement Fee: 1.8)	
	4%Rh-2%Re/Al ₂ O ₃ + ST-OS (4.8% SiO ₂)		(Performance Stability Improvement Fee: 2.0)	
4%Rh-2%Ru/Al ₂ O ₃ + ST-OS (4.8% SiO ₂)		(Performance Stability Improvement Fee: 1.3)		

1.3.2. Coke formation

From 1.3.1, the author considers that coke is the biggest problem for reformed EGR engine catalysts, so it will be explained in detail here. The coke deposited at the inlet of the catalyst bed is mainly derived from substrate (fuel) decomposition (Eqs. 1 and 2), while that at the outlet of the catalyst bed is derived from CO disproportionation (Eq. 3), especially when the conversion is high [31]. The deposited coke types are mainly classified into (a) whisker carbon, (b) encapsulating carbon, and (c) pyrolytic carbon. The main characteristics of these cokes are summarized below [32, 33].



(a) Whisker carbon

It is well known that the dissociation of carbon monoxide, methane, and higher hydrocarbons on the active metal such as Ni leads to the formation of carbons in the form of whiskers [34, 35]. The formation temperature was > 720 K, increased with lower $\text{H}_2\text{O}/\text{C}_n\text{H}_m$ and low activity aromatic feed. The combustion temperature is high (> 773 K). Growing whisker carbon lifts a nickel particle as shown in **Fig. 1.4 (a)** and may result in a break-down of the catalyst structure, without deactivation of catalytic activity. There is also a danger of whisker carbon growing and causing blockage of the device.

(b) Encapsulating carbon

Carbon adsorbed on the active metal due to slow polymerization of C_nH_m radicals on the active metal surface encapsulates the catalyst as the non-reactive film. The encapsulating film leads to the deactivation of the active metal. The forming temperature is < 770 K, increased with lower $\text{H}_2/\text{C}_n\text{H}_m$. The combustion temperature is low (> 573 K). A typical example of the carbon film encapsulating the ruthenium metal particle is shown in **Fig. 1.4 (b)**.

(c) Pyrolytic carbon

The pyrolytic carbon was formed by thermal cracking of hydrocarbon (steam cracking) on catalyst surface at > 870 K and the formation, may also proceed in steam reforming reaction above ca.920 K. The pyrolytic carbon is normally found as dense shales on the tube wall, or deposits encapsulating the catalyst particles and eventually filling out the void between the particles. The pyrolytic carbon also deactivates active metal. The combustion temperature is low (> 473 K), increased with lower H_2O/C_nH_m and higher pressure. The acidity of the catalyst also has an impact on the formation. A typical example of pyrolytic carbon is shown in **Fig. 1.4 (c)** [36].

As described above, coke deposition causes blockage of the system, destruction of the catalyst structure, and deactivation of the active metal by coating. The catalyst must be regenerated to remove these coke deposits. Among the precipitated coke, blockage of the system by whisker carbon is very dangerous and can cause serious accidents. In order to remove these coke deposits, it is necessary to regenerate the catalyst, and it is considered important to control the disproportionation of CO and direct decomposition of hydrocarbons that cause coke deposition.

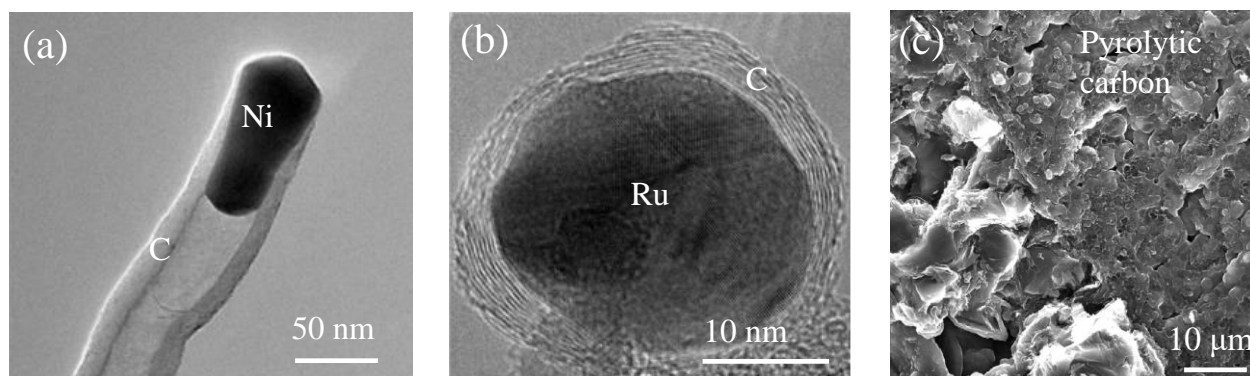


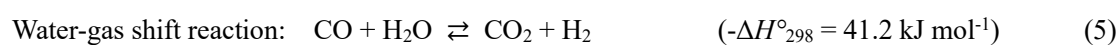
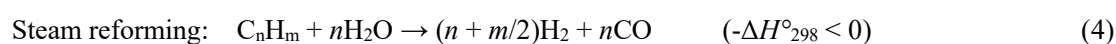
Figure 1.4 HR-TEM images of (a) whisker and (b) encapsulating carbon and (c) SEM image of pyrolytic carbon [34, 36]

1.4. Catalytic reforming of hydrocarbons

Reforming reactions are produced synthesis gas from hydrocarbons with the reforming agent and are important reactions in many fields such as refining of petroleum, the cracking of biomass tar and the conversion of hydrocarbon or natural gas as well as Reformed EGR, and they have been extensively studied. The product, syngas, is the valuable raw material that can be used to produce a wide variety of fuels and chemicals such as hydrogen, methanol, Fischer-Tropsch oil, and dimethyl ether. Here, the author describes the general hydrocarbon reforming reactions to obtain the guidance for the development of new catalysts for Reformed EGR.

1.4.1. Steam reforming

Steam reforming the process using steam for converting hydrocarbons, such as natural gas and oil, into syngas (a mixture of carbon monoxide and hydrogen) [32, 37, 38]. Because the reaction is highly endothermic, higher reaction temperatures are favorable for thermodynamics. When oxygen is added to the feed gas (oxidative reforming), oxidation of hydrocarbons, an exothermic reaction, occurs, and the temperature in the system can be raised. Therefore, the oxidative reforming valid as the supply of heat source of steam reforming, since the heat supplied rate to the reformer tube wall is a major issue in industrially steam reforming. The steam reforming reaction (Eq. 4) [32, 37, 38], the water gas shift reactions (Eq. 5) [39], and the methanation reaction (Eq. 6) are also involved and they are reversible.



These reactions may accompany side reactions that cause the carbon deposits described as Eqs. 1-3 (Section 1.3.2). The carbon monoxide disproportionation (Eq. 3) is more likely to occur at lower reaction temperatures, while the hydrocarbon decomposition (Eqs. 1 and 2) is more likely to occur at higher reaction temperatures. At high temperatures ($> 920 \text{ K}$), a carbonaceous deposit can form via pyrolysis of hydrocarbons without catalysts (Eq. 2). Since coke can cause various problems such as equipment blockage as described in Section 1.3.2, it is necessary to

avoid the risk of coke deposition in industrial operations.

The TOF [h^{-1}] of various active metals for steam reforming of toluene on Al_2O_3 support is reported to be in the order of Rh (470) > Pd (128) > Pt (88) > Ni (77) > Co (67) > Ru (64) > Ir (59) and that on SiO_2 support is Rh (94) > Ni (69) > Co (64) > Ru (61) > Pd (54) > Ir (45) > Pt (16) [40]. The coke deposition resistance is reported to be the order of Ru > Pt > Ir > Rh > Pd > Ni [37]. In addition, it is reported that Rh has high resistance to oxidation as indicated by that the activity of Rh keeps but those of Ni, Pt, and Pd decrease during oxidative reforming [41, 42].

Among these, Ni and Al_2O_3 have been widely studied because of their lower catalyst cost [37,43-46]. However, Ni/ α - Al_2O_3 catalysts have the disadvantage of being rapidly deactivated under high temperature reactions due to carbon deposition (encapsulated carbon and whisker carbon) and sintering of Ni particles [47, 48].

On the other hand, the addition of secondary metals such as Rh, Pt, Fe and Cu to form alloys with Ni has been reported to improve the catalytic performance of steam reforming various hydrocarbons [41, 49-63]. In particular, as shown in **Table 1.3**, the addition of Fe improved the coke deposition resistance and sometimes activity, which is thought to be due to the high oxygen affinity of Fe [43, 49, 50-53, 55-63].

Table 1.3 Effect of Fe addition to Ni catalysts for steam reforming reactions

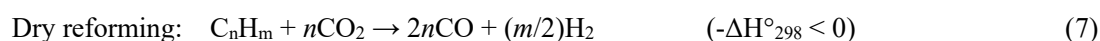
Entry	Catalyst	Reaction condition	Conv. [%]	Amount of coke deposition	Ref.
				[g _{coke} g _{cat} ⁻¹ h ⁻¹]	
2	LaNiO ₃	$F_{\text{toluene}} = 188 \mu\text{mol min}^{-1}$, $F_{\text{H}_2\text{O}} = 4444 \mu\text{mol min}^{-1}$, $F_{\text{H}_e} = 5357 \mu\text{mol min}^{-1}$, $W = 30 \text{ mg}$, $T = 923 \text{ K}$, $t = 60 \text{ min}$.	51.1	0.08	[56]
	LaNi _{0.8} Fe _{0.2} O ₃		53.1	0.04	
	LaNi _{0.5} Fe _{0.5} O ₃		22.4	0.03	
	LaNi _{0.2} Fe _{0.8} O ₃		14.7	0.01	
	LaFeO ₃		-	-	
3	Pal	toluene conc. = 3000 ppm, S/C = 1, W = 0.5 g, T = 823 K, t = 120 min.	70 - 24		[59]
	Fe ₃ /Pal		78 - 44		
	Ni ₈ /Pal		77 - 65		
	Fe ₃ Ni ₈ /Pal		81 - 79		
4	Zeolite	toluene conc. = 320 μmol , W = 70 mg, T = 873 K, t = 80 min.	20		[60]
	Ni/Zeolite		39		
	Ni-Fe/Zeolite		60		
5	7Ni/SBA-15	$F_{\text{biomass}} = 150 \text{ mg min}^{-1}$, W = 250 mg, T = 873 K, t = 80 min.	72	0.51	[61]
	6Ni-1Fe/SBA-15		82	0.19	
	5Ni-2Fe/SBA-15		75	0.19	
	3.5Ni-3.5Fe/SBA-15		56		
7	Ni/HTc	C ₇ H ₈ = 9000 ppm, WHSV = 12000 ml h _{cat} ⁻¹ , S/C = 3.4, W = 500 mg, T = 773 K.	100		[52]
	Ni-Fe/HTc		100		

Chapter 1

Entry	Catalyst	Reaction condition	Conv. [%]	Amount of coke deposition [gcoke gcat-1 h-1]	Ref.
8	Ni/Mg/Al	Toluene/H ₂ O/N ₂ = 0.38/4.4/26.8 (molar ratio), $W/F = 0.11 \text{ g h mol}^{-1}$, $S/C = 1.1$, $W = 100$ mg, $T = 873 \text{ K}$, $t = 80 \text{ min}$.	60	0.16	[31]
		Toluene/H ₂ O/N ₂ = 0.38/4.4/26.8 (molar ratio), $W/F = 0.11 \text{ g h mol}^{-1}$, $S/C = 1.7$, $W = 100$ mg, $T = 873 \text{ K}$, $t = 80 \text{ min}$.	79	0.15	
		Toluene/H ₂ O/N ₂ = 0.38/4.4/26.8 (molar ratio), $W/F = 0.11 \text{ g h mol}^{-1}$, $S/C = 3.3$, $W = 100$ mg, $T = 873 \text{ K}$, $t = 80 \text{ min}$.	92	0.04	
	Ni-Fe/Mg/Al (Fe/Ni = 0.25)	Toluene/H ₂ O/N ₂ = 0.38/4.4/26.8 (molar ratio), $W/F = 0.11 \text{ g h mol}^{-1}$, $S/C = 1.1$, $W = 100$ mg, $T = 873 \text{ K}$, $t = 80 \text{ min}$.	82	0.07	
		Toluene/H ₂ O/N ₂ = 0.38/4.4/26.8 (molar ratio), $W/F = 0.11 \text{ g h mol}^{-1}$, $S/C = 1.7$, $W = 100$ mg, $T = 873 \text{ K}$, $t = 80 \text{ min}$.	100	0.01	
		Toluene/H ₂ O/N ₂ = 0.38/4.4/26.8 (molar ratio), $W/F = 0.11 \text{ g h mol}^{-1}$, $S/C = 3.3$, $W = 100$ mg, $T = 873 \text{ K}$, $t = 80 \text{ min}$.	100	0.00	
9	Ni/Mg/Al	Toluene/H ₂ O/N ₂ = 1/11.8/71.1, $W/F = 0.05 \text{ g h mol}^{-1}$, $S/C = 1.7$, $W = 100 \text{ mg}$, $T = 873 \text{ K}$, $t =$	53.3		[53]
	Ni-Fe/Mg/Al (Fe/Ni = 0.1)	30 min.	61.7		
	Ni-Fe/Mg/Al (Fe/Ni = 0.25)		83.2		
	Ni-Fe/Mg/Al (Fe/Ni = 0.5)		82.7		
	Ni-Fe/Mg/Al (Fe/Ni = 1)		58.2		
	Ni/ α -Al ₂ O ₃		26.5		
	Ni-Fe/ α -Al ₂ O ₃ (Fe/Ni = 0.5)		26.3		
	Ni/Mg/Al		70	0.75	
	Ni-Fe/Mg/Al (Fe/Ni = 0.25)		100	0.02	

1.4.2. Dry reforming

Dry reforming (Eq. 7) is the reforming reaction using CO₂ as the reforming agent. The most typical reactant is methane [37, 44, 46, 64-66]. The side reactions are the same as those in the steam reforming reactions (Eqs. 2-6). The advantages of this reaction include the fact that, unlike steam reforming, it produces synthesis gas with a low H₂/CO ratio, making it suitable for use with the Fischer-Tropsch method, and the effective use of the greenhouse gases methane and CO. In addition, the reaction is a much endothermic reaction even compared to steam reforming. Therefore, the reaction is often carried out under high temperature conditions of 973 - 1273 K.



On the other hand, one of the problems in the dry reforming reaction is that carbon tends to precipitate. This is due to the fact that the stoichiometric composition of the reaction gas contains a large proportion of carbon. Carbon is produced mainly by the pyrolysis reaction of CH₄ (Eq. 1) and the CO disproportionation reaction (Eq. 3).

In dry reforming, catalysts with supported group VIII metals such as Pt, Rh, Ru, Ni, and Co show activity [64]. Among them, supported Ni catalysts have been widely studied because they are the least expensive and have relatively high activity [44, 46, 64-66]. However, degradation of catalyst activity due to coke deposition, oxidation of the metal, and sintering of the metal particles are inevitable. It has been reported that the addition of a second metal (M = Pt, Rh, Pd, Ru, Fe, Cu, Mn, Co) to Ni is an effective way to prevent catalyst activity degradation [66], and the main reason for the improved stability of Ni-M alloys can be attributed to the reduced coke deposition.

1.4.3. Combined dry-steam reforming

Combined dry-steam reforming is the reforming using both steam and CO₂ as reforming agents. Generally, the combined dry-steam reaction is used to produce synthesis gas with an H₂/CO ratio of about 2, which is suitable for methanol synthesis and Fischer-Tropsch synthesis [54, 67-70]. This reaction can be controlled to the H₂/CO ratio about the range to 3 from 1 with the change to feed ratio of steam and CO₂ since the H₂/CO ratio in the product is about 1 in dry reforming and about 3 in steam reforming. In addition, the combined dry-steam reaction can reduce carbon

production.

The catalytic reforming in Reformed EGR engine can be regarded as one of combined dry-steam reforming systems because used exhaust gas contains both steam and CO₂. However, the feed ratio of steam and CO₂ in the exhaust gas cannot be changed, unlike a generally combined dry-steam reforming. The partial pressure of steam in the exhaust gas is smaller than that of generally combined dry-steam reforming, and the CO₂/H₂O ratio is larger than generally combined dry-steam reforming. It is considered that the activity and coke deposition resistance are expected to be lower than the case of generally combined dry-steam reforming. In addition, the reaction temperature of Reformed EGR is determined by main the temperature of EGR gas (≤ 773 K), and it is lower than that in generally combined dry-steam reforming. This low reaction temperature is thought to cause the formation of whisker carbon due to CO disproportionation.

Gasoline, the hydrocarbon source for reforming EGR, is composed of various hydrocarbons such as paraffins, olefins, and aromatics. Steam reforming of aromatics is known to be more likely to suffer coke deposition than that of aliphatic hydrocarbons which are the other major component of gasoline because of the lower H/C ratio [71]. Toluene is the largest aromatic component of gasoline [72]. Therefore, the author selects toluene as a model compound of gasoline in this study in terms of the investigation of coke deposition resistance as well as catalytic activity. Toluene is also a model compound of biomass tar, and the steam reforming of toluene has been intensively investigated [73-76], although higher steam/carbon ratio (typically ≥ 2) and higher reaction temperature (typically ≥ 873 K) than those encountered in Reformed EGR system has been typically applied. It is expected that the difference in between steam/carbon ratio greatly influences the catalytic performance.

1.5. Hydrotalcite-like-compound-derived Ni catalyst

Many researchers have investigated the support effect on Ni catalysts in order to improve the catalytic performance. Li et al. reported that the addition of CeO₂ improves the reducibility of Ni and catalytic performance in steam reforming of tar and that the combination of CeO₂ and Al₂O₃ results in the formation of Ni-CeO₂ nanocomposite structure, which exhibits high activity and high coke deposition resistance [77]. The author's group also reported that the addition of MgO can redisperse by reduction of the calcined Ni particles via NiO-MgO solid solution formation.

On the other hand, Al_2O_3 and MgAl_2O_4 were reported to be superior to pure CeO_2 and ZrO_2 as supports for Ni catalysts in dry reforming [67]. These results suggest that the reforming catalysts can be more resistant to sintering and coking by the strong interaction between the metal and the support, which in turn improves the stability of the catalyst. The acidity of the support also has a significant effect on the adsorption and reaction of hydrocarbon and carbon dioxide as well as the interaction between the metal and the support.

Hydrotalcite-like compounds (HTlcs) form mixed oxides when calcined and exhibit important properties such as high dispersibility, thermal stability, high specific surface area, and basicity, and in the presence of reducing cations, the reduction process yields highly dispersed metal particles with thermal stability. Due to these excellent properties, Ni/Mg/Al catalysts using hydrotalcite-like compounds as precursors exhibit higher activity, higher coke deposition resistance, and higher structural stability than Ni/ Al_2O_3 and Ni/MgO in the steam reforming of tar [52, 78-81]. While a low steam/carbon ratio (e.g. 1.7) was successfully applied to these catalysts, the reaction temperature was high (e.g. 873 K) and the effect of CO_2 has not been investigated. The structure of Ni/Mg/Al catalysts is the mixture of Ni metal particles with MgO-based oxide particles containing Al^{3+} and unreduced Ni (which can be also denoted as Mg (Ni, Al) O) with similar size (about 10 nm), and this structure can be regarded as nanocomposite of Ni metal and Mg (Ni, Al) O (**Fig. 1.5**). On the other hand, conventional supported metal catalysts such as Ni/ Al_2O_3 have a much larger particle size of the oxide support than that of metal particles. The formation of this kind of nanocomposite structure of Ni/Mg/Al catalyst and other modified Ni/Mg/Al catalysts can give the large number of interface sites between metal (Ni) and support oxide (Mg(Ni, Al)O), which can be active sites with excellent performance such as high activity, suppression of the aggregation of metal particles, and coke deposition resistance [31, 52, 53, 74, 78, 82, 83]. In addition, the reusability is due to the characteristic structure change that the oxidation treatment of the Ni metal nanoparticles induces the incorporation of Ni ions into the near surface of support oxide (Mg (Ni, Al) O periclase) and the reduction regenerates uniform Ni metal nanoparticles.

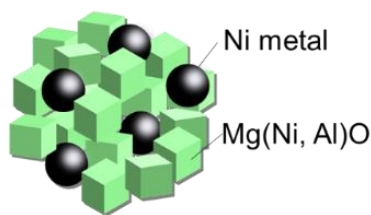


Figure 1.5 The model structure of Ni/Mg/Al catalyst [53, 78]

Utilization of HTlcs as precursors offers a feasible route for the controlled preparation of alloy catalysts [52, 53, 64, 78, 82, 84, 85]. By incorporating Ni^{2+} and Fe^{3+} (or Cu^{2+}) into the Mg-Al HTlcs, followed by calcination and reduction treatments, the author's group have successfully prepared a well dispersed Ni-Fe (or Ni-Cu) alloy catalyst with relatively uniform composition [53, 78, 82, 83] in comparison with simply supported catalysts prepared by co-impregnation. The Ni-Fe/Mg/Al and Ni-Cu/Mg/Al catalysts showed improved activity and coke deposition resistance in steam reforming of biomass tar or model compounds of biomass tar [31, 53, 82, 83, 86]. Several other research groups also reported good performance of Ni-Fe and Ni-Cu catalysts derived from HTlcs in CO_2 methanation [85], dry reforming of methane [64, 65, 66], and steam reforming of toluene [52, 78].

The reusability is due to the characteristic structure change in oxidation-reduction treatments in the same manner as Ni/Mg/Al. The oxidation treatment of the Ni-Fe alloy nanoparticles induces the incorporation of Ni and Fe ions into the near surface of support oxide (Mg (Ni, Fe, Al) O periclase) and the reduction regenerates uniform Ni-Fe alloy nanoparticles.

In the steam reforming of biomass tar, the addition of noble metals such as Rh and Pd to Ni/Mg/Al catalyst enhanced the activity in the oxidative steam reforming reaction. In particular, Pd showed higher activity than the other noble metals with increasing oxygen partial pressures. It also showed high resistance to coke deposition [87]. It has also been reported that self-activation occurs when precious metals are added [88].

1.6. Purpose of this thesis

In recent years, the depletion of fossil resources has become an issue, and there is a need to improve the fuel economy of automobiles. In this context, an exhaust gas recirculation (EGR) engine system has been developed that can significantly improve fuel economy at a relatively low cost, and a modified EGR engine that combines this system

with fuel reforming technology has also been developed. The reforming reaction in the modified EGR engine is severer than the conventional steam reforming reactions because of the relatively low reaction temperature (below 773 K) and the use of exhaust gas (low vapor partial pressure and coexistence of carbon dioxide) as the reforming agent. The reforming catalysts for reformed EGR engines are required to have (i) high activity at relatively low temperatures (< 773 K), (ii) high coke deposition resistance, (iii) high structural stability, and (iv) high start-up performance. Therefore, the author thought of replacing the main metal with Ni, which is known to have high activity at a low cost. However, supported Ni catalysts cannot achieve the performance of (i)-(iv) above due to their low coke deposition tolerance and structural stability in general steam reforming reactions. On the other hand, it has been reported that Ni/Mg/Al with the hydrotalcite-like compound as a precursor has high coke deposition tolerance and high structural stability in general steam reforming reaction. Therefore, the author considered the application of Ni/Mg/Al with hydrotalcite-like precursors to modified EGR.

In this study, the author aimed to develop Ni-based catalysts with properties of (i) - (iv) in reforming of toluene which is a model compound of gasoline as the typical source of coke under relatively low temperature (≤ 773 K) with model exhaust gas (low partial pressure of steam and carbon dioxide coexistence: $\text{H}_2\text{O}/\text{N}_2/\text{CO}_2 = 11.8/71.2/11.8$).

This research is a challenging work to apply Ni catalysts to severe reaction conditions such as relatively low temperature (≤ 773 K), low water vapor partial pressure, and carbon dioxide coexistence, which have not been the target of Ni/Mg/Al and the related catalysts so far. In addition, the results of this research will be useful in the development of catalysts in fuel cells and other applications, where their use is much broader than that of conventional catalysts.

1.7. Outline of thesis

This thesis presents the results of catalytic performance and characterization of Ni-based catalysts for the reforming of toluene as model compounds of gasoline with exhaust gas. This thesis includes five chapters. Each chapter except for chapters 1 and 5 is written based on one different publication or manuscript for publication which can/will be read dependently.

Chapter 1 presents a general introduction. A world energy consumption and fossil resource depletion, technologies

to improve automotive fuel economy, advanced research on fuel reforming catalysts, advanced research on catalysts for steam reforming of hydrocarbons, and advanced research on hydrotalcite precursor catalysts are presented in this chapter. The purpose of this thesis is also described therein.

In Chapter 2, Ni/Mg/Al catalysts prepared from the calcination and reduction of hydrotalcite-like compounds containing Ni, Mg, and Al were applied to the reforming of toluene with model exhaust gas. The Ni/Mg/Al catalyst prepared from hydrotalcite-like precursor compound showed higher performance than Ni/ α -Al₂O₃ catalyst in terms of activity, stability, and coke deposition resistance. The amount of coke deposition on Ni/Mg/Al catalyst was increased with increases of W/F or partial pressure of toluene, especially at the outlet of the catalyst bed. Similar to the case of simple steam reforming, the Ni/Mg/Al catalyst after reaction can be regenerated by the combination of oxidation (at 773 K) and reduction (at 1073 K) treatments. The effect of feed ratio of H₂O:N₂:CO₂ showed that low partial pressure of steam in model EGR gas in comparison with standard feed gas for steam reforming is the main reason for low toluene conversion and coke deposition resistance. On the other hand, the presence of CO₂ did not affect the conversion and the coke deposition behavior so significantly.

In Chapter 3, catalysts with the addition of a second metal (Fe, Co, Cu) to a Ni/Mg/Al catalyst were prepared and their effect on the Reforming EGR performance was investigated. The Ni-Fe/Mg/Al (Fe/Ni = 0.25) catalyst showed higher performance than Ni/Mg/Al, Ni-M/Mg/Al (M/Ni = 0.25, M = Co, Cu) and Ni-Fe/ α -Al₂O₃ (Fe/Ni = 0.25) catalysts in terms of activity, stability and coke deposition resistance. The Ni-Fe/Mg/Al (Fe/Ni = 0.25) catalyst showed high coke deposition resistance at both inlet and outlet positions of the catalyst bed, indicating that both substrate decomposition to coke and CO disproportionation were suppressed. The coke amount hardly increased even under low reaction temperature or higher concentration of toluene; however, the activity gradually decreased under such conditions. The regeneration of deactivated catalyst under higher toluene conversion was tested with several methods. The activity was recovered to a similar level to the fresh catalyst by treatment with N₂ flow at 873 K, catalytic use at 973 K, or re-reduction.

In Chapter 4, the addition of trace amounts of noble metals to Ni-Fe/Mg/Al catalysts was investigated to impart startability. When the catalyst in the unreduced state was heated with the reaction gas aeration, the addition of Rh showed higher starting ability than Pt, Ir, Pd, and Ru, but it did not reach the toluene conversion over Ni-Fe/Mg/Al

after reduction as pretreatment. The starting temperature was lower and toluene conversion rates were higher over the powder mixture of Rh/CeO₂ and Ni-Fe/Mg/Al than those over Rh/Ni-Fe/Mg/Al prepared by impregnation as Rh mixing method. In both mixing methods, there was an improvement in the reducibility of Ni and Fe.

In Chapter 5, all findings of this thesis are summarized.

Reference

- [1] International Energy Outlook (IEO) 2019 (2019). Available from www.eia.gov/ieo
- [2] International Energy Outlook (IEO) 2020 (2020). Available from www.eia.gov/ieo
- [3] BP statistical review of world energy 2020. Available from www.bp.com/
- [4] AUTOMOTIVE TECHNOLOGIES IN JAPAN, Japan Automobile Manufacturers Association, Inc.
- [5] H. Wei, T. Zhu, G. Shu, L. Tan, Y. Wang, Gasoline engine exhaust gas recirculation - A review, *Appl. Energy*, 2012, 99, 534-544. <https://doi.org/10.1016/j.apenergy.2012.05.011>
- [6] S. R. Gomes, N. Bion, D. Duprez, F. Epron, Hydrogen production from hydrocarbons over Rh supported on Ce-based oxides for automotive applications, *Appl. Catal. B: Environ.*, 2016, 197, 138-145. <https://doi.org/10.1016/j.apcatb.2016.01.022>
- [7] Y. Jamal, T. Wagner, M. L. Wyszynski, Exhaust Gas Reforming of Gasoline at Moderate Temperatures, *Int. J. Hydrogen Energy*, 1996, 21, 507-519. [https://doi.org/10.1016/0360-3199\(95\)00103-4](https://doi.org/10.1016/0360-3199(95)00103-4)
- [8] S. Peucheret, M. L. Wyszynski, R.S. Lehrle, S. Golunski, H.Xu, Use of catalytic reforming to aid natural gas HCCI combustion in engines: experimental and modelling results of open-loop fuel reforming, *Int. J. Hydrogen Energy*, 2005, 30, 1583-1594. <https://doi.org/10.1016/j.ijhydene.2005.02.001>
- [9] A. Tsolakis, A. Megaritis, D. Yap, Application of exhaust gas fuel reforming in diesel and homogeneous charge compression ignition (HCCI) engines fuelled with biofuels, *Energy*, 2008, 33, 462-470. <https://doi.org/10.1016/j.energy.2007.09.011>
- [10] L. Tartakovsky, M. Sheintuch, Fuel reforming in internal combustion engines, *Prog. Energy Combust. Sci.*, 2018, 67, 88-114. <https://doi.org/10.1016/j.peccs.2018.02.003>
- [11] Nissan Motor Co., Ltd., Fuel reforming catalyst and method of using the same, JP2001-170486.

- [12] A. Tsolakis, A. Megaritis, Partially premixed charge compression ignition engine with on-board H₂ production by exhaust gas fuel reforming of diesel and biodiesel, *Int. J. Hydrogen Energy*, 2005, 30, 731-745. <https://doi.org/10.1016/j.ijhydene.2004.06.013>
- [13] S. Peucheret, M. Feaviour, S. Golunski, Exhaust-gas reforming using precious metal catalysts, *Appl. Catal. B: Environ.*, 2006, 65, 201-206. <https://doi.org/10.1016/j.apcatb.2006.01.009>
- [14] D. Fennell, J. Herreros, A. Tsolakis, Improving gasoline direct injection (GDI) engine efficiency and emissions with hydrogen from exhaust gas fuel reforming, *Int. J. Hydrogen Energy*, 2014, 39, 5153-5162. <https://doi.org/10.1016/j.ijhydene.2014.01.065>
- [15] JOGMEC (Japan Oil, Gas and Metals National Corporation), Resource Library.
- [16] S. Peucheret, M. Feaviour, S. Golunski, Exhaust-gas reforming using precious metal catalysts, *Appl. Catal. B: Environ.*, 2006, 65, 201-206. <https://doi.org/10.1016/j.apcatb.2006.01.009>
- [17] J. Thormann, L. Maier, P. Pfeifer, U. Kunz, O. Dautschmann, K. Schubert, Steam reforming of hexadecane over a Rh/CeO₂ catalyst in microchannels: Experimental and numerical investigation, *Int. J. Hydrogen Energy*, 2009, 34, 5108-5120. <https://doi.org/10.1016/j.ijhydene.2009.04.031>
- [18] M. Asadullah, K. Tomishige, K. Fujimoto, A novel catalytic process for cellulose gasification to synthesis gas, *Catal. Commun.*, 2001, 2, 63-68. [https://doi.org/10.1016/S1566-7367\(01\)00011-5](https://doi.org/10.1016/S1566-7367(01)00011-5)
- [19] M. Asadullah, K. Fujimoto, K. Tomishige, Catalytic Performance of Rh/CeO₂ in the Gasification of Cellulose to Synthesis Gas at Low Temperature, *Ind. Eng. Chem. Res.*, 2001, 40, 5894-5900. <https://doi.org/10.1021/ie010160z>
- [20] A. Tsolakis, S. E. Golunski, Sensitivity of process efficiency to reaction routes in exhaust-gas reforming of diesel fuel, *Chem. Eng. J.*, 2006, 117, 131-136. <https://doi.org/10.1016/j.cej.2005.12.017>
- [21] K. Theinnoi, W. Temwutthikun, T. Wongchang, B. Sawatmongkhon, Application of Exhaust Gas Fuel Reforming in Diesel Engines Towards the Improvement Urban Air Qualities, *Energy Procedia*, 2018, 152, 875-882. <https://doi.org/10.1016/j.egypro.2018.09.257>

- [22] P. Leung, A. Tsolakis, J. Rodriguez-Fernandez, S. Golunski, Raising the fuel heating value and recovering exhaust heat by on-board oxidative reforming of bioethanol, *Energy Environ. Sci.*, 2010, 3, 780-788. <https://doi.org/10.1039/b927199f>
- [23] D. Fennell, J. Herreros, A. Tsolakis, K. Cockle, J. Pignon, P. Millington, Thermochemical recovery technology for improved modern engine fuel economy - part 1: analysis of a prototype exhaust gas fuel reformer, *RSC Adv.*, 2015, 5, 35252-35261. <https://doi.org/10.1039/c5ra03111g>
- [24] E. Ambroise, C. Courson, A. C. Roger, A. Kiennemann, G. Blanchard, S. Rousseau, X. Carrier, E. Marceau, C. La Fontaine, F. Villain, Exhaust gas recirculation for on-board hydrogen production by isooctane reforming: Comparison of performances of metal/ceria-zirconia based catalysts prepared through pseudo sol-gel or impregnation methods, *Catal. Today*, 2010, 154, 133-141. <https://doi.org/10.1016/j.cattod.2009.12.010>
- [25] A. Tsolakis, A. Megaritis, M. L. Wyszynski, Application of Exhaust Gas Fuel Reforming in Compression Ignition Engines Fueled by Diesel and Biodiesel Fuel Mixtures, *Energy Fuels*, 2003, 17, 1464-1473. <https://doi.org/10.1021/ef0300693>
- [26] V. Chintala, D. Banaerjee, P. K. Ghodke, E. Porpatham, Hydrogen rich exhaust gas recirculation (H₂EGR) for performance improvement and emissions reduction of a compression ignition engine, *Int. J. Hydrogen. Energy*, 2019, 44, 18545-18558. <https://doi.org/10.1016/j.ijhydene.2019.05.141>
- [27] S. R. Gomes, N. Bion, G. Blanchard, S. Rousseau, V. Bellière-Baca, V. Harlé, D. Duprez, F. Epron, Thermodynamic and experimental studies of catalytic reforming of exhaust gas recirculation in gasoline engines, *Appl. Catal. B: Environ.*, 2011, 102, 44-53. <https://doi.org/10.1016/j.apcatb.2010.11.023>
- [28] Nissan Motor Co., Ltd., Fuel reforming catalyst and hydrogen rich gas production method, P2004-57869A.
- [29] Nissan Motor Co., Ltd., Fuel reforming catalyst and its manufacturing method, P2013-144266A.
- [30] Nissan Motor Co., Ltd., Fuel reforming catalyst, P2014-113518A.
- [31] M. Koike, D. Li, H. Watanabe, Y. Nakagawa, K. Tomishige, Comparative study on steam reforming of model aromatic compounds of biomass tar over Ni and Ni-Fe alloy nanoparticles, *Appl. Catal. A: Gen.*, 2015, 506, 151-162. <https://doi.org/10.1016/j.apcata.2015.09.007>

- [32] J. R. Rostrup-Nielsen, Catalytic Steam Reforming, in J. R. Anderson and M. Boudart, Eds., Catalytic Steam Reforming, *Catalysis Science and Technology*, Springer-Verlag, New York, 1984, pp.1-117.
https://doi.org/10.1007/978-3-642-93247-2_1
- [33] H. S. Benggaard, J. K. Nørskov, J. Sehested, B. S. Clausen, L. P. Nielsen, A. M. Molenbroek, J. R. Rostrup-Nielsen, Steam Reforming and Graphite Formation on Ni Catalysts, *J. Catal.*, 2002, 209, 365-384.
<https://doi.org/10.1006/jcat.2002.3579>
- [34] S. Helveg, J. Sehested, J.R. Rostrup-Nielsen, Whisker carbon in perspective, *Catal. Today*, 2011, 178, 42-46.
<https://doi.org/10.1016/j.cattod.2011.06.0>
- [35] S. Helveg, C. Lopez-Cartes, J. Sehested, P.L. Hansen, B.S. Clausen, J.R. Rostrup-Nielsen, F. Abild-Pedersen, J.K. Nørskov, Atomic-scale imaging of carbon nanofibre growth, *Nature*, 2004, 427, 426-429. <https://doi.org/10.1038/nature02278>
- [36] X. He, J. Song, H. Xia, J. Tan, B. Zhang, Z. He, X. Zhou, Z. Zhu, M. Zhao, X. Liu, L. Xu, S. Bai, Direct characterization of ion implanted pyrolytic carbon coatings deposited from natural gas, *Carbon*, 2014, 68, 95-103. <https://doi.org/10.1016/j.carbon.2013.10.058>
- [37] J. R. Rostrup-Nielsen, J. H. B. Hansen, CO₂-Reforming og Methane over Transition Metals, *J. Catal.*, 1991, 144, 38-49. <https://doi.org/10.1006/jcat.1993.1312>
- [38] M. A. Pena, J. P. Gdmez, J. L. G. Fierro, New catalytic routes for syngas and hydrogen production, *Appl. Catal. A: Gen.*, 1996, 144, 7-57. [https://doi.org/10.1016/0926-860X\(96\)00108-1](https://doi.org/10.1016/0926-860X(96)00108-1)
- [39] C. Ratnasamy, J. P. Wegner, Water Gas Shift Catalysis, *Catal. Rev.*, 2009, 51, 325-440.
<https://doi.org/10.1080/01614940903048661>
- [40] D. Duprez, Selective steam reforming of aromatic compounds on metal catalysts, *Appl. Catal. A: Gen.*, 1992, 82, 111-157. [https://doi.org/10.1016/0926-860X\(92\)85001-R](https://doi.org/10.1016/0926-860X(92)85001-R)
- [41] D. Li, Y. Nakagawa, K. Tomishige, Methane reforming to synthesis gas over Ni catalysts modified with noble metals, *Appl. Catal. A: Gen.*, 2011, 408, 1-24. <https://doi.org/10.1016/j.apcata.2011.09.018>

- [42] A. Remiro, A. Arandia, J. Bilbao, A. G. Gayubo, Comparison of Ni Based and Rh Based Catalyst Performance in the Oxidative Steam Reforming of Raw Bio-Oil, *Energy Fuels*, 2017, 31, 7147-7156. <https://doi.org/10.1021/acs.energyfuels.7b00735>
- [43] B. Li, X. Yuan, B. Li, X. Wang, Impact of pore structure on hydroxyapatite supported nickel catalysts (Ni/HAP) for dry reforming of methane, *Fuel Proc. Technol.*, 2020.202, 106359. <https://doi.org/10.1016/j.fuproc.2020.106359>
- [44] J. Kobayashi, K. Kawamoto, N. Kobayashi, Effect of porous silica on the removal of tar components generated from waste biomass during catalytic reforming, *Fuel Proc. Technol.*, 2019, 194, 106104. <https://doi.org/10.1016/j.fuproc.2019.05.027>
- [45] T. Y. Liang, H. H. Chen, D. H. Tsai, Nickel hybrid nanoparticle decorating on alumina nanoparticle cluster for synergistic catalysis of methane dry reforming, *Fuel Proc. Technol.*, 2020, 201, 106335. <https://doi.org/10.1016/j.fuproc.2020.106335>
- [46] S. S. Maluf, E. M. Assaf, Ni catalysts with Mo promoter for methane steam reforming, *Fuel*, 2009, 88, 1547-1553. <https://doi.org/10.1016/j.fuel.2009.03.025>
- [47] P. Wu, X. Li, S. Ji, B. Lang, F. Habimana, C. Li, Steam reforming of methane to hydrogen over Ni-based metal monolith catalysts, *Catal. Today*, 2009, 146, 82-86. <https://doi.org/10.1016/j.cattod.2009.01.031>
- [48] J. Ashok, S. Kawi, Nickel-Iron Alloy Supported over Iron-Alumina Catalysts for Steam Reforming of Biomass Tar Model Compound, *ACS Catal.*, 2014, 4, 289-301. <https://doi.org/10.1021/cs400621p>
- [49] K. Tomishige, D. Li, M. Tamura, Y. Nakagawa, Nickel-iron alloy catalysts for reforming of hydrocarbons: preparation, structure, and catalytic properties, *Catal. Sci. Technol.*, 2017, 7, 3952-3979. <https://doi.org/10.1039/c7cy01300k>
- [50] L. Wang, D. Li, M. Koike, S. Koso, Y. Nakagawa, Y. Xu, K. Tomishige, Catalytic performance and characterization of Ni-Fe catalysts for the steam reforming of tar from biomass pyrolysis to synthesis gas, *Appl. Catal. A: Gen.*, 2011, 392, 248-255. <https://doi.org/10.1016/l.apcata.2010.11.013>

- [51] F. Zhou, N. Pan, H. Chen, X. Xu, C. Wang, Y. Du, Y. Guo, Z. Zeng, L. Li, Hydrogen production through steam reforming of toluene over Ce, Zr or Fe promoted Ni-Mg-Al hydrotalcite-derived catalysts at low temperature, *Energy Convers. Manag.*, 2019, 196, 677-687. <https://doi.org/10.1016/j.enconman.2019.06.047>
- [52] M. Koike, D. Li, Y. Nakagawa, and K. Tomishige, A Highly Active and Coke-Resistant Steam Reforming Catalyst Comprising Uniform Nickel-Iron Alloy Nanoparticles, *ChemSusChem*, 2012, 5, 2312-2314. <https://doi.org/10.1002/cssc.201200507>
- [53] Y. Khani, Z. Shariatnia, F. Bahadoran, High catalytic activity and stability of ZnLaAlO₄ supported Ni, Pt and Ru nanocatalysts applied in the dry, steam and combined dry-steam reforming of methane, *Chem. Eng. J.*, 2016, 299, 353-366. <https://doi.org/10.1016/j.cej.2016.04.108>
- [54] B. Li, Y. Luo, B. Li, X. Yuan, X. Wang, Catalytic performance of iron-promoted nickel-based ordered mesoporous alumina FeNiAl catalysts in dry reforming of methane, *Fuel Process. Technol.*, 2019, 193, 348-360. <https://doi.org/10.1016/j.fuproc.2019.05.033>
- [55] U. Oemar, P.S. Ang, K. Hidajat, S. Kawi, Promotional effect of Fe on perovskite LaNi_xFe_{1-x}O₃ catalyst for hydrogen production via steam reforming of toluene, *Int. J. Hydrogen Energy*, 2013, 38, 5525-5534. <https://doi.org/10.1016/j.ijhydene.2013.02.083>
- [56] G. Wang, Y. Jin, G. Liu, Y. Li, Production of Hydrogen and Nanocarbon from Catalytic Decomposition of Methane over a Ni-Fe/Al₂O₃ Catalyst, *Energy Fuels*, 2013, 27, 4448-4456. <https://doi.org/10.1021/ef3019707>
- [57] X. Song, X. Dong, S. Yin, M. Wang, M. Li, H. Wang, Effects of Fe partial substitution of La₂NiO₄/LaNiO₃ catalyst precursors prepared by wet impregnation method for the dry reforming of methane, *Appl. Catal. A: Gen.*, 2016, 526, 132-138. <https://doi.org/10.1016/j.apcata.2016.07.024>
- [58] X. Zou, T. Chen, P. Zhang, D. Chen, J. He, Y. Dang, Z. Ma, Y. Chen, P. Toloueinia, C. Zhu, J. Xie, H. Liu, S. L. Suib, High catalytic performance of Fe-Ni/Palygorskite in the steam reforming of toluene for hydrogen production, *Appl. Energy*, 2018, 226, 827-837. <https://doi.org/10.1016/j.apenergy.2018.06.005>
- [59] T. Ahmed, S. Xiu, L. Wang, A. Shahbazi, Investigation of Ni/Fe/Mg zeolite-supported catalysts in steam reforming of tar using simulated-toluene as model compound, *Fuel*, 2018, 211, 566-571. <https://doi.org/10.1016/j.fuel.2017.09.051>

- [60] Y. Kathiraser, J. Ashok, S. Kawi, Synthesis and evaluation of highly dispersed SBA-15 supported Ni-Fe bimetallic catalysts for steam reforming of biomass derived tar reaction, *Catal. Sci. Technol.*, 2016, 6, 4327-4336. <https://doi.org/10.1039/c5cy01910a>
- [61] T.u Baidya, R. J. Cattolica, R. Seiser, High performance Ni-Fe-Mg catalyst for tar removal in producer gas, *Appl. Catal. A: Gen.*, 2018, 558, 131-139. <https://doi.org/10.1016/j.apcata.2018.03.026>
- [62] T. Zhang, Z. Liu, Y. A. Zhu, Z. Liu, Z. Sui, K. Zhu, X. Zhou, Dry reforming of methane on Ni-Fe-MgO catalysts: Influence of Fe on carbon-resistant property and kinetics, *Appl. Catal. B: Environ.*, 2020, 264, 118497. <https://doi.org/10.1016/j.apcatb.2019.118497>
- [63] K. Song, M. Lu, S. Xu, C. Chen, Y. Zhan, D. Li, C. Au, L. Jiang, K. Tomishige, Effect of alloy composition on catalytic performance and coke-resistance property of Ni-Cu/Mg(Al)O catalysts for dry reforming of methane, *Appl. Catal. B: Environ.*, 2018, 239, 324-333. <https://doi.org/10.1016/j.apcatb.2018.08.023>
- [64] C. Wan, K. Song, J. Pan, M. Huang, R. Luo, D. Li, L. Jiang, Ni-Fe/Mg(Al)O alloy catalyst for carbon dioxide reforming of methane: Influence of reduction temperature and Ni-Fe alloying on coking, *Int. J. Hydrogen Energy*, 2020, 45, 33574-33585. <https://doi.org/10.1016/j.ijhydene.2020.09.129>
- [65] S. M. Kim, P. M. Abdala, T. Margossian, D. Hosseini, L. Foppa, A. Armutlulu, W. Beek, A. Comas-Vives, C. Copéret, C. Müller, Cooperativity and Dynamics Increase the Performance of Ni Fe Dry Reforming Catalysts, *J. Am. Chem. Soc.*, 2017, 139, 1937-1949. <https://doi.org/10.1021/jacs.6b11487>
- [66] C. Liu, J. Ye, J. Jiang, Y. Pan, Progresses in the Preparation of Coke Resistant Ni-based Catalyst for Steam and CO₂ Reforming of Methane, *ChemCatChem*, 2011, 3, 529-541. <https://doi.org/10.1002/cctc.201000358>
- [67] C. Zhang, K. W. Jun, K. S. Ha, Y. J. Lee, S. C. Kang, Efficient Utilization of Greenhouse Gases in a Gas-to-Liquids Process Combined with CO₂/Steam-Mixed Reforming and Fe-Based Fischer-Tropsch Synthesis, *Environ. Sci. Technol.*, 2014, 48, 8251-8257. <https://doi.org/10.1021/es501021u>
- [68] G. A. Olah, A. Goepfert, M. Czaun, G. K. S. Prakash, Bi-reforming of Methane from Any Source with Steam and Carbon Dioxide Exclusively to Metgas (CO-2H₂) for Methanol and Hydrocarbon Synthesis, *J. Am. Chem. Soc.*, 2013, 135, 648-650. <https://doi.org/10.1021/ja311796n>

- [69] G. A. Olah, A. Goeppert, M. Czaun, T. Mathew, R. B. May, G. K. S. Prakash, Single Step Bi-reforming and Oxidative Bi-reforming of Methane (Natural Gas) with Steam and Carbon Dioxide to Metgas (CO-2H₂) for Methanol Synthesis: Self-Sufficient Effective and Exclusive Oxygenation of Methane to Methanol with Oxygen, *J. Am. Chem. Soc.*, 2015, 137, 8720-8729. <https://doi.org/10.1021/jacs.5b02029>
- [70] L. Barbarias, G. Lopez, M. Amutio, M. Artetxe, J. Alvarez, A. Arregi, J. Bilbao, M. Olazar, Steam reforming of plastic pyrolysis model hydrocarbons and catalyst deactivation, *Appl. Catal. A: Gen.*, 2016, 527, 152-160. <https://doi.org/10.1016/j.apcata.2016.09.003>
- [71] L. Sileghem, V. A. Alekseev, J. Vancoillie, K. M. Van Geem, E. J. K. Nilsson, S. Verhelst, A. A. Konnov, Laminar burning velocity of gasoline and the gasoline surrogate components iso-octane, n-heptane and toluene, *Fuel*, 2013, 112, 355-365. <https://doi.org/10.1016/j.fuel.2013.05.049>
- [72] J. Ashok, N. Dewangan, S. Das, P. Hongmanorm, M. H. Wai, K. Tomishige, S. Kawi, Recent progress in the development of catalysts for steam reforming of biomass tar model reaction, *Fuel Proc. Technol.*, 2020, 199, 106252. <https://doi.org/10.1016/j.fuproc.2019.106252>
- [73] D. Li, M. Tamura, Y. Nakagawa, K. Tomishige, Metal catalysts for steam reforming of tar derived from the gasification of lignocellulosic biomass, *Bioresource Technol.*, 2015, 178, 53-64. <https://doi.org/10.1016/j.biortech.2014.10.010>
- [74] J. Ren, J. P. Cao, F. L. Yang, X. Y. Zhao, W. Tang, X. Cui, Q. Chen, X. Y. Wei, Layered uniformly delocalized electronic structure of carbon supported Ni catalyst for catalytic reforming of toluene and biomass tar, *Energy Convers. Manag.*, 2019, 183, 182-192. <https://doi.org/10.1016/j.enconman.2018.12.093>
- [75] V. Claude, J. G. Mahy, J. Geens, C. Courson, S. D. Lambert, Synthesis of Ni/ γ -Al₂O₃-SiO₂ catalysts with different silicon precursors for the steam toluene reforming, *Microporous Mesoporous Mater.*, 2019, 284, 304-315. <https://doi.org/10.1016/j.micromeso.2019.04.027>
- [76] D. Li, Y. Nakagawa, K. Tomishige, Development of Ni-Based Catalysts for Steam Reforming of Tar Derived from Biomass Pyrolysis, *Chin. J. Catal.*, 2012, 33, 583-594. [https://doi.org/10.1016/S1872-2067\(11\)60359-8](https://doi.org/10.1016/S1872-2067(11)60359-8)

- [77] D. Li, L. Wang, M. Koike, Y. Nakagawa, K. Tomishige, Steam reforming of tar from pyrolysis of biomass over Ni/Mg/Al catalysts prepared from hydrotalcite-like precursors, *Appl. Catal. B: Environ.*, 2011, 102, 528-538. <https://doi.org/10.1016/j.apcatb.2010.12.035>
- [78] H. Cheng, Y. Zhang, X. Lu, W. Ding, Q. Li, Hydrogen Production from Simulated Hot Coke Oven Gas by Using Oxygen-Permeable Ceramics, *Energy Fuels*, 2009, 23, 414-421. <https://doi.org/10.1021/ef8007618>
- [79] O. C. V. Silva, E. B. Silveira, R. C. Rabelo-Neto, L. E. P. Borges, F. B. Noronha, Hydrogen Production Through Steam Reforming of Toluene Over Ni Supported on MgAl Mixed Oxides Derived from Hydrotalcite-Like Compounds, *Catal. Lett.*, 2018, 148, 1622-1633. <https://doi.org/10.1007/s10562-018-2390-8>
- [80] C. Wu, J. Huang, P. T. Williams, Carbon nanotubes and hydrogen production from the reforming of toluene, *Int. J. Hydrogen Energy*, 2013, 38, 8790-8797. <https://doi.org/10.1016/j.ijhydene.2013.05.028>
- [81] D. Li, M. Koike, L. Wang, Y. Nakagawa, Y. Xu, K. Tomishige, Regenerability of Hydrotalcite-Derived Nickel-Iron Alloy Nanoparticles for Syngas Production from Biomass Tar, *ChemSusChem*, 2014, 7, 510-522. <https://doi.org/10.1002/cssc.201300855>
- [82] D. Li, M. Koike, J. Chen, Y. Nakagawa, K. Tomishige, Preparation of Ni-Cu/Mg/Al catalysts from hydrotalcite-like compounds for hydrogen production by steam reforming of biomass tar, *Int. J. Hydrogen Energy*, 2014, 39, 10959-10970. <https://doi.org/10.1016/j.ijhydene.2014.05.062>
- [83] L. Wang, J. Chen, H. Watanabe, Y. Xu, M. Tamura, Y. Nakagawa, K. Tomishige, Catalytic performance and characterization of Co-Fe bcc alloy nanoparticles prepared from hydrotalcite-like precursors in the steam gasification of biomass-derived tar, *Appl. Catal. B: Environ.*, 2014, 160-161, 701-715. <http://dx.doi.org/10.1016/j.apcatb.2014.06.021>
- [84] C. Mebrahtu, F. Krebs, S. Perathoner, S. Abate, G. Centi, R. Palkovits, Hydrotalcite based Ni-Fe/(Mg, Al)Ox catalysts for CO₂ methanation - tailoring Fe content for improved CO dissociation, basicity, and particle size, *Catal. Sci. Technol.*, 2018, 8, 1016-1027. <https://doi.org/10.1039/c7cy02099f>
- [85] D. Li, M. Lu, K. Aragaki, M. Koike, Y. Nakagawa, K. Tomishige, Characterization and catalytic performance of hydrotalcite-derived Ni-Cu alloy nanoparticles catalysts for steam reforming of 1-methylnaphthalene, *Appl. Catal. B: Environ.*, 2016, 192, 171-181. <https://doi.org/10.1016/j.apcatb.2016.03.052>

- [86] J. Chen, M. Tamura, Y. Nakagawa, K. Okumura, K. Tomishige, Promoting effect of trace Pd on hydrotalcite-derived Ni/Mg/Al catalyst in oxidative steam reforming of biomass tar, *Appl. Catal. B: Environ.*, 2015, 179, 412-421. <https://doi.org/10.1016/j.apcatb.2015.05.042>
- [87] K. Takehira, "Intelligent" reforming catalysts: Trace noble metal-doped Ni/Mg(Al)O derived from hydrotalcites, *Journal of Natural Gas Chemistry*, 2009, 18, 237-259. [https://doi.org/10.1016/S1003-9953\(08\)60123-1](https://doi.org/10.1016/S1003-9953(08)60123-1)

Chapter 2

Reforming of toluene with simulated automobile exhaust gas over hydrotalcite-like-compound-derived Ni catalyst

* Reproduced from Ref. “M. Betchaku, Y. Nakagawa, M. Tamura, K. Tomishige, *Fuel Process. Technol.*, 2020, 209, 106545.” with permission from Elsevier.

2.1. Introduction

Liquid fuels, because of energy density, cost, and chemical properties, continue to be the predominant transportation fuel and an important industrial feedstock, and our life keeps receiving the benefit.

Techniques to improve fuel economy of engines of automobiles have been extensively developed. Exhaust Gas Recirculation (EGR) system was developed at first for decrease of NO_x emission [1, 2], however, currently, EGR system is regarded as one of the methods to improve fuel economy of engines [1, 3, 4]. Especially, EGR with reforming techniques (denoted as Reformed EGR) is promising where a small amount of gasoline is mixed with the circulating exhaust gas and is reformed over catalyst to highly flammable synthesis gas [1, 5-7]. The addition of synthesis gas produced by the catalytic reforming to engine feed gas (mixture of gasoline and air) stabilizes the combustion of gasoline, which enables higher dilution of feed gas with exhaust gas to improve the fuel economy [1, 5, 6]. This Reformed EGR system can be relatively simple and inexpensive since it only requires the addition of a reformer containing a reforming catalyst to a conventional EGR system. The reforming catalyst should have high activity at relatively low temperature (673-773 K or less), good reusability and startability [8]. Here, high startability means that the catalyst can exhibit activity just when the engine in a resting state starts up.

Generally, supported Rh catalysts have been investigated for Reformed EGR system, since they have high activity, reducibility (startability) and high coke deposition resistance [7, 9]. CeO₂-based supports have been typically used [10, 11], and catalyst development by modification of support [3, 12] or adding second metal such as Pt [7, 13-15] and Co [16]

has been carried out to improve the performance. For example, Gomes et al. reported the effect of support of Rh catalyst for reforming of isooctane at 853 K with simulated exhaust gas ($\text{H}_2\text{O}:\text{CO}_2:\text{N}_2:\text{O}_2 = 12:14:71:1$), and Rh/CeZrAl catalyst showed higher activity (57% conv.) than Rh/CeO₂ (47% conv.) and Rh/Al₂O₃ (39% conv.) [3]. However, Rh is a very expensive noble metal and development of reforming catalyst with lower cost is necessary.

Among non-noble metals, Ni has low cost and is often investigated as steam reforming catalyst because the activity of Ni in steam reforming tends to be comparable to those of noble metal catalysts and therefore the development of Ni catalysts has been intensively carried out for various substrates [17-22]. However, Ni catalysts can be deactivated easily because of aggregation and coke (carbon) deposition. The coke may cause serious operational problems, by forming a non-reactive film deposit on the nickel surface to cause deactivation and whisker like structures to cause reactor plugging and breakdown of the catalyst granules to powders [23]. Periodical removal of coke by combustion of the catalyst is necessary for catalysts that are suffered from coking. However, the combustion procedure can also cause catalyst deactivation by sintering of the support and aggregation of the metal particles. After all, suppression of coke deposition is one of the most important functions of reforming catalysts in Reformed EGR system as well as conventional hydrogen and/or syngas production systems.

Conventional steam reforming system, operated under sufficient partial pressure of steam, can change feed ratio of all reactants [24]. The combination of steam reforming with dry reforming (reforming with CO₂) is well known which can adjust the H₂/CO ratio of the produced synthesis gas [25, 26]. On the other hand, Reformed EGR system has limitation in the feed ratio of H₂O, CO₂, and N₂ because the supply of gasoline and air to engines is controlled by the stoichiometry of the gasoline combustion (when air with O₂:N₂ = 20:80 stoichiometrically reacts with (CH₂)_n hydrocarbon molecule the exhaust gas is composed of H₂O:CO₂:N₂ = 13:13:80 ($2/3(\text{CH}_2)_n + n\text{O}_2 \rightarrow 2/3n\text{CO}_2 + 2/3n\text{H}_2\text{O}$)). In Reformed EGR system, the feed amount of gasoline into the reformer can vary, and the system should work at any feed amount. Up to now, there is no report focusing on Ni catalysts for reforming in EGR of gasoline engine. Zhang et al. tested Ni catalyst for reforming of CH₄ with LNG-diesel dual fuel engine; however, the reactants (CH₄ and exhaust gas of diesel fuel) were much different from Reformed EGR system for gasoline engine, because exhaust gas of diesel fuel contains substantial amount of O₂ [27].

Gasoline is composed of various type of hydrocarbons such as paraffins, olefins and aromatics. Steam reforming of

aromatics is known to be more likely to suffer coke deposition than that of aliphatic hydrocarbons which are the other major component of gasoline because of lower H/C ratio [28]. Toluene is the largest aromatic component of gasoline [29]. Therefore, I selected toluene as a model compound of gasoline in this study in terms of the investigation of coke deposition resistance as well as catalytic activity. Toluene is also a model compound of biomass tar, and the steam reforming of toluene has been intensively investigated [30-33], although higher steam/carbon ratio (typically ≥ 2) and higher reaction temperature (typically ≥ 873 K) than those encountered in Reformed EGR system has been typically applied. It is expected that the difference of steam/carbon ratio greatly influences the catalytic performance. Previous studies on steam reforming of toluene as a tar model compound showed that Ni/Mg/Al catalysts prepared by calcination and subsequent reduction of hydrotalcite-like compounds containing Ni have higher activity and higher coke deposition resistance than other Ni supported catalysts such as Ni/Al₂O₃ [34-38]. While low steam/carbon ratio (e.g. 1.7) was successfully applied to these catalysts, the reaction temperature was high (e.g. 873 K) and the effect of CO₂ has not been investigated. The structure of Ni/Mg/Al catalysts is the mixture of Ni metal particles with MgO-based oxide particles containing Al³⁺ and unreduced Ni (which can be also denoted as Mg(Ni, Al)O) with similar size (about 10 nm), and this structure can be regarded as nanocomposite of Ni metal and Mg(Ni, Al)O (**Figure 2.1**). On the other hand, conventional supported metal catalysts such as Ni/Al₂O₃ have much larger particle size of the oxide support than that of metal particles. The formation of this kind of nanocomposite structure of Ni/Mg/Al catalyst and other modified Ni/Mg/Al catalysts can give large number of interface sites between metal (Ni) and support oxide (Mg(Ni, Al)O), which can be active sites with excellent performance such as high activity, suppression of the aggregation of metal particles, and coke deposition resistance [31, 34, 35, 39-42]. In addition, Ni-Fe alloy-oxide nanocomposite catalysts from hydrotalcite-like compound has high catalytic activity and high reusability in oxidation-reduction treatments [39, 43]. The reusability is due to the characteristic structure change that the oxidation treatment of the Ni-Fe alloy nanoparticles induces the incorporation of Ni and Fe ions into the near surface of support oxide (Mg (Ni, Fe, Al) O periclase) and the reduction regenerates uniform Ni-Fe alloy nanoparticles.

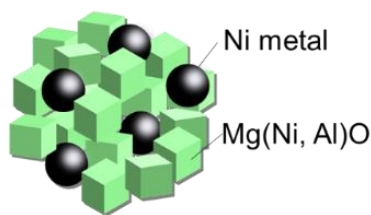


Figure 2.1 The model structure of Ni/Mg/Al catalyst ^[34, 40]

In this chapter, the author applied the Ni/Mg/Al catalyst to the reforming of toluene with model EGR gas of gasoline engine as the model reaction of Reformed EGR. The activity, stability and coke deposition resistance of Ni/Mg/Al catalysts were compared with those of Ni/ α -Al₂O₃ and Rh/CeO₂ catalysts under the severer conditions of Reformed EGR than simple steam reforming, although startability (reducibility) was not compared in this study. The effects of contact time (W/F), toluene feeding rate, reaction temperature and feed ratio on the Ni/Mg/Al catalyst were investigated under conditions of Reformed EGR. In addition, the reusability of Ni/Mg/Al catalyst by regeneration was confirmed in the model EGR system. The difference of stability and coke deposition behavior between Reformed EGR and simple steam reforming system was also discussed.

2.2. Experimental

2.2.1. Catalyst preparation

Ni/Mg/Al catalyst derived from hydrotalcite-like compound was prepared according to our previous paper ^[34] on the basis of the method reported by Miyata ^[44]. Briefly, a mixed aqueous solution of nickel, magnesium and aluminum nitrates with specific concentration ratio (molar ratio 9:66:25) was added slowly into Na₂CO₃ aq in the beaker under stirring at room temperature. During this procedure, pH of the solution was kept constant at 10 ± 0.5 by using NaOH aq. The resulting suspension was kept at room temperature for 24 h. The obtained precipitate was collected by filtration, washed with water, and then dried at 383 K overnight. The solid was ground to fine powders, and calcination at 1073 K for 5 h was carried out. The granule size of the catalyst material was controlled to 30-60 mesh size (0.3-0.6 mm ϕ) by pressing, crushing and sieving. The loading amount of Ni was 12 wt%. The composition of the Ni/Mg/Al catalyst was the optimized one in the steam reforming of toluene in our previous paper ^[34]. The BET surface area was 120 m² g⁻¹. The Ni⁰_{surface}/Ni_{total} ratio determined from the crystallite size (XRD; 7.6 nm) and the

reduction degree (0.54; determined by TPR (**Fig. 2.2**)) was 0.069 (**Table 2.1**). These values were almost the same as the reported values in our previous report ^[34].

Table 2.1 Physicochemical properties of the supports and prepared catalysts.

Entry	Catalyst	Loading amount of metal [wt%]	Particle size [nm]		BET surface area ^a [m ² g ⁻¹]	Reduction degree of Ni ^b [-]	Ni ⁰ _{surface} /Ni ⁰ _{total} [-]	Dispersion by H ₂ adsorption [-]
			XRD	TEM				
1	Ni/Mg/Al	12	7.6	5.5	120	0.54	0.069	n.d.
1'	Ni/Mg/Al ^[34]	12	8.5	10.8	146	0.54	0.062	0.077
2	Ni/ α -Al ₂ O ₃	12	14.1	38.6	12	1.0	0.069	n.d.
2'	Ni/ α -Al ₂ O ₃ ^[47]	12	24	-	8	0.94	0.038	0.043
3	α -Al ₂ O ₃	0	-	-	12	-	-	-
4	Rh/CeO ₂	1	- ^d	n.d.	82	-	-	1.0
5	Rh/CeO ₂	0.1	- ^d	n.d.	n.d.	-	-	0.85
6	CeO ₂	0	-	-	87	-	-	-

^a Measured to catalysts after calcination. ^b Calculated on the basis of H₂ consumption in TPR (**Fig. 2.2**) by assuming NiO + H₂ → Ni⁰ + H₂O from 293 to 1073 K. ^c Calculated by the following equation: Ni⁰_{surface}/Ni⁰_{total} ratio = 9.71/(Ni particle size/nm × 10) × reduction degree. ^d Metal peaks were not observed because of the low loading amount. n.d.: no data. Reduction conditions before particle size determination: 50%/50% H₂/N₂, 1073 K, 0.5 h (Ni/Mg/Al) and 100% H₂, 773 K, 0.5 h (Ni/ α -Al₂O₃)

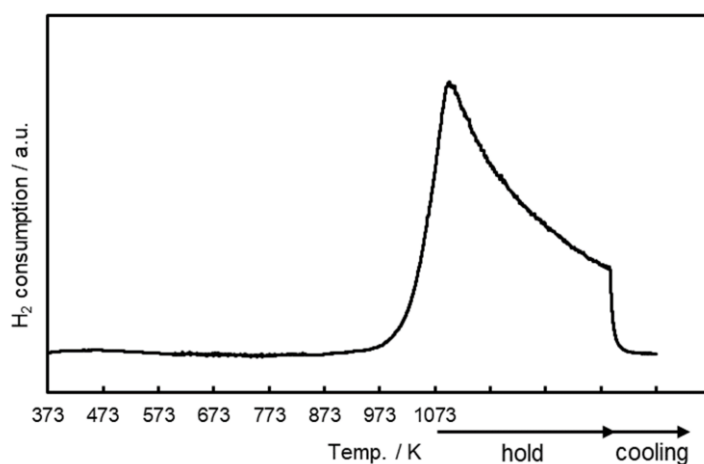


Figure 2.2 TPR profile of Ni/Mg/Al.

Measurement conditions: 5% H₂/Ar, 30 ml min⁻¹; room temperature to 1073 K at a rate of 10 K min⁻¹, then the temperature was maintained at 1073 K for 30 min; sample, 50 mg.

The Ni/ α -Al₂O₃ catalyst was prepared on the basis of our previous reports [45, 46]. The α -Al₂O₃ support was prepared by the calcination of α -Al₂O₃ (Sumitomo Chemical, KHO-24) in air at 1423 K for 3 h. The BET surface area of the α -Al₂O₃ support was 12.1 m² g⁻¹. The support before impregnation was crushed and sieved to granule size between 30 and 60 mesh size. Ni/ α -Al₂O₃ catalyst (Ni 12 wt%) was prepared by an impregnation method using Ni(NO₃)₂ aq. The resulting catalyst was dried in an oven at 383 K for 12 h. Subsequently, the sample was calcined at 773 K for 3 h. The Ni⁰_{surface}/Ni_{total} ratio determined from the crystallite size (XRD; 14.1 nm) and the reduction degree (TPR; 1.0) was 0.069 (**Table 2.1**). In comparison with the Ni/ α -Al₂O₃ catalyst in our previous paper [47], the catalyst in this study had slightly higher dispersion (0.069; in previous study: 0.038). The difference is probably due to the larger surface area of α -Al₂O₃ support in this study (12 m² g⁻¹) than in previous study (8 m² g⁻¹).

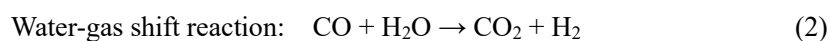
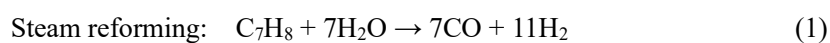
The CeO₂ support was prepared by the calcination of commercial ceria (Daiichi Kigenso, HS) in air at 873 K for 3 h. The BET surface area of the calcined support was 87 m² g⁻¹. Rh/CeO₂ catalyst (Rh 1 or 0.1 wt%) was prepared by an impregnation method using Rh(NO₃)₃ aq. The resulting powder was dried in an oven at 383 K for 12 h and then calcined at 773 K for 3 h. The granule size was controlled to 30-60 mesh by pressing, crushing and sieving after calcination. The dispersion of Rh in Rh/CeO₂ catalyst (Rh 1 and 0.1 wt%) determined by H₂ adsorption at 183 K was 1.0 and 0.85, respectively (**Table 2.1**).

2.2.2. Catalyst characterization

X-ray diffraction (XRD) patterns were recorded with Rigaku MiniFlex600 diffractometer with Cu K α ($\lambda=0.15418$ nm) radiation at 45 kV and 40 mA. The average size of Ni metal particles in the catalyst was calculated on the basis of width of the $d(200)$ spacing in XRD and the Scherrer equation. Transmission electron microscope (TEM) images were obtained on a Hitachi HD-2700 instrument. The samples after reduction or reaction were dispersed in ethanol under supersonic waves and the mixture was dropped on Cu grids. Average particle size was calculated by $\sum n_i d_i^3 / \sum n_i d_i^2$ (d_i : particle size; n_i : number of particles with d_i). H₂-TPR was carried out with home-made apparatus equipped with quartz tube reactor and TCD. The sample was reduced with 5% H₂ in Ar from room temperature to 1073 K at a heating rate of 10 K min⁻¹. The reduction degree of Ni/Mg/Al and Ni/ α -Al₂O₃ was determined on the basis of H₂ consumption in H₂-TPR by assuming NiO + H₂ \rightarrow Ni + H₂O.

2.2.3. Activity test of reforming of toluene

Reforming of toluene (WAKO Pure Chemical Industries, Ltd., 99.5 %) as a model compound of gasoline was carried out using a 6 mm i.d. fixed-bed reactor made of quartz. For the temperature control of the catalyst bed, the thermocouple, covered with thin glass tube, was inserted into the outlet of the catalyst bed. About 100 mg catalyst was used for the activity test and the height of the catalyst bed was about 10 mm. Before the activity test, the reduction pretreatment of the catalysts was carried out in the catalyst bed. The mixture gas of 30 ml min⁻¹ H₂ and 30 ml min⁻¹ N₂ was fed to the catalyst bed at 1073 K for 0.5 h. The reduction pretreatment can transform Ni²⁺ species in Mg (Ni, Al) O particles to well-dispersed Ni particles [39]. Ni/ α -Al₂O₃ catalyst was reduced in flowing H₂ (60 ml min⁻¹) at 773 K for 0.5 h and Rh/CeO₂ catalyst was reduced in flowing H₂ and N₂ mixture (H₂/N₂ = 15 ml min⁻¹/15 ml min⁻¹) at 573 K for 1 h [48] in the reactor. After the catalyst pretreatment, the reactor was purged with N₂, and the reactant liquids (such as toluene and H₂O) were supplied by syringe pumps through a heating chamber at 523 K. In the heating chamber toluene and H₂O were vaporized and they were swept out by carrier gas (N₂ mixed with CO₂) to the catalyst bed. The standard feed ratio (molar ratio) of reactants and carrier gas was toluene/H₂O/N₂/CO₂ = 1/11.8/71.2/11.8 (the ratio of steam to carbon in hydrocarbon reactant (S/C_{HC}) = 1.7), corresponding to the contact time $W/F = 0.19$ g_{cat} h mol⁻¹. Here, F represents the total flow rate of the hydrocarbon gas (6 mmol h⁻¹), steam (65 mmol h⁻¹), CO₂ (64 mmol h⁻¹) and N₂ (382 mmol h⁻¹) carrier and W is the catalyst weight. The H₂O/N₂/CO₂ ratio corresponds to the exhaust gas of stoichiometric combustion of (CH₂)_n molecule in air, which was defined as the model EGR gas. The standard reaction temperature was 773 K, which was clearly lower than the case of usual studies on steam reforming of toluene [31]. The effluent gas sampling was carried out using a heated syringe and the analysis of the collected gas was conducted by using gas chromatograph (GC). The concentration of CO, CO₂ and CH₄ was determined by FID-GC (Gaskuropack 54) equipped with a methanator. The concentration of H₂ was determined by TCD-GC (MS-13X), and that of toluene and benzene was measured by FID-GC (DB-1). A bubble flow meter was used for the measurement of the flow rate of the non-condensable effluent gas. The main reaction schemes are shown below (Eqs. 1- 3).



Toluene conversion and carbon balance were calculated by the following equations.

$$\text{Toluene conversion (\%)}: \left(1 - \left(\frac{\text{unreacted toluene} \times 7}{\text{fed toluene} \times 7} \right) \right) \times 100 \quad (4)$$

$$\text{Carbon balance (\%)}: \left(\frac{\text{unreacted toluene} \times 7 + \text{CO} + \text{CH}_4 + \text{CO}_2 + \text{C}_6\text{H}_6 \times 6}{\text{fed toluene} \times 7 + \text{fed CO}_2} \right) \times 100 \quad (5)$$

The experimental error of the carbon balance was within 10% ($100 \pm 10\%$), which can be derived from the fluctuations of CO_2 and toluene feeds and sampling error with a heated syringe.

CO_2 formation amount or rate was calculated by subtraction of fed CO_2 from the detected CO_2 . In all the experiments, thermogravimetric (TG-DTA) analysis was used for the determination of the deposited coke (carbon) as described below. The amount of the deposited carbon was at most $< 0.93\%$, which was clearly smaller than the formation amount of $\text{CO} + \text{CO}_2 + \text{CH}_4$ (+ benzene). Therefore, the author neglected the contribution of carbon formation in the calculation of selectivity and carbon balance.

The amount of coke deposition was measured by TG-DTA with Rigaku Thermo Plus EVO-II instrument. The amount of carbon was determined separately on the samples at three different positions (inlet, middle and outlet) in the catalyst bed [49]. TG-DTA data were obtained in the air atmosphere from room temperature to 1173 K at the heating rate of 10 K min^{-1} , and 10 mg of sample was used by each TG-DTA analysis. The exothermic weight loss around 600-900 K (on example was shown in **Fig. 2.3**) was assigned to the combustion of coke (carbon) [50]. The weight increase before the combustion of coke was assigned to the oxidation of Ni metal to NiO.

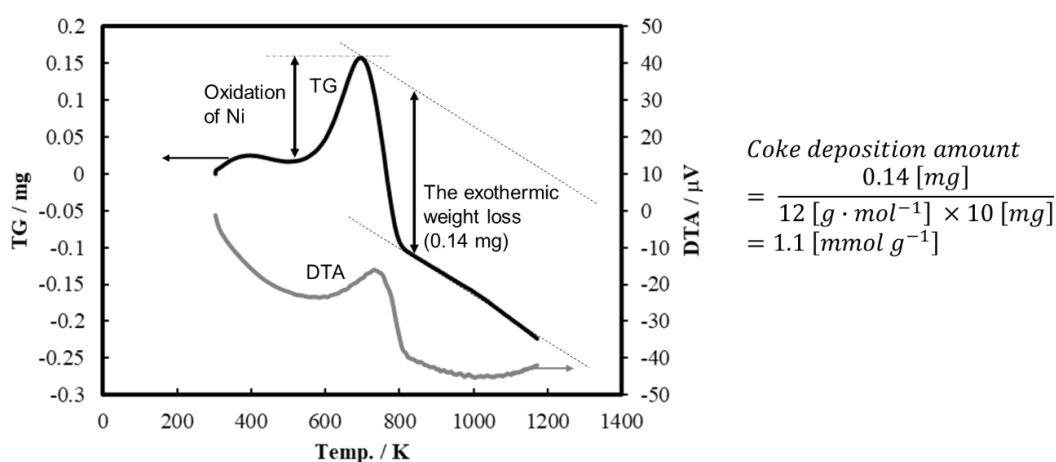


Figure 2.3 TG-DTA profile of Ni/ α - Al_2O_3 catalyst after reaction (**Table 2.2** and **Fig. 2.4**)
Conditions: Air; room temperature to 1173 K at the heating rate of 10 K min^{-1} ; sample, 10 mg.

2.3. Results and discussion

2.3.1. Catalytic performance in the reforming of toluene with model EGR gas

Ni/ α -Al₂O₃, Ni/Mg/Al and Rh/CeO₂ catalysts were tested for the reforming of toluene with model EGR gas (in the presence of CO₂; low partial pressure of steam). Conversion and formation rates of products at 773 K as a function of time on stream are shown in **Fig. 2.4** and **Table 2.2**. The activity of Ni/ α -Al₂O₃, which is a typical Ni catalyst for steam reforming, rapidly decreased during the first 30 min and became almost constant at longer reaction time. In the case of Ni/Mg/Al catalyst (**Fig. 2.4 (b)-(d)**), the activity gradually decreased during 60 ~ 180 min (depending on the *W/F* conditions) and became almost constant. In the case of Rh/CeO₂ catalysts (**Fig. 2.4 (e) and (f)**) the performance very slowly decreased during the first 180 min. The reaction results are also summarized in **Table 2.2**. The amount of coke after the 5 h reaction was measured at three different positions of the catalyst bed (inlet, middle and outlet) and the data are also listed in **Table 2.2**. The coke deposited at the inlet of the catalyst bed was mainly derived from substrate (toluene) decomposition, while that at the outlet of the catalyst bed was derived from CO disproportionation, especially when the conversion was high [41]. It is difficult to compare the initial activities of Ni/ α -Al₂O₃ and Ni/Mg/Al catalysts only from these data since the catalysts, especially Ni/ α -Al₂O₃, deactivated quickly. The toluene conversion of Ni/Mg/Al was higher than that of Ni/ α -Al₂O₃ (**Fig. 2.4 (a) and (d)**, **Table 2.2, Entries 1 and 4**) after 20 min time on stream. Ni/ α -Al₂O₃ catalyst was deactivated more quickly and more severely to steady state than Ni/Mg/Al. The steady state activity of Ni/Mg/Al was higher than that of Ni/ α -Al₂O₃. The difference of toluene conversion at the steady state between the catalysts was larger than the difference of Ni⁰_{surface}/Ni_{total} ratio (Ni/Mg/Al: 0.069; Ni/ α -Al₂O₃: 0.069), indicating that the toluene conversion at steady state based on surface Ni site in Ni/Mg/Al can be higher than Ni/ α -Al₂O₃. The higher activity at the steady state of Ni/Mg/Al than that of Ni/ α -Al₂O₃ was also reported in the simple steam reforming of toluene without CO₂ addition at 873 K [40]. The amount of coke deposited on Ni/Mg/Al was slightly smaller than that on Ni/ α -Al₂O₃. Considering the higher activity at the steady state of Ni/Mg/Al, the coke yield based on converted toluene was significantly lower on Ni/Mg/Al than that on Ni/ α -Al₂O₃. Therefore, Ni/Mg/Al is a superior catalyst to Ni/ α -Al₂O₃ in terms of steady state activity (both total Ni-based and surface Ni-based) and coke deposition resistance.

In the case of Ni/ α -Al₂O₃, there was large loss of carbon balance in the initial stage. The loss might be due to the

coke formation. The rapid coke formation can be related to the rapid deactivation of Ni/ α -Al₂O₃. The coke amount at the inlet of catalyst bed of Ni/ α -Al₂O₃ was relatively small (1.1 mmol g⁻¹). This amount was not so much larger than the surface Ni⁰ amount (0.2 mmol g⁻¹). It is interpreted that the coke produced by toluene decomposition effectively covers the surface of Ni.

The results at different W/F values over Ni/Mg/Al are shown in **Table 2.2, Entries 2-4**. The initial conversion at $W/F = 0.19 \text{ g}_{\text{cat}} \text{ h mol}^{-1}$ was almost twice of that at $W/F = 0.09 \text{ g}_{\text{cat}} \text{ h mol}^{-1}$, indicating that the conversion is proportional to the contact time (W/F). However, at the steady state the conversion was lower than the proportional level to higher W/F , indicating that the catalyst deactivated more severely at larger W/F . The coke amount at the inlet of catalyst bed was similar (0.04 g_{coke} g_{cat}⁻¹) between $W/F = 0.09 - 0.39 \text{ g}_{\text{cat}} \text{ h mol}^{-1}$. This suggests that the catalyst at the inlet can be similarly deactivated regardless of W/F values. On the other hand, the coke amount became larger at higher W/F , at the outlet of the catalyst bed. The coke formation at higher conversion level (high CO partial pressure) can decrease the activity of the catalyst in the downstream positions of the catalyst bed. It seems to be difficult to obtain high conversion of toluene with this toluene concentration in the feed over Ni catalysts.

Reforming of toluene with simulated automobile exhaust gas over hydrotalcite-like-compound-derived Ni catalyst

Table 2.2 Summary of performance of Ni and Rh catalysts in reforming of toluene with simulated exhaust gas (**Fig. 2.4**)

Entry	Catalyst	Loading		Toluene conv.	Formation rate [mmol h ⁻¹ g _{cat} ⁻¹]					H ₂ /CO ratio	Carbon balance	Amount of coke deposition ^c [g _{coke} g _{cat} ⁻¹]		
		amount of Ni or Rh	W/F											
		[wt%]	[g _{cat} h mol ⁻¹]		[%]	H ₂	CH ₄	CO	CO ₂			C ₆ H ₆	[-]	[%]
1	Ni/ α -Al ₂ O ₃	12	0.39	65 ^a	155	3	43	0	0	3.8	84	0.01	0.15	0.16
				26 ^b	92	0	21	-16	0	4.4	91			
2	Ni/Mg/Al	12	0.09	39 ^a	452	2	123	115	2	3.7	97	0.04	0.04	0.05
				24 ^b	284	0	61	95	1	4.7	99			
3	Ni/Mg/Al	12	0.19	84 ^a	450	37	170	84	1	2.6	97	0.04	0.05	0.06
				34 ^b	304	0	81	85	2	3.7	104			
4	Ni/Mg/Al	12	0.39	>99 ^a	242	44	108	44	0	2.2	101	0.04	0.08	0.14
				56 ^b	225	1	71	20	1	3.2	98			
5	Rh/CeO ₂	1	0.19	97 ^a	476	5	147	121	25	3.2	105	0.00	0.00	0.00
				92 ^b	430	2	118	91	29	3.6	103			
6	Rh/CeO ₂	0.1	0.19	65 ^a	247	0	69	47	20	3.6	98	0.00	0.00	0.00
				54 ^b	217	0	59	-7	17	3.7	95			

Reaction conditions: $W_{\text{cat}} = 100$ mg; $S/C_{\text{HC}} = 1.7$ (toluene/H₂O/N₂/CO₂ = 1.0/11.8/71.2/11.8 (molar ratio)), reaction temperature, 773 K; reaction time, 5 h. Feeding rate of Entries 1 and 4: toluene 3 mmol h⁻¹, steam 33 mmol h⁻¹, N₂ 197 mmol h⁻¹, CO₂ 33 mmol h⁻¹. Feeding rate of Entry 2: toluene 11 mmol h⁻¹, steam 131 mmol h⁻¹, N₂ 766 mmol h⁻¹, CO₂ 127 mmol h⁻¹. Feeding rate of Entries 3, 5 and 6: toluene 6 mmol h⁻¹, steam 65 mmol h⁻¹, N₂ 382 mmol h⁻¹, CO₂ 64 mmol h⁻¹. ^a Initial: at 10-30 min, ^b Steady state: at 280-300 min, ^c After 5 h.

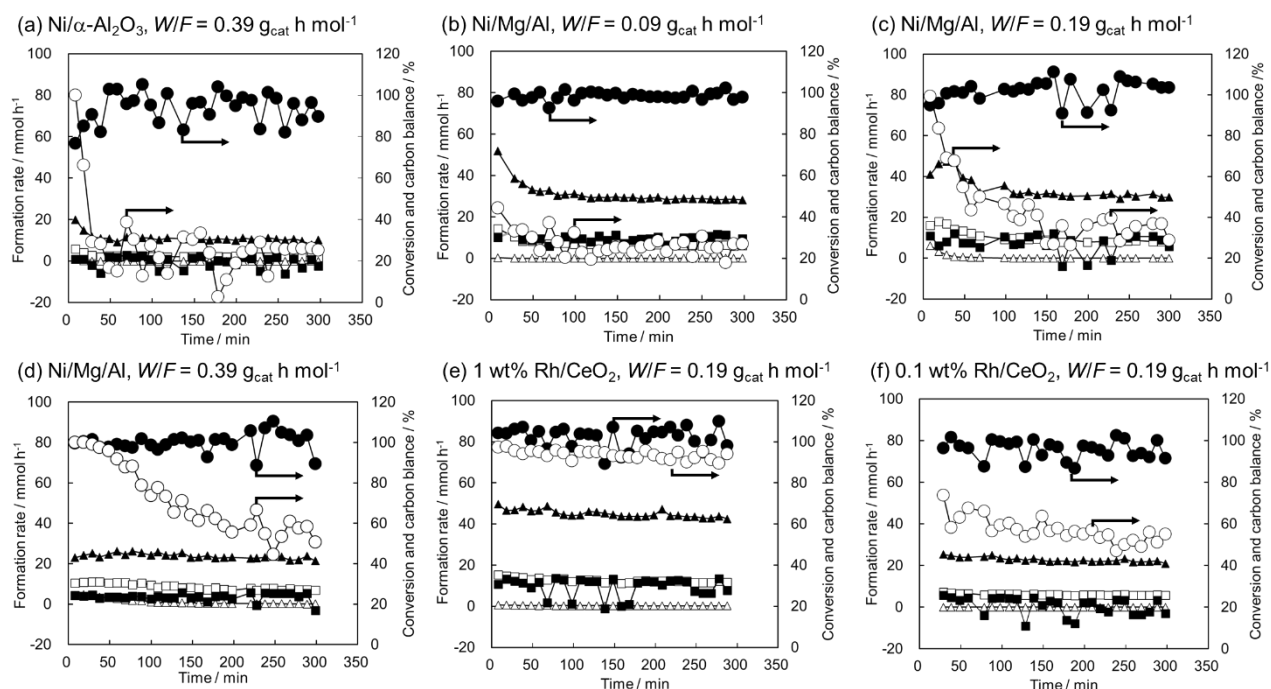


Figure 2.4 Reforming of toluene over (a) Ni/ α -Al₂O₃, (b-d) Ni/Mg/Al, (e) Rh/CeO₂ (1 wt%Rh) and (f) Rh/CeO₂ (0.1 wt%Rh) catalysts. \circ : toluene conversion, \bullet : carbon balance \blacktriangle : H₂, \triangle : CH₄, \square : CO, \blacksquare : CO₂. Reaction conditions: S/C_{H_C} = 1.7 (Toluene/H₂O/N₂/CO₂ = 1.0/11.8/71.2/11.8 (molar ratio)); W_{cat} = 100 mg; reaction temperature, 773 K; reaction time, 5 h. (a and d) W/F = 0.39 g h mol⁻¹; feeding rate: toluene 3 mmol h⁻¹, steam 33 mmol h⁻¹, N₂ 197 mmol h⁻¹, CO₂ 33 mmol h⁻¹. (b) W/F = 0.09 g h mol⁻¹; feeding rate: toluene 11 mmol h⁻¹, steam 131 mmol h⁻¹, N₂ 766 mmol h⁻¹, CO₂ 127 mmol h⁻¹. (c, e and f) W/F = 0.19 g h mol⁻¹; feeding rate: toluene 6 mmol h⁻¹, steam 65 mmol h⁻¹, N₂ 382 mmol h⁻¹, CO₂ 64 mmol h⁻¹.

The results over Rh/CeO₂ catalysts with two different Rh loading amount are shown in **Table 2.2, Entries 5 and 6**. The dispersion of Rh was almost 1 for both catalysts. The initial toluene conversion over 0.1 wt% Rh/CeO₂ and 1 wt% Rh/CeO₂ at W/F = 0.19 g_{cat} h mol⁻¹ was 65% and 97%, respectively, and that over Ni/Mg/Al (12 wt% Ni) (84%) fell between those values (**Table 2.2, Entry 3**). These data indicate that Rh/CeO₂ catalyst had 101 ~ 102 fold higher activity than Ni/Mg/Al based on active metal weight. At the steady state the conversion level at W/F = 0.19 g_{cat} h mol⁻¹ over 0.1 wt% Rh/CeO₂ was similar to that at W/F = 0.39 g_{cat} h mol⁻¹ over Ni/Mg/Al. The difference became ca. 200 fold based on toluene conversion per weight of active metal. On the other hand, the price of Rh (3×10^2 US\$ g⁻¹)^[51] is more than 3×10^4 times of Ni (0.01 US\$ g⁻¹)^[52]. The turnover frequency (TOF) based on initial toluene conversion and number of surface metal atoms of 0.1 wt% Rh/CeO₂ and 1 wt% Rh/CeO₂ at W/F = 0.19 g_{cat} h mol⁻¹ was 5.5×10^2 h⁻¹ and 1.9×10^3 h⁻¹, respectively, and that of Ni/Mg/Al (12 wt% Ni) was 1.3×10^2 h⁻¹. Therefore,

the activity of Ni is still attractive. However, the resistance to coke of Ni catalysts was much inferior to Rh catalysts where the detected coke amount was negligible at all positions of the catalyst bed. The coke deposition resistance of Ni/Mg/Al catalyst should be improved especially at high conversion level and high toluene partial pressure.

2.3.2. Effect of toluene feeding ratio to EGR gas

In the Reformed EGR system, the composition in EGR gas is unchangeable while the fuel feeding amount is variable. Here, the effect of toluene amount in the feed of the Reformed EGR system over Ni/Mg/Al catalyst was investigated. **Table 2.3** shows the summary of results, and the detailed results during the time on stream are shown in **Fig. 2.5** The initial conversion of toluene reached almost 100% at low toluene feed (toluene/H₂O/N₂/CO₂ = 0.5/11.8/71.2/11.8, 0.8/11.8/71.2/11.8). The initial conversion decreased at higher toluene feed. On the other hand, the initial H₂ formation rate became larger with increase of toluene feed up to toluene/H₂O/N₂/CO₂ = 1/11.8/71.2/11.8, which can be explained simply by larger supply of toluene, however, it did not increase or even decreased when toluene feed further increased. The low H₂ formation rate at too high toluene feed can be explained by very rapid deactivation even in the initial stage as shown by the small difference of initial and steady-state formation rates at higher toluene feed. At very low toluene feed (toluene/H₂O/N₂/CO₂ = 0.5/11.8/71.2/11.8), the deactivation was clearly less significant than other cases. In fact, the largest steady state H₂ formation rate was observed at this low toluene feed condition. The steady state conversion as well as H₂ formation rate tends to decrease with increasing molar ratio of toluene.

The amount of coke deposited on these catalysts was measured after 1 h and 5 h reactions. The amount of deposited coke at 1 h reaction was about 1/3-1/2 times of that at 5 h reaction, indicating that coke continued to be formed after initial deactivation. In addition, for all positions and for both reaction times, the amount of deposited coke increased with increase of molar ratio of toluene.

Table 2.3 Effect of toluene feed amount on the reforming of toluene with model EGR gas over Ni/Mg/Al catalyst (details: Fig. 2.5)

Entry	Feed ratio [-]				Toluene conv. [%]	Formation rate [mmol h ⁻¹ g _{cat} ⁻¹]					H ₂ /CO ratio [-]	Carbon balance [%]	Amount of coke deposition ^c [g _{coke} g _{cat} ⁻¹]		
	Toluene	H ₂ O	N ₂	CO ₂		H ₂	CH ₄	CO	CO ₂	C ₆ H ₆			Inlet	Middle	Outlet
1	0.5	11.8	71.2	11.8	>99	286	8	82	66	0	3.6	95	0.01	0.01	0.01
					94	361	12	107	114	0	3.4	106	0.02	0.02	0.02
2	0.8	11.8	71.2	11.8	98	416	45	153	101	0	2.7	99	0.01	0.01	0.02
					52	314	0	74	1	0	4.2	92	0.03	0.04	0.04
3	1	11.8	71.2	11.8	84	450	37	170	84	1	2.6	97	0.01	0.02	0.02
					34	304	0	81	85	2	3.7	104	0.04	0.05	0.06
4	1.2	11.8	71.2	11.8	63	435	11	156	76	2	2.8	96	0.02	0.03	0.04
					27	269	0	75	72	1	3.6	103	0.04	0.06	0.07
5	1.5	11.8	71.2	11.8	55	447	5	148	69	2	3.1	93	0.03	0.04	0.04
					20	286	0	79	86	2	3.6	105	0.04	0.06	0.06
6	2	11.8	71.2	11.8	30	268	0	92	52	2	3.0	95	0.04	0.06	0.06
					22	244	0	64	56	2	3.8	97	0.07	0.09	0.09

Reaction conditions: Ni/Mg/Al (12 wt% Ni) catalyst; $W_{\text{cat}} = 100$ mg (Entry 4: 126 mg); feeding rate: toluene 3-11 mmol h⁻¹, steam 65 mmol h⁻¹ (Entry 4: 82 mmol h⁻¹), N₂ 382 mmol h⁻¹ (Entry 4: 480 mmol h⁻¹), CO₂ 64 mmol h⁻¹ (Entry 4: 79 mmol h⁻¹); S/C_{H_C} = 0.8-3.4; $W/F = 0.19$ g_{cat} h mol⁻¹; reaction temperature, 773 K; reaction time, 5 h. ^a Initial: at 10-30 min, ^b Steady state: at 280-300 min, ^c Upper: after 1 h; lower: after 5 h.

Reforming of toluene with simulated automobile exhaust gas over hydrotalcite-like-compound-derived Ni catalyst

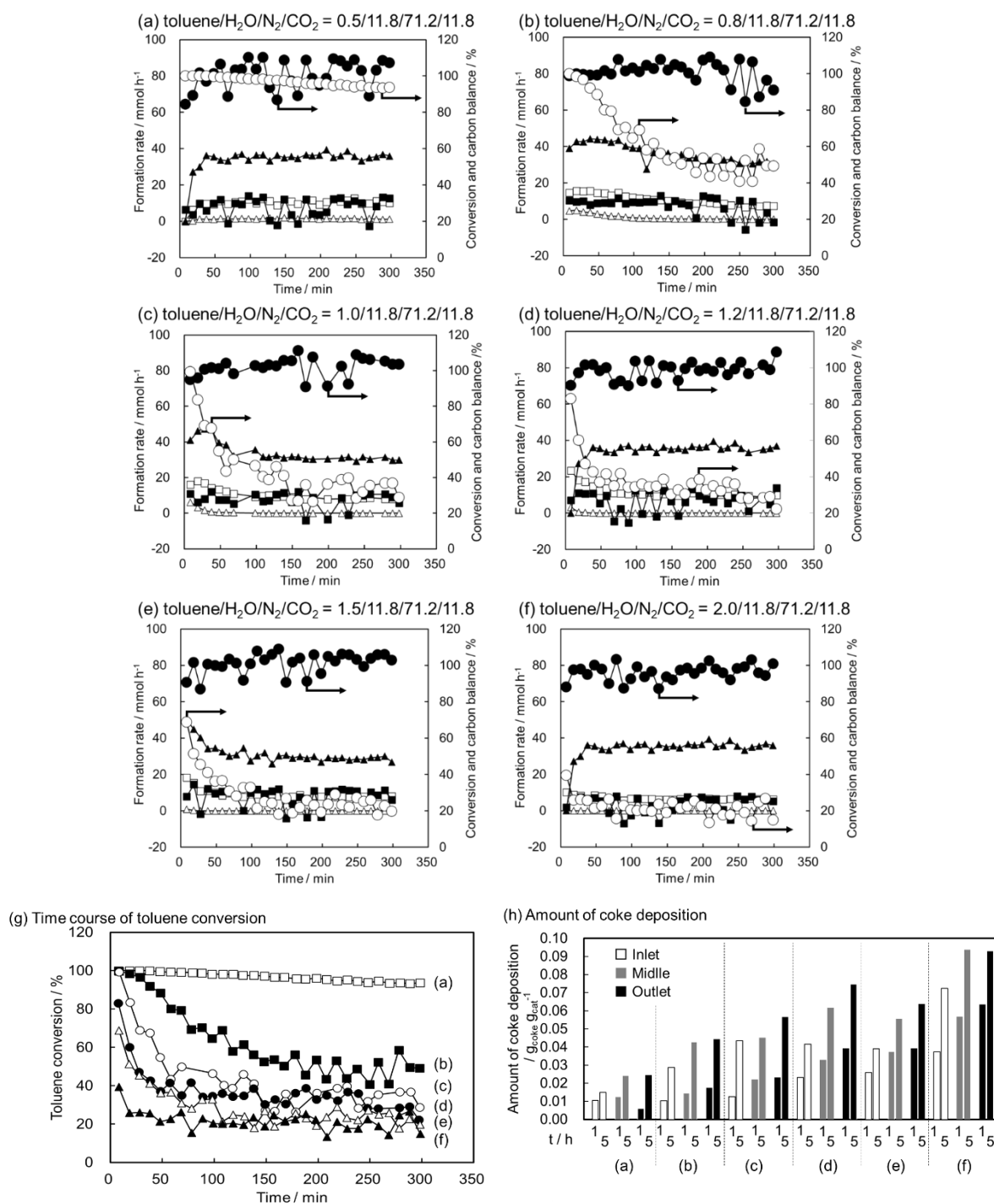


Figure 2.5 Time dependence of reforming of toluene over Ni/Mg/Al catalyst at (a) toluene/H₂O/N₂/CO₂ = 0.5/11.8/71.2/11.8, (b) toluene/H₂O/N₂/CO₂ = 0.8/11.8/71.2/11.8, (c) toluene/H₂O/N₂/CO₂ = 1.0/11.8/71.2/11.8, (d) toluene/H₂O/N₂/CO₂ = 1.2/11.8/71.2/11.8, (e) toluene/H₂O/N₂/CO₂ = 1.5/11.8/71.2/11.8, (f) toluene/H₂O/N₂/CO₂ = 2.0/11.8/71.2/11.8 (molar ratio). ○: toluene conversion, ●: carbon balance, ▲: H₂, △: CH₄, □: CO, ■: CO₂. Reaction conditions: Feeding rate: toluene, 3-11 mmol h⁻¹; steam, 65 mmol h⁻¹; N₂, 382 mmol h⁻¹; CO₂, 64 mmol h⁻¹. S/C_{HC} = 0.8-1.7. \bar{W}_{cat} = 100 mg ((d): 126 mg); W/F = 0.19 g h mol⁻¹; reaction temperature, 773 K.

2.3.3. Effect of reaction temperature

The temperature of the EGR gas is typically 573 – 773 K^[8], which is clearly lower than that of the simple reforming of hydrocarbons for the hydrogen or syngas production (873-1273 K). Here, the effect of reaction temperature with Ni/Mg/Al catalyst was investigated at 873 and 773 K. **Table 2.4** shows the summary of results, and the detailed results during the time of stream are shown in **Fig. 2.6**. The toluene conversion at 773 K decreased to 38% from 84% during the first 150 min. In contrast, the toluene conversion at 873 K was kept very high (>99%) during the first 300 min.

The amount of coke after the 5 h reaction was measured at three different positions of the catalyst bed (inlet, middle and outlet) and the data are also shown in **Table 2.4**. As described in Section 2.3.1, for 773 K the coke amount at the outlet of catalyst bed was larger than that at other positions, suggesting that CO disproportionation was a major route of coke formation. In contrast, for 873 K the coke amount at the inlet of catalyst bed was larger than that at the other positions, suggesting that toluene decomposition was a major route of coke formation. The major route of coke formation seems to be changed by reaction temperatures. However, the total amount of coke deposition was hardly changed between these temperatures.

Table 2.4 Reaction temperature dependence in the reforming of toluene with EGR gas over Ni/Mg/Al (details: **Fig. 2.6**)

Entry	Reaction temp. [K]	Toluene conv. [%]	Formation rate [mmol h ⁻¹ g _{cat} ⁻¹]					H ₂ /CO ratio [-]	Carbon balance [%]	Amount of coke deposition ^c [g _{coke} g _{cat} ⁻¹]		
			H ₂	CH ₄	CO	CO ₂	C ₆ H ₆			Inlet	Middle	Outlet
			1	773	84 ^a	450	37			170	84	1
		34 ^b	304	0	81	85	2	3.7	104	0.04	0.05	0.06
2	873	>99 ^a	531	10	353	-1	0	1.5	98			
		>99 ^b	559	15	404	15	0	1.4	105	0.07	0.05	0.04

Reaction conditions: $W_{\text{cat}} = 100$ mg; feeding rate: toluene 6 mmol h⁻¹, steam 65 mmol h⁻¹, N₂ 382 mmol h⁻¹, CO₂ 64 mmol h⁻¹. S/C_{HC} = 1.7. $W/F = 0.19$ g_{cat} h mol⁻¹; reaction time, 5 h. ^a Initial: at 10-30 min, ^b Steady state: at 280-300 min, ^c After 5 h.

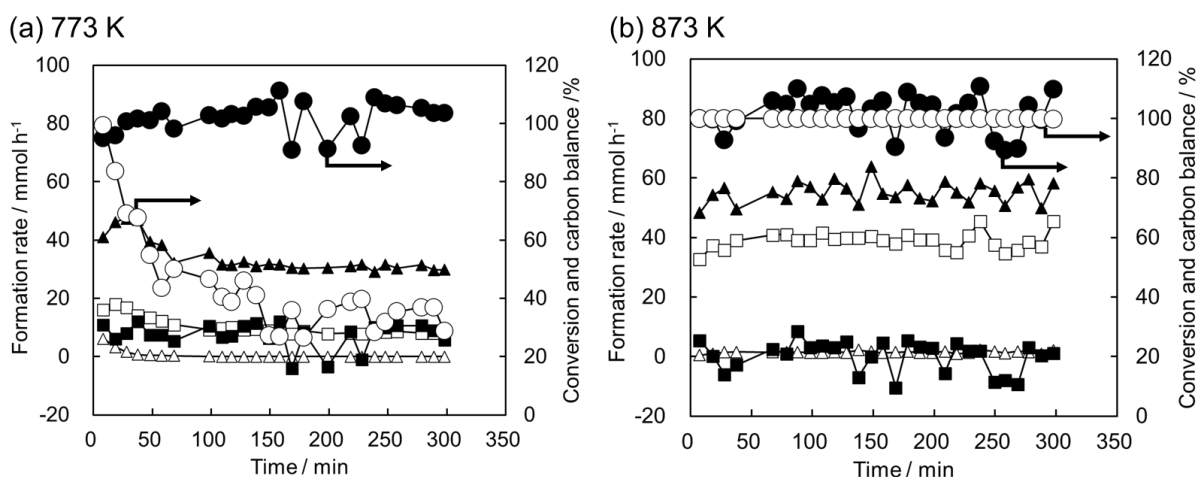


Figure 2.6 Reaction temperature dependence in the reforming of toluene with model EGR gas reformer on reforming of toluene over Ni/Mg/Al catalyst at (a) 773 K and (b) 873 K. ○: toluene conversion, ●: carbon balance, ▲: H₂, △: CH₄, □: CO, ■: CO₂. Reaction conditions: Feeding rate: toluene, 6 mmol h⁻¹; steam, 65 mmol h⁻¹; N₂, 382 mmol h⁻¹; CO₂, 64 mmol h⁻¹. S/C_{HC} = 1.7 (Toluene/H₂O/N₂/CO₂ = 1.0/11.8/71.2/11.8 (molar ratio)). W_{cat} = 100 mg; W/F = 0.19 g h mol⁻¹.

2.3.4. Characterization of used catalysts and regeneration of Ni/Mg/Al

Figure 2.7 shows the TEM images of Ni/ α -Al₂O₃ and Ni/Mg/Al after H₂ reduction at 1073 K or after reaction for 5 h at 773 K (activity tests in Fig. 2.4 and Table 2.2). The Ni particle size was not largely changed during the reaction for both catalysts except Ni/Mg/Al at the outlet position of the catalyst bed. Severe deposition of whisker carbon was observed on the surface of Ni/ α -Al₂O₃ after reaction at both inlet and outlet positions in the catalyst bed (Figs. 2.7c and e). In the case of Ni/Mg/Al, the formation of whisker carbon was more evident at the outlet of the catalyst bed (Figs. 2.7d and f) than at the inlet. The growth of the whisker carbon generally proceeds via the tip-growth mechanism, where coke deposits within the Ni particle and moves to form long whisker carbon which lifts the Ni particle above the support [23]. This mechanism has been reported to be characteristic to large Ni particles which weakly interact with the support and are prone to coke deposition [53]. The smaller deposited amount of whisker carbon on Ni/Mg/Al can be due to smaller Ni particle size of Ni/Mg/Al than that of Ni/ α -Al₂O₃.

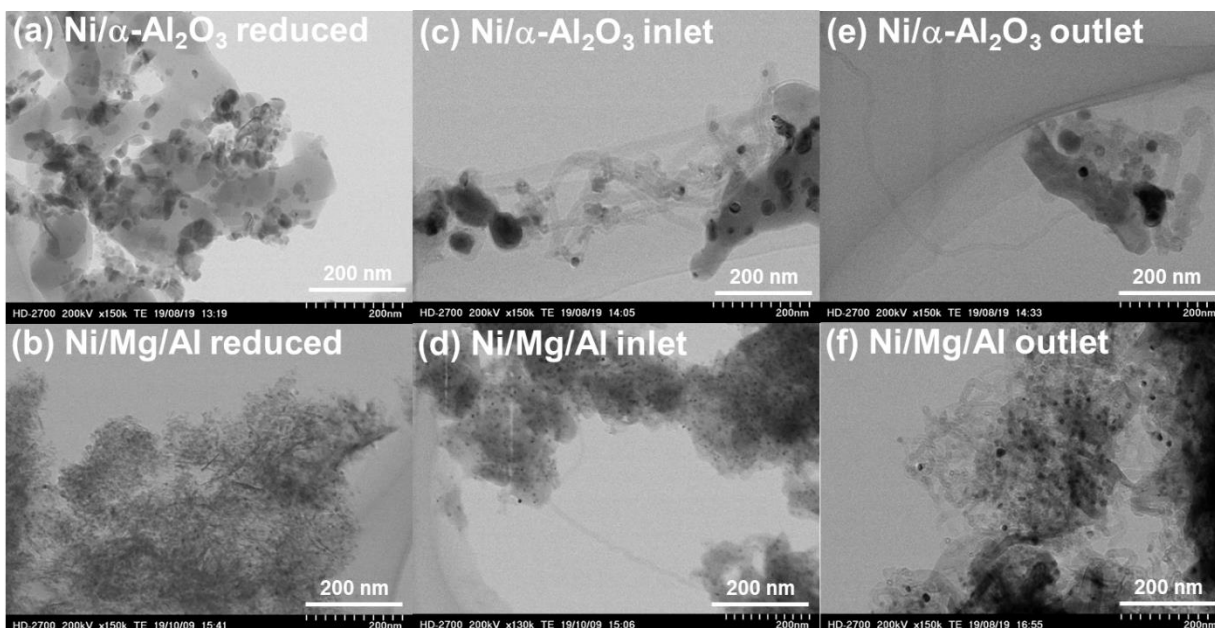


Figure 2.7 TEM images of Ni/ α -Al₂O₃ (a, c, e) and Ni/Mg/Al (b, d, f) catalysts. (a) and (b): after reduction. Reduction conditions: 100% H₂, 773 K, 0.5 h (a) and 50%/50% H₂/N₂, 1073 K, 0.5 h (b). (c) and (d): used catalysts at the inlet of catalyst bed; (e) and (f): used catalysts at the outlet of catalyst bed; reaction conditions were the same to **Table 2.2, Entries 1 and 4**.

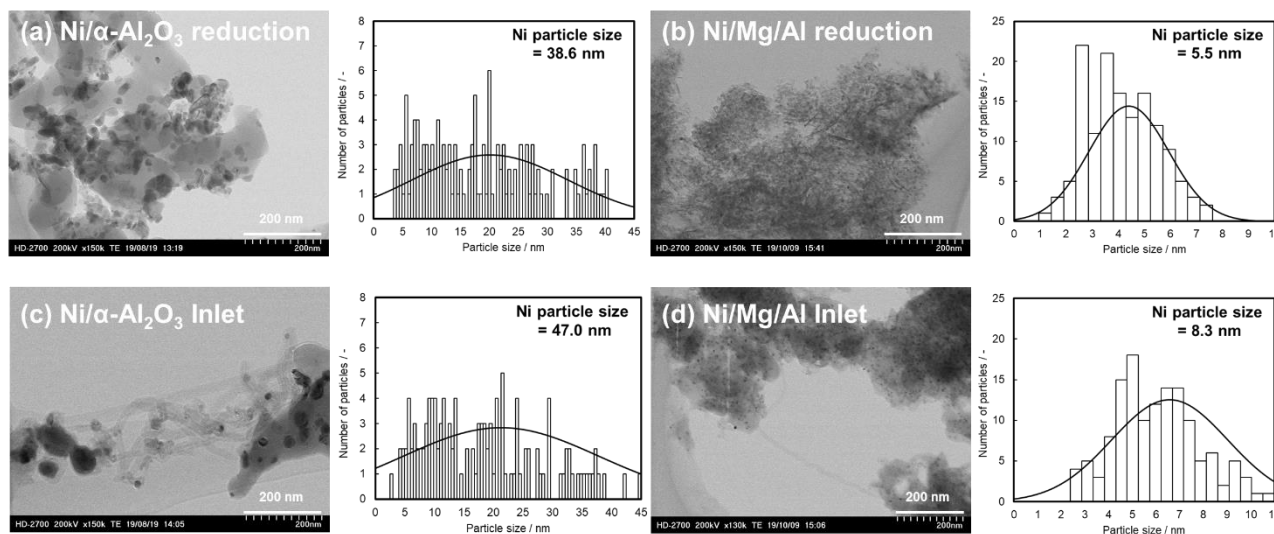


Figure 2.8 TEM images of Ni/ α -Al₂O₃ (a, c) and Ni/Mg/Al (b, d) catalysts. (a) and (b): after reduction. Reduction conditions: 100% H₂, 773 K, 0.5 h (a) and 50%/50% H₂/N₂, 1073 K, 0.5 h (b). (c) and (d): used catalysts at the inlet of catalyst bed; reaction conditions were the same to **Table 2.2, Entries 1 and 4**.

Regeneration of the deactivated Ni/Mg/Al catalyst by combustion of coke was carried out. Here, the reforming of toluene over Ni/Mg/Al under a feed ratio of toluene/H₂O/N₂/CO₂ = 1/11.8/71.2/11.8 (molar ratio) was carried out at 773 K for 1 h and the catalyst was regenerated after each reaction. The procedure for the regeneration was as follows:

the catalyst after each reaction test was oxidized in air (30 ml min⁻¹) flow at 723 K for 1 h for the removal of the deposited carbonaceous species, and then the oxidized catalysts were reduced similarly to the fresh catalyst (H₂/N₂ = 1/1, 1073 K, 0.5 h). **Figure 2.9** shows the results of three cycles of reactions. The oxidation-reduction treatments regenerated the Ni/Mg/Al catalyst almost completely to the level of the fresh one, although the gradual deactivation of the catalyst in the second and third runs was observed. In order to evaluate the effect of the oxidation-reduction treatments on the catalyst structure, fresh Ni/Mg/Al catalyst was subjected to three catalytic runs with two times of regeneration cycles, and the change of the structure was analyzed by XRD (**Fig. 2.10**). The average particle size of Ni metal on Ni/Mg/Al catalyst after the reduction and after the third reaction was almost unchanged (6.4 nm and 5.6 nm, respectively). The peak intensity of Ni metal phase was also unchanged, indicating the same reduction degree. As a result, the deactivation of Ni/Mg/Al was suggested to be caused by the deposited carbon. The stability of hydrotalcite-like-compound-derived nanocomposite catalysts consisting of Ni-based metal particles and MgO-based oxides in the reaction-regeneration cycles has been also reported in steam reforming of biomass tar ^[39], which is explained by the reversible structural change of Ni species between Ni⁰ particles and Ni²⁺ species enriched near the surface of Mg (Ni, Al) O periclase particles.

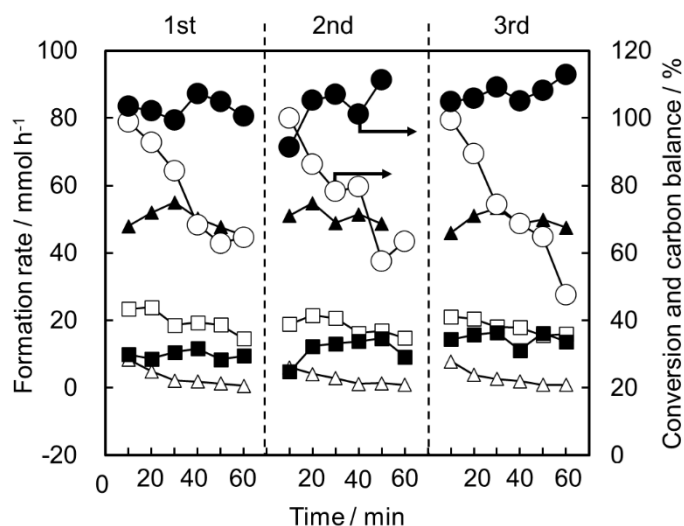


Figure 2.9 Effect of regeneration treatment on the performance of Ni/Mg/Al catalyst. ○: toluene conversion, ●: carbon balance, ▲: H₂, △: CH₄, □: CO, ■: CO₂. Reaction conditions: $W_{cat} = 100$ mg; Feeding rate: toluene 6 mmol h⁻¹, steam 65 mmol h⁻¹, N₂ 382 mmol h⁻¹, CO₂ 64 mmol h⁻¹; S/C_{HC} = 1.7; W/F = 0.19 g h mol⁻¹; reaction temperature, 773 K; reaction time, 1 h. After each reaction, the catalyst was regenerated by treatment in an air gas flow at 723 K for 1 h, followed by reduction in the H₂/N₂ (30 ml min⁻¹/30 ml min⁻¹) gas flow at 1073 K for 0.5 h.

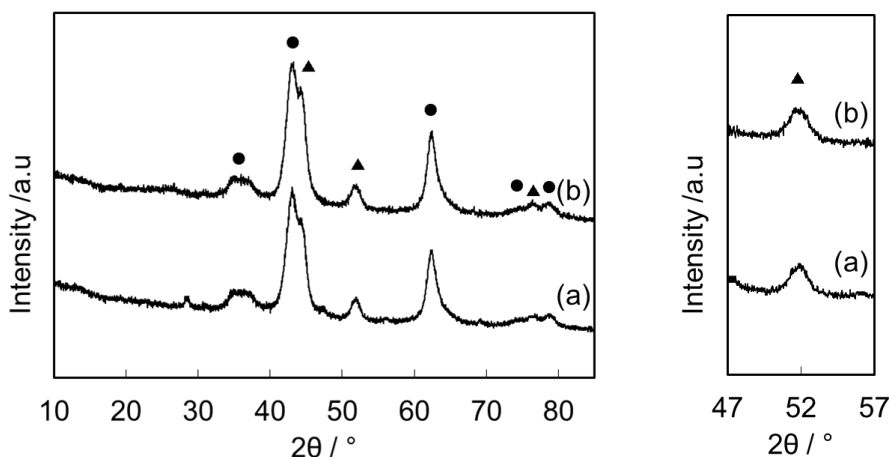


Figure 2.10 XRD patterns of Ni/Mg/Al (a) after reduction and (b) after third reaction in **Fig. 2.9**. Crystalline phases: periclase (●), Ni metal (▲).

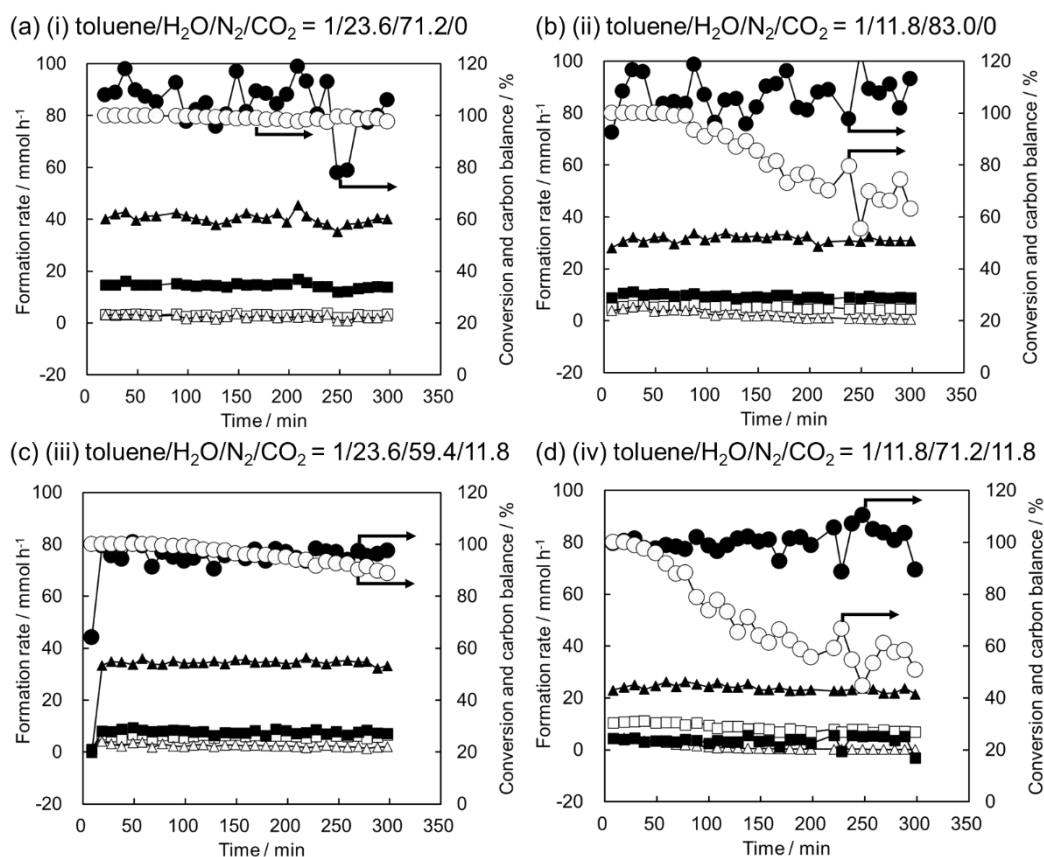
2.3.5. Influence of feed ratio

Here, the performance of Ni/Mg/Al catalyst between EGR condition and simple steam reforming conditions was compared. **Table 2.5** and **Fig. 2.11** shows the results of reforming of toluene under four types of conditions: toluene/H₂O/N₂/CO₂ = (i)1/23.6/71.2/0; (ii)1/11.8/83.0/0; (iii) 1/23.6/59.4/11.8; (iv) 1/11.8/71.2/11.8. The condition (i) is a standard one of simple steam reforming (high partial pressure of steam, without CO₂), and the condition (iv) is reforming with EGR gas (low partial pressure steam, with CO₂). In the condition (i), the toluene conversion was kept 98% even at 300 min. The amount of the deposited coke during the reaction was determined to be 0.02 g_{coke} g_{cat}⁻¹ for all positions of the catalyst bed. In contrast, the toluene conversion of the condition (iv) was decreased from 100% to ca. 54% at 300 min. The amount of the deposited coke of inlet, middle and outlet positions was determined to be 0.04 g_{coke} g_{cat}⁻¹, 0.08 g_{coke} g_{cat}⁻¹, 0.14 g_{coke} g_{cat}⁻¹, respectively. The condition (iv) gave much lower toluene conversion and coke deposition resistance than the condition (i). Differences between these conditions were presence or absence of CO₂ and partial pressure of steam (S/C_{HC} = 1.7 or 3.4). Next, we determined which point (CO₂ or steam) was the major cause of the performance difference.

Table 2.5 Influence of feed ratio on reforming of toluene over Ni/Mg/Al (details: Fig. 2.11)

Entry	Feed ratio [-]				Toluene conv. [%]	Formation rate [mmol h ⁻¹ g _{cat} ⁻¹]					H ₂ /CO ratio [-]	Carbon balance [%]	Amount of coke deposition ^c [g _{coke} g _{cat} ⁻¹]		
	Toluene	H ₂ O	N ₂	CO ₂		H ₂	CH ₄	CO	CO ₂	C ₆ H ₆			Inlet	Middle	Outlet
	(i)	1	23.6	71.2	0.0	>99 ^a 99 ^b	411 400	31 22	32 31	147 140	0 0	12.9 12.9	108 101	0.02	0.02
(ii)	1	11.8	83.0	0.0	>99 ^a 68 ^b	304 309	46 6	56 46	103 90	0 1	5.5 6.7	106 109	0.05	0.09	0.10
(iii)	1	23.6	59.4	11.8	>99 ^a 90 ^b	343 335	37 18	64 59	81 78	0 0	5.4 5.7	98 96	0.01	0.01	0.01
(iv)	1	11.8	71.2	11.8	>99 ^a 56 ^b	242 225	44 1	108 71	44 20	0 1	2.2 3.2	101 98	0.04	0.08	0.14

Reaction conditions: $W_{\text{cat}} = 100$ mg; feeding rate: toluene 6 mmol h⁻¹, steam 33 or 65 mmol h⁻¹, CO₂ 0 or 33 mmol h⁻¹, N₂ 159 or 191 or 223 mmol h⁻¹; S/C_{HC} = 1.7 or 3.4; $W/F = 0.39$ g_{cat} h mol⁻¹; reaction temperature, 773 K; reaction time, 5 h. ^a Initial: at 10-30 min, ^b Steady state: at 280-300 min, ^c After 5 h.



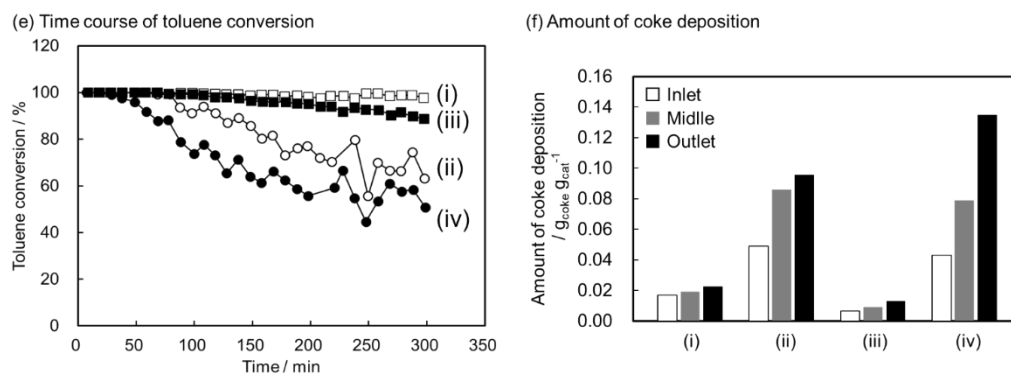


Figure 2.11 Influence of feed ratio in reforming of toluene over Ni/Mg/Al: (a) toluene/H₂O/N₂/CO₂ = 1/23.6/71.2/0, (b) toluene/H₂O/N₂/CO₂ = 1/11.8/83.0/0, (c) toluene/H₂O/N₂/CO₂ = 1/23.6/59.4/11.8, (d) toluene/H₂O/N₂/CO₂ = 1/11.8/71.2/11.8 (molar ratio), (e) toluene conversion and (f) amount of coke deposition over Ni/Mg/Al catalyst. ○: toluene conversion, ●: carbon balance, ▲: H₂, △: CH₄, □: CO, ■: CO₂. □; (i) toluene/H₂O/N₂/CO₂ = 1/23.6/71.2/0, ○: (ii) toluene/H₂O/N₂/CO₂ = 1/11.8/83.0/0, ■; (iii) toluene/H₂O/N₂/CO₂ = 1/23.6/59.4/11.8, ●: (iv) toluene/H₂O/N₂/CO₂ = 1/11.8/71.2/11.8 (molar ratio). Reaction conditions: Feeding rate: toluene 3 mmol h⁻¹, steam 65 or 33 mmol h⁻¹, N₂ 159 or 191 or 223 mmol h⁻¹, CO₂ 0 or 32 mmol h⁻¹, S/C_{H_C} = 1.7 or 3.4; W_{cat} = 100 mg; W/F = 0.39 g_{cat} h mol⁻¹; reaction temperature, 773 K; reaction time, 5 h.

In the condition (iii) (high partial pressure of steam, with CO₂), the toluene conversion was kept > 89% even at 300 min. The amount of the deposited coke in the condition (iii) was determined to be 0.01 g_{coke} g_{cat}⁻¹ for all the positions, and this value was even lower than the case of condition (i). In contrast, the toluene conversion in the condition (ii) (low partial pressure of steam, without CO₂) was decreased to 71% at 300 min. In addition, the amount of the deposited coke was large: 0.05 g_{coke} g_{cat}⁻¹, 0.09 g_{coke} g_{cat}⁻¹ and 0.10 g_{coke} g_{cat}⁻¹, for inlet, middle, and outlet positions, respectively. Therefore, lower partial pressure of steam more decreased toluene conversion and resistance to coke deposition than presence of CO₂.

In the case of higher partial pressure of steam ((i) and (iii)), the presence of CO₂ decreased the amount of coke deposition. In contrast, in the cases of lower partial pressure of steam ((ii) and (iv)), the presence of CO₂ rather increased the amount of coke deposition at the outlet of the catalyst bed, while the coke amount at inlet or middle positions was similar between these two conditions. As described above, coke can be formed via two different routes: substrate decomposition which mainly proceeds at the inlet of catalyst bed and CO disproportionation (2CO → C + CO₂). The presence of CO₂ seems to suppress CO disproportionation at the outlet and to decrease the amount of carbon at the inlet by the gasification of carbon with CO₂ aided by steam.

2.4. Conclusions

1. The reforming of toluene was carried out with model exhaust gas of gasoline engine (model EGR gas) where CO₂ is present and steam partial pressure is lower than simple steam reforming systems. The Ni/Mg/Al catalyst, prepared by the calcination and the subsequent reduction of the hydrotalcite-like precursor containing Ni²⁺, exhibited much higher catalytic activity at steady state and coke deposition resistance than Ni/ α -Al₂O₃ catalyst.
2. The difference of activity at steady state of the reforming in toluene with the model EGR gas between Ni/Mg/Al and Rh/CeO₂ was about 1:200 based on the weight of active metal, while the difference of price is in the order of 1:10⁴. The activity of Ni based on the price of activity was further higher at the initial stage. However, coke deposition was a major problem of Ni/Mg/Al catalyst.
3. The activity and coke deposition resistance decreased with increase of molar ratio of toluene in the reforming of toluene with model EGR gas.
4. The Ni/Mg/Al catalyst can be regenerated by oxidation and reduction treatments for the removal of deposited coke and the reduction of oxidized Ni species, respectively.
5. Lower partial pressure of steam can decrease the toluene conversion and the resistance to coke deposition significantly in the toluene reforming with steam in the presence and absence of CO₂ over Ni/Mg/Al catalyst. In contrast, the addition effect of CO₂ on the toluene conversion and the resistance to coke deposition was not significant in toluene reforming with steam over the Ni/Mg/Al catalyst.
6. Further suppression of coke formation and addition of startability are probably necessary for the practical use of Ni catalysts in Reformed EGR system.

Acknowledgments

This work was partially supported by JSPS KAKENHI 18H05247 and JST.

References

- [1] L. Tartakovsky, M. Sheintuch, Fuel reforming in internal combustion engines, *Prog. Energy Combust. Sci.*, 2018, 67, 88-114. <https://doi.org/10.1016/j.pecs.2018.02.003>

- [2] N. Ladommatos, R. Balian, R. Horrocks, L. Cooper, The Effect of Exhaust gas Recirculation on Combustion and NO_x Emissions in a High-Speed Direct-injection Diesel Engine, *SAE Technical Paper*, 1996, 960840. <https://doi.org/10.4271/960840>
- [3] S. R. Gomes, N. Bion, D. Duprez, F. Epron, Hydrogen production from hydrocarbons over Rh supported on Ce-based oxides for automotive applications, *Appl. Catal. B: Environ.*, 2016, 197, 138-145. <https://doi.org/10.1016/j.apcatb.2016.01.022>.
- [4] Y. Jamal, M. L. Wyszynski, On-board generation of hydrogen-rich gaseous fuels—a review, *Int. J. Hydrogen Energy*, 1994, 19, 557-572. [https://doi.org/10.1016/0360-3199\(94\)90213-5](https://doi.org/10.1016/0360-3199(94)90213-5)
- [5] Nissan Motor Co., Ltd., Fuel reforming catalyst and method of using the same, JP2001-170486.
- [6] A. Tsolakis, A. Megaritis, Partially premixed charge compression ignition engine with on-board H₂ production by exhaust gas fuel reforming of diesel and biodiesel, *Int. J. Hydrogen Energy*, 2005, 30, 731-745. <https://doi.org/10.1016/j.ijhydene.2004.06.013>
- [7] S. Peucheret, M. Feaviour, S. Golunski, Exhaust-gas reforming using precious metal catalysts *Appl. Catal. B: Environ.*, 2006, 65, 201-206. <https://doi.org/10.1016/j.apcatb.2006.01.009>
- [8] V. Chintala, D. Banaerjee, P. K. Ghodke, E. Porpatham, Hydrogen rich exhaust gas recirculation (H₂EGR) for performance improvement and emissions reduction of a compression ignition engine, *Int. J. Hydrogen Energy*, 2019, 44, 18545-18558. <https://doi.org/10.1016/j.ijhydene.2019.05.141>
- [9] J. Thormann, L. Maier, P. Pfeifer, U. Kunz, O. Dautschmann, K. Schubert, Steam reforming of hexadecane over a Rh/CeO₂ catalyst in microchannels: Experimental and numerical investigation, *Int. J. Hydrogen Energy*, 2009, 34, 5108-5120. <https://doi.org/10.1016/j.ijhydene.2009.04.031>
- [10] M. Asadullah, K. Tomishige, K. Fujimoto, A novel catalytic process for cellulose gasification to synthesis gas, *Catal. Commun.*, 2001, 2, 63-68. [https://doi.org/10.1016/S1566-7367\(01\)00011-5](https://doi.org/10.1016/S1566-7367(01)00011-5)
- [11] M. Asadullah, K. Fujimoto, K. Tomishige, Catalytic Performance of Rh/CeO₂ in the Gasification of Cellulose to Synthesis Gas at Low Temperature, *Ind. Eng. Chem. Res.*, 2001, 40, 5894-5900. <https://doi.org/10.1021/ie010160z>

- [12] A. Tsolakis, S. E. Golunski, Sensitivity of process efficiency to reaction routes in exhaust-gas reforming of diesel fuel, *Chem. Eng. J.*, 2006, 117, 131-136. <https://doi.org/10.1016/j.cej.2005.12.017>
- [13] K. Theinnoi, W. Temwutthikun, T. Wongchang, B. Sawatmongkhon, Application of Exhaust Gas Fuel Reforming in Diesel Engines Towards the Improvement Urban Air Qualities, *Energy Procedia*, 2018, 152, 875-882. <https://doi.org/10.1016/j.egypro.2018.09.257>
- [14] P. Leung, A. Tsolakis, J. Rodriguez-Fernandez, S. Golunski, Raising the fuel heating value and recovering exhaust heat by on-board oxidative reforming of bioethanol, *Energy Environ. Sci.*, 2010, 3, 780-788. <https://doi.org/10.1039/b927199f>
- [15] D. Fennell, J. Herreros, A. Tsolakis, K. Cockle, J. Pignon, P. Millington, Thermochemical recovery technology for improved modern engine fuel economy – part 1: analysis of a prototype exhaust gas fuel reformer, *RSC Adv.*, 2015, 5, 35252-35261. <https://doi.org/10.1039/c5ra03111g>
- [16] E. Ambroise, C. Courson, A. C. Roger, A. Kiennemann, G. Blanchard, S. Rousseau, X. Carrier, E. Marceau, C. La Fontaine, F. Villain, Exhaust gas recirculation for on-board hydrogen production by isooctane reforming: Comparison of performances of metal/ceria–zirconia based catalysts prepared through pseudo sol–gel or impregnation methods, *Catal. Today*, 2010, 154, 133-141. <https://doi.org/10.1016/j.cattod.2009.12.010>
- [17] J. R. Rostrup-Nielsen, J. H. B. Hansen, CO₂-Reforming of Methane over Transition Metals, *J. Catal.*, 1993, 144, 38-49. <https://doi.org/10.1006/jcat.1993.1312>
- [18] B. Li, X. Yuan, B. Li, X. Wang, Impact of pore structure on hydroxyapatite supported nickel catalysts (Ni/HAP) for dry reforming of methane, *Fuel Proc. Technol.*, 2020, 202, 106359. <https://doi.org/10.1016/j.fuproc.2020.106359>
- [19] B. Li, Y. Luo, B. Li, X. Yuan, X. Wang, Catalytic performance of iron-promoted nickel-based ordered mesoporous alumina FeNiAl catalysts in dry reforming of methane, *Fuel Proc. Technol.*, 2019, 193, 348-360. <https://doi.org/10.1016/j.fuproc.2019.05.033>
- [20] J. Kobayashi, K. Kawamoto, N. Kobayashi, Effect of porous silica on the removal of tar components generated from waste biomass during catalytic reforming, *Fuel Proc. Technol.*, 2019, 194, 106104. <https://doi.org/10.1016/j.fuproc.2019.05.027>

- [21] T. Y. Liang, H. H. Chen, D. H. Tsai, Nickel hybrid nanoparticle decorating on alumina nanoparticle cluster for synergistic catalysis of methane dry reforming, *Fuel Proc. Technol.*, 2020, 201, 106335. <https://doi.org/10.1016/j.fuproc.2020.106335>
- [22] Q. Ma, L. Guo, Y. Fang, H. Li, J. Zhang, T. S. Zhao, G. Yang, Y. Yoneyama, N. Tsubaki, Combined methane dry reforming and methane partial oxidization for syngas production over high dispersion Ni based mesoporous catalyst, *Fuel Proc. Technol.*, 2019, 188, 98-104. <https://doi.org/10.1016/j.fuproc.2019.02.013>
- [23] C. H. Bartholomew, Carbon Deposition in Steam Reforming and Methanation, *Catal. Rev. Sci. Eng.*, 1982, 24, 67-112. <https://doi.org/10.1080/03602458208079650>
- [24] O. Yamazaki, K. Tomishige, K. Fujimoto, Development of highly stable nickel catalyst for methane-steam reaction under low steam to carbon ratio, *Appl. Catal. A: Gen.*, 1996, 136, 49-56. [https://doi.org/10.1016/0926-860X\(95\)00268-5](https://doi.org/10.1016/0926-860X(95)00268-5)
- [25] J. R. Rostrup-Nielsen, Production of synthesis gas, *Catal. Today*, 1993, 18, 305-324. [https://doi.org/10.1016/0920-5861\(93\)80059-A](https://doi.org/10.1016/0920-5861(93)80059-A)
- [26] K. Tomishige, Syngas production from methane reforming with CO₂/H₂O and O₂ over NiO–MgO solid solution catalyst in fluidized bed reactors, *Catal. Today*, 2004, 89, 405-418. <https://doi.org/10.1016/j.cattod.2004.01.003>
- [27] Z. Zhang, P. Jia, G. Zhong, J. Liang, G. Li, Numerical study of exhaust reforming characteristics on hydrogen production for a marine engine fueled with LNG, *Appl. Therm. Eng.*, 2017, 124, 241-249. <https://doi.org/10.1016/j.applthermaleng.2017.06.012>
- [28] I. Barbarias, G. Lopez, M. Amutio, M. Artetxe, J. Alvarez, A. Arregi, J. Bilbao, M. Olazar, Steam reforming of plastic pyrolysis model hydrocarbons and catalyst deactivation, *Appl. Catal. A: Gen.*, 2016, 527, 152-160. <https://doi.org/10.1016/j.apcata.2016.09.003>
- [29] L. Sileghem, V. A. Alekseev, J. Vancoillie, K. M. Van Geem, E. J. K. Nilsson, S. Verhelst, A. A. Konnov, Laminar burning velocity of gasoline and the gasoline surrogate components iso-octane, n-heptane and toluene, *Fuel*, 2013, 112, 355-365. <https://doi.org/10.1016/j.fuel.2013.05.049>

- [30] J. Ashok, N. Dewangan, S. Das, P. Hongmanorm, M. H. Wai, K. Tomishige, S. Kawi, Recent progress in the development of catalysts for steam reforming of biomass tar model reaction, *Fuel Proc. Technol.*, 2020, 199, 106252. <https://doi.org/10.1016/j.fuproc.2019.106252>
- [31] D. Li, M. Tamura, Y. Nakagawa, K. Tomishige, Metal catalysts for steam reforming of tar derived from the gasification of lignocellulosic biomass, *Bioresource Technol.*, 2015, 178, 53-64. <https://doi.org/10.1016/j.biortech.2014.10.010>
- [32] J. Ren, J. P. Cao, F. L. Yang, X. Y. Zhao, W. Tang, X. Cui, Q. Chen, X. Y. Wei, Layered uniformly delocalized electronic structure of carbon supported Ni catalyst for catalytic reforming of toluene and biomass tar, *Energy Convers. Manag.*, 2019, 183, 182-192. <https://doi.org/10.1016/j.enconman.2018.12.093>
- [33] V. Claude, J. G. Mahy, J. Geens, C. Courson, S. D. Lambert, Synthesis of Ni/ γ -Al₂O₃-SiO₂ catalysts with different silicon precursors for the steam toluene reforming, *Microporous Mesoporous Mater.*, 2019, 284, 304-315. <https://doi.org/10.1016/j.micromeso.2019.04.027>
- [34] D. Li, L. Wang, M. Koike, Y. Nakagawa, K. Tomishige, Steam reforming of tar from pyrolysis of biomass over Ni/Mg/Al catalysts prepared from hydrotalcite-like precursors, *Appl. Catal. B: Environ.*, 2011, 102, 528-538. <https://doi.org/10.1016/j.apcatb.2010.12.035>
- [35] F. Zhou, N. Pan, H. Chen, X. Xu, C. Wang, Y. Du, Y. Guo, Z. Zeng, L. Li, Hydrogen production through steam reforming of toluene over Ce, Zr or Fe promoted Ni-Mg-Al hydrotalcite-derived catalysts at low temperature, *Energy Convers. Manag.*, 2019, 196, 677-687. <https://doi.org/10.1016/j.enconman.2019.06.047>
- [36] H. Cheng, Y. Zhang, X. Lu, W. Ding, Q. Li, Hydrogen Production from Simulated Hot Coke Oven Gas by Using Oxygen-Permeable Ceramics, *Energy Fuels*, 2009, 23, 414-421. <https://doi.org/10.1021/ef8007618>
- [37] O. C. V. Silva, E. B. Silveira, R. C. Rabelo-Neto, L. E. P. Borges, F. B. Noronha, Hydrogen Production Through Steam Reforming of Toluene Over Ni Supported on MgAl Mixed Oxides Derived from Hydrotalcite-Like Compounds, *Catal. Lett.*, 2018, 148, 1622-1633. <https://doi.org/10.1007/s10562-018-2390-8>
- [38] C. Wu, J. Huang, P. T. Williams, Carbon nanotubes and hydrogen production from the reforming of toluene, *Int. J. Hydrogen Energy*, 2013, 38, 8790-8797. <https://doi.org/10.1016/j.ijhydene.2013.05.028>

- [39] D. Li, M. Koike, L. Wang, Y. Nakagawa, Y. Xu, K. Tomishige, Regenerability of Hydrotalcite-Derived Nickel–Iron Alloy Nanoparticles for Syngas Production from Biomass Tar, *ChemSusChem*, 2014, 7, 510-522. <https://doi.org/10.1002/cssc.201300855>
- [40] M. Koike, D. Li, Y. Nakagawa, and K. Tomishige, A Highly Active and Coke-Resistant Steam Reforming Catalyst Comprising Uniform Nickel–Iron Alloy Nanoparticles, *ChemSusChem*, 2012, 5, 2312-2314. <https://doi.org/10.1002/cssc.201200507>
- [41] M. Koike, D. Li, H. Watanabe, Y. Nakagawa, K. Tomishige, Comparative study on steam reforming of model aromatic compounds of biomass tar over Ni and Ni–Fe alloy nanoparticles, *Appl. Catal. A: Gen.*, 2015, 506, 151-162. <https://doi.org/10.1016/j.apcata.2015.09.007>
- [42] D. Li, M. Koike, J. Chen, Y. Nakagawa, K. Tomishige, Preparation of Ni-Cu/Mg/Al catalysts from hydrotalcite-like compounds for hydrogen production by steam reforming of biomass tar, *Int. J. Hydrogen Energy*, 2014, 39, 10959-10970. <https://doi.org/10.1016/j.ijhydene.2014.05.062>
- [43] K. Tomishige, D. Li, M. Tamura, Y. Nakagawa, Nickel–iron alloy catalysts for reforming of hydrocarbons: preparation, structure, and catalytic properties, *Catal. Sci. Technol.*, 2017, 7, 3952-3979. <https://doi.org/10.1039/c7cy01300k>
- [44] S. Miyata, The Syntheses of Hydrotalcite-Like Compounds and Their Structures and Physico-Chemical Properties—I: the Systems $Mg^{2+}-Al^{3+}-NO_3^-$, $Mg^{2+}-Al^{3+}-Cl^-$, $Mg^{2+}-Al^{3+}-ClO_4^-$, $Ni^{2+}-Al^{3+}-Cl^-$ and $Zn^{2+}-Al^{3+}-Cl^-$ Clays *Clay Miner.*, 1975, 23, 369-375. <https://doi.org/10.1346/CCMN.1975.0230508>
- [45] K. Yoshida, K. Okumura, T. Miyao, S. Naito, S. Ito, K. Kunimori, K. Tomishige, Oxidative steam reforming of methane over $Ni/\alpha-Al_2O_3$ modified with trace Pd, *Appl. Catal. A: Gen.*, 2008, 351, 217-225. <https://doi.org/10.1016/j.apcata.2008.09.014>
- [46] K. Yoshida, N. Begum, S. Ito, K. Tomishige, Oxidative steam reforming of methane over $Ni/\alpha-Al_2O_3$ modified with trace noble metals, *Appl. Catal. A: Gen.*, 2009, 358, 186-192. <https://doi.org/10.1016/j.apcata.2009.02.025>
- [47] L. Wang, D. Li, M. Koike, S. Koso, Y. Nakagawa, Y. Xu, K. Tomishige, Catalytic performance and characterization of Ni-Fe catalysts for the steam reforming of tar from biomass pyrolysis to synthesis gas, *Appl. Catal. A: Gen.*, 2011, 392, 248-255. <https://doi.org/10.1016/j.apcata.2010.11.013>

- [48] A. Vita, C. Italiano, L. Pino, M. Laganà, V. Recupero, Hydrogen-rich gas production by steam reforming of n-dodecane. Part II: Stability, regenerability and sulfur poisoning of low loading Rh-based catalyst, *Appl. Catal. B: Environ.*, 2017, 218, 317-326. <https://doi.org/10.1016/j.apcatb.2017.06.059>
- [49] K. Tomishige, Y. Himeno, Y. Matsuo, Y. Yoshinaga, K. Fujimoto, Catalytic Performance and Carbon Deposition Behavior of a NiO-MgO Solid Solution in Methane Reforming with Carbon Dioxide under Pressurized Conditions, *Ind. Eng. Chem. Res.*, 2000, 39, 1891-1897. <https://doi.org/10.1021/ie990884z>
- [50] K. Tomishige, Y. Matsuo, Y. Yoshinaga, Y. Sekine, M. Asadullah, K. Fujimoto, Comparative study between fluidized bed and fixed bed reactors in methane reforming combined with methane combustion for the internal heat supply under pressurized condition, *Appl. Catal. A: Gen.*, 2002, 223, 225-238. [https://doi.org/10.1016/S0926-860X\(01\)00757-8](https://doi.org/10.1016/S0926-860X(01)00757-8)
- [51] KITCO, <https://www.kitco.com/charts/rhodium.html>, accessed on March 23rd, 2020.
- [52] KITCO, <https://www.kitco.com/charts/interactive-charts/?Symbol=NICKEL&Currency=USD&multiCurrency=false&langId=EN&period=7862400000>, accessed on March 23rd, 2020.
- [53] Y. G. Chen, K. Tomishige, K. Yokoyama, K. Fujimoto, Catalytic Performance and Catalyst Structure of Nickel-Magnesia Catalysts for CO₂ Reforming of Methane, *J. Catal.*, 1999, 184, 479-490. <https://doi.org/10.1006/jcat.1999.2469>

Chapter 3

Catalytic performance of hydrotalcite-like-compound-derived Ni-metal alloy catalyst for toluene reforming with gasoline engine exhaust model gas as reforming agent

* submitted

3.1. Introduction

As described in Chapter 2, some researches focused on the Exhaust Gas Recirculation (EGR) engine system combined with reforming to improve the fuel economy ^[1, 2], was defined to Reformed EGR. In addition, the properties required for the reforming catalyst for Reformed EGR are as follows: workable at wide range of temperature including low temperature (active at 673-773 K or less), stability (no change of performance during use), resistance to coke deposition, reusability (no change of catalyst properties by regeneration), startability (easy activation), etc. ^[3]. As described in Chapter 2, supported Rh catalysts, especially those using CeO₂-based supports, have been typically investigated in Reformed EGR system for gasoline engine or diesel fuel ^[4-11]. However, reforming catalysts with lower cost are desired to be developed since Rh is a very expensive element.

In our previous study shown Chapter 2, Ni/Mg/Al catalyst prepared from hydrotalcite-like compounds (HTLcs) containing Ni as a precursor was applied to reforming of toluene with model EGR gas which contains CO₂ and low concentration (partial pressure) of steam ^[12]. Toluene was selected as a model compound of gasoline because reforming of toluene is more difficult especially in view of coke deposition than those of other gasoline components such as paraffins and olefins ^[13-19]. The activity, structure stability and coke deposition resistance of Ni/Mg/Al catalyst higher than that Ni/ α -Al₂O₃ catalyst, but lower than that Rh/CeO₂ ^[12]. The amount of coke deposition on Ni/Mg/Al catalyst increased with the increase of *W/F*, especially at the outlet of the catalyst bed, which can be due to the coke formation from CO disproportionation. The deactivation and coke deposition were also severer in higher partial pressure of toluene, when only the toluene concentration was changed in the feed. The Ni/Mg/Al catalyst needs more

improvement of stability and coke deposition resistance [12].

On the other hand, the alloying of Ni with other transition metals such as Rh, Pt, Pd, Fe, Co and Cu is a frequently-used method to improve the performance such as activity, stability and coke deposition resistance of Ni catalysts in reforming reactions [20-34]. Especially, alloying nickel with iron has been intensively investigated, and the improvement in activity and coke deposition resistance has been reported in steam reforming of toluene [33, 35-43], other model compounds [34, 44-46, 73], and biomass tar which is produced by biomass gasification [38, 44-48] and dry reforming of methane [40, 51-53]. Other first-row transition metals such as Co [54-59] and Cu [59-64] have been also used as counterparts of Ni-based alloy catalysts. These alloy catalysts exhibited improved coke deposition resistance in steam reforming of aromatic compounds including toluene, although the increase of formation rate of CO was generally less clear than the cases of Ni-Fe alloy catalysts.

The utilization of HTICs as precursors is an effective method for the preparation of alloy catalysts with good homogeneity [34, 39, 49, 65-67]. By incorporating Ni²⁺ and Fe³⁺ (or Cu²⁺) into the Mg-Al HTICs before calcination and reduction steps, the author has prepared a well-dispersed Ni-Fe (or Ni-Cu) alloy catalyst with relatively uniform composition [35, 49, 60] in comparison with supported catalysts prepared by simple co-impregnation. The Ni-Fe/Mg/Al and Ni-Cu/Mg/Al catalysts showed improved activity and coke deposition resistance in steam reforming of biomass tar or model compounds of biomass tar [35, 36, 49, 60, 61]. Several other research groups also reported good performance of Ni-Fe and Ni-Cu catalysts derived from HTICs in CO₂ methanation [66], dry reforming of methane [53, 67, 68] and steam reforming of toluene [39].

In this paper, the author applied the Ni-M/Mg/Al (M = Fe, Co, Cu) catalysts to a model reaction of Reformed EGR: the reaction of toluene with model EGR gas of gasoline engine to synthesis gas. The conditions of this model reaction of Reformed EGR are severer than those of simple steam reforming including our previous studies using Ni-M/Mg/Al catalysts. Although startability (reducibility) was still not considered in this study, the Ni-Fe/Mg/Al catalyst showed higher activity, stability and coke deposition resistance than Ni/Mg/Al, Ni-Co/Mg/Al, Ni-Cu/Mg/Al and Ni-Fe/ α -Al₂O₃. In addition, various regeneration methods were tested for the Ni-Fe/Mg/Al catalyst, and the author found that simple high-temperature treatment or the use for reforming reaction at higher temperature can regenerate the catalyst.

3.2. Experimental

3.2.1. Catalyst preparation

Ni/Mg/Al catalyst was the same one used in Chapter 2.

As similarity described in Chapter 2, Ni-M/Mg/Al (M = Fe, Cu) catalysts derived from HTlcs were prepared according to our previous papers [35, 60, 69]. Ni-Co/Mg/Al catalyst derived from HTlc was prepared by the same method as that of Ni-Cu/Mg/Al. The molar ratio of $(\text{Ni} + \text{M}^{2+} + \text{Mg}) / (\text{Al} + \text{M}^{3+})$ ($\text{M}^{2+} = \text{Co}^{2+}, \text{Cu}^{2+}$; $\text{M}^{3+} = \text{Fe}^{3+}$) was 3 for all the catalysts. For Ni-Co/Mg/Al and Ni-Cu/Mg/Al, the Ni content was 12.0 wt% as a weight percentage in the calcined sample, and the molar ratio of Co/Ni or Cu/Ni was 0.25. For Ni-Fe/Mg/Al catalysts, the Fe content was set at 1, 3 and 5 wt% while the Ni content in the calcined sample was set at 14, 12 and 10 wt%, respectively, to obtain a molar ratio of Fe/Ni of 0.1, 0.25 and 0.5, respectively. The composition of the Ni/Mg/Al catalyst was 9/66/25 (Ni 12 wt% in the calcined sample), which the author has determined as the best composition for the steam reforming of toluene as a model reaction of tar reforming in biomass gasification [69].

The Ni-Fe catalyst supported on $\alpha\text{-Al}_2\text{O}_3$ (Ni-Fe/ $\alpha\text{-Al}_2\text{O}_3$) was prepared also according to our previous reports [70, 71]. The $\alpha\text{-Al}_2\text{O}_3$ support (BET surface area $12.1 \text{ m}^2 \text{ g}^{-1}$) was the same one used in Chapter 2. It was granulated to the same size as that of Ni-M/Mg/Al. Ni-Fe/ $\alpha\text{-Al}_2\text{O}_3$ catalyst (Ni 12 wt%, molar ratio of Fe/Ni 0.25) was prepared by a co-impregnation method using a mixed solution of Ni^{2+} and Fe^{3+} nitrates in water. The catalyst after impregnation was dried in an oven at 383 K for 12 h, and the dried catalyst was calcined at 773 K for 3 h.

For all catalysts, the reduction pretreatment was carried out just before catalytic use or characterization. The reduction conditions are shown in the details of each experiment.

3.2.2. Catalyst characterization

X-ray diffraction (XRD) patterns were recorded as described in Chapter 2. For the catalysts after reduction, the catalyst sample was mixed with silicon powder as an internal standard to determine the shift of Ni-M alloy peaks from pure Ni phase peaks accurately. The average particle size of active metal in the catalyst was calculated as described in Chapter 2., although this value might be underestimated for alloy catalysts because of the heterogeneity of alloy composition. The TEM images were taken with HD-2700 instrument. The M/Ni ratio in each Ni-M alloy

particle was determined by point analysis of Energy Dispersive X-ray Spectroscopy (EDX; HORIBA EMAX ENERGY EX-250) combined with TEM. The size of analyzed area in the point analysis was about 1 nm. Temperature-programmed reduction with H₂ (H₂-TPR) was measurement as described in Chapter 2. The reduction degree of Ni/Mg/Al and Ni-M/Mg/Al (M = Fe, Co, Cu) was calculated from the H₂ consumption in H₂-TPR and alloy composition determined by EDX. Here, the author assumed the following formulae for the reduction: NiO + H₂ → Ni + H₂O, Fe₂O₃ + 3H₂ → 2Fe + 3H₂O, CoO + H₂ → Co + H₂O and CuO + H₂ → Cu + H₂O. The reduced amount of Ni²⁺ was calculated by (H₂ consumption amount) × 2/(2 + n × (M/Ni ratio in alloy)), while that of Mⁿ⁺ was calculated by (H₂ consumption amount) × 2 × (M/Ni ratio in alloy)/(2 + n × (M/Ni ratio in alloy)). The reduction degree of Ni, M or Ni+M was calculated by the ratio of the reduced amount of Ni²⁺, Mⁿ⁺ or Ni²⁺ + Mⁿ⁺ to the Ni²⁺, Mⁿ⁺ or Ni²⁺ + Mⁿ⁺ amount in the simple, respectively.

3.2.3. Activity test of reforming of toluene

The used fixed-bed flow reactor was the same one used in Chapter 2. After the catalysts in the oxidized form were loaded, the reactor was purged with N₂, and the reactant liquids (such as toluene and H₂O) were supplied as described in Chapter 2. The standard feed ratio (molar ratio) of reactants and carrier gas was toluene/H₂O/N₂/CO₂ = 1/11.8/71.2/11.8 (the ratio of steam to carbon in hydrocarbon reactant (S/C_{HC}) = 1.7), corresponding to the contact time $W/F = 0.19 \text{ g}_{\text{cat}} \text{ h mol}^{-1}$, which were the same conditions as the standard experiments in Chapter 2. Here, F represents the total flow rate and W is the catalyst weight. The main reaction schemes were shown in Chapter 2 (Eqs. 1- 3).

In addition, the coke amount deposited on the catalyst was measured as described in Chapter 2. The author evaluated the carbon amount on the catalyst sample at each position ^[71]. In TG-DTA profile, the decrease of weight accompanying exothermic DTA signals at the temperature range between 600 and 900 K was assigned to the combustion of coke ^[72].

3.3. Results and discussion

3.3.1. Catalyst characterization

Figure 3.1 shows the XRD patterns of reduced catalysts: Ni/Mg/Al and Ni-M/Mg/Al ($M/Ni = 0.25$, $M = Fe, Co, Cu$). The strongest peak of Ni metal or Ni-based alloy (fcc (1 1 1); $\sim 44^\circ$) was overlapped with a peak of the periclase phase, and therefore the author discussed the metallic phase with the second strongest peak at around 52° ((2 0 0)). The peak due to Ni metal with the width corresponding to 7.6 nm particle size was observed at $2q = 51.9^\circ$ on Ni/Mg/Al [12]. On Ni-M/Mg/Al ($M/Ni = 0.25$, $M = Fe, Co, Cu$) catalysts, the peak was shifted to smaller angle which can be interpreted by the formation of Ni-rich Ni-M solid solution alloy [60, 73]. The peak in Ni-Cu/Mg/Al was very broad, which means the formation of small alloy particles. The width of the peak in Ni-Fe/Mg/Al and Ni-Co/Mg/Al was slightly broader than that in Ni/Mg/Al. However, it is difficult to determine the particle size of alloy accurately from XRD because of the heterogeneity of the alloy composition.

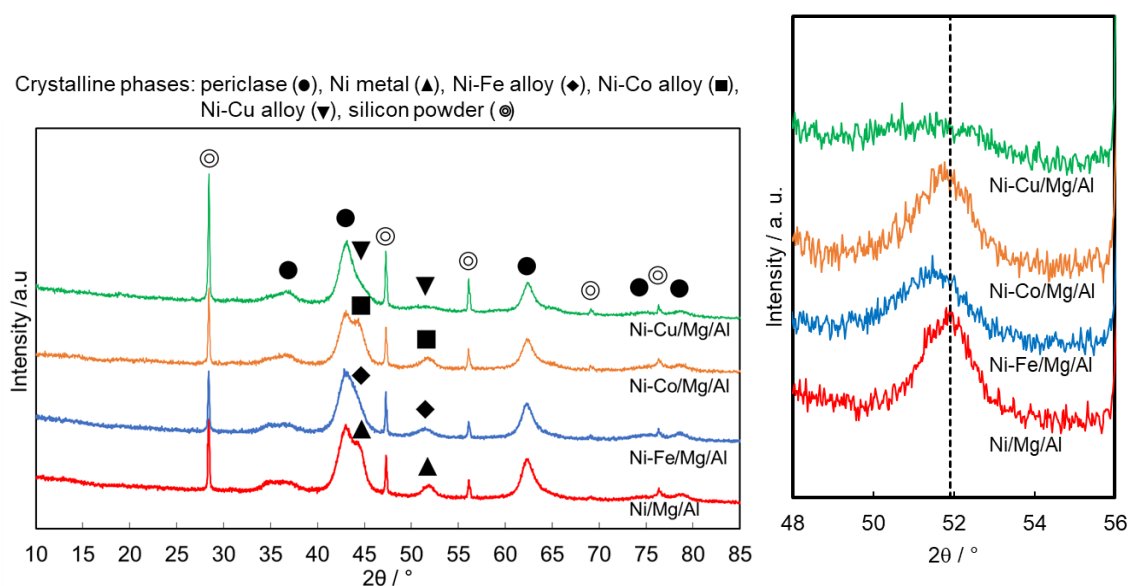


Figure 3.1 XRD patterns of Ni/Mg/Al and Ni-M/Mg/Al ($M = Fe, Co, Cu$; $M/Ni = 0.25$) after reduction.

The author calculated the composition of the Ni-M alloy particles from the $d(2\ 0\ 0)$ spacing value and Vegard's law, as listed in Table 3.1. Fe/Ni molar ratio in the alloy was calculated to be 0.22, consistent with Fe/Ni molar ratio in the catalyst ($Fe/Ni = 0.25$) [35], suggesting that the Ni and Fe were reduced simultaneously to form an alloy. On the other hand, Co/Ni and Cu/Ni molar ratio in the alloy was larger than that in the whole catalyst, although the

calculation of the molar ratio in Ni-Co and Ni-Cu alloy had large errors because of the close peak positions of Ni⁰ and Co⁰ and the very broad XRD signal of Ni-Cu alloy (**Fig. 3.2**).

Table 3.1 Physicochemical properties of catalysts.

Entry	Catalyst	Loading amount of metal [wt%]		M/Ni molar ratio [-]	Particle size [nm]		BET surface area ^a [m ² g ⁻¹]	M/Ni molar ratio in alloy [-]		H ₂ consumption in TPR ^d [mmol g _{cat} ⁻¹]
		Ni	M		XRD	TEM		XRD ^b	EDX ^c	
		1 ^g	Ni/Mg/Al	12	0	-	7.6	5.5	120	-
2	Ni-Fe/Mg/Al	14	1	0.1	4.9	6.2	130	0.13	0.10	1.96
3	Ni-Fe/Mg/Al	12	3	0.25	5.1	4.3	75	0.22	0.30	1.89
4	Ni-Fe/Mg/Al	10	5	0.5	4.1	6.5	126	0.40	0.49	1.93
5	Ni-Co/Mg/Al	12	3	0.25	5.4	5.0	106	0.43	0.29	1.86
6	Ni-Cu/Mg/Al	12	3	0.25	3.4	6.1	108	0.31	(0.30) ^h	1.93
7	Ni-Fe/ α -Al ₂ O ₃	12	3	0.25	6.4	19.8	15	0.11	0.59	2.53

Entry	Catalyst	Loading amount of metal [wt%]		M/Ni molar ratio [-]	Reduction degree ^e [-]			(Ni ⁰ +M ⁰) _{surface} / (Ni ⁰ +M ⁰) _{total} ^f [-]	H ₂ adsorption [μmol g _{cat} ⁻¹]	Dispersion by H ₂ adsorption [-]
		Ni	M		Ni	M	Ni+M			
		1 ^g	Ni/Mg/Al	12	0	-	0.54	-	0.54	0.069
2	Ni-Fe/Mg/Al	14	1	0.1	0.7	1.11	0.74	0.145	65.9	0.07
3	Ni-Fe/Mg/Al	12	3	0.25	0.65	0.71	0.66	0.126	28.9	0.03
4	Ni-Fe/Mg/Al	10	5	0.5	0.64	0.62	0.63	0.151	5.6	0.01
5	Ni-Co/Mg/Al	12	3	0.25	0.71	0.82	0.73	0.131	45.5	0.05
6	Ni-Cu/Mg/Al	12	3	0.25	0.64	1.04	0.70	0.199	31.7	0.04
7	Ni-Fe/ α -Al ₂ O ₃	12	3	0.25	0.65	1.49	0.89	0.135	10.3	0.01

^a Measured after calcination. ^b Atomic ratio in particles determined by the $d(2\ 0\ 0)$ spacing from XRD and Vegard's law (**Fig. 3.2**). ^c Average of 14 - 23 points. ^d From room temperature to 1073 K. ^e Calculated from the H₂-TPR results by assuming NiO + H₂ → Ni⁰ + H₂O, Fe₂O₃ + 3H₂ → 2Fe⁰ + 3H₂O, CoO + H₂ → Co⁰ + H₂O and CuO + H₂ → Cu⁰ + H₂O: Reduction degree of Ni²⁺ = (H₂ consumption amount) × 2 / (2 + n × (M/Ni ratio in alloy)) / (Ni amount), Reduction degree of Mⁿ⁺ = (H₂ consumption amount) × 2 × (M/Ni ratio in alloy) / (2 + n × (M/Ni ratio in alloy)) / (M amount). Reduction degree of (Ni+M) = (H₂ consumption amount) × (2 + (2 × (M/Ni ratio in alloy)) / (2 + n × (M/Ni ratio in alloy))) / (Ni amount + M amount). The M/Ni molar ratios in alloy were determined by XRD and Vegard's law. ^f Calculated by the following equation: (Ni⁰+M⁰)_{surface} / (Ni+M)_{total} = 9.71 / (Ni or Ni-M alloy particle size/nm × 10) × reduction degree of (Ni+M). ^g Ref. [12]. ^h Average for only Ni-Cu alloy particles; there were monometallic Cu particles in addition to these alloy particles. n.d.: no data.

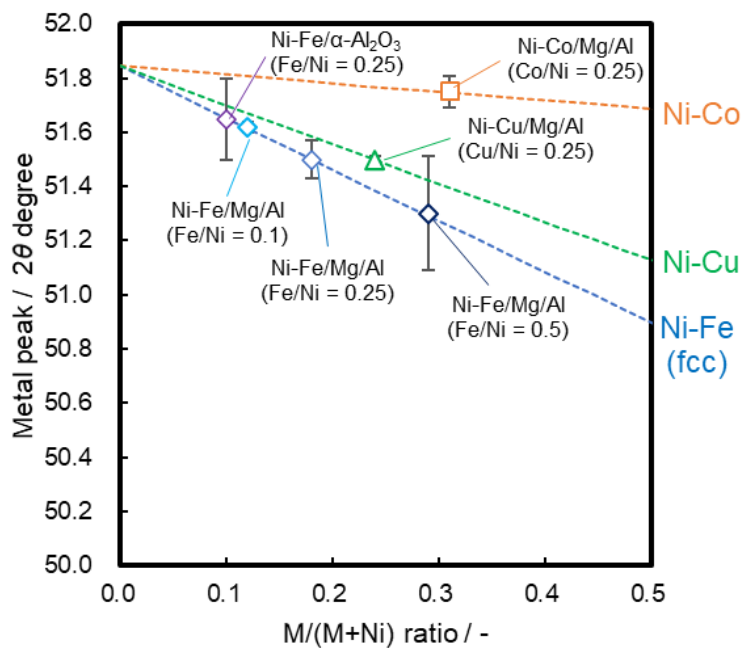


Figure 3.2 Determination of M/Ni ratio in alloy phase in Ni-M/Mg/Al (M = Fe, Co, Cu, M/Ni = 0.25) and Ni-Fe/α-Al₂O₃ (Fe/Ni = 0.25) catalysts after reduction by XRD patterns and Vegard's law.

TEM-EDX analysis was carried out to obtain the morphology of catalysts and the M/Ni ratio in each metal particle. **Figure 3.3** shows the TEM-EDX results of Ni/Mg/Al and Ni-M/Mg/Al catalysts after reduction. Raw EDX data of a representative measurement are shown in **Table 3.2**. The morphology of the Ni-M/Mg/Al catalysts was similar to that of Ni/Mg/Al: nanocomposites of oxide and metal particles with less than 10 nm size. The presence of Ni and M (M = Fe, Co, Cu) in the same particle was confirmed by EDX, indicating the formation of a Ni-M (M = Fe, Co, Cu) alloy (**Fig.3.3**). In the case of M = Fe (**Fig. 3.3 (b)**), the Fe/Ni molar ratio in all metal particles was similar to that in the whole catalyst, as reported in our previous study ^[35], also agreeing with the XRD result. In the Ni-Fe/Mg/Al catalysts with Fe/Ni = 0.1 and 0.5, the average Fe/Ni molar ratio in metal particles by EDX was close to that in the whole catalyst, as reported in our previous study ^[49], also corresponding with XRD (**Figs. 3.4 (a), 3.5 (a) and (b)**). Ni-Co alloy particles with similar uniform composition were observed for Ni-Co/Mg/Al (**Fig. 3.3 (c)**), and the composition was similar to that in the whole catalyst. On the other hand, the alloy composition in the Ni-Cu/Mg/Al catalyst was heterogeneous, and some metal particles in the Ni-Cu/Mg/Al catalyst contained only Cu (**Fig. 3.3 (d)**). The particle size of Ni-Fe and Ni-Co alloys measured by TEM was similar to those calculated from XRD. On the

other hand, the Ni-Cu alloy particle size measured by TEM was larger than that calculated by XRD, which can be due to the heterogeneity of alloy composition of Ni-Cu as shown by EDX. In the case of Ni-Fe/ α -Al₂O₃, the average Fe/Ni molar ratio in metal particles by EDX was significantly larger than that in the whole catalyst (**Fig. 3.5 (c)**). On the other hand, the Fe/Ni ratio in the metal phase of Ni-Fe/ α -Al₂O₃ determined by XRD was significantly lower than that in the whole catalyst (**Fig. 3.4 (b)**). This behavior can be explained by that larger metal particles in Ni-Fe (α -Al₂O₃) tended to be more Ni-rich.

H₂-TPR measurement was carried out to investigate the reduction behavior and to determine the reduction degree of catalysts (**Fig. 3.6**). The profile was recorded up to 1073 K which was the actual reduction temperature for the catalytic test. The reduction of Ni/Mg/Al was not completed at 1073 K, and the reduction degree after the reduction at 1073 K for 30 min was 0.54 [12]. As reported in our previous paper [49], the profile of Ni-Fe/Mg/Al had similar shape to that of Ni/Mg/Al, while the intensity was significantly larger, indicating that the reduction of Ni and Fe occurred simultaneously. The TPR profile of Ni-Co/Mg/Al had similar shape to those of Ni/Mg/Al and Ni-Fe/Mg/Al, and the intensity was also significantly larger than that of Ni/Mg/Al. The reduction of Ni and Co occurred also simultaneously. The reduction degree of Ni, and Fe or Co was determined by the total consumption amount of H₂ and alloy composition determined by EDX (**Table 3.1**). The reduction degree of Ni in Ni-Fe/Mg/Al and Ni-Co/Mg/Al was similar to that in Ni/Mg/Al. The reduction degree of Fe and Co was 0.7 and 0.8, respectively. Larger amount of Co was reduced to form Ni-based alloy than the case of Fe. On the other hand, two peaks were observed in the TPR profile of Ni-Cu/Mg/Al, which has been also reported in our previous paper [60]. The first peak at 573 K was due to the reduction of part of Cu species to Cu metal (reduction degree of Cu: 0.09) and the second peak was due to the simultaneous reduction of Ni and Cu to form Ni-Cu alloy (reduction degree of Cu: 1.04, including the first peak). Large temperature difference between Cu and Ni reductions can be connected to the formation of monometallic Cu particles.

Catalytic performance of hydrotalcite-like-compound-derived Ni-metal alloy catalyst for toluene reforming with gasoline engine exhaust model gas as reforming agent

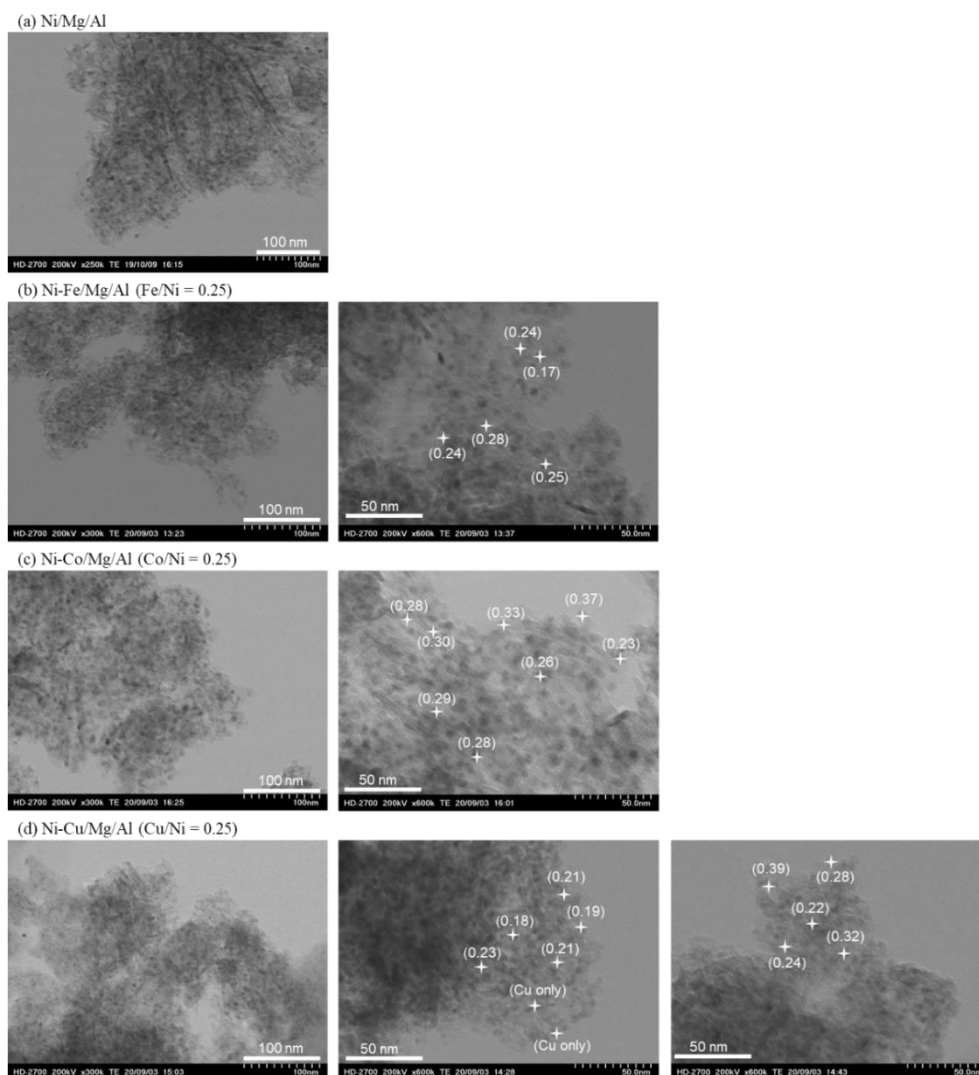
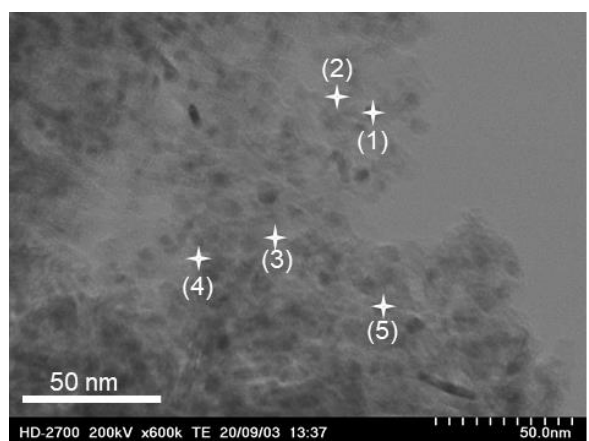


Figure 3.3 TEM images of Ni/Mg/Al (a), Ni-Fe/Mg/Al (b), Ni-Co/Mg/Al (c) and Ni-Cu/Mg/Al (d) catalysts after reduction.

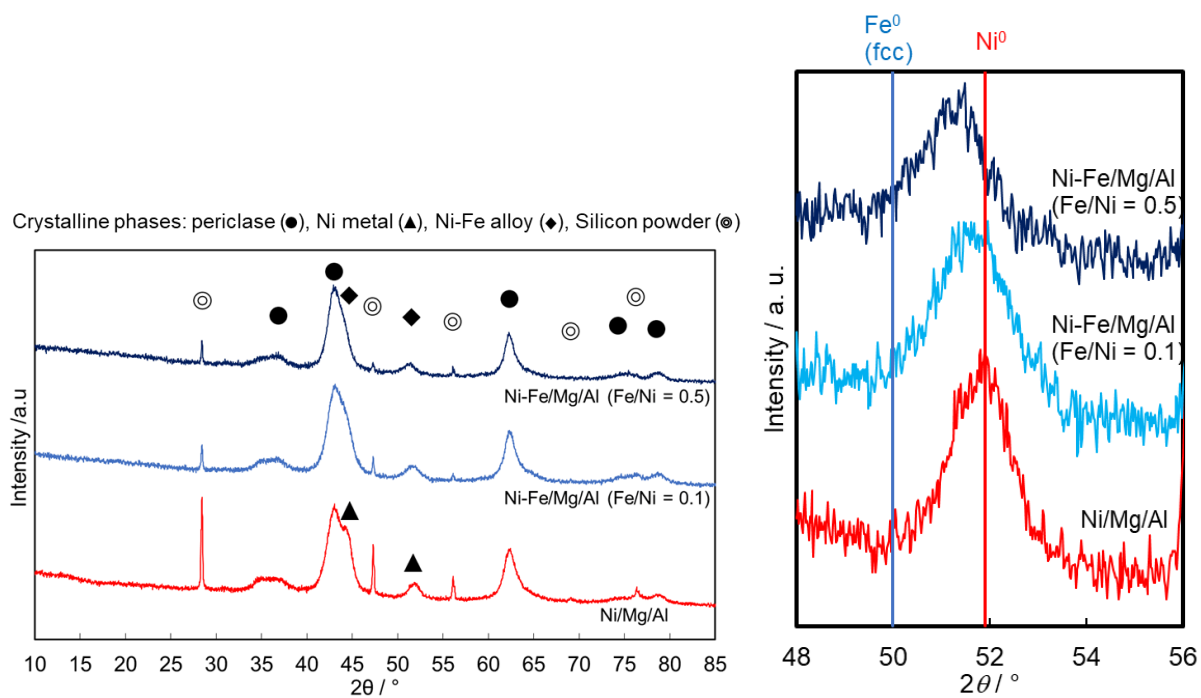
Reduction conditions: 50%/50% H₂/N₂, 1073 K, 30 min.

Table 3.2 EDX analysis of Ni-Fe/Mg/Al (Fe/Ni = 0.25, **Fig. 3.3 (b)**)



Point No.	Atomic concentration [-]				M/Ni ratio at EDX [-]
	Ni	Fe	Mg	Al	
1	0.307	0.052	0.429	0.213	0.17
2	0.134	0.032	0.517	0.317	0.24
3	0.140	0.039	0.580	0.240	0.28
4	0.157	0.038	0.560	0.245	0.24
5	0.127	0.031	0.583	0.259	0.25
Bulk ^a	0.090	0.023	0.660	0.227	0.25

^a Ratio of used precursors.



(a) Ni/Mg/Al and Ni-Fe/Mg/Al (Fe/Ni = 0.1, 0.5)

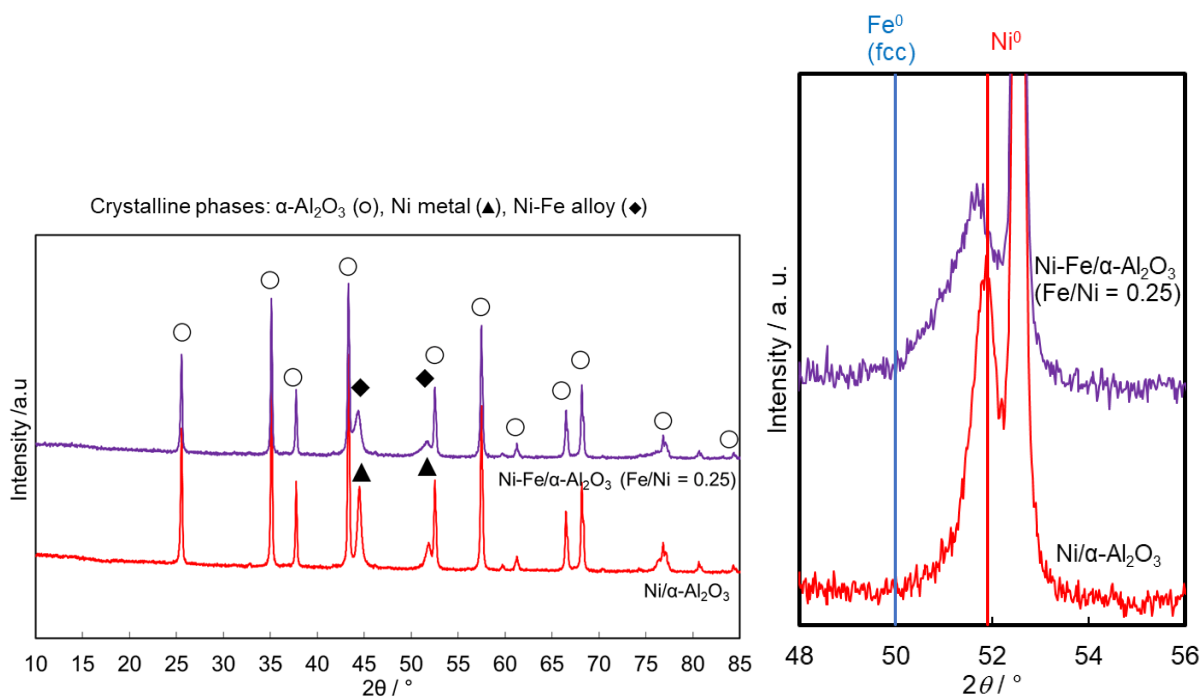
(b) Ni/ α -Al₂O₃ and Ni-Fe/ α -Al₂O₃ (Fe/Ni = 0.25)

Figure 3.4 XRD patterns of Ni and Ni-Fe catalysts after reduction.

Reduction conditions: $W_{cat} = 100$ mg, $T = 1073$ K, $H_2/N_2 = 30$ ml min⁻¹/30 ml min⁻¹, $t = 0.5$ h.

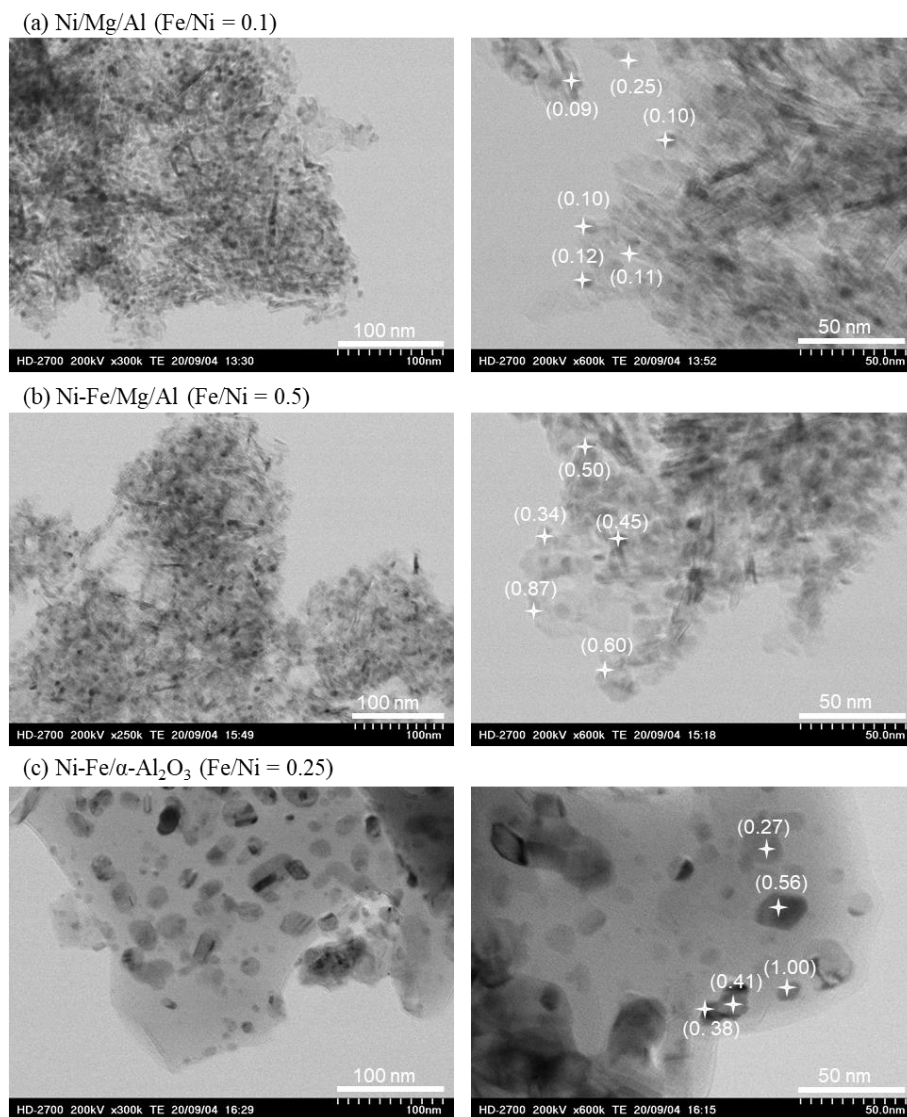


Figure 3.5 TEM images of Ni-Fe/Mg/Al (Fe/Ni = 0.1, (a)), Ni-Fe/Mg/Al (Fe/Ni = 0.5, (b)) and Ni-Fe/ α -Al₂O₃ (Fe/Ni = 0.25, (c)) catalysts after reduction.

Reduction conditions: 50%/50% H₂/N₂, 1073 K, 0.5 h.

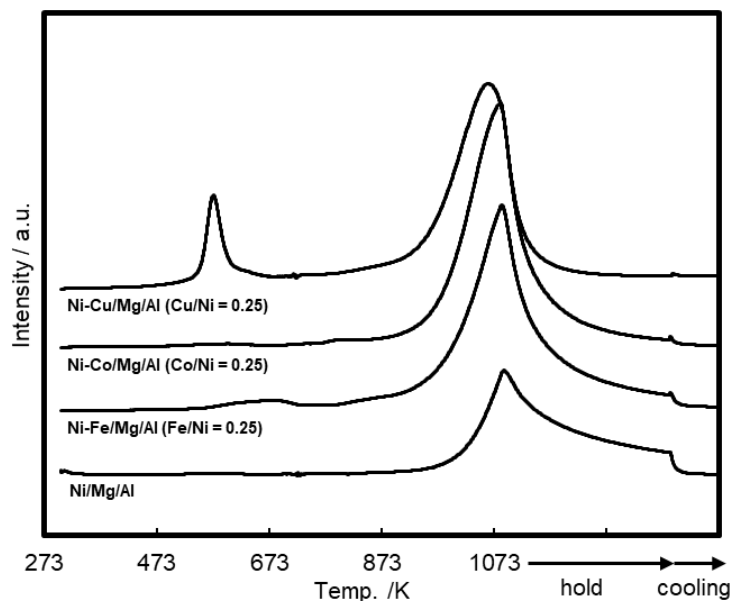


Figure 3.6 TPR profiles of Ni/Mg/Al and Ni-M/Mg/Al (M = Fe, Co, Cu) catalysts.

Measurement conditions: 5% H₂/Ar, 30 ml min⁻¹; room temperature to 1073 K at a rate of 10 K min⁻¹, then the temperature was maintained at 1073 K for 30 min; sample, 50 mg. The profile of Ni/Mg/Al was reported in ref. [12].

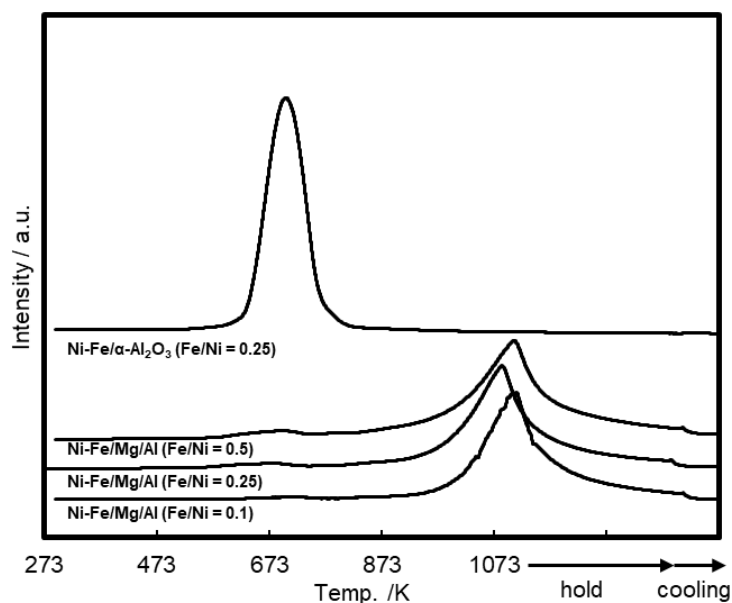


Figure 3.7 TPR profiles of Ni-Fe/Mg/Al (Fe/Ni = 0.1, 0.25, 0.5) and Ni-Fe/α-Al₂O₃ (Fe/Ni = 0.25) catalysts.

Measurement conditions: 5% H₂/Ar, 30 ml min⁻¹; room temperature to 1073 K at a rate of 10 K min⁻¹, then the temperature was maintained at 1073 K for 30 min; sample, 50 mg.

3.3.2. Catalytic performance of Ni-M/Mg/Al in the reforming of toluene with model EGR gas

The reforming of toluene with model EGR gas which contains CO₂ and low partial pressure of steam was tested with Ni-M/Mg/Al (M/Ni = 0.25, M = Fe, Co, Cu) catalysts. The results were compared with that of Ni/Mg/Al catalyst reported in our previous paper [12]. The reactions were performed for 300 min of time on stream. Toluene conversion and formation rates of each product at 773 K are shown in **Table 3.3** and **Fig. 3.8**. The activity of Ni-Co/Mg/Al (Co/Ni = 0.25) and Ni-Cu/Mg/Al (Cu/Ni = 0.25) gradually decreased during 0 ~ 100 min, and toluene conversion decreased from > 80% to about 30% after 300 min. These behaviors of the rapid deactivation were similar to the case of Ni/Mg/Al catalyst. In contrast, the activity of Ni-Fe/Mg/Al (Fe/Ni = 0.25) decreased much slower: the conversion was kept > 80% up to 180 min, and at 300 min the conversion was still 70%. The Ni-Fe/Mg/Al catalyst showed clearly higher steady-state activity than Ni/Mg/Al, Ni-Co/Mg/Al and Ni-Cu/Mg/Al catalysts. The amount of coke after the 300 min reaction was measured at the inlet, middle and outlet positions of the catalyst bed. Generally, the coke deposited at the inlet of the catalyst bed is mainly generated by substrate (toluene) decomposition, and that deposited at the outlet is generated also by CO disproportionation, especially at high conversion levels [36]. As shown in **Table 3.3**, the amount of coke on Ni-Co/Mg/Al (Co/Ni = 0.25) and Ni-Cu/Mg/Al (Cu/Ni = 0.25) catalysts were almost the same as that on Ni/Mg/Al catalyst for all the three positions. By contrast, the amount of coke on Ni-Fe/Mg/Al (Fe/Ni = 0.25) catalyst was much smaller than those on Ni-Co/Mg/Al, Ni-Cu/Mg/Al and Ni/Mg/Al catalysts for all the three positions. Ni-Fe/Mg/Al catalyst showed higher coke deposition resistance from both substrate decomposition and CO disproportionation and higher steady-state activity. Similar better coke deposition resistance of Ni-Fe/Mg/Al catalyst than that of Ni/Mg/Al has been also reported for simple steam reforming of toluene, benzene, phenol and biomass tar [36, 49]. It has been proposed that H₂O is activated on Fe site and the oxygen species reacted with and removed carbon species adsorbed on Ni metal [40].

Table 3.3 Reforming of toluene with model EGR gas over Ni/Mg/Al and Ni-M/Mg/Al (M = Fe, Co, Cu; M/Ni = 0.25) catalysts.

Entry	Catalyst	Toluene conv. [%]	Average formation rate [mmol h ⁻¹ g _{cat} ⁻¹]					H ₂ /CO ratio [-]	Amount of coke deposition ^d [g _{coke} g _{cat} ⁻¹]		
			H ₂	CH ₄	CO	CO ₂	C ₆ H ₆		Inlet	Middle	Outlet
1 ^a	Ni/Mg/Al	84 ^b	450	37	170	84	1	2.6			
		34 ^c	304	0	81	85	2	3.7	0.04	0.05	0.06
2	Ni-Fe/Mg/Al	100 ^b	497	75	244	128	0	2.0			
		70 ^c	500	8	171	154	3	3.0	0.01	0.01	0.01
3	Ni-Co/Mg/Al	89 ^b	449	51	175	63	1	2.6			
		36 ^c	314	0	84	53	2	3.8	0.04	0.04	0.06
4	Ni-Cu/Mg/Al	69 ^b	291	9	84	72	10	3.6			
		32 ^c	178	0	43	28	10	4.2	0.03	0.08	0.06

Reaction conditions: $W_{cat} = 100$ mg; $W/F = 0.19$ g h mol⁻¹ (total feeding rate 517 mmol h⁻¹); Toluene/H₂O/N₂/CO₂ = 1.0/11.8/71.2/11.8; reaction temperature (T) = 773 K; reaction time, 300 min. $S/C_{HC} = 1.7$. ^a Ref. [12], ^b Initial: at 10-30 min, ^c Steady state: at 280-300 min, ^d After 300 min.

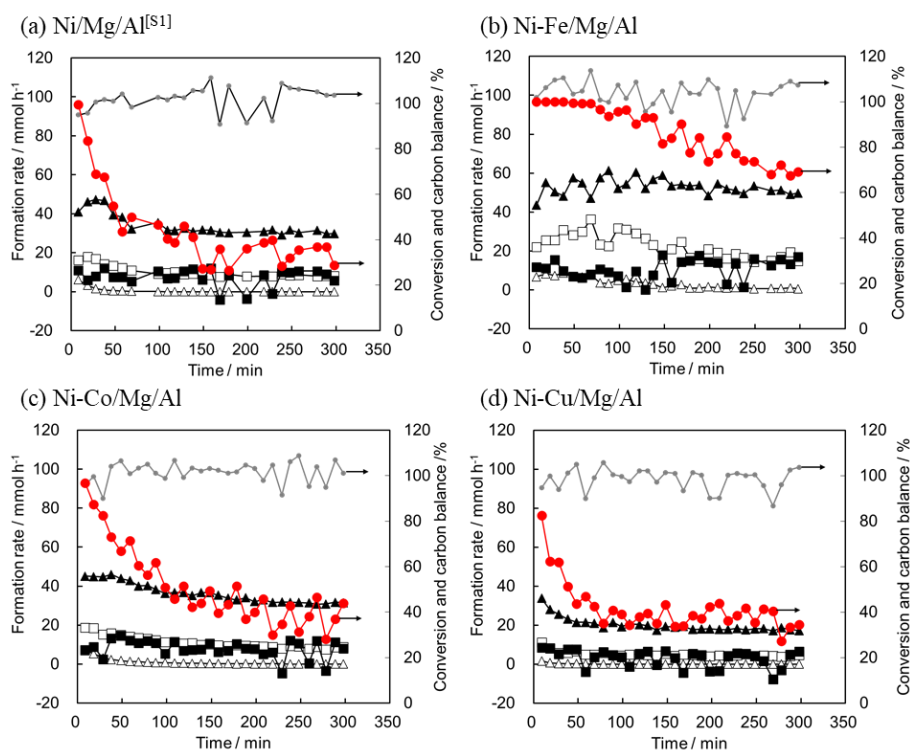


Figure 3.8 Time dependence of reforming of toluene over Ni/Mg/Al and Ni-M/Mg/Al (M = Fe, Co, Cu; M/Ni = 0.25) catalysts. (Detailed data of Table 3.3)

● (red circle): toluene conversion, ● (gray circle): carbon balance, ▲: H₂, △: CH₄, □; CO, ■; CO₂. Reaction conditions: $W_{cat} = 100$ mg; $W/F = 0.19$ g h mol⁻¹. reaction temperature, 773 K; reaction time, 300 min. $S/C_{HC} = 1.7$ (Toluene/H₂O/N₂/CO₂ = 1.0/11.8/71.2/11.8 (molar ratio)). Feeding rate: toluene, 6 mmol h⁻¹; steam, 65 mmol h⁻¹; N₂, 382 mmol h⁻¹; CO₂, 64 mmol h⁻¹.

3.3.3. Effect of Fe/Ni ratio

Next, Ni-Fe/Mg/Al catalysts with different molar ratios of Fe/Ni (0.1, 0.25 and 0.5) were tested. The results of 300 min reactions are shown in **Table 3.4** and **Fig. 3.9**. On the Fe/Ni = 0.1 catalyst, the activity (conversion) gradually decreased during 70 ~ 300 min, and toluene conversion decreased from > 95% to about 45% at 300 min. The conversion value at 300 min was much lower than that over the standard Fe/Ni = 0.25 catalyst. The activity of the Fe/Ni = 0.5 catalyst gradually decreased during 0 ~ 300 min, and toluene conversion decreased from 97% to about 80% during the 300 min. However, clearly higher amount of benzene was formed (15 mol% yield at 300 min) over the Fe/Ni = 0.5 catalyst than that over Fe/Ni = 0.25 (5 mol% yield at 300 min). The smaller ensemble size of surface Ni atoms for activation of hydrocarbons on Ni-Fe alloy with higher Fe/Ni ratio may decrease the activity in total decomposition of hydrocarbon molecules^[37, 40]. All the three Ni-Fe/Mg/Al catalysts exhibited high resistance of coke deposition as demonstrated by the small amount of coke deposition (0.01 g_{coke} g_{cat}⁻¹) for all the positions.

Table 3.4 Reforming of toluene with model EGR gas over Ni-Fe catalysts.

Entry	Catalyst	Fe/Ni molar ratio [-]	Toluene conv. [%]	Average formation rate [mmol h ⁻¹ g _{cat} ⁻¹]					H ₂ /CO ratio [-]	Amount of coke deposition ^c [g _{coke} g _{cat} ⁻¹]		
				H ₂	CH ₄	CO	CO ₂	C ₆ H ₆		Inlet	Middle	Outlet
				1	Ni-Fe/Mg/Al	0.1	100 ^a 45 ^b	423 391		70 7	145 110	111 91
2	Ni-Fe/Mg/Al	0.25	100 ^a 70 ^b	497 500	75 8	244 171	128 154	0 3	2.0 3.0	0.01	0.01	0.01
3	Ni-Fe/Mg/Al	0.5	97 ^a 80 ^b	610 555	13 0	295 207	52 98	2 9	2.1 2.7	0.01	0.01	0.01
4	Ni-Fe/ α -Al ₂ O ₃	0.25	70 ^a 19 ^b	448 163	2 0	153 47	73 45	3 1.2	3.0 3.6	0.00	0.01	0.06

Reaction conditions: $W_{cat} = 100$ mg; $W/F = 0.19$ g h mol⁻¹ (total feeding rate 517 mmol h⁻¹); Toluene/H₂O/N₂/CO₂ = 1.0/11.8/71.2/11.8; $T = 773$ K; reaction time, 300 min. S/C_{HC} = 1.7. ^a Initial: at 10-30 min, ^b Steady state: at 280-300 min, ^c After 300 min.

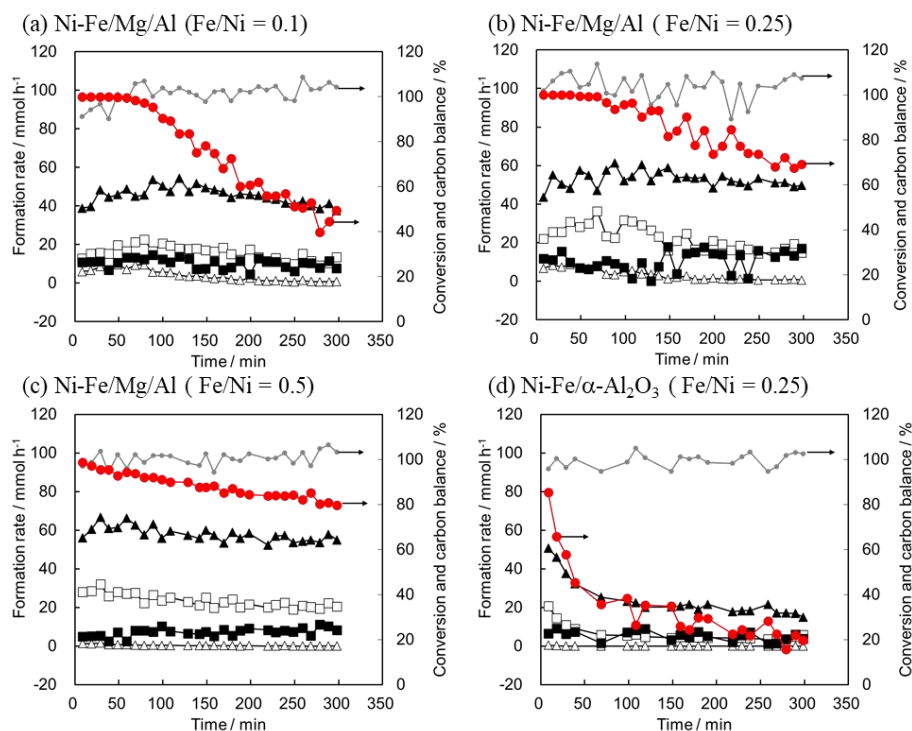


Figure 3.9 Time dependence of reforming of toluene over Ni-Fe/Mg/Al (Fe/Ni = 0.1, 0.25, 0.5) and Ni-Fe/ α -Al₂O₃ (Fe/Ni = 0.25) catalysts. (Detailed data of **Table 3.4**)

● (red circle): toluene conversion, ● (gray circle): carbon balance, ▲: H₂, △: CH₄, □: CO, ■: CO₂. Reaction conditions: $W_{cat} = 100$ mg; $W/F = 0.19$ g h mol⁻¹. reaction temperature, 773 K; reaction time, 300 min. $S/C_{HC} = 1.7$ (Toluene/H₂O/N₂/CO₂ = 1.0/11.8/71.2/11.8 (molar ratio)). Feeding rate: toluene, 6 mmol h⁻¹; steam, 65 mmol h⁻¹; N₂, 382 mmol h⁻¹; CO₂, 64 mmol h⁻¹.

The author compared the performance of Ni-Fe/Mg/Al (Fe/Ni = 0.25) catalyst with that of Ni-Fe/ α -Al₂O₃ (Fe/Ni = 0.25), which is a simple Ni-Fe catalyst prepared by co-impregnation. The activity of Ni-Fe/ α -Al₂O₃ was lower than Ni-Fe/Mg/Al with the same Ni and Fe amounts during all the reaction time. The deactivation of Ni-Fe/ α -Al₂O₃ was clearly more rapid. The amount of coke on the Ni-Fe/ α -Al₂O₃ at the outlet of the catalyst bed was higher than that on Ni-Fe/Mg/Al, while those on Ni-Fe/ α -Al₂O₃ at the inlet and middle of the catalyst bed were similarly very low to those on Ni-Fe/Mg/Al. The Ni-Fe/ α -Al₂O₃ catalyst seems to be vulnerable to coke deposition by CO disproportionation. From the data shown above, the author used Ni-Fe/Mg/Al (Fe/Ni = 0.25) catalyst in the following studies because of the high activity, stability, small coke amount and low selectivity to benzene.

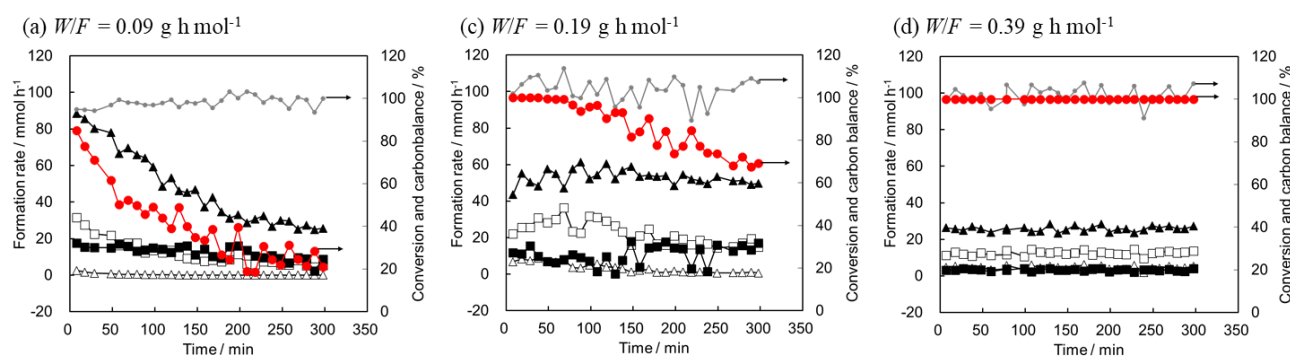
3.3.4. Effect of W/F

The results at different W/F values over Ni-Fe/Mg/Al (Fe/Ni = 0.25) are shown in **Table 3.5** and **Fig. 3.10**. The initial conversion at $W/F = 0.19$ and $0.39 \text{ g}_{\text{cat}} \text{ h mol}^{-1}$ was 100%, and that at $W/F = 0.09 \text{ g}_{\text{cat}} \text{ h mol}^{-1}$ was 78%. The deactivation was severer at lower W/F , although the coke amount at three positions was similar at all the W/F conditions. It should be noted that the formation rates of H_2 and CO per catalyst amount at 300 min were higher at $W/F = 0.19 \text{ g}_{\text{cat}} \text{ h mol}^{-1}$ than those at $W/F = 0.09$ and $0.39 \text{ g}_{\text{cat}} \text{ h mol}^{-1}$. The formation rates of H_2 and CO at $W/F = 0.09 \text{ g}_{\text{cat}} \text{ h mol}^{-1}$ after deactivation were similar to those over Ni/Mg/Al. This agreement suggests that the effect of addition of Fe to Ni/Mg/Al on activity was lost during deactivation, while the resistance to coke deposition of Ni-Fe/Mg/Al was still much higher than that of Ni/Mg/Al. The role of Fe in Ni-Fe alloy surface has been proposed to be the activation of H_2O to improve the activity and the supply of oxygen atom to suppress coke formation [49]. In addition, the Fe in Ni-Fe alloy was not oxidized because the Ni-Fe alloy peak after the reaction was not shifted. The author then inferred that the surface Fe site was blocked by some deposited species in the deactivated catalyst and tested the treatment of used catalyst with inert gas (N_2) to desorb the species as regeneration. After the used catalyst was treated with N_2 flow at 773 K, the reaction profile exhibited almost the same behavior as that of fresh catalyst (**Table 3.6** and **Fig. 3.11**). The structure change of Ni-Fe/Mg/Al catalyst during reaction and regeneration by N_2 flow was investigated by XRD (**Fig. 3.12**). Compared with the reduced fresh catalyst (before reaction), the intensity of (2 0 0) Ni-Fe alloy peak decreased after the 1st use (**Fig. 3.12 (a)**), while the peak position was hardly changed for all the positions of the catalyst bed, indicating that part of Ni-Fe alloy was oxidized. However, the decrease of XRD peak intensity was smaller than the decrease of activity, and most Ni-Fe alloy particles can be maintained after the deactivation. After the treatment with N_2 flow, the peak intensity gradually increased during the reuse, especially for the outlet of the catalyst bed. Considering that the activity decreased again during the reuse, the activity decrease during uses is mainly due to the adsorption of some species on the catalyst rather than the decrease of alloy phase by oxidation. The increase of the XRD peak in the regenerated catalyst during the reuse is probably due to the reduction by the synthesis gas formed in the upper (near inlet) position of the catalyst bed. However, as described later, deeply deactivated catalyst cannot be regenerated by the N_2 flow at 773 K. In addition, it is difficult to carry out this inert gas treatment in the engine of an automobile. The regeneration methods will be further discussed later.

Table 3.5 W/F dependence of the reforming of toluene with model EGR gas over Ni-Fe/Mg/Al (Fe/Ni = 0.25) catalyst

Entry	W/F [g _{cat} h mol ⁻¹]	Toluene conv. [%]	Average formation rate [mmol h ⁻¹ g _{cat} ⁻¹]					H ₂ /CO ratio [-]	Amount of coke deposition ^c [g _{coke} g _{cat} ⁻¹]		
			H ₂	CH ₄	CO	CO ₂	C ₆ H ₆		Inlet	Middle	Outlet
			1	0.09	78 ^a 24 ^b	848 259	17 0		272 50	160 67	7 3
2	0.19	100 ^a 70 ^b	497 500	75 8	244 171	128 154	0 3	2.0 3.0			
3	0.39	100 ^a 100 ^b	257 263	48 46	121 131	35 31	0 0	2.1 2.0			

Reaction conditions: $W_{\text{cat}} = 100$ mg; total feeding rate 1035 (Entry 1), 517 (Entry 2), 267 (Entry 3) mmol h⁻¹; Toluene/H₂O/N₂/CO₂ = 1.0/11.8/71.2/11.8; $T = 773$ K; reaction time, 300 min. $S/C_{\text{HC}} = 1.7$. ^a Initial: at 10-30 min, ^b Steady state: at 280-300 min, ^c After 300 min.

Figure 3.10 W/F dependence in the reforming of toluene with EGR gas over Ni-Fe/Mg/Al (Fe/Ni = 0.25) catalyst.

(Detailed data of Table 3.5)

● (red circle): toluene conversion, ● (gray circle): carbon balance, ▲: H₂, △: CH₄, □: CO, ■: CO₂. Reaction conditions: $W_{\text{cat}} = 100$ mg; $S/C_{\text{HC}} = 1.7$ (toluene/H₂O/N₂/CO₂ = 1.0/11.8/71.2/11.8 (molar ratio)), reaction temperature, 773 K; reaction time, 300 min. Feeding rate of (a): toluene 11 mmol h⁻¹, steam 131 mmol h⁻¹, N₂ 766 mmol h⁻¹, CO₂ 127 mmol h⁻¹. Feeding rate of (b): toluene 6 mmol h⁻¹, steam 65 mmol h⁻¹, N₂ 382 mmol h⁻¹, CO₂ 64 mmol h⁻¹. Feeding rate of (c): toluene 3 mmol h⁻¹, steam 33 mmol h⁻¹, N₂ 197 mmol h⁻¹, CO₂ 33 mmol h⁻¹. (b): After reduction of used catalyst.

Table 3.6 Reuse experiment of Ni-Fe/Mg/Al (Fe/Ni = 0.25) catalyst with N₂ treatment of used catalyst

Entry	Post-catalysis treatment	Toluene conv. [%]	Average formation rate [mmol h ⁻¹ g _{cat} ⁻¹]					H ₂ /CO ratio [-]	Amount of coke deposition ^c [g _{coke} g _{cat} ⁻¹]		
			H ₂	CH ₄	CO	CO ₂	C ₆ H ₆		Inlet	Middle	Outlet
			1	Fresh	78 ^a	848	17		272	160	7
		24 ^b	259	0	50	67	3	5.2	0.01	0.01	0.02
2	N ₂ flow ^d	67 ^a	863	11	310	133	6	2.8			
		26 ^b	324	0	81	77	3	4.1	0.01	0.01	0.01

Reaction conditions: $W_{\text{cat}} = 100$ mg; $W/F = 0.09$ g h mol⁻¹ (total feeding rate 1035 mmol h⁻¹); Toluene/H₂O/N₂/CO₂ = 1.0/11.8/71.2/11.8; $T = 773$ K; reaction time, 300 min. $S/C_{\text{HC}} = 1.7$. ^a Initial: at 10-30 min, ^b Steady state: at 280-300 min, ^c After 300 min, ^d N₂ flow (60 ml min⁻¹) at 773 K for 170 min.

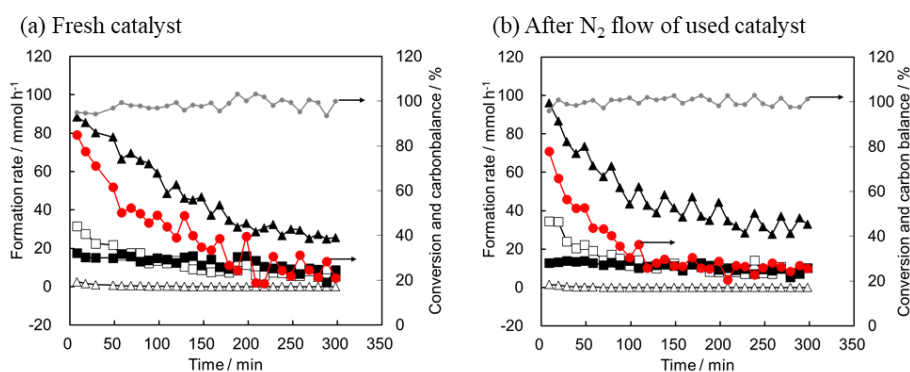


Figure 3.11 Effect of N₂ treatment of used catalyst on reforming of toluene with EGR gas over Ni-Fe/Mg/Al (Fe/Ni = 0.25) catalyst. (Detailed data of **Table 3.6**)

● (red circle): toluene conversion, ● (gray circle): carbon balance, ▲: H₂, △: CH₄, □: CO, ■: CO₂. Reaction conditions: $W_{\text{cat}} = 100$ mg; $W/F = 0.09$ g h mol⁻¹, $S/C_{\text{HC}} = 1.7$ (toluene/H₂O/N₂/CO₂ = 1.0/11.8/71.2/11.8 (molar ratio)); reaction temperature, 773 K; reaction time, 300 min. Feeding rate: toluene 11 mmol h⁻¹, steam 131 mmol h⁻¹, N₂ 766 mmol h⁻¹, CO₂ 127 mmol h⁻¹. Regeneration conditions: temperature, 773 K; N₂ 60 ml min⁻¹; feed time, 170 min.

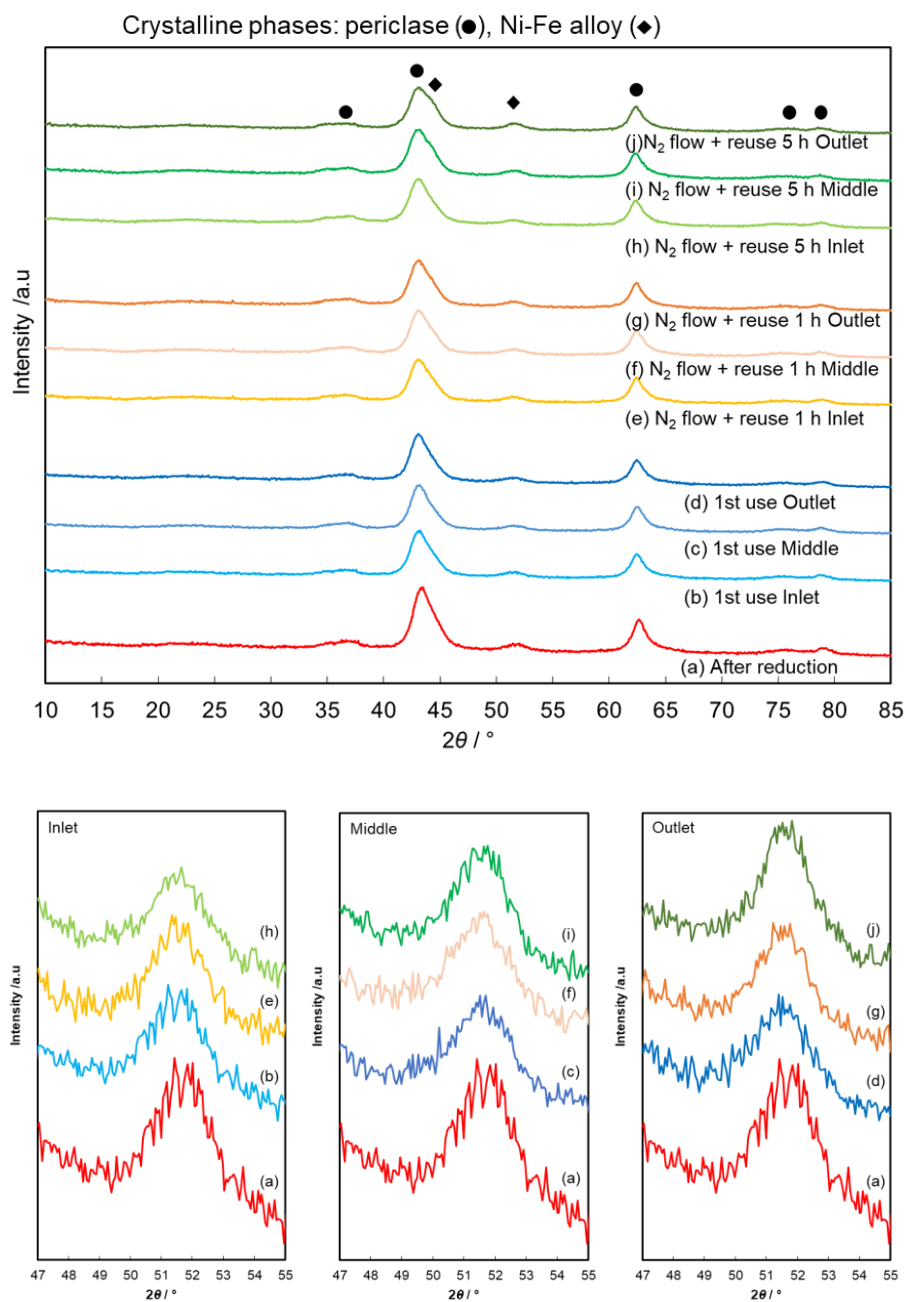


Figure 3.12 XRD patterns of Ni-Fe/Mg/Al (Fe/Ni = 0.25) after reduction, after use of fresh catalyst and after use of regenerated catalyst with N₂ flow in **Table 3.6**. Red lines: after reduction (a), Blue lines: after 1st use (b)-(d), Yellow/orange lines: after 1st use, N₂ treatment and 2nd use for 60 min (e)-(g), Green lines: after 1st use, N₂ treatment and 2nd use for 300 min (h)-(j).

3.3.5. Effect of reaction temperature

The temperature of the recirculating gas in EGR system is typically 573 – 773 K [12], which is clearly lower than the reaction temperature of the conventional steam reforming of hydrocarbons (873-1273 K) [33]. Here, the effect of reaction temperature on the catalysis of Ni-Fe/Mg/Al (Fe/Ni = 0.25) was investigated in the range of 673-873 K. **Table 3.7** shows the summary of results, and the detailed results including those at each time of stream are shown in **Fig. 3.13**. The toluene conversion at 673 K decreased from 42% to 5% during the first 100 min, and that at 773 K was kept almost 100% for the first 70 min and then decreased to 70% during 70-300 min. At 873 K, the toluene conversion was kept very high (>99%) during 300 min. In order to check whether high conversion can be obtained at 673 K with enough catalyst or not, the reaction test at higher W/F ($0.39 \text{ g}_{\text{cat}} \text{ h mol}^{-1}$) was carried out at 673 K. The initial toluene conversion was indeed increased from the case at $W/F = 0.19 \text{ g}_{\text{cat}} \text{ h mol}^{-1}$ (42% → 79%). However, at 300 min, the toluene conversion was much decreased (10%). It is difficult to compare such low conversion values because of the experimental errors in the analysis of unreacted toluene amount. Then the author compared the H_2 formation rates between the two runs. The H_2 formation rate per catalyst amount was lower in the case at $W/F = 0.39 \text{ g}_{\text{cat}} \text{ h mol}^{-1}$ than that at $W/F = 0.19 \text{ g}_{\text{cat}} \text{ h mol}^{-1}$, indicating that the catalyst was more severely deactivated at $W/F = 0.19 \text{ g}_{\text{cat}} \text{ h mol}^{-1}$. Based on the small increase in the H_2 formation rate with the increase of W/F , it seems to be difficult to obtain high toluene conversion at too low reaction temperature such as 673 K.

Table 3.7 Reaction temperature (T) dependence of the reforming of toluene with model EGR gas over Ni-Fe/Mg/Al (Fe/Ni = 0.25) catalyst

Entry	T [K]	W/F [g _{cat} h mol ⁻¹]	Toluene conv. [%]	Average formation rate [mmol h ⁻¹ g _{cat} ⁻¹]					H_2/CO ratio [-]	Amount of coke deposition ^c [g _{coke} g _{cat} ⁻¹]		
				H ₂	CH ₄	CO	CO ₂	C ₆ H ₆		Inlet	Middle	Outlet
				1	673	0.19	42	256		0	27	89
			5	85	0	12	80	1	10.6	0.01	0.02	0.01
2	673	0.39	79	219	9	32	34	3	6.8			
			10	50	0	3	-10	0	15.7	0.01	0.01	0.01
3	773	0.19	100	497	75	244	128	0	2.0			
			70	500	8	171	154	3	3.0	0.01	0.01	0.01
4	873	0.19	100	531	15	394	45	0	1.3			
			100	554	18	394	6	0	1.4	0.01	0.02	0.02

Reaction conditions: $W_{cat} = 100$ mg; $W/F = 0.19$ g h mol⁻¹, total feeding rate 517 mmol h⁻¹ (Entry 2: $W/F = 0.39$ g h mol⁻¹, total feeding rate 258 mmol h⁻¹); Toluene/H₂O/N₂/CO₂ = 1.0/11.8/71.2/11.8; $T = 673, 773$ or 873 K; reaction time, 300 min. $S/C_{HC} = 1.7$. ^a Initial: at 10-30 min, ^b Steady state: at 280-300 min, ^c After 300 min.

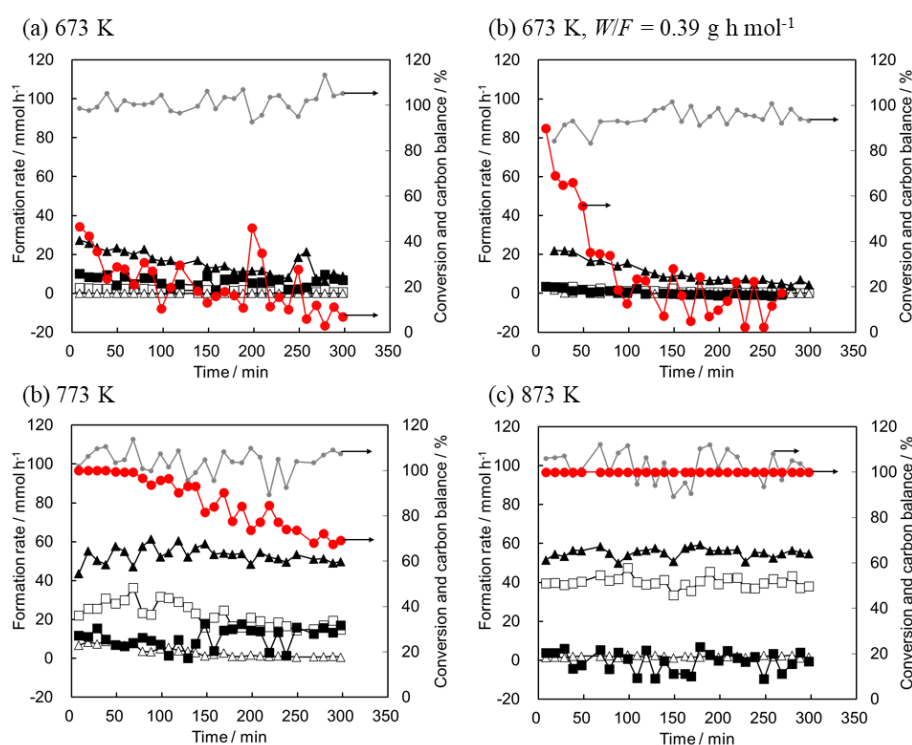


Figure 3.13 Reaction temperature dependence in the reforming of toluene with EGR gas over Ni-Fe/Mg/Al (Fe/Ni = 0.25) catalyst. (Detailed data of **Table 3.7**)

● (red circle): toluene conversion, ● (gray circle): carbon balance, ▲: H₂, △: CH₄, □: CO, ■: CO₂. Reaction conditions: $W_{cat} = 100$ mg; $W/F = 0.19$ g h mol⁻¹ (unless noted). reaction temperature, 673-873 K; reaction time, 300 min. $S/C_{HC} = 1.7$ (Toluene/H₂O/N₂/CO₂ = 1.0/11.8/71.2/11.8 (molar ratio)). Feeding rate: toluene, 6 ((b): 3) mmol h⁻¹; steam, 65 ((b): 33) mmol h⁻¹; N₂, 382 ((b): 191) mmol h⁻¹; CO₂, 64 ((b): 31) mmol h⁻¹.

3.3.6. Effect of feeding ratio of toluene to EGR gas

The composition in EGR gas (the ratio of $\text{H}_2\text{O}/\text{N}_2/\text{CO}_2$) cannot be changed under the stoichiometric combustion conditions in the engine. Only the concentration of the fuel can be changed in the feed of the reformer. In our previous paper, the effect of toluene concentration in the feed on the catalysis of Ni/Mg/Al was investigated in the model reaction of Reformed EGR [12]. Here, the author investigated the effect of toluene concentration in the feed on the catalysis of Ni-Fe/Mg/Al (Fe/Ni = 0.25). The results are shown in **Table 3.8** (summary) and **Fig. 3.14** (detailed results during the time on stream). The conversion of toluene at short reaction time was almost 100% at low toluene feed (toluene/ $\text{H}_2\text{O}/\text{N}_2/\text{CO}_2 = 0.5/11.8/71.2/11.8$, $0.8/11.8/71.2/11.8$), and the high conversion was kept during 300 min. The toluene conversion at longer reaction time began to decrease at the feed of toluene/ $\text{H}_2\text{O}/\text{N}_2/\text{CO}_2 = 1/11.8/71.2/11.8$, and the initial toluene conversion began to decrease at the feed of toluene/ $\text{H}_2\text{O}/\text{N}_2/\text{CO}_2 = 1.2/11.8/71.2/11.8$. At the feed of toluene/ $\text{H}_2\text{O}/\text{N}_2/\text{CO}_2 = 1.5/11.8/71.2/11.8$, the toluene conversion at 300 min was 20% and this value was almost the same as that over Ni/Mg/Al catalyst under the same reaction conditions [12]. The initial H_2 formation rate at 773 K became larger when the toluene feed was increased up to toluene/ $\text{H}_2\text{O}/\text{N}_2/\text{CO}_2 = 1/11.8/71.2/11.8$; however, it began to decrease with further increase of toluene feed because of the severer deactivation under higher concentration of toluene. The largest H_2 formation rate was obtained at the feed of toluene/ $\text{H}_2\text{O}/\text{N}_2/\text{CO}_2 = 1.2/11.8/71.2/11.8$ and $1/11.8/71.2/11.8$ at initial state and steady state, respectively. Although coke amount gradually increased with the increase of toluene feed, the coke amount was still much smaller on Ni-Fe/Mg/Al than that on Ni/Mg/Al (toluene/ $\text{H}_2\text{O}/\text{N}_2/\text{CO}_2 = 1.2/11.8/71.2/11.8$: $0.06 \text{ g}_{\text{coke}} \text{ g}_{\text{cat}}^{-1}$) [12]. In order to examine whether high conversion can be obtained or not at high toluene concentration, higher W/F was applied to the conditions of high toluene feed (toluene/ $\text{H}_2\text{O}/\text{N}_2/\text{CO}_2 = 1.5/11.8/71.2/11.8$). At $W/F = 0.58 \text{ g}_{\text{cat}} \text{ h mol}^{-1}$, which is 3 times higher than standard W/F , the initial toluene conversion reached 100%, and the toluene conversion at 300 min was 63% which was about 3 times higher than that obtained at standard W/F . Therefore, also in high toluene feed (toluene/ $\text{H}_2\text{O}/\text{N}_2/\text{CO}_2 = 1.5/11.8/71.2/11.8$), high toluene conversion can be obtained with enough amount of catalyst. This behavior is different from Ni/Mg/Al, where even at standard toluene concentration (toluene/ $\text{H}_2\text{O}/\text{N}_2/\text{CO}_2 = 1/11.8/71.2/11.8$) it is difficult to obtain high toluene conversion with a large amount of catalyst [12].

Table 3.8 Effect of toluene feed amount (toluene/H₂O/N₂/CO₂ = x/11.8/71.2/11.8) on the reforming of toluene with model EGR gas over Ni-Fe/Mg/Al (Fe/Ni = 0.25) catalyst

Entry	Feed ratio of toluene x [-]	W/F [g _{cat} h mol ⁻¹]	Toluene conv. [%]	Average formation rate [mmol h ⁻¹ g _{cat} ⁻¹]					H ₂ /CO ratio [-]	Amount of coke deposition ^c [g _{coke} g _{cat} ⁻¹]		
				H ₂	CH ₄	CO	CO ₂	C ₆ H ₆		Inlet	Middle	Outlet
1	0.5	0.19	100 ^a	295	8	81	58	0	3.6			
			100 ^b	366	12	107	71	0	3.4	0.01	0.01	0.01
2	0.8	0.19	100 ^a	438	44	164	108	0	2.7			
			98 ^b	493	36	199	95	0	2.5	0.00	0.01	0.01
3	1	0.19	100 ^a	497	75	244	128	0	2.0			
			70 ^b	500	8	171	154	3	3.0	0.01	0.01	0.01
4	1.2	0.19	92 ^a	706	39	218	170	2	3.3			
			30 ^b	324	0	44	109	3	7.2	0.01	0.01	0.01
5	1.5	0.19	65 ^a	562	23	249	-15	3	3.0			
			20 ^b	276	0	83	30	4	3.4	0.02	0.02	0.02
6	1.5	0.39	84 ^a	282	28	129	14	1	2.3			
			26 ^b	136	0	39	19	2	3.5	0.01	0.03	0.02
7	1.5	0.58	100 ^a	194	51	112	30	0	1.7			
			63 ^b	211	8	98	37	2	2.2	0.01	0.03	0.10

Reaction conditions: $W_{\text{cat}} = 100$ mg (Entry 4: 126 mg, Entry 6: 200 mg, Entry 7: 300 mg); feeding rate: toluene 3-11 mmol h⁻¹, steam+N₂+CO₂ 511 mmol h⁻¹ (Entry 4: 641 mmol h⁻¹); $T = 773$ K; reaction time, 300 min. S/C_{HC} = 0.8-3.4. ^a Initial: at 10-30 min, ^b Steady state: at 280-300 min, ^c After 300 min.

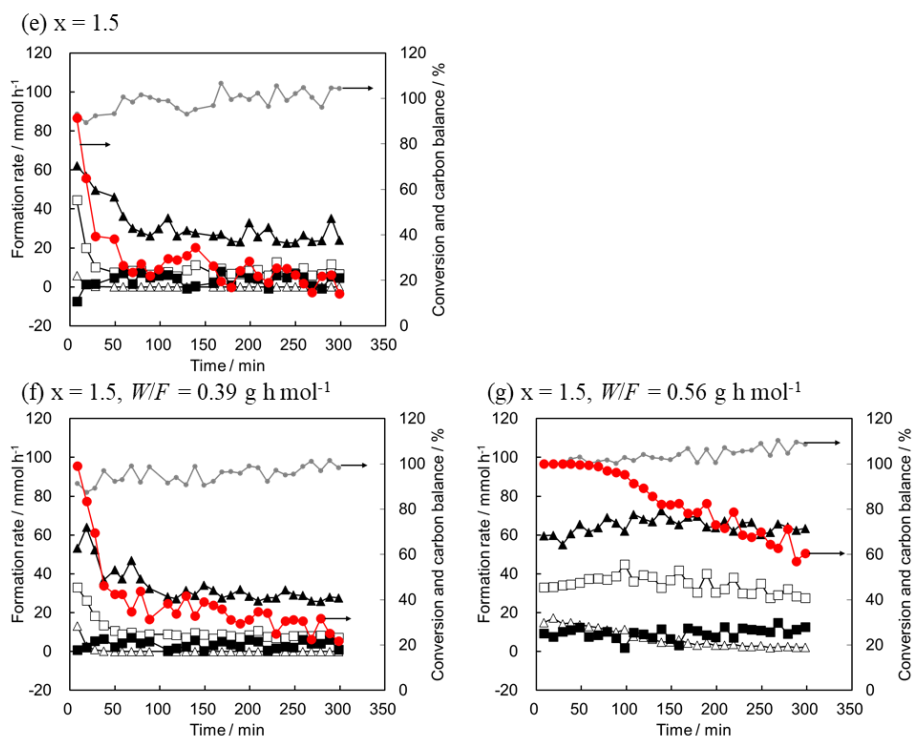


Figure 3.14 Effect of toluene feed amount (toluene/H₂O/N₂/CO₂ = x/11.8/71.2/11.8) on the reforming of toluene with model EGR gas over Ni-Fe/Mg/Al (Fe/Ni = 0.25) catalyst. (Detailed data of **Table 3.8**)

● (red circle): toluene conversion, ● (gray circle): carbon balance, ▲: H₂, △: CH₄, □; CO, ■; CO₂. Reaction conditions: $W_{\text{cat}} = 100$ mg ((d): 126 mg, (f): 200 mg, (g): 300 mg); feeding rate: toluene 3-11 mmol h⁻¹, steam 65 mmol h⁻¹ ((d): 82 mmol h⁻¹), N₂ 382 mmol h⁻¹ ((d): 480 mmol h⁻¹), CO₂ 64 mmol h⁻¹ ((d): 79 mmol h⁻¹); S/C_{HC} = 0.8-3.4; $W/F = 0.19$ g_{cat} h mol⁻¹ ((f): 0.39 g_{cat} h mol⁻¹, (g): 0.56 g_{cat} h mol⁻¹); reaction temperature, 773 K; reaction time, 300 min.

3.3.7. Regeneration of Ni-Fe/Mg/Al catalyst with various methods

In section 3.4, the author have demonstrated that the used Ni-Fe/Mg/Al (Fe/Ni = 0.25) catalyst under the standard conditions (toluene/H₂O/N₂/CO₂ = 1/11.8/71.2/11.8, 773 K) can be almost regenerated by the treatment with N₂ flow to desorb the organic species. However, the reduction degree of the reused catalyst was different from that of the fresh one. Here, the regeneration of the catalyst deactivated under severer conditions was investigated. First, the reaction was carried out at high toluene feed (toluene/H₂O/N₂/CO₂ = 1.5/11.8/71.2/11.8) for 150 min. The catalyst was treated with various conditions, and then the catalyst was reused under the standard reaction conditions (toluene/H₂O/N₂/CO₂ = 1.0/11.8/71.2/11.8). The results were shown in **Table 3.9** and **Figs. 3.15** and **3.16**. First, re-reduction with H₂/N₂ mixture at 1073 K (**Fig. 3.15** (g)), the same conditions for the fresh catalyst, was applied as

regeneration, which can totally remove the adsorbed organic molecules and reset the reduction degree of catalyst. The regenerated catalyst by reduction showed a similar behavior to the fresh one (**Fig. 3.15(h)**) (reaction time > 250 min).

Table 3.9 The various treatments for regeneration of used catalyst on reforming of toluene with model EGR gas over Ni-Fe/Mg/Al (Fe/Ni = 0.25) catalyst

Entry	Feed ratio of toluene [-]	Post-catalysis treatment	Toluene conv. [%]	Formation rate [mmol h ⁻¹ g _{cat} ⁻¹]					H ₂ /CO ratio [-]	Amount of coke deposition [g _{coke} g _{cat} ⁻¹]		
				H ₂	CH ₄	CO	CO ₂	C ₆ H ₆		Inlet	Middle	Outlet
1	1.5	N ₂ flow at 773 K	59 ^a	563	19	257	16	3	2.3			
			31 ^b	276	1	101	40	5	2.7			
	1		91 ^a	618	11	284	63	3	2.2			
			62 ^b	454	1	142	100	5	3.2	0.01	0.02	0.01
2	1.5	N ₂ flow at 873 K	95 ^a	648	106	327	70	2	2.0			
			35 ^b	419	4	151	80	4	3.0			
	1		100 ^a	580	51	272	87	0	2.1			
			94 ^b	634	18	259	99	2	2.4	0.01	0.01	0.01
3	1.5	EGR gas flow at 873 K	63 ^a	532	12	156	-59	5	3.8			
			34 ^b	326	2	77	-1	6	4.4			
	1		10 ^a	0	0	0	-104	0	-			
			0 ^b	0	0	0	-48	0	-	0.00	0.00	0.00
4	1.5	Steam flow at 873 K	64 ^a	527	13	204	-13	4	2.8			
			30 ^b	318	0	75	34	4	4.3			
	1		1 ^a	0	0	0	-87	0	-			
			7 ^b	0	0	0	-91	0	-	0.00	0.00	0.02
5	1.5	873 K reaction	86 ^a	595	58	273	48	2	2.2			
			32 ^b	297	0	86	45	4	3.6			
	1		90 ^a	580	13	237	105	2	2.5			
			75 ^b	490	4	171	94	3	2.9	0.00	0.00	0.02
6	1.5	973 K reaction	84 ^a	633	50	279	6	3	2.4			
			37 ^b	340	1	91	66	4	3.8			
	1		99 ^a	505	65	241	66	0	2.1			
			97 ^b	552	49	239	104	0	2.3	0.05	0.01	0.02

Catalytic performance of hydrotalcite-like-compound-derived Ni-metal alloy catalyst for toluene reforming with gasoline engine exhaust model gas as reforming agent

Entry	Feed ratio of toluene [-]	Post-catalysis treatment	Toluene conv. [%]	Formation rate [mmol h ⁻¹ g _{cat} ⁻¹]					H ₂ /CO ratio [-]	Amount of coke deposition [g _{coke} g _{cat} ⁻¹]		
				H ₂	CH ₄	CO	CO ₂	C ₆ H ₆		Inlet	Middle	Outlet
7	1.5	Reduction	76 ^a	584	49	281	17	3	2.1			
			18 ^b	282	1	113	41	3	3.4			
	1		99 ^a	507	78	246	72	0	2.1			
			95 ^b	538	56	236	98	1	2.3	0.01	0.01	0.02

Reaction conditions: $W_{\text{cat}} = 100$ mg; feeding rate: toluene 8 (1st), 6 (2nd) mmol h⁻¹, steam 65 mmol h⁻¹, N₂ 382 mmol h⁻¹, CO₂ 64 mmol h⁻¹; S/C_{HC} = 1.1 (1st), 1.7 (2nd); $W/F = 0.19$ g_{cat} h mol⁻¹; toluene/H₂O/N₂/CO₂ = 1.5 (1st), 1.0 (2nd)/11.8/71.2/11.8, reaction temperature, 773 K; reaction time, 150 + 150 min, Regeneration conditions: (Entry 1) N₂ flow (30 ml min⁻¹) at 773 K for 90 min; (Entry 2) N₂ flow (30 ml min⁻¹) at 873 K for 30 min; (Entry 3) EGR gas flow (steam 65 mmol h⁻¹, N₂ 382 mmol h⁻¹, CO₂ 64 mmol h⁻¹) at 873 K for 30 min; (Entry 4) steam flow (steam 65 mmol h⁻¹, N₂ 382 mmol h⁻¹) at 873 K for 30 min; (Entry 5) reactant feed (toluene/H₂O/N₂/CO₂ = 1.0/11.8/71.2/11.8) for 30 min at 873 K; (Entry 6) reactant feed (toluene/H₂O/N₂/CO₂ = 1.0/11.8/71.2/11.8) for 30 min at 973 K; (Entry 7) reduction (1073 K, 30 min, H₂/N₂ = 30 ml min⁻¹/30 ml min⁻¹). ^a Initial: at 10-30 or 160-180 min, ^b Steady state: at 130-150 or 280-300 min, ^c After reaction.

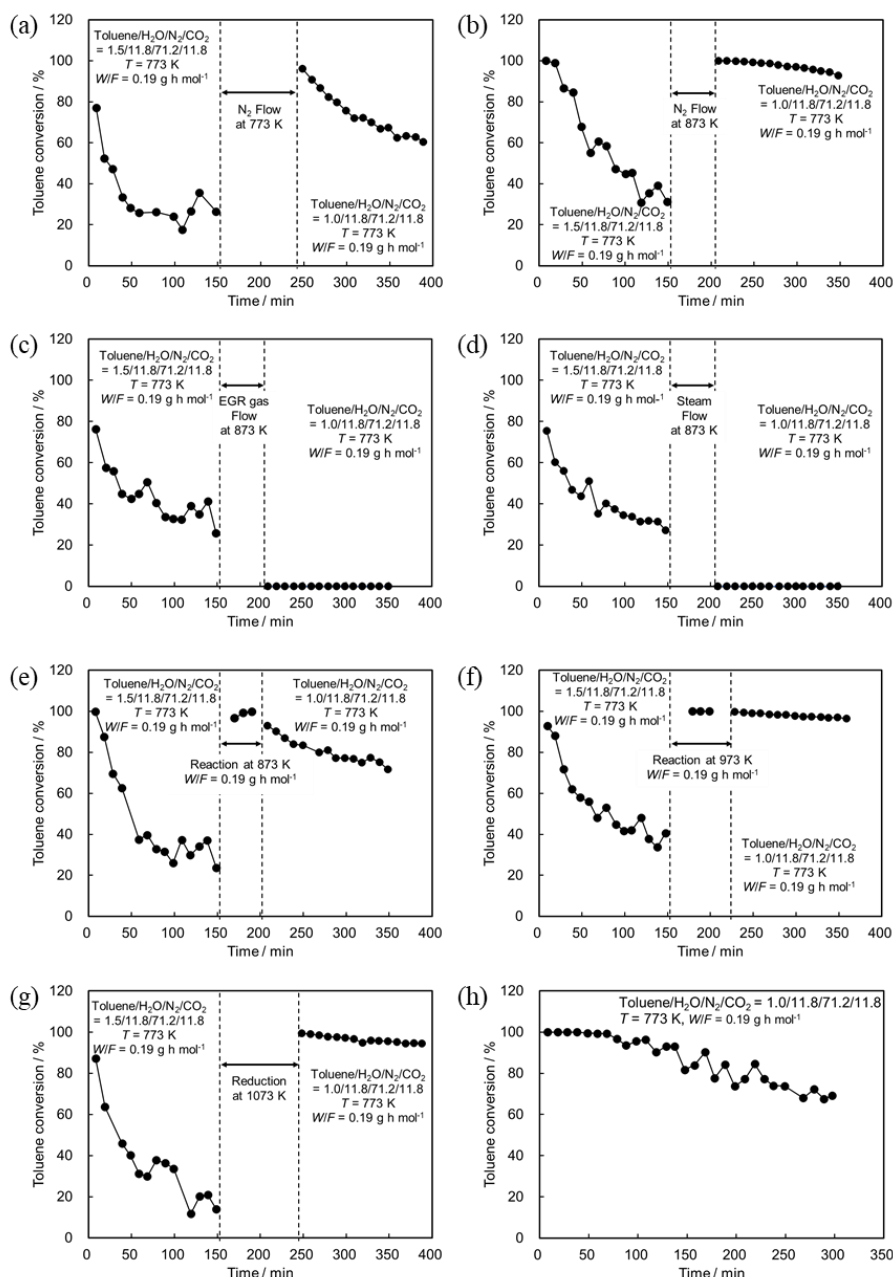


Figure 3.15 Effect of various treatments for regeneration of used Ni-Fe/Mg/Al (Fe/Ni = 0.25) catalyst. Formation rate of each product is show in **Fig. 3.16**.

Reaction conditions: $W_{\text{cat}} = 100$ mg; feeding rate: toluene 8 (1st), 6 (2nd) mmol h^{-1} , steam 65 mmol h^{-1} , N_2 382 mmol h^{-1} , CO_2 64 mmol h^{-1} ; $S/C_{\text{HC}} = 1.1$ (1st), 1.7 (2nd); $W/F = 0.19$ g cat h mol^{-1} ; toluene/ $\text{H}_2\text{O}/\text{N}_2/\text{CO}_2 = 1.5$ (1st) or 1.0 (2nd)/11.8/71.2/11.8, $T = 773$ K; reaction time, 150 (1st) + 150 (2nd) min. Regeneration conditions: (a) N_2 flow (30 ml min^{-1}) at 773 K for 90 min; (b) N_2 flow (30 ml min^{-1}) at 873 K for 30 min; (c) EGR gas flow (steam 65 mmol h^{-1} , N_2 382 mmol h^{-1} , CO_2 64 mmol h^{-1}) at 873 K for 30 min; (d) reactant feed (toluene/ $\text{H}_2\text{O}/\text{N}_2/\text{CO}_2 = 1.0/11.8/71.2/11.8$) for 30 min at 873 K; (e) reactant feed (toluene/ $\text{H}_2\text{O}/\text{N}_2/\text{CO}_2 = 1.0/11.8/71.2/11.8$) for 30 min at 973 K; (f) reduction (1073 K, 30 min, $\text{H}_2/\text{N}_2 = 30$ $\text{ml min}^{-1}/30$ ml min^{-1}), (g) standard condition (773 K, $t = 300$ min, toluene/ $\text{H}_2\text{O}/\text{N}_2/\text{CO}_2 = 1.0/11.8/71.2/11.8$).

Catalytic performance of hydrotalcite-like-compound-derived Ni-metal alloy catalyst for toluene reforming with gasoline engine exhaust model gas as reforming agent

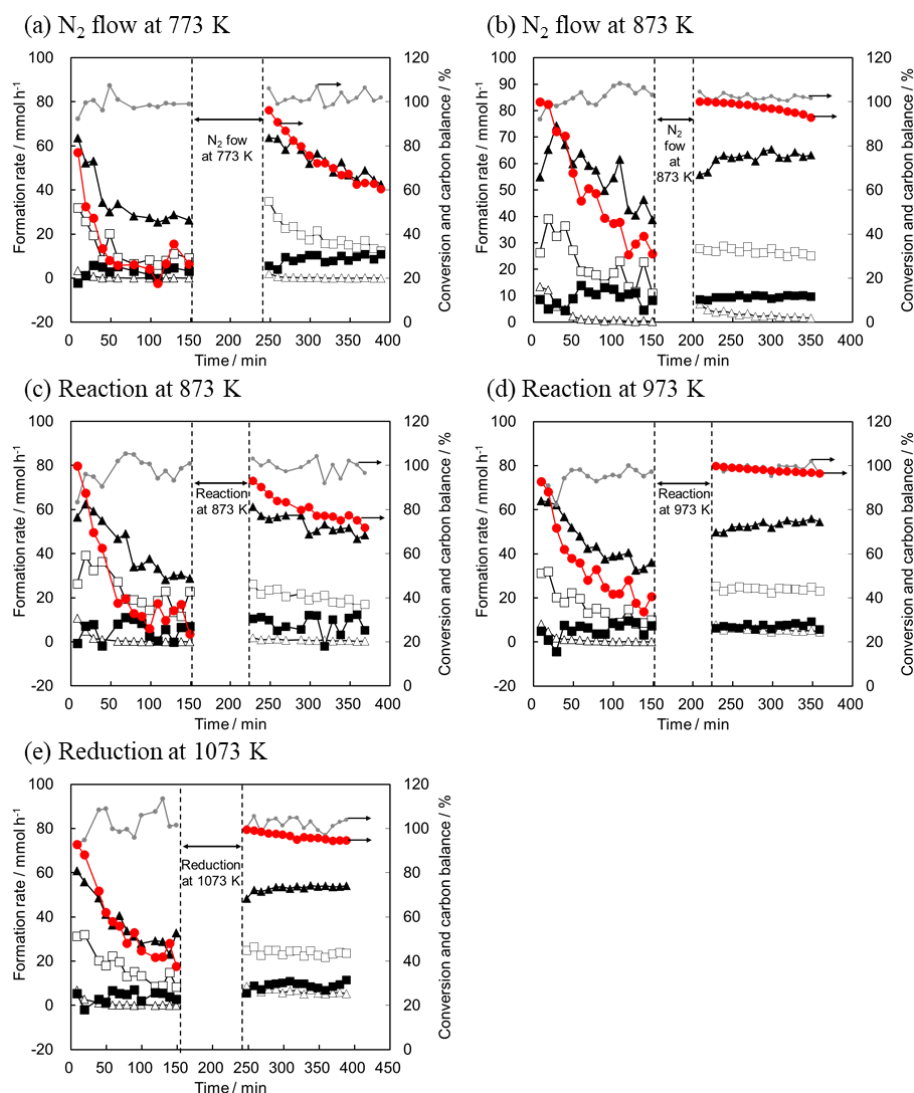


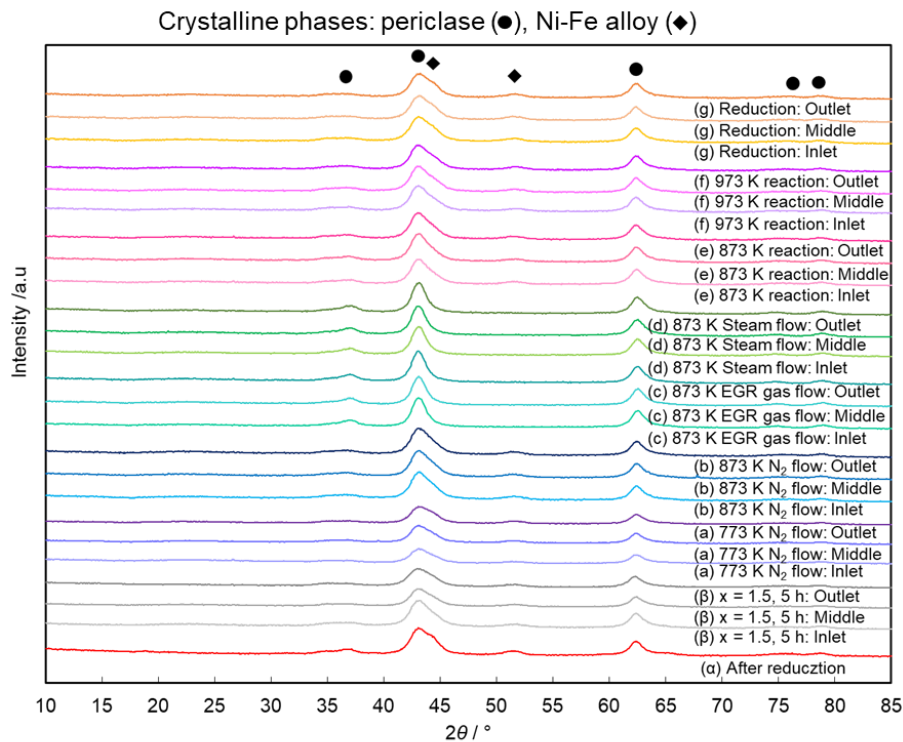
Figure 3.16 Effect of various treatments for regeneration of used Ni-Fe/Mg/Al (Fe/Ni = 0.25) catalyst. (Detailed data of Fig. 3.15)

● (red circle): toluene conversion, ● (gray circle): carbon balance, ▲: H₂, △: CH₄, □: CO, ■: CO₂. Reaction conditions: $W_{\text{cat}} = 100$ mg; feeding rate: toluene 8 (1st), 6 (2nd) mmol h⁻¹, steam 65 mmol h⁻¹, N₂ 382 mmol h⁻¹, CO₂ 64 mmol h⁻¹; S/C_{HC} = 1.1 (1st), 1.7 (2nd); W/F = 0.19 g_{cat} h mol⁻¹; toluene/H₂O/N₂/CO₂ = 1.5 (1st), 1.0 (2nd)/11.8/71.2/11.8, reaction temperature, 773 K; reaction time, 150 + 150 min, Regeneration conditions: (a) N₂ flow (30 ml min⁻¹) at 773 K for 90 min; (b) N₂ flow (30 ml min⁻¹) at 873 K for 30 min; (c) EGR gas flow (steam 65 mmol h⁻¹, N₂ 382 mmol h⁻¹, CO₂ 64 mmol h⁻¹) at 873 K for 30 min; (d) reactant feed (toluene/H₂O/N₂/CO₂ = 1.0/11.8/71.2/11.8) for 30 min at 873 K; (e) reactant feed (toluene/H₂O/N₂/CO₂ = 1.0/11.8/71.2/11.8) for 30 min at 973 K; (f) reduction (1073 K, 30 min, H₂/N₂ = 30 ml min⁻¹/30 ml min⁻¹), (g) standard condition (773 K, t = 300 min, toluene/H₂O/N₂/CO₂ = 1.0/11.8/71.2/11.8).

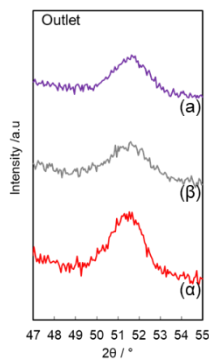
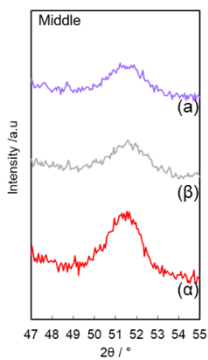
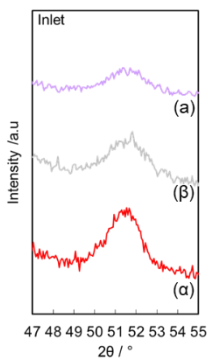
Next, the N₂ flow at 773 K was applied (**Fig. 3.15 (a)**), which was used in section 3.4 for the deactivated catalyst under the standard reaction conditions. However, the regenerated catalyst decreased the conversion more rapidly, indicating that the activity was not recovered completely. On the other hand, when the temperature for N₂ flow was raised to 873 K (**Fig. 3.15 (b)**), the reaction profile of the regenerated catalyst became almost the same as the fresh one (**Fig. 3.15 (h)**). The species deposited under the conditions of higher toluene feed are more difficult to be removed. However, it is difficult to flow inert gas to the catalyst bed in the real engine system of automobiles. Then, the author tested the model EGR gas (toluene/H₂O/N₂/CO₂ = 0/11.8/71.2/11.8) flow at 873 K as the regeneration of deactivated catalyst (**Fig. 3.15 (c)**). The catalyst after this treatment showed no activity. The color of catalyst after the treatment and reaction was returned from black to yellow-green, which is the same color as that of the calcined catalyst, indicating that the Ni-Fe alloy was oxidized with the model EGR gas. Next, the author tested the reactions at high temperatures as the regeneration of the deactivated catalyst. When the deactivated catalyst was used for the reaction under the conditions of toluene/H₂O/N₂/CO₂ = 1.0/11.8/71.2/11.8 at 873 K for 30 min (**Fig. 3.15 (e)**), the activity surely increased, although not completely recovered. The activity in the reuse was similar to the catalyst used under the standard conditions for 150 min. When the reaction temperature for regeneration was raised to 973 K (**Fig. 3.15 (f)**), the activity was totally recovered to the fresh catalyst. Therefore, the deactivated catalyst can be regenerated by the reaction at higher temperature, which can be relatively easily carried out in the real engine system.

The XRD patterns of the reused catalysts in the runs for **Fig. 3.15** were measured to investigate the effect of treatments in the catalyst structure (**Fig. 3.17**). The XRD patterns of the fresh reduced catalyst and used catalyst under the conditions of toluene/H₂O/N₂/CO₂ = 1.5/11.8/71.2/11.8 at 773 K for 5 h (essentially the same for the first stage of the reaction before regeneration) are also shown. When the activity of the used catalyst was regenerated (N₂ flow at 873 K, reaction at 973 K and reduction), the Ni-Fe peak intensity increased during the reuse, especially for the outlet of the catalyst bed. As discussed in section 3.4, the activity decrease during reactions was mainly due to the adsorption of some species on the catalyst rather than the decrease of Ni-Fe alloy phase by oxidation, although total oxidation of the metal phase surely loses the activity. The increase of the XRD peak in the regenerated catalysts during the reuse can be due to the reduction by the synthesis gas formed in the upper (near inlet) position of the catalyst bed.

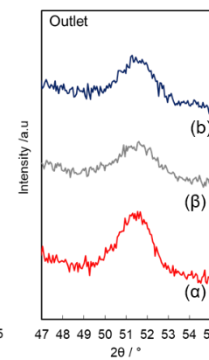
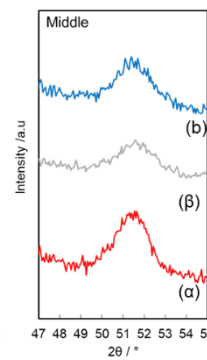
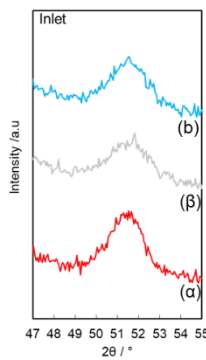
Catalytic performance of hydrotalcite-like-compound-derived Ni-metal alloy catalyst for toluene reforming with gasoline engine exhaust model gas as reforming agent



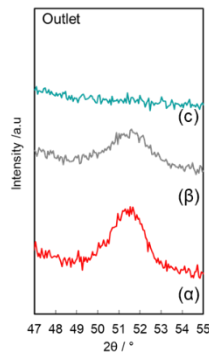
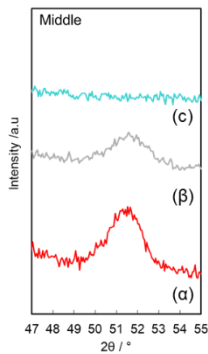
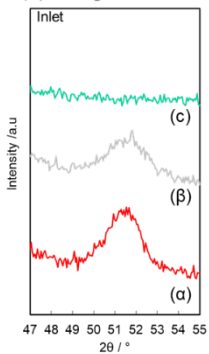
(i) N₂ flow at 773 K



(ii) N₂ flow at 873 K



(iii) EGR gas flow at 873 K



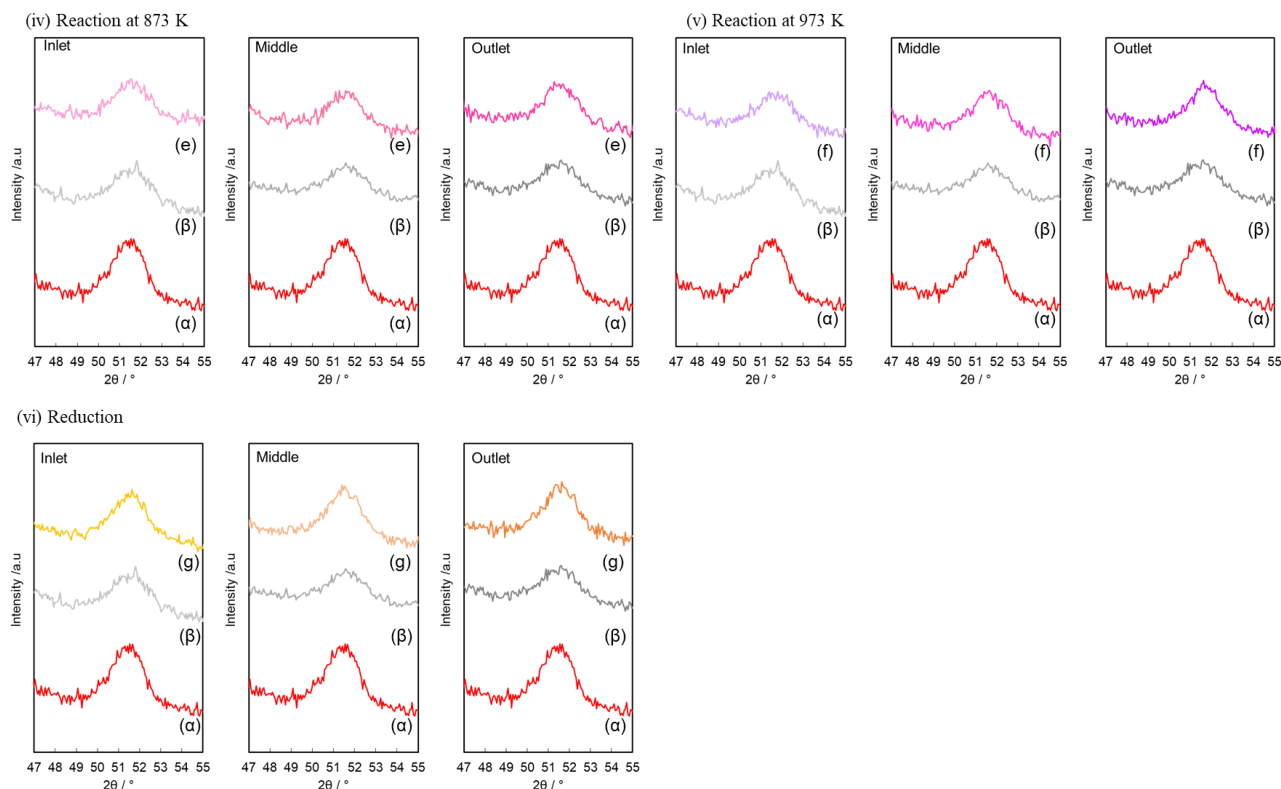


Figure 3.17 XRD patterns of Ni-Fe/Mg/Al (Fe/Ni = 0.25) after reduction, after reaction of fresh catalyst and after reaction of regenerated catalyst with reduction in **Figs. 3.15 and 3.16**. Red lines: after reduction, Gray lines: after reaction of fresh (Toluene/H₂/N₂/CO₂ = 1.5/11.8/71.2/11.8, t = 300 min), Blue-purple lines: after reaction of regenerated catalyst with N₂ flow at 773 K, Blue lines: after reaction of regenerated catalyst with N₂ flow at 873 K, Blue-green lines: after reaction of regenerated catalyst with EGR gas flow at 873 K, Green lines: after reaction of regenerated catalyst with steam flow at 873 K, Pink lines: after reaction of regenerated catalyst with reaction at 873 K, Red-purple lines: after reaction of regenerated catalyst with reaction at 973 K, Orange lines: after reaction of regenerated catalyst with reduction at 1073 K.

Three regeneration methods, N₂ flow at 873 K, model EGR gas flow at 873 K and reaction at 973 K, were also applied to Ni/Mg/Al and Ni-Fe/ α -Al₂O₃ catalysts for comparison (**Tables 3.10 and 3.11, Figs. 3.18 and 3.19**). For both catalysts, the activity recovered slightly, but not completely, by N₂ flow. Treatment with model EGR gas completely deactivated the catalysts as was the Ni-Fe/Mg/Al catalyst. On the other hand, the activity was almost recovered by the use in the reaction at 973 K. In the XRD patterns of catalysts after treatment with N₂ flow or reaction as regeneration, the Ni or Ni-Fe peak intensity increased during the reuse, especially for the outlet of the catalyst bed (**Figs. 3.22 and 3.23**). This behavior on XRD was similar to the case of Ni-Fe/Mg/Al catalyst. Therefore, both the N₂ flow treatment and catalytic use of high temperature can regenerate Ni-based catalysts. While high temperature

reaction can almost totally regenerate all the tested catalysts (Ni/Mg/Al, Ni-Fe/Mg/Al and Ni-Fe/ α -Al₂O₃), the treatment with N₂ flow is only very effective in Ni-Fe/Mg/Al catalyst. Because N₂ flow cannot remove the deposited coke, the high coke deposition resistance of Ni-Fe/Mg/Al can be related to the effectiveness of N₂ flow treatment.

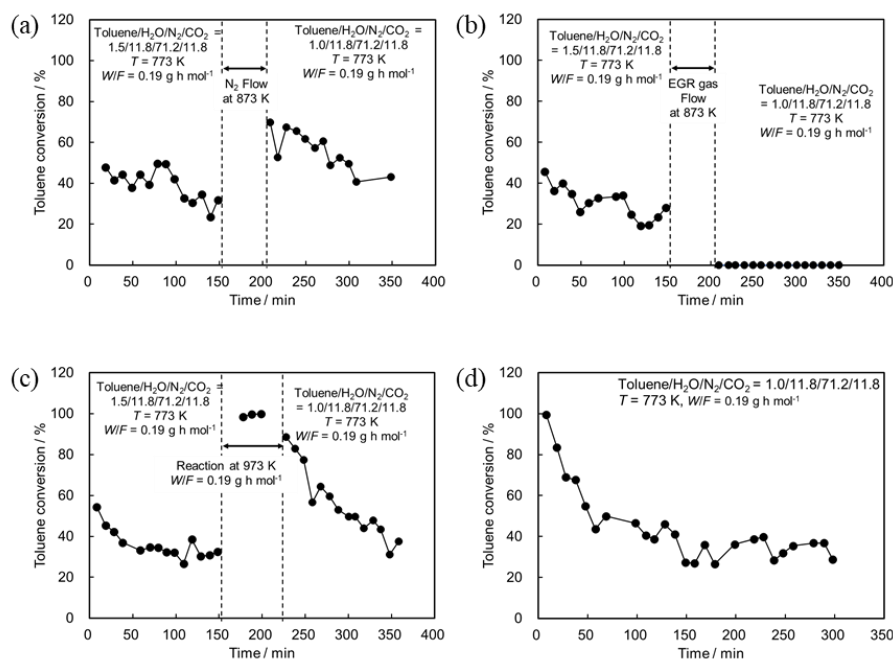


Figure 3.18 Effect of various treatments for regeneration of used Ni/Mg/Al catalyst. (Detailed data of **Table 3.10**). Formation rate of each product is show in **Fig. 3.20**.

Reaction conditions: $W_{\text{cat}} = 100$ mg; feeding rate: toluene 8 (1st), 6 (2nd) mmol h⁻¹, steam 65 mmol h⁻¹, N₂ 382 mmol h⁻¹, CO₂ 64 mmol h⁻¹; S/C_{HC} = 1.1 (1st), 1.7 (2nd); $W/F = 0.19$ g_{cat} h mol⁻¹; toluene/H₂O/N₂/CO₂ = 1.5 (1st) or 1.0 (2nd)/11.8/71.2/11.8, $T = 773$ K; reaction time, 150 + 150 min. Regeneration conditions: (Entry 1) N₂ flow (30 ml min⁻¹) at 873 K for 30 min; (Entry 2) EGR gas flow (steam 65 mmol h⁻¹, N₂ 382 mmol h⁻¹, CO₂ 64 mmol h⁻¹) at 873 K for 30 min; (Entry 3) reactant feed (toluene/H₂O/N₂/CO₂ = 1.0/11.8/71.2/11.8) for 30 min at 973 K.

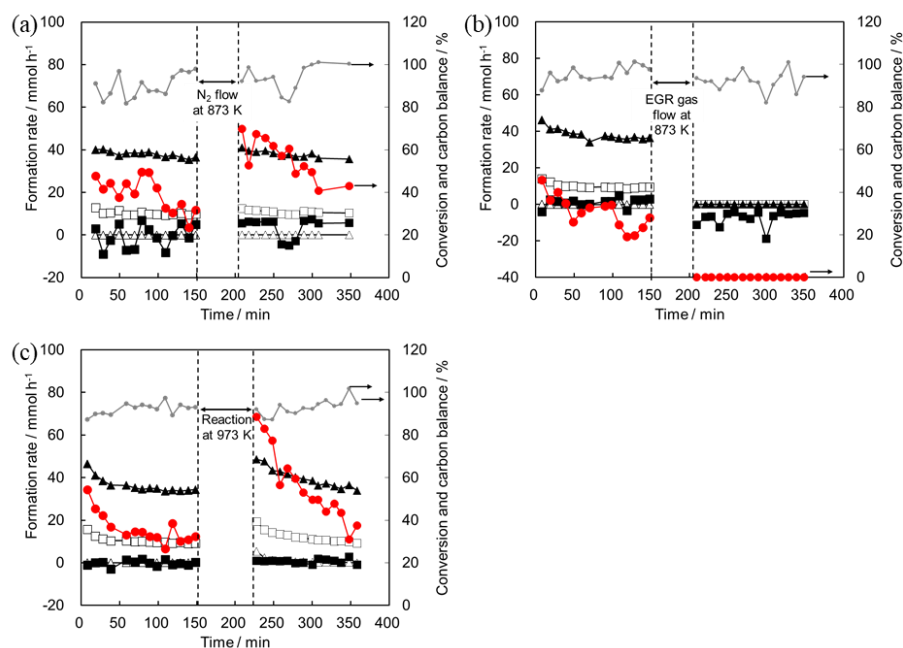


Figure 3.20 Effect of various treatments for regeneration of used Ni/Mg/Al catalyst. (Detailed data of **Table 3.10**)

● (red circle): toluene conversion, ● (gray circle): carbon balance, ▲: H₂, △: CH₄, □; CO, ■; CO₂.

Reaction conditions: $W_{\text{cat}} = 100$ mg; feeding rate: toluene 8 (1st), 6 (2nd) mmol h⁻¹, steam 65 mmol h⁻¹, N₂ 382 mmol h⁻¹, CO₂ 64 mmol h⁻¹; S/C_{HC} = 1.1 (1st), 1.7 (2nd); $W/F = 0.19$ g_{cat} h mol⁻¹; toluene/H₂O/N₂/CO₂ = 1.5 (1st), 1.0 (2nd)/11.8/71.2/11.8, reaction temperature, 773 K; reaction time, 150 + 150 min, Regeneration conditions: (a) N₂ flow (30 ml min⁻¹) at 873 K for 30 min; (b) EGR gas flow (steam 65 mmol h⁻¹, N₂ 382 mmol h⁻¹, CO₂ 64 mmol h⁻¹) at 873 K for 30 min; (c) reactant feed (toluene/H₂O/N₂/CO₂ = 1.0/11.8/71.2/11.8) for 30 min at 973 K.

Catalytic performance of hydrotalcite-like-compound-derived Ni-metal alloy catalyst for toluene reforming with gasoline engine exhaust model gas as reforming agent

Table 3.10 The various treatments for regeneration of used catalyst on reforming of toluene with model EGR gas over Ni/Mg/Al catalyst

Entry	Feed ratio of toluene	Post-catalysis treatment	Toluene conv. [%]	Formation rate [mmol h ⁻¹ g _{cat} ⁻¹]					H ₂ /CO ratio [-]	Carbon balance [%]	Amount of coke deposition [g _{coke} g _{cat} ⁻¹]		
				H ₂	CH ₄	CO	CO ₂	C ₆ H ₆			Inlet	Middle	Outlet
1	1.5	N ₂ flow at 873 K	45	401	0	116	-30	2	3.5	87			
			30	361	0	99	30	2	3.6	97			
	1		63	399	0	118	59	2	3.4	94			
			43	303	0	104	57	2	3.4	100	0.08	0.06	0.15
2	1.5	EGR gas flow at 873 K	41	430	0	123	1	2	3.5	92			
			24	364	0	94	27	2	3.9	100			
	1		-2	0	0	0	-83	0	-	93			
			4	0	0	0	-49	0	-	94	0.00	0.00	0.00
3	1.5	973 K reaction	47	420	0	132	-2	2	3.2	89			
			51	390	18	125	1	2	3.4	93			
	1		72	446	16	143	7	1	3.1	90			
			33	352	1	95	9	2	3.7	98	0.06	0.08	0.07

Reaction conditions: $W_{\text{cat}} = 100$ mg; feeding rate: toluene 8 (1st), 6 (2nd) mmol h⁻¹, steam 65 mmol h⁻¹, N₂ 382 mmol h⁻¹, CO₂ 64 mmol h⁻¹; S/C_{HC} = 1.1 (1st), 1.7 (2nd); $W/F = 0.19$ g_{cat} h mol⁻¹; toluene/H₂O/N₂/CO₂ = 1.5 (1st), 1.0 (2nd)/11.8/71.2/11.8, reaction temperature, 773 K; reaction time, 150 + 150 min, Regeneration conditions: (Entry 1) N₂ flow (30 ml min⁻¹) at 873 K for 30 min; (Entry 2) EGR gas flow (steam 65 mmol h⁻¹, N₂ 382 mmol h⁻¹, CO₂ 64 mmol h⁻¹) at 873 K for 30 min; (Entry 3) reactant feed (toluene/H₂O/N₂/CO₂ = 1.0/11.8/71.2/11.8) for 30 min at 973 K. ^a Initial: at 10-30 or 160-180 min, ^b Steady state: at 130-150 or 280-300 min, ^c After reaction.

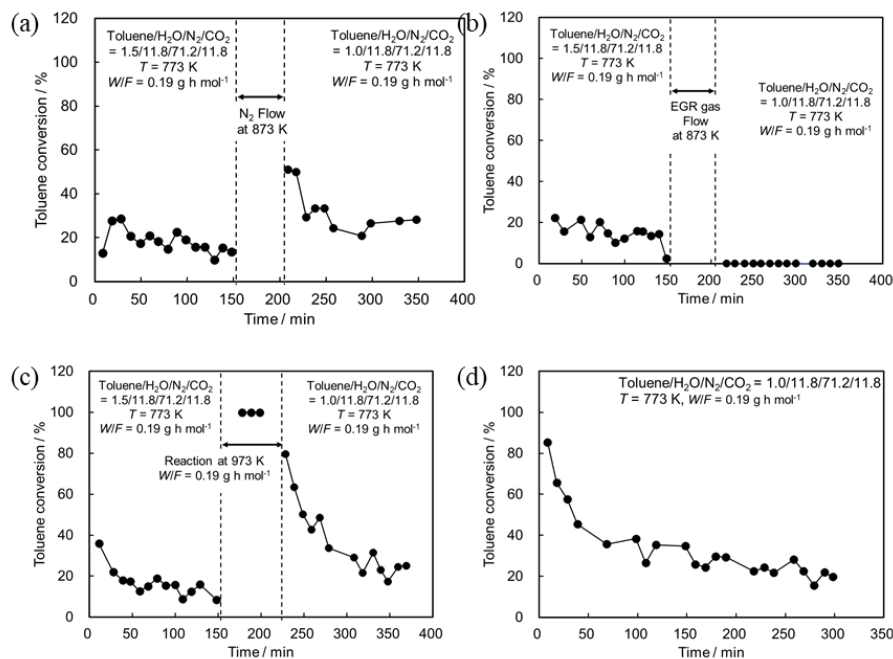


Figure 3.19 Effect of various treatments for regeneration of used Ni-Fe/ α -Al₂O₃ (Fe/Ni = 0.25) catalyst. (Detailed data of **Table 3.11**). Formation rate of each product is show in **Fig. 3.21**.

Reaction conditions: $W_{\text{cat}} = 100$ mg; feeding rate: toluene 8 (1st), 6 (2nd) mmol h⁻¹, steam 65 mmol h⁻¹, N₂ 382 mmol h⁻¹, CO₂ 64 mmol h⁻¹; S/C_{HC} = 1.1 (1st), 1.7 (2nd); $W/F = 0.19$ g_{cat} h mol⁻¹; toluene/H₂O/N₂/CO₂ = 1.5 (1st), 1.0 (2nd)/11.8/71.2/11.8, $T = 773$ K; reaction time, 150 + 150 min, Regeneration conditions: (Entry 1) N₂ flow (30 ml min⁻¹) at 873 K for 30 min; (Entry 2) EGR gas flow (steam 65 mmol h⁻¹, N₂ 382 mmol h⁻¹, CO₂ 64 mmol h⁻¹) at 873 K for 30 min; (Entry 3) reactant feed (toluene/H₂O/N₂/CO₂ = 1.0/11.8/71.2/11.8) for 30 min at 973 K. ^a Initial: at 10-30 or 160-180 min, ^b Steady state: at 130-150 or 280-300 min, ^c After reaction.

Catalytic performance of hydrotalcite-like-compound-derived Ni-metal alloy catalyst for toluene reforming with gasoline engine exhaust model gas as reforming agent

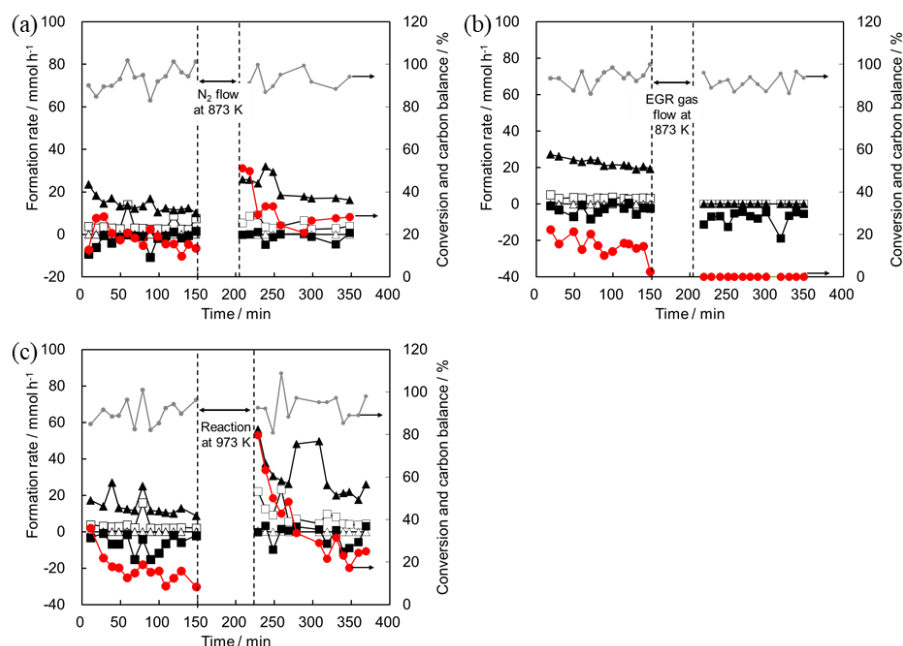


Figure 3.21 Effect of various treatments for regeneration of used Ni-Fe/ α -Al₂O₃ (Fe/Ni = 0.25) catalyst. (Detailed data of **Table 3.11**)

● (red circle): toluene conversion, ● (gray circle): carbon balance, ▲: H₂, △: CH₄, □: CO, ■: CO₂.

Reaction conditions: $W_{\text{cat}} = 100$ mg; feeding rate: toluene 8 (1st), 6 (2nd) mmol h⁻¹, steam 65 mmol h⁻¹, N₂ 382 mmol h⁻¹, CO₂ 64 mmol h⁻¹; S/C_{HC} = 1.1 (1st), 1.7 (2nd); $W/F = 0.19$ g_{cat} h mol⁻¹; toluene/H₂O/N₂/CO₂ = 1.5 (1st), 1.0 (2nd)/11.8/71.2/11.8, reaction temperature, 773 K; reaction time, 150 + 150 min, Regeneration conditions: (a) N₂ flow (30 ml min⁻¹) at 873 K for 30 min; (a) EGR gas flow (steam 65 mmol h⁻¹, N₂ 382 mmol h⁻¹, CO₂ 64 mmol h⁻¹) at 873 K for 30 min; (c) reactant feed (toluene/H₂O/N₂/CO₂ = 1.0/11.8/71.2/11.8) for 30 min at 973 K.

Table 3.11 The various treatments for regeneration of used catalyst on reforming of toluene with model EGR gas over Ni-Fe/ α -Al₂O₃ (Fe/Ni = 0.25) catalyst

Entry	Feed ratio of toluene [-]	Post-catalysis treatment	Toluene conv. [%]	Formation rate [mmol h ⁻¹ g _{cat} ⁻¹]					H ₂ /CO ratio [-]	Carbon balance [%]	Amount of coke deposition [g _{coke} g _{cat} ⁻¹]		
				H ₂	CH ₄	CO	CO ₂	C ₆ H ₆			Inlet	Middle	Outlet
1	1.5	N ₂ flow at 873 K	23 ^a	188	1	35	-53	1	5.3	88			
			13 ^b	114	0	41	-1	0	3.9	97			
	1		43 ^a	252	0	77	3	2	3.5	93			
			22 ^b	154	0	29	-16	1	5.5	93	0.01	0.03	0.03
2	1.5	EGR gas flow at 873 K	19 ^a	268	0	41	-20	2	6.8	93			
			10 ^b	196	0	33	-32	1	6.0	96			
	1		0 ^a	0	0	0	-85	0	-	92			
			0 ^b	0	0	0	-72	0	-	92	0.00	0.00	0.00
3	1.5	973 K reaction	29 ^a	156	0	34	-20	2	4.6	88			
			12 ^b	109	0	22	-39	1	5.0	93			
	1		64 ^a	415	3	146	-23	1	3.0	89			
			22 ^b	218	0	40	-39	1	5.5	92	0.00	0.01	0.03

Reaction conditions: $W_{\text{cat}} = 100$ mg; feeding rate: toluene 8 (1st), 6 (2nd) mmol h⁻¹, steam 65 mmol h⁻¹, N₂ 382 mmol h⁻¹, CO₂ 64 mmol h⁻¹; S/C_{HC} = 1.1 (1st), 1.7 (2nd); $W/F = 0.19$ g_{cat} h mol⁻¹; toluene/H₂O/N₂/CO₂ = 1.5 (1st), 1.0 (2nd)/11.8/71.2/11.8, reaction temperature, 773 K; reaction time, 150 + 150 min, Regeneration conditions: (Entry 1) N₂ flow (30 ml min⁻¹) at 873 K for 30 min; (Entry 2) EGR gas flow (steam 65 mmol h⁻¹, N₂ 382 mmol h⁻¹, CO₂ 64 mmol h⁻¹) at 873 K for 30 min; (Entry 3) reactant feed (toluene/H₂O/N₂/CO₂ = 1.0/11.8/71.2/11.8) for 30 min at 973 K. ^a Initial: at 10-30 or 160-180 min, ^b Steady state: at 130-150 or 280-300 min, ^c After reaction.

Catalytic performance of hydrotalcite-like-compound-derived Ni-metal alloy catalyst for toluene reforming with gasoline engine exhaust model gas as reforming agent

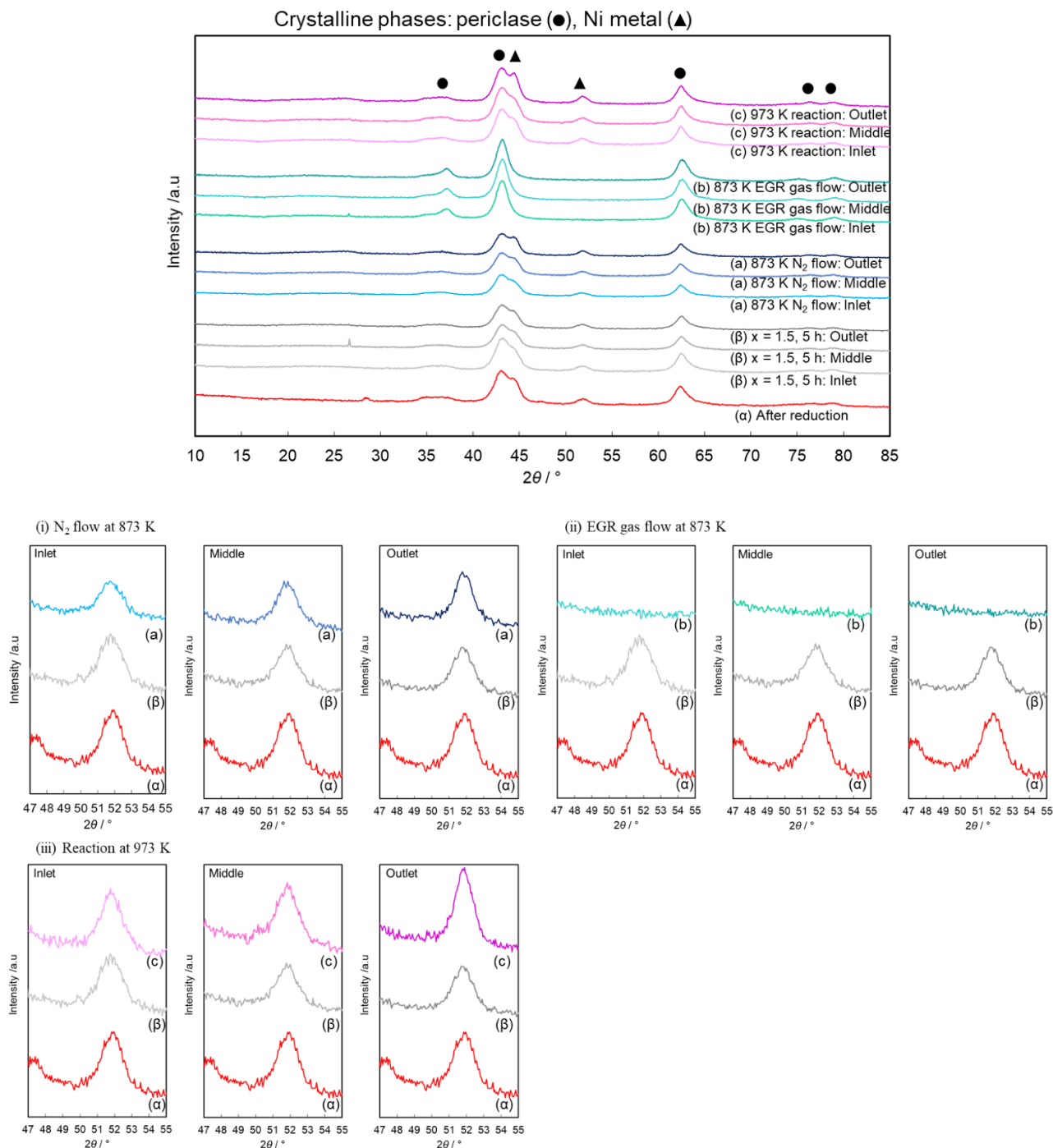


Figure 3.22 XRD pattern of Ni /Mg/Al after reduction, after the various treatments for regeneration of used catalyst on reforming of toluene with model EGR gas in **Table 3.10**. Red lines: after reduction, Gray lines: after reaction of fresh (Toluene/ H_2 / N_2 / CO_2 = 1.5/11.8/71.2/11.8, t = 300 min), Blue lines: after reaction of regenerated catalyst with N_2 flow at 873 K, Blue-green lines: after reaction of regenerated catalyst with EGR gas flow at 873 K, Red-purple lines: after reaction of regenerated catalyst with reaction at 973 K.

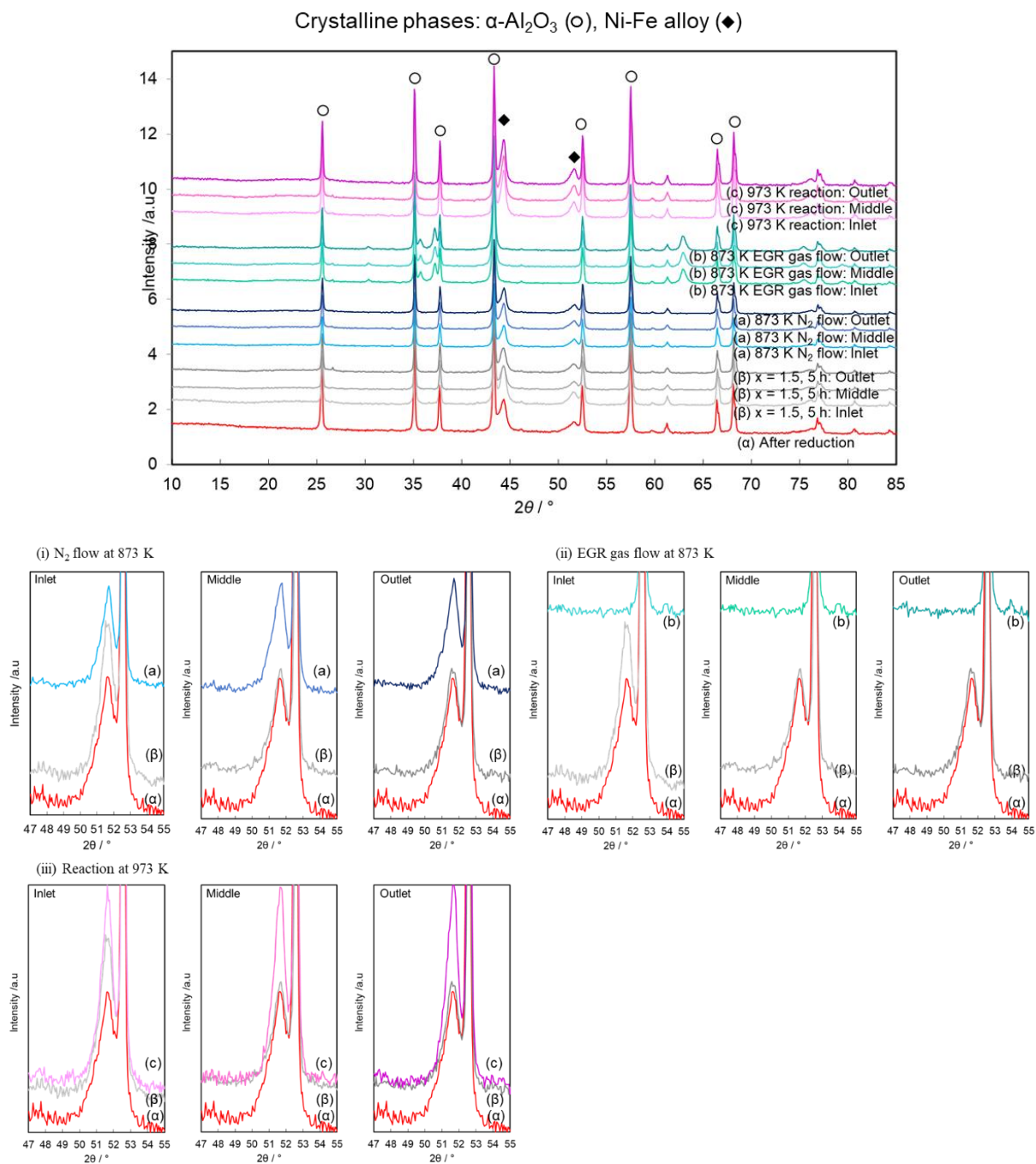


Figure 3.23 XRD pattern of Ni /Mg/Al after reduction, after the various treatments for regeneration of used catalyst on reforming of toluene with model EGR gas in **Table 3.11**. Red lines: after reduction, Gray lines: after reaction of fresh (Toluene/H₂/N₂/CO₂ = 1/11.8/71.2/11.8, t = 300 min), Blue lines: after reaction of regenerated catalyst with N₂ flow at 873 K, Blue-green lines: after reaction of regenerated catalyst with EGR gas flow at 873 K, Red-purple lines: after reaction of regenerated catalyst with reaction at 973 K.

3.4. Conclusions

1. In the reforming of toluene with diluted CO₂ and H₂O in N₂ as model reaction of Reformed EGR, the addition of Fe to Ni/Mg/Al catalyst prepared from the hydrotalcite-like compound improves toluene conversion and resistance to coke deposition. The optimized Fe/Ni ratio is 0.25 in views of decomposition of aromatic ring to synthesis gas. The additions of Co or Cu are less effective.
2. Ni-Fe/Mg/Al catalyst gradually loses activity during time on steam especially at short contact time (*W/F*) or at low reaction temperature. It is difficult to obtain high conversion at low reaction temperature even at longer contact time. Nevertheless, the amount of deposited coke is very small in such conditions.
3. Similar to Ni/Mg/Al, Ni-Fe/Mg/Al catalyst shows higher conversion and slower deactivation at low toluene/EGR gas ratio. However, even at high toluene/EGR gas ratio the conversion can be increased by increase of contact time on Ni-Fe/Mg/Al catalyst, while Ni/Mg/Al catalyst is difficult to increase the toluene conversion by increase of contact time.
4. The deactivated Ni-Fe/Mg/Al catalyst recovered the activity by N₂ treatment at 873 K, catalytic use at 973 K, or re-reduction. The removal of adsorbed organic species by these treatments probably causes the recovery of activity. The treatment of EGR gas without toluene rather deactivates the catalyst, which is due to the total oxidation of metal phase.
5. Ni/Mg/Al and Ni-Fe/ α -Al₂O₃ catalysts can be also regenerated by N₂ treatment or catalytic use at high temperature, to some extent. However, the effectiveness of N₂ treatment is lower than the case of Ni-Fe/Mg/Al catalyst. The very low amount of coke, which is difficult to remove with N₂ flow, on Ni-Fe/Mg/Al can be related to the effectiveness.

Acknowledgments

JSPS (KAKENHI 18H05247) and JST financially supported this work.

References

- [1] L. Tartakovsky, M. Sheintuch, Fuel reforming in internal combustion engines, *Prog. Energy Combust. Sci.*,

- 2018, 67, 88-114. <https://doi.org/10.1016/j.pecs.2018.02.003>
- [2] S. Golunski, What is the point of on-board fuel reforming?, *Energy Environ. Sci.*, 2010, 3, 1918–1923. <https://doi.org/10.1039/c0ee00252f>
- [3] V. Chintala, D. Banaerjee, P. K. Ghodke, E. Porpatham, Hydrogen rich exhaust gas recirculation (H₂EGR) for performance improvement and emissions reduction of a compression ignition engine, *Int. J. Hydrogen Energy*, 2019, 44, 18545-18558. <https://doi.org/10.1016/j.ijhydene.2019.05.141>
- [4] S. R. Gomes, N. Bion, D. Duprez, F. Epron, Hydrogen production from hydrocarbons over Rh supported on Ce-based oxides for automotive applications, *Appl. Catal. B: Environ.*, 2016, 197, 138-145. <https://doi.org/10.1016/j.apcatb.2016.01.022>
- [5] S. Peucheret, M. Feaviour, S. Golunski, Exhaust-gas reforming using precious metal catalysts, *Appl. Catal. B: Environ.*, 2006, 65, 201-206. <https://doi.org/10.1016/j.apcatb.2006.01.009>
- [6] J. Thormann, L. Maier, P. Pfeifer, U. Kunz, O. Dautschmann, K. Schubert, Steam reforming of hexadecane over a Rh/CeO₂ catalyst in microchannels: Experimental and numerical investigation, *Int. J. Hydrogen Energy*, 2009, 34, 5108-5120. <https://doi.org/10.1016/j.ijhydene.2009.04.031>
- [7] Nissan Motor Co., Ltd., Fuel reforming catalyst and method of using the same, JP2001-170486.
- [8] A. Tsolakis, A. Megaritis, Partially premixed charge compression ignition engine with on-board H₂ production by exhaust gas fuel reforming of diesel and biodiesel, *Int. J. Hydrogen Energy*, 2005, 30, 731-745. <https://doi.org/10.1016/j.ijhydene.2004.06.013>
- [9] D. W. Brookshear, J. A. Pihl, J. P. Szybist, Catalytic Steam and Partial Oxidation Reforming of Liquid Fuels for Application in Improving the Efficiency of Internal Combustion Engines, *Energy Fuels*, 2018, 32, 2267-2281. <https://doi.org/10.1021/acs.energyfuels.7b02576>
- [10] S. R. Gomes, N. Bion, G. Blanchard, S. Rousseau, V. Bellière-Baca, V. Harlé, D. Duprez, F. Epron, Thermodynamic and experimental studies of catalytic reforming of exhaust gas recirculation in gasoline engines, *Appl. Catal. B: Environ.*, 2011, 102, 44-53. <https://doi.org/10.1016/j.apcatb.2010.11.023>
- [11] S. Rijo Gomes, N. Bion, G. Blanchard, S. Rousseau, D. Duprez, F. Epron, Study of the main reactions involved in reforming of exhaust gas recirculation (REGR) in gasoline engines, *RSC Adv.*, 2011, 1, 109-116.

<https://doi.org/10.1039/c1ra00003a>

- [12] M. Betchaku, Y. Nakagawa, M. Tamura, K. Tomishige, Reforming of toluene with simulated automobile exhaust gas over hydrotalcite-like-compound-derived Ni catalyst, *Fuel Process. Technol.*, 2020, 209, 106545. <https://doi.org/10.1016/j.fuproc.2020.106545>
- [13] I. Barbarias, G. Lopez, M. Amutio, M. Artetxe, J. Alvarez, A. Arregi, J. Bilbao, M. Olazar, Steam reforming of plastic pyrolysis model hydrocarbons and catalyst deactivation, *Appl. Catal. A: Gen.*, 2016, 527, 152-160. <https://doi.org/10.1016/j.apcata.2016.09.003>
- [14] T. Higo, T. Hashimoto, D. Mukai, S. Nagatake, S. Ogo, Y. Sugiura, Y. Sekine, Effect of Hydrocarbon Structure on Steam Reforming over Ni/perovskite Catalyst, *J. Jpn. Petrol. Inst.*, 2015, 58, 86-96. <https://doi.org/10.1627/jpi.58.86>
- [15] G. Guan, M. Kaewpanha, X. Hao, A. Abudula, Catalytic steam reforming of biomass tar: Prospects and challenges, *Renew. Sust. Energ. Rev.*, 2016, 58, 450-461. <https://doi.org/10.1016/j.rser.2015.12.316>
- [16] D. G. Ju, S. B. Jo, D. S. Ha, T. Y. Kim, S. Y. Jung, H. J. Chae, S. C. Lee, J. C. Kim, Enhanced Ni-Al-Based Catalysts and Influence of Aromatic Hydrocarbon for Autothermal Reforming of Diesel Surrogate Fuel, *Catalysts*, 2019, 9, 573. <https://doi.org/10.3390/catal9070573>
- [17] A. Jess, Mechanisms and kinetics of thermal reactions of aromatic hydrocarbons from pyrolysis of solid fuels, *Fuel*, 1996, 75, 144101448. [https://doi.org/10.1016/0016-2361\(96\)00136-6](https://doi.org/10.1016/0016-2361(96)00136-6)
- [18] S. R. de la Rama, S. Kawai, H. Yamada, and T. Tagawa, Preliminary Assessment of Oxidation Pretreated Hastelloy as Hydrocarbon Steam Reforming Catalyst, *J. Catal.*, 2014, 210371. <http://doi.org/10.1155/2014/210371>
- [19] G. Chen, X. Zhang, Z. Mi, Effects of pressure on coke and formation of its precursors during catalytic cracking of toluene over USY catalyst, *J. Fuel Chem. Technol.*, 2007, 35, 211-216. [https://doi.org/10.1016/S1872-5813\(07\)60018-8](https://doi.org/10.1016/S1872-5813(07)60018-8)
- [20] J. Ashok, N. Dewangan, S. Das, P. Hongmanorom, M. H. Wai, K. Tomishige, S. Kawi, Recent progress in the development of catalysts for steam reforming of biomass tar model reaction, *Fuel Process. Technol.*, 2020, 199, 106252. <https://doi.org/10.1016/j.fuproc.2019.106252>

- [21] B. Dou, H. Zhang, Y. Song, L. Zhao, B. Jiang, M. He, C. Ruan, H. Chen, Y. Xu, Hydrogen production from the thermochemical conversion of biomass: issues and challenges, *Sustain. Energy Fuels*, 2019, 3, 314-342. <https://doi.org/10.1039/c8se00535d>
- [22] M. Mosinska, M. I. Szyrkowska, P. Mierczynski, Oxy-Steam Reforming of Natural Gas on Ni Catalysts - A Minireview, *Catalysts*, 2020, 10, 896. <https://doi.org/10.3390/catal10080896>
- [23] S. Bepari, D. Kuila, Steam reforming of methanol, ethanol and glycerol over nickel-based catalysts - A review, *Int. J. Hydrogen Energy*, 2020, 45, 18090-18113. <https://doi.org/10.1016/j.ijhydene.2019.08.003>
- [24] T. K. Phung, T. L. M. Pham, A.-N. T. Nguyen, K. B. Vu, H. N. Giang, T.-A. Nguyen, T. C. Huynh, H. D. Pham, Effect of Supports and Promoters on the Performance of Ni-Based Catalysts in Ethanol Steam Reforming, *Chem. Eng. Technol.*, 2020, 43, 672-688. <https://doi.org/10.1002/ceat.201900445>
- [25] U. Sikander, S. Sufian, M. A. Salam, A review of hydrotalcite based catalysts for hydrogen production systems, *Int. J. Hydrogen Energy*, 2017, 42, 19851-19868. <https://doi.org/10.1016/j.ijhydene.2017.06.089>
- [26] D. Li, Y. Nakagawa, K. Tomishige, Development of Ni-Based Catalysts for Steam Reforming of Tar Derived from Biomass Pyrolysis, *Chin. J. Catal.*, 2012, 33, 583-594. [https://doi.org/10.1016/S1872-2067\(11\)60359-8](https://doi.org/10.1016/S1872-2067(11)60359-8)
- [27] Y. Mukainakano, B. Li, S. Kado, T. Miyazawa, K. Okumura, T. Miyao, S. Naito, K. Kunimori, K. Tomishige, Surface modification of Ni catalysts with trace Pd and Rh for oxidative steam reforming of methane, *Appl. Catal. A: Gen.*, 2007, 318, 252-264. <https://doi.org/10.1016/j.apcata.2006.11.017>
- [28] K. Nakamura, T. Miyazawa, T. Sakurai, T. Miyao, S. Naito, N. Begum, K. Kunimori, K. Tomishige, Promoting effect of MgO addition to Pt/Ni/CeO₂/Al₂O₃ in the steam gasification of biomass, *Appl. Catal. B: Environ.*, 2009, 86, 36-44. <https://doi.org/10.1016/j.apcatb.2008.07.016>
- [29] J. Nishikawa, T. Miyazawa, K. Nakamura, M. Asadullah, K. Kunimori, K. Tomishige, Promoting effect of Pt addition to Ni/CeO₂/Al₂O₃ catalyst for steam gasification of biomass, *Catal. Commun.*, 2008, 9, 195-201. <https://doi.org/10.1016/j.catcom.2007.05.045>
- [30] M. Nurunnabi, Y. Mukainakano, S. Kado, B. Li, K. Kunimori, K. Suzuki, K. Fujimoto, K. Tomishige, Additive effect of noble metals on NiO-MgO solid solution in oxidative steam reforming of methane under atmospheric and pressurized conditions, *Appl. Catal. A: Gen.*, 2006, 299, 145-156.

<https://doi.org/10.1016/j.apcata.2005.10.020>

- [31] B. Li, S. Kado, Y. Mukainakano, M. Nurunnabi, T. Miyao, S. Naito, K. Kunimori, K. Tomishige, Temperature profile of catalyst bed during oxidative steam reforming of methane over Pt-Ni bimetallic catalysts, *Appl. Catal. A: Gen.*, 2006, 304, 62-71. <https://doi.org/10.1016/j.apcata.2006.02.025>
- [32] J. Chen, M. Tamura, Y. Nakagawa, K. Okumura, K. Tomishige, Promoting effect of trace Pd on hydrotalcite-derived Ni/Mg/Al catalyst in oxidative steam reforming of biomass tar, *Appl. Catal. B: Environ.*, 2015, 179, 412-421. <https://doi.org/10.1016/j.apcatb.2015.05.042>
- [33] V. Claude, J. G. Mahy, S. Douven, S. L. Pirard, C. Courson, S. D. Lambert, Ni- and Fe-doped γ -Al₂O₃ or olivine as primary catalyst for toluene reforming, *Mater. Today Chem.*, 2019, 14, 100197. <https://doi.org/10.1016/j.mtchem.2019.100197>
- [34] F. L. Yang, J. P. Cao, X. Y. Zhao, J. Ren, W. Tang, X. Huang, X. B. Feng, M. Zhao, X. Cui, X. Y. Wei, Acid washed lignite char supported bimetallic Ni-Co catalyst for low temperature catalytic reforming of corncob derived volatiles, *Energy Convers. Manag.*, 2019, 196, 1257-1266. <https://doi.org/10.1016/j.enconman.2019.06.075>
- [35] M. Koike, D. Li, Y. Nakagawa, and K. Tomishige, A Highly Active and Coke-Resistant Steam Reforming Catalyst Comprising Uniform Nickel-Iron Alloy Nanoparticles, *ChemSusChem*, 2012, 5, 2312-2314. <https://doi.org/10.1002/cssc.201200507>
- [36] M. Koike, D. Li, H. Watanabe, Y. Nakagawa, K. Tomishige, Comparative study on steam reforming of model aromatic compounds of biomass tar over Ni and Ni-Fe alloy nanoparticles, *Appl. Catal. A: Gen.*, 2015, 506, 151-162. <https://doi.org/10.1016/j.apcata.2015.09.007>
- [37] U. Oemar, P. S. Ang, K. Hidajat, S. Kawi, Promotional effect of Fe on perovskite LaNi_xFe_{1-x}O₃ catalyst for hydrogen production via steam reforming of toluene, *Int. J. Hydrogen Energy*, 2013, 38, 5525-5534. <https://doi.org/10.1016/j.ijhydene.2013.02.083>
- [38] T. Ahmed, S. Xiu, L. Wang, A. Shahbazi, Investigation of Ni/Fe/Mg zeolite-supported catalysts in steam reforming of tar using simulated-toluene as model compound, *Fuel*, 2018, 211, 566-571. <https://doi.org/10.1016/j.fuel.2017.09.051>

- [39] F. Zhou, N. Pan, H. Chen, X. Xu, C. Wang, Y. Du, Y. Guo, Z. Zeng, L. Li, Hydrogen production through steam reforming of toluene over Ce, Zr or Fe promoted Ni-Mg-Al hydrotalcite-derived catalysts at low temperature, *Energy Convers. Manag.*, 2019, 196, 677-687. <https://doi.org/10.1016/j.enconman.2019.06.047>
- [40] K. Tomishige, D. Li, M. Tamura, Y. Nakagawa, Nickel-iron alloy catalysts for reforming of hydrocarbons: preparation, structure, and catalytic properties, *Catal. Sci. Technol.*, 2017, 7, 3952-3979. <https://doi.org/10.1039/c7cy01300k>
- [41] X. Zou, T. Chen, P. Zhang, D. Chen, J. He, Y. Dang, Z. Ma, Y. Chen, P. Toloueinia, C. Zhu, J. Xie, H. Liu, S. L. Suib, High catalytic performance of Fe-Ni/Palygorskite in the steam reforming of toluene for hydrogen production, *Appl. Energy*, 2018, 226, 827-837. <https://doi.org/10.1016/j.apenergy.2018.06.005>
- [42] S. Hu, L. He, Y. Wang, S. Su, L. Jiang, Q. Chen, Q. Liu, H. Chi, J. Xiang, L. Sun, Effects of oxygen species from Fe addition on promoting steam reforming of toluene over Fe-Ni/Al₂O₃ catalysts, *Int. J. Hydrogen Energy*, 2016, 41, 17967-17975. <https://doi.org/10.1016/j.ijhydene.2016.07.271>
- [43] J. Ashok, S. Kawi, Nickel-Iron Alloy Supported over Iron-Alumina Catalysts for Steam Reforming of Biomass Tar Model Compound, *ACS Catal.*, 2014, 4, 289-301. <https://doi.org/10.1021/cs400621p>
- [44] J. Meng, Z. Zhao, X. Wang, A. Zheng, D. Zhang, Z. Huang, K. Zhao, G. Wei, H. Li, Comparative study on phenol and naphthalene steam reforming over Ni-Fe alloy catalysts supported on olivine synthesized by different methods, *Energy Convers. Manag.*, 2018, 168, 60-73. <https://doi.org/10.1016/j.enconman.2018.04.112>
- [45] J. Ashok, S. Kawi, Steam reforming of biomass tar model compound at relatively low steam-to-carbon condition over CaO-doped nickel-iron alloy supported over iron-alumina catalysts, *Appl. Catal. A: Gen.*, 2015, 490, 24-35. <https://doi.org/10.1016/j.apcata.2014.10.057>
- [46] R. Michel, A. Łamacz, A. Krzton, G. Djéga-Mariadassou, P. Burg, C. Courson, R. Gruber, Steam reforming of *a*-methyl-naphthalene as a model tar compound over olivine and olivine supported nickel, *Fuel*, 2013, 109, 653-660. <https://doi.org/10.1016/j.fuel.2013.03.017>
- [47] D. Swierczynski, S. Libs, C. Courson, A. Kiennemann, Steam reforming of tar from a biomass gasification process over Ni/olivine catalyst using toluene as a model compound, *Appl. Catal. B: Environ.*, 2007, 74, 211-

222. <https://doi.org/10.1016/j.apcatb.2007.01.017>

- [48] Y. Kathiraser, J. Ashok, S. Kawi, Synthesis and evaluation of highly dispersed SBA-15 supported Ni-Fe bimetallic catalysts for steam reforming of biomass derived tar reaction, *Catal. Sci. Technol.*, 2016, 6, 4327-4336. <https://doi.org/10.1039/c5cy01910a>
- [49] D. Li, M. Koike, L. Wang, Y. Nakagawa, Y. Xu, K. Tomishige, Regenerability of Hydrotalcite-Derived Nickel-Iron Alloy Nanoparticles for Syngas Production from Biomass Tar, *ChemSusChem*, 2014, 7, 510-522. <https://doi.org/10.1002/cssc.201300855>
- [50] J. N. Kuhn, Z. Zhao, A. Senefeld-Naber, L. G. Felix, R. B. Slimane, C. W. Choi, U. S. Ozkan, Ni-olivine catalysts prepared by thermal impregnation: Structure, steam reforming activity, and stability, *Appl. Catal. A: Gen.*, 2008, 341, 43-49. <https://doi.org/10.1016/j.apcata.2007.12.037>
- [51] T. Zhang, Z. Liu, Y.-A. Zhu, Z. Liu, Z. Sui, K. Zhu, X. Zhou, Dry reforming of methane on Ni-Fe-MgO catalysts: Influence of Fe on carbon-resistant property and kinetics, *Appl. Catal. B: Environ.*, 2020, 264, 118497. <https://doi.org/10.1016/j.apcatb.2019.118497>
- [52] B. Li, Y. Luo, B. Li, X. Yuan, X. Wang, Catalytic performance of iron-promoted nickel-based ordered mesoporous alumina FeNiAl catalysts in dry reforming of methane, *Fuel Process. Technol.*, 2019, 193, 348-360. <https://doi.org/10.1016/j.fuproc.2019.05.033>
- [53] C. Wan, K. Song, J. Pan, M. Huang, R. Luo, D. Li, L. Jiang, Ni-Fe/Mg(Al)O alloy catalyst for carbon dioxide reforming of methane: Influence of reduction temperature and Ni-Fe alloying on coking, *Int. J. Hydrogen Energy*, 2020, 45, 33574-33585. <https://doi.org/10.1016/j.ijhydene.2020.09.129>
- [54] L. Wang, D. Li, M. Koike, H. Watanabe, Y. Xu, Y. Nakagawa, K. Tomishige, Catalytic performance and characterization of Ni-Co catalysts for the steam reforming of biomass tar to synthesis gas, *Fuel*, 2013, 112, 654-661. <https://doi.org/10.1016/j.fuel.2012.01.073>
- [55] H. S. M. Yahya, N. A. S. Amin, Catalytic Steam Reforming of Toluene for Hydrogen Production over Nickel-Cobalt Supported Activated Carbon, *Int. J. Integr. Eng.*, 2019, 11, 209-218. <https://doi.org/10.30880/ijie.2019.11.07.027>
- [56] M. Lu, Z. Xiong, J. Li, X. Li, K. Fang, T. Li, Catalytic steam reforming of toluene as model tar compound

- using Ni/coal fly ash catalyst, *Asia-Pac. J. Chem. Eng.*, 2020, e2529. <https://doi.org/10.1002/apj.2529>
- [57] N. Gao, Y. Han, C. Quan, Study on steam reforming of coal tar over Ni-Co/ceramic foam catalyst for hydrogen production: Effect of Ni/Co ratio, *Int. J. Hydrogen Energy*, 2018, 43, 22170-22186. <https://doi.org/10.1016/j.ijhydene.2018.10.119>
- [58] Z. Li, M. Li, J. Ashok, K. Sibudjing, NiCo@NiCo phyllosilicate@CeO₂ hollow core shell catalysts for steam reforming of toluene as biomass tar model compound, *Energy Convers. Manag.*, 2019, 180, 822-830. <https://doi.org/10.1016/j.enconman.2018.11.034>
- [59] A. D. Shejale, G. D. Yadav, Ni-Cu and Ni-Co Supported on La-Mg Based Metal Oxides Prepared by Coprecipitation and Impregnation for Superior Hydrogen Production via Steam Reforming of Glycerol, *Ind. Eng. Chem. Res.*, 2018, 57, 4785-4797. <https://doi.org/10.1021/acs.iecr.7b05150>
- [60] D. Li, M. Koike, J. Chen, Y. Nakagawa, K. Tomishige, Preparation of Ni-Cu/Mg/Al catalysts from hydrotalcite-like compounds for hydrogen production by steam reforming of biomass tar, *Int. J. Hydrogen Energy*, 2014, 39, 10959-10970. <https://doi.org/10.1016/j.ijhydene.2014.05.062>
- [61] D. Li, M. Lu, K. Aragaki, M. Koike, Y. Nakagawa, K. Tomishige, Characterization and catalytic performance of hydrotalcite-derived Ni-Cu alloy nanoparticles catalysts for steam reforming of 1-methylnaphthalene, *Appl. Catal. B: Environ.*, 2016, 192, 171-181. <https://doi.org/10.1016/j.apcatb.2016.03.052>
- [62] M. Khzouz, E. I. Gkanas, S. Du, J. Wood, Catalytic performance of Ni-Cu/Al₂O₃ for effective syngas production by methanol steam reforming, *Fuel*, 2018, 672-683. <https://doi.org/10.1016/j.fuel.2018.06.025>
- [63] T. Liang, Y. Wang, M. Chen, Z. Yang, S. Liu, Z. Zhou, X. Li, Steam reforming of phenol-ethanol to produce hydrogen over bimetallic Ni-Cu catalysts supported on sepiolite, *Int. J. Hydrogen Energy*, 2017, 42, 28233-28246. <https://doi.org/10.1016/j.ijhydene.2017.09.134>
- [64] J. Ashok, Y. Kathiraser, M. L. Ang, S. Kawi, Ni and/or Ni-Cu alloys supported over SiO₂ catalysts synthesized via phyllosilicate structures for steam reforming of biomass tar reaction, *Catal. Sci. Technol.*, 2015, 5, 4398-4409. <https://doi.org/10.1039/c5cy00650c>
- [65] L. Wang, J. Chen, H. Watanabe, Y. Xu, M. Tamura, Y. Nakagawa, K. Tomishige, Catalytic performance and characterization of Co-Fe bcc alloy nanoparticles prepared from hydrotalcite-like precursors in the steam

- gasification of biomass-derived tar, *Appl. Catal. B: Environ.*, 2014, 160-161, 701-715.
<http://dx.doi.org/10.1016/j.apcatb.2014.06.021>
- [66] C. Mebrahtu, F. Krebs, S. Perathoner, S. Abate, G. Centi, R. Palkovits, Hydrotalcite based Ni-Fe/(Mg, Al)Ox catalysts for CO₂ methanation - tailoring Fe content for improved CO dissociation, basicity, and particle size, *Catal. Sci. Technol.*, 2018, 8, 1016-1027. <https://doi.org/10.1039/c7cy02099f>
- [67] K. Song, M. Lu, S. Xu, C. Chen, Y. Zhan, D. Li, C. Au, L. Jiang, K. Tomishige, Effect of alloy composition on catalytic performance and coke-resistance property of Ni-Cu/Mg(Al)O catalysts for dry reforming of methane, *Appl. Catal. B: Environ.*, 2018, 239, 324-333. <https://doi.org/10.1016/j.apcatb.2018.08.023>
- [68] S. M. Kim, P. M. Abdala, T. Margossian, D. Hosseini, L. Foppa, A. Armutlulu, W. Beek, A. Comas-Vives, C. Copéret, C. Müller, Cooperativity and Dynamics Increase the Performance of NiFe Dry Reforming Catalysts, *J. Am. Chem. Soc.*, 2017, 139, 1937-1949. <https://doi.org/10.1021/jacs.6b11487>
- [69] D. Li, L. Wang, M. Koike, Y. Nakagawa, K. Tomishige, Steam reforming of tar from pyrolysis of biomass over Ni/Mg/Al catalysts prepared from hydrotalcite-like precursors, *Appl. Catal. B: Environ.*, 2011, 102, 528-538. <https://doi.org/10.1016/j.apcatb.2010.12.035>
- [70] L. Wang, D. Li, M. Koike, S. Koso, Y. Nakagawa, Y. Xu, K. Tomishige, Catalytic performance and characterization of Ni-Fe catalysts for the steam reforming of tar from biomass pyrolysis to synthesis gas, *Appl. Catal. A: Gen.*, 2011, 392, 248 -255. <https://doi.org/10.1016/j.apcata.2010.11.013>
- [71] K. Yoshida, N. Begum, S. Ito, K. Tomishige, Oxidative steam reforming of methane over Ni/ α -Al₂O₃ modified with trace noble metals, *Appl. Catal. A: Gen.*, 2009, 358, 186-192. <https://doi.org/10.1016/j.apcata.2009.02.025>
- [72] K. Tomishige, Y. Matsuo, Y. Yoshinaga, Y. Sekine, M. Asadullah, K. Fujimoto, Comparative study between fluidized bed and fixed bed reactors in methane reforming combined with methane combustion for the internal heat supply under pressurized condition, *Appl. Catal. A: Gen.*, 2002, 223, 225-238. [https://doi.org/10.1016/S0926-860X\(01\)00757-8](https://doi.org/10.1016/S0926-860X(01)00757-8)
- [73] K. Gheisari, S. Javadpour, J.T. Oh, M. Ghaffari, The effect of milling speed on the structural properties of mechanically alloyed Fe-45%Ni powders, *J. Alloys Compd.*, 2009, 472, 416-420. <https://doi.org/10.1016/j.jallcom.2008.04.074>

Chapter 4

Effect of addition of noble metal to hydrotalcite-derived Ni-Fe alloy catalyst for steam reforming of toluene using exhaust gas as reforming agent

* in preparation

4.1. Introduction

As described in Chapter 2, the Exhaust Gas Recirculation engine system with reforming techniques (denoted as Reformed EGR) was studied to improve the fuel economy of engines ^[1, 2]. The requirement for the reforming catalysts are as follows: activity at relatively low temperature (≤ 773 K), stability as resistance to coke deposition and aggregation of metal particles, reusability as no change of catalyst properties by regeneration, startability as easy activation, etc. ^[3]. The Rh-based catalysts using CeO₂-based supports as described in Chapter 2 have been typically investigated for the Reformed EGR system of gasoline engine ^[4, 5, 6]. However, reforming catalysts with a lower cost are desired to be developed since Rh is a very expensive noble metal.

As described in Chapter 3, Ni-Fe/Mg/Al (Fe/Ni = 0.25) catalyst derived to hydrotalcite-like compounds (HTLcs) shows higher activity, coke deposition resistance and structure stability than Ni/Mg/Al catalyst in reforming of toluene with model EGR gas (in the presence of CO₂; low partial pressure of steam). In addition, the activity can be recovered to a similar level to the fresh catalyst by treatment with N₂ flow at 873 K, catalytic use at 973 K, or re-reduction. On the other hand, the Ni-Fe/Mg/Al (Fe/ Ni = 0.25) is easily deactivated by the oxidation of catalyst. However, the formation of Ni-Fe alloy as an active site requires high temperature (1073 K) and supply of H₂, neither of which are available for automobiles. Therefore, the reducibility of catalysts should be much.

In the steam reforming of methane, the addition of noble metals such as Rh and Pt to Ni-based catalysts has been reported to enable self-activation ^[7-19]. In the reforming of biomass tar, the addition of noble metals such as Rh and

Pd to Ni/Mg/Al catalyst enhanced the activity in the oxidative steam reforming reaction [8]. In particular, Pd showed higher activity than the other noble metals under higher oxygen partial pressures. It also showed high coke deposition resistance. It has also been reported that self-activation occurs when noble metals are added to Ni/Mg(Al)O in steam reforming of methane [13].

In this chapter, the author investigated that addition effect on startability (reducibility) of noble metal to Ni-Fe/Mg/Al (Fe/Ni = 0.25) in reforming of toluene with model EGR gas of gasoline engine. Mixing Rh/CeO₂ powder to Ni-Fe/Mg/Al powder was found to be a better method of Rh addition to increase the startability of Ni-Fe/Mg/Al than mixing Rh/CeO₂ granule to Ni-Fe/Mg/Al granule, setting Rh/CeO₂ catalyst bed above Ni-Fe/Mg/Al catalyst bed and impregnation of Ni-Fe/Mg/Al with Rh. The author confirmed that the reducibility of Rh/CeO₂+Ni-Fe/Mg/Al (Powder Mixture) and Rh/Ni-Fe/Mg/Al catalyst was surely improved from Ni-Fe/Mg/Al.

4.2. Experimental

4.2.1. Catalyst preparation

The Ni-Fe/Mg/Al (Ni: 12 wt%, Fe/Ni = 0.25, (Ni+Mg)/(Al+Fe) = 3) catalyst was the same one used in Chapter 3 [20, 21].

The CeO₂ support and the Rh/CeO₂ (Rh 1 or 0.1 wt%) catalysts were the same ones used in Chapter 2 [22]. The M/CeO₂ catalysts (M = Pt, Ir, Pd, Ru, M 0.1 wt%) were prepared by an impregnation method using H₂PtCl₆ aq, IrCl₃ aq, PdCl₂ aq, and RuCl₃ aq, respectively. The resulting powder was dried in an oven at 383 K for 12 h and then calcined at 773 K for 3 h [23]. The granule size was controlled to 30-60 mesh by pressing, crushing, and sieving after calcination.

The M/CeO₂ + Ni-Fe/Mg/Al (including the amount of M was 0.1 wt%, M = Rh, Pt, Ir, Pd, Ru) catalysts were prepared by mixed each powder at 10:90 wt%, which is defined as Powder Mixture. Also, other two types of Rh/CeO₂ + Ni-Fe/Mg/Al (including the amount of Rh was 0.1 wt%) catalysts were prepared other two types: (i) Separate; Rh/CeO₂ after granulating was set upstream of the catalyst bed and Ni-Fe/Mg/Al after granulating located downstream of the catalyst bed, (ii) Granule Mixture; Rh/CeO₂ and Ni-Fe/Mg/Al after granulating were mixed.

The Rh/Ni-Fe/Mg/Al catalyst (Rh 0.1 wt%, Ni: 12 wt%, Fe/Ni = 0.25, (Ni+Mg)/(Al+Fe) = 3) was prepared by an impregnation method using Rh(NO₃)₃ aq and calcinated Ni-Fe/Mg/Al. The resulting powder was dried in an oven at 383 K for 12 h and then calcined at 773 K for 3 h. The granule size was controlled to 30-60 mesh by pressing, crushing, and sieving after calcination.

4.2.2. Catalyst characterization

X-ray diffraction (XRD) patterns, temperature-programmed reduction profiles with H₂ (H₂-TPR), and Transmission electron microscope (TEM) images were taken with the same instruments as described in Chapters 2 and 3. As described in Chapter 3, Energy Dispersive X-ray Spectroscopy (EDX; HORIBA EMAX ENERGY EX-250) combined with TEM, was used to obtain element distribution mapping.

4.2.3. Activity test of reforming of toluene

The used fixed-bed flow reactor was the same one used in Chapter 2. After the catalysts in the oxidized form were loaded, the reactor was purged with N₂, and the reactant liquids (such as toluene and H₂O) were supplied as described in Chapter 2. The standard feed ratio (molar ratio) of reactants and carrier gas was toluene/H₂O/N₂/CO₂ = 1/11.8/71.2/11.8 (the ratio of steam to carbon in hydrocarbon reactant (S/C_{H_C}) = 1.7), corresponding to the contact time $W/F = 0.19 \text{ g}_{\text{cat}} \text{ h mol}^{-1}$, which were the same conditions as the standard experiments in Chapter 2. Here, F represents the total flow rate and W is the catalyst weight. In the standard reaction, the catalyst bed temperature was raised from 523 K to 873 K in 50 K increments while the reaction gas was aerated, and then cooled to 773 K and 523 K. At each temperature, the reaction was carried out for 40 min and then moved to the next temperature. The analysis of products was the same as described in Chapter 2. The main reaction schemes were shown in Chapter 2 (Eqs. 1- 3).

CO₂ formation amount or rate was calculated by subtraction of fed CO₂ from the detected CO₂. In all the experiments, thermogravimetric (TG-DTA) analysis was used for the determination of the deposited coke (carbon) as described in Chapter 2.

4.3. Results and discussion

4.3.1. Effect of the method of adding Rh to Ni-Fe/Mg/Al

The results of the toluene reforming reaction with model EGR gas over the unreduced physical mixture of Rh/CeO₂ and Ni-Fe/Mg/Al catalysts at 10:90 wt% are shown in **Fig. 4.1**. The physical mixing was carried out in three ways: (i) Separate (Rh/CeO₂ catalyst upstream and Ni-Fe/Mg/Al catalyst downstream), (ii) Granule mixture (mixing the catalysts after granulation), and (iii) Powder mixture (mixing in powder form and then granulation).

The conversion of toluene was observed from 673 K for all the catalysts, and the active site was probably Rh metal. For all the catalysts, the toluene conversion increased with the increase of reaction temperature. The toluene conversion of the Separate and Granule mixture increased with increased reaction temperature with almost the same behavior, although the toluene conversion of the Granule mixture was slightly higher. In contrast, the Powder mixture showed higher toluene conversion than the Separate and Granule mixture from 773 K as also shown in **Table 4.1, Entries 2-3**, and reached 100% at 873 K. In all the catalysts, when the temperature was lowered from 873 K to 773 K, the toluene conversion was almost the same as the initial toluene conversion at 773 K, suggesting high structural stability. However, the toluene conversion of the Rh/CeO₂ + Ni-Fe/Mg/Al catalyst at 773 K was not as high as that of the Ni-Fe/Mg/Al catalyst reduced at 1073 K (100%; Chapter 2). For Rh/CeO₂ + Ni-Fe/Mg/Al catalysts, the toluene conversion at 773-873 K was Powder mixture > Granule mixture \approx Separate, which may be related to the high dispersion of Rh/CeO₂ catalyst and the close distance between Ni-Fe/Mg/Al and Rh/CeO₂ catalysts.

Effect of addition of noble metal to hydrotalcite-derived Ni-Fe alloy catalyst for steam reforming of toluene using exhaust gas as reforming agent

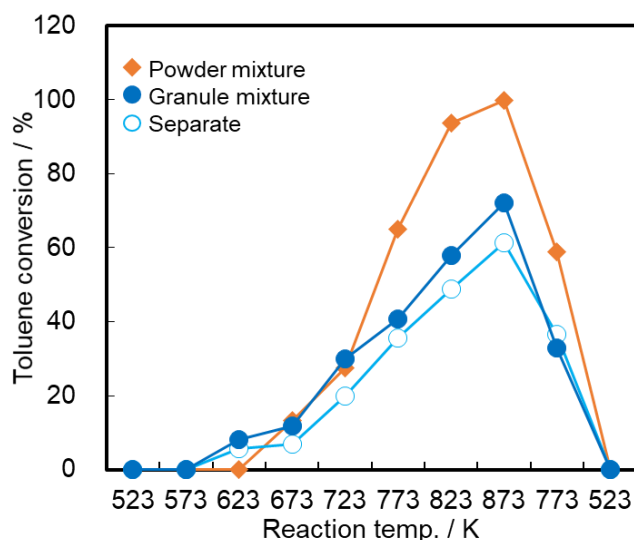


Figure 4.1 Reforming of toluene over Rh/CeO₂ (Rh: 1 wt%) + Ni-Fe/Mg/Al (Ni: 12 wt%, Fe/Ni = 0.25, (Ni+Mg)/(Al+Fe) = 3) catalysts (10:90 wt% mixture). Reaction conditions: $W_{cat} = 100$ mg; $W/F = 0.19$ g h mol⁻¹. reaction temperature, 523-873 K; reaction time, 470 min. $S/C_{HC} = 1.7$ (Toluene/H₂O/N₂/CO₂ = 1.0/11.8/71.2/11.8 (molar ratio)). Feeding rate: toluene, 6 mmol h⁻¹; steam, 65 mmol h⁻¹; N₂, 382 mmol h⁻¹; CO₂, 64 mmol h⁻¹.

Table 4.1 Reforming of toluene over Rh/CeO₂ (Rh: 1 wt%) + Ni-Fe/Mg/Al or Mg/Al (Ni: 12 wt%, Fe/Ni = 0.25, (Ni+Mg)/(Al+Fe) and Mg/Al = 3, mixture; 10:90 wt%) and Rh/Ni-Fe/Mg/Al or Mg/Al (Rh: 0.1 wt%, Ni: 12 wt%, Fe/Ni = 0.25, (Ni+Mg)/(Al+Fe) and Mg/Al = 3) catalysts.

Entry	Catalyst	At 773 K during heating							After heating and cooling	
		Toluene conv. [%]	Formation rate [mmol h ⁻¹]					H ₂ /CO ratio [-]	Carbon balance [%]	Coke deposition [g _{coke} g _{cat} ⁻¹]
			H ₂	CH ₄	CO	CO ₂	C ₆ H ₆			
1	Ni-Fe/Mg/Al	0	0	0	0	-7	0	-	92	0.04
2	Rh/CeO ₂ + Ni-Fe/Mg/Al (Separate)	36	19	0	4	-2	1	4.2	94	0.00
3	Rh/CeO ₂ + Ni-Fe/Mg/Al (Granule mixture)	41	24	0	6	0	1	-0.3	96	0.00
4	Rh/CeO ₂ + Ni-Fe/Mg/Al (Powder mixture)	65	26	0	8	1	2	3.4	93	0.03
5	Rh/CeO ₂ + Mg/Al (Powder mixture)	42	18	0	4	0	1	4	96	0.00
6	Rh/Ni-Fe/Mg/Al	22	3	0	1	-5	0	3.4	89	0.04
7	Rh/Mg/Al	5	2	0	1	-9	0	3.0	90	0.00

Reaction conditions: $W_{cat} = 100$ mg; $W/F = 0.19$ g h mol⁻¹. reaction temperature, 523-873 K; reaction time, 470 min. $S/C_{HC} = 1.7$ (Toluene/H₂O/N₂/CO₂ = 1.0/11.8/71.2/11.8 (molar ratio)). Feeding rate: toluene, 6 mmol h⁻¹; steam, 65 mmol h⁻¹; N₂, 382 mmol h⁻¹; CO₂, 64 mmol h⁻¹.

The same activity tests were performed for Rh/Ni-Fe/Mg/Al with Rh addition by impregnation method and the results are shown in **Fig. 4.2** along with the results for the Powder mixture of Rh/CeO₂ + Ni-Fe/Mg/Al catalyst. Here, the same experiments were performed for the case of Mg/Al instead of Ni-Fe/Mg/Al catalyst, and the effect on the coexistence of non-noble metal active elements, Ni and Fe, was also investigated. In the case of Rh/Ni-Fe/Mg/Al catalyst, the conversion of toluene started at 723 K, 50 K higher than that of Rh/CeO₂ + Ni-Fe/Mg/Al (Powder mixture, 10:90 wt%) catalyst. Thereafter, the toluene conversion increased with the increase of temperature and reached 100% at 873 K. On the other hand, the toluene conversion of Rh/CeO₂ + Ni-Fe/Mg/Al (Powder mixture, 10:90 wt%) catalyst was higher than that of Rh/Ni-Fe/Mg/Al catalyst in the temperature range above 673 K, and of toluene conversion at 773 K as an example was shown in **Table 4.1, Entries 4 and 6**. This may be due to the high modification activity of Rh/CeO₂. In both catalysts, when the temperature was lowered from 873 K to 773 K, the toluene conversion rate was almost the same as the initial toluene conversion rate at 773 K, suggesting high structural stability. A comparison of the Rh/Ni-Fe/Mg/Al and Rh/CeO₂ + Ni-Fe/Mg/Al (Powder mixture, 10:90 wt%) catalysts with the Rh/Mg/Al and Rh/CeO₂ + Mg/Al catalysts showed that the toluene conversion was higher than the Ni-Fe/Mg/Al catalyst for both addition methods. This suggests that Ni and Fe are activated by Rh. In the Rh/CeO₂ + Ni-Fe/Mg/Al (Powder mixture, 10:90 wt%) catalyst, Rh which was not present on the same support was able to activate Ni and Fe. This could be due to the that the H₂ produced by Rh was spilt over the CeO₂ surface, which supplied hydrogen to Ni and Fe. These results indicate that the mixing of Rh/CeO₂ and Ni-Fe/Mg/Al is the most suitable method of adding Rh.

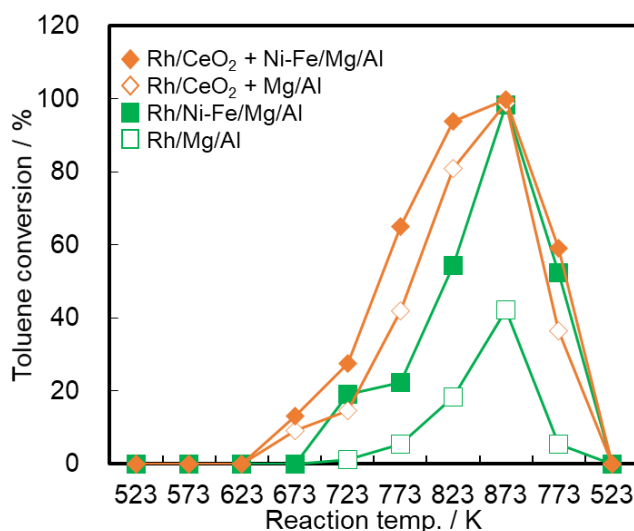


Figure 4.2 Reforming of toluene over Rh/CeO₂ (Rh: 1 wt%) + Ni-Fe/Mg/Al or Mg/Al (Ni: 12 wt%, Fe/Ni = 0.25, (Ni+Mg)/(Al+Fe) and Mg/Al = 3, Powder mixture; 10:90 wt%) and Rh/Ni-Fe/Mg/Al or Mg/Al (Rh: 0.1 wt%, Ni: 12 wt%, Fe/Ni = 0.25, (Ni+Mg)/(Al+Fe) and Mg/Al = 3) catalysts. Reaction conditions: $W_{cat} = 100$ mg; $W/F = 0.19$ g h mol⁻¹. reaction temperature, 523-873 K; reaction time, 470 min. $S/C_{HC} = 1.7$ (Toluene/H₂O/N₂/CO₂ = 1.0/11.8/71.2/11.8 (molar ratio)). Feeding rate: toluene, 6 mmol h⁻¹; steam, 65 mmol h⁻¹; N₂, 382 mmol h⁻¹; CO₂, 64 mmol h⁻¹.

4.3.2. Noble metals screening

The results of the toluene reforming reaction with model EGR gas over M/CeO₂ (M = Rh, Pt, Ir, Pd, Ru) + Ni-Fe/Mg/Al and M/CeO₂ (M = Rh, Pt, Ir, Pd, Ru) + Mg/Al (Powder mixture, 10:90 wt%) catalysts are shown in **Fig. 4.3**. In the case of M/CeO₂ (M = Rh, Pt, Ir, Pd, Ru) + Ni-Fe/Mg/Al (Powder mixture, 10:90 wt%) catalyst, the conversion of toluene started at 673 K for Rh, 723 K for Pd, and 773 K for Pt, Ir, and Ru, while no conversion of toluene was observed with Ni-Fe/Mg/Al catalyst alone. The toluene conversion increased with increasing reaction temperature for Rh-, Ir- and Ru-added catalysts, while it did not change much for Pd- and Pt-added ones. The toluene conversion of Pd-added catalyst decreased at 873 K, suggesting that it has low thermal stability. In addition, when the temperature was lowered from 873 K to 773 K, for Pt-, Pd- and Ru-added catalysts, the toluene conversion was much lower than that at the first 773 K, suggesting catalyst degradation. When compared with the corresponding M/CeO₂ (M = Rh, Pt, Ir, Pd, Ru) + Mg/Al catalyst, the toluene conversion over the catalysts containing Ni and Fe was higher except in the case of Pd addition, was an example as toluene as shown in **Table 4.2** which summarizes the toluene conversion at 773 K. This suggests that Ni and Fe were activated by the addition

of most noble metals. For the mixture catalysts using Mg/Al, Pd- and Ru-added catalysts which showed activity at 773 K were deactivated when the temperature was lowered from 873 K to 773 K. Only Rh-added catalyst showed high activity and stability.

Duprez reported that in the steam reforming reaction of toluene with $M/\text{Al}_2\text{O}_3$ ($M = \text{Rh}, \text{Pt}, \text{Ir}, \text{Pd}, \text{Ru}$) the activity (TOF [h^{-1}]) was in the order of $\text{Rh} (470) > \text{Pd} (128) > \text{Pt} (88) > \text{Ru} (64) > \text{Ir} (59)$ [24]. These literature results fairly agreed to the order in **Fig. 4.3**. Therefore, it is suggested that the reaction of $\text{Rh}/\text{CeO}_2 + \text{Ni-Fe/Mg/Al}$ and $\text{Rh}/\text{CeO}_2 + \text{Mg/Al}$ started at a lower temperature than that of other noble metals because of the higher reforming activity of Rh, and that these mixture catalysts were self-activated by the H_2 obtained in the reforming reaction.

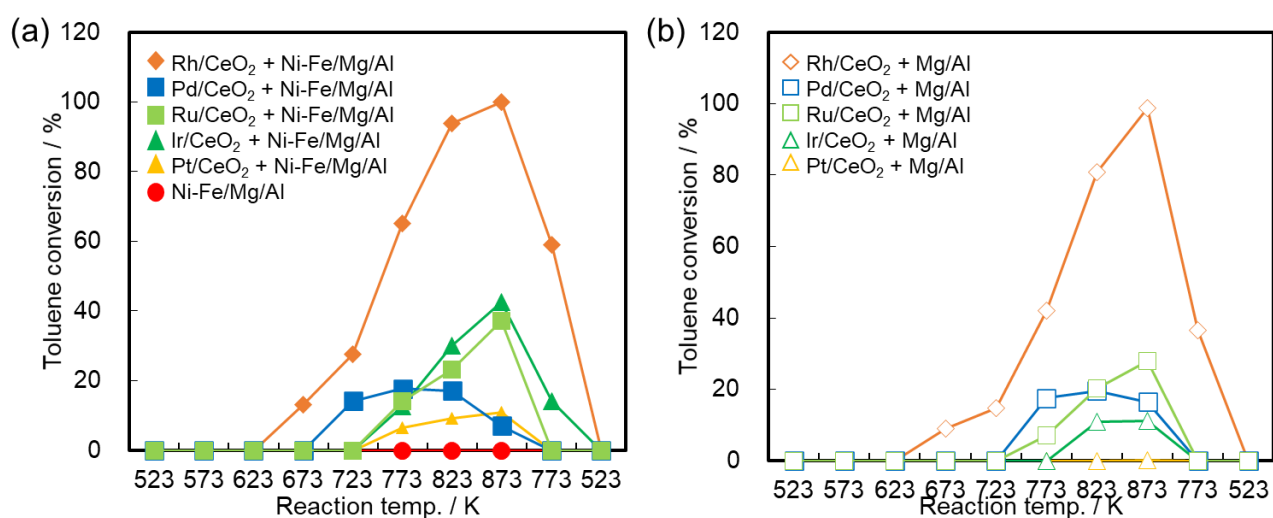


Figure 4.3 Reforming of toluene over M/CeO_2 (M : 1 wt%, $M = \text{Rh}, \text{Pt}, \text{Ir}, \text{Pd}, \text{Ru}$) + Ni-Fe/Mg/Al (Ni : 12 wt%, $\text{Fe}/\text{Ni} = 0.25$, $(\text{Ni}+\text{Mg})/(\text{Al}+\text{Fe}) = 3$) and M/CeO_2 (M : 1 wt%, $M = \text{Rh}, \text{Pt}, \text{Ir}, \text{Pd}, \text{Ru}$) + Mg/Al ($\text{Mg}/\text{Al} = 3$) catalysts (10:90 wt% Powder mixture). Reaction conditions: $W_{\text{cat}} = 100$ mg; $W/F = 0.19$ g h mol $^{-1}$. reaction temperature, 523-873 K; reaction time, 470 min. $S/C_{\text{HC}} = 1.7$ (Toluene/ $\text{H}_2\text{O}/\text{N}_2/\text{CO}_2 = 1.0/11.8/71.2/11.8$ (molar ratio)). Feeding rate: toluene, 6 mmol h $^{-1}$; steam, 65 mmol h $^{-1}$; N_2 , 382 mmol h $^{-1}$; CO_2 , 64 mmol h $^{-1}$.

Table 4.2 Reforming of toluene over M/CeO₂ (M: 1 wt%, M = Rh, Pt, Ir, Pd, Ru) + Ni-Fe/Mg/Al (Ni: 12 wt%, Fe/Ni = 0.25, (Ni+Mg)/(Al+Fe) = 3) and M/CeO₂ (M: 1 wt%, M = Rh, Pt, Ir, Pd, Ru) + Mg/Al (Mg/Al = 3) catalysts (10:90 wt% Powder mixture).

Entry	Catalyst	At 773 K during heating							After heating and cooling	
		Toluene conv. [%]	Formation rate [mmol h ⁻¹]					H ₂ /CO ratio [-]	Carbon balance [%]	Coke deposition [g _{coke} g _{cat} ⁻¹]
			H ₂	CH ₄	CO	CO ₂	C ₆ H ₆			
1	Ni-Fe/Mg/Al	0	0	0	0	-7	0	-	92	0.04
4	Rh/CeO ₂ + Ni-Fe/Mg/Al	65	26	0	8	1	2	3.4	93	0.03
5	Rh/CeO ₂ + Mg/Al	42	18	0	4	0	1	4	96	0.00
8	Pt/CeO ₂ + Ni-Fe/Mg/Al	7	0	0	0	-5	0	-	92	0.01
9	Pt/CeO ₂ + Mg/Al	0	0	0	0	-6	0	-	92	0.01
10	Ir/CeO ₂ + Ni-Fe/Mg/Al	13	2	0	0	-9	0	5.7	87	0.00
11	Ir/CeO ₂ + Mg/Al	0	0	0	0	-2	0	0.0	96	0.01
12	Pd/CeO ₂ + Ni-Fe/Mg/Al	18	1	0	0	-10	0	3.9	85	0.02
13	Pd/CeO ₂ + Mg/Al	18	1	0	0	-3	0	2.8	92	0.00
14	Ru/CeO ₂ + Ni-Fe/Mg/Al	14	1	0	0	-3	0	3.6	92	0.00
15	Ru/CeO ₂ + Mg/Al	7	2	0	4	-5	0	3.2	96	0.00

Reaction conditions: $W_{cat} = 100$ mg; $W/F = 0.19$ g h mol⁻¹. reaction temperature, 523-873 K; reaction time, 470 min. $S/CHC = 1.7$ (Toluene/H₂O/N₂/CO₂ = 1.0/11.8/71.2/11.8 (molar ratio)). Feeding rate: toluene, 6 mmol h⁻¹; steam, 65 mmol h⁻¹; N₂, 382 mmol h⁻¹; CO₂, 64 mmol h⁻¹.

4.3.3. Performance of reduced Rh/CeO₂ + Ni-Fe/Mg/Al

The results of the toluene reforming reaction with model EGR gas over Rh/CeO₂ (Rh: 1 wt%) + Ni-Fe/Mg/Al (Powder mixture, 10:90 wt%), Ni-Fe/Mg/Al and Rh/CeO₂ (Rh: 0.1 wt%) catalysts at a constant temperature of 773 K are shown in **Fig. 4.4** and **Table 4.3**. Over the Rh/CeO₂ (Rh: 1 wt%) + Ni-Fe/Mg/Al (Powder mixture, 10:90 wt%) catalyst without reduction, the toluene conversion was decreased to 56% from 76% at 300 min (**Fig. 4.4 (a)** and **Table 4.3, Entry 1**). On the other hand, the toluene conversion of Rh/CeO₂ (Rh: 1 wt%) + Ni-Fe/Mg/Al (Powder mixture, 10:90 wt%) catalyst after reduction at 773 K was decreased to 71% from 86% at 300 min (**Fig. 4.4 (b)** and **Table 4.3, Entry 2**). In addition, the toluene conversion of Rh/CeO₂ (Rh: 0.1 wt%) catalyst after reduction at 573 K was decreased to 54% from 74% at 300 min (**Fig. 4.4 (e)** and **Table 4.3, Entry 5**). It is suggested that the Rh/CeO₂ (Rh: 1 wt%) + Ni-Fe/Mg/Al (powder mixture, 10:90 wt%) catalyst is self-reduced by the feed gas (toluene/H₂O/N₂/CO₂ = 1/11.8/71.2/11.8) to the same extent as the reduction at 773 K, and the active

site was mainly Rh. In the Rh/CeO₂ (Rh: 1 wt%) + Ni-Fe/Mg/Al (Powder mixture, 10:90 wt%) catalyst after reduction at 1073 K, the toluene conversion was decreased to 86% from 100% at 300 min (**Fig. 4.4 (c)** and **Table 4.3, Entry 3**). Compared with Ni-Fe/Mg/Al catalyst after reduction at 1073 K (**Fig. 4.4 (d)** and **Table 4.3, Entry 4**), the Rh/CeO₂ (Rh: 1 wt%) + Ni-Fe/Mg/Al (Powder mixture, 10:90 wt%) catalyst after reduction at 1073 K kept high activity. The high stability of activity of Rh/CeO₂ (Rh: 1 wt%) + Ni-Fe/Mg/Al (Powder mixture, 10:90 wt%) catalyst is probably related to the higher activity and better coke deposition resistance of the Rh/CeO₂ catalyst.

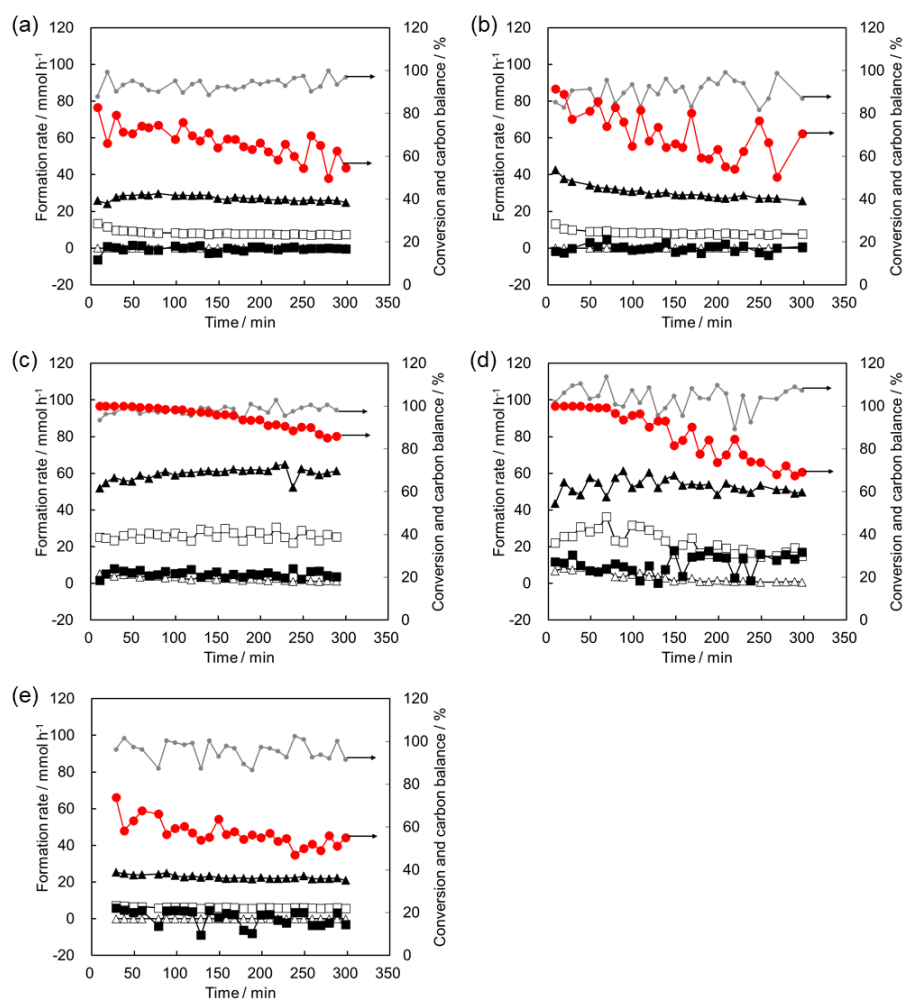


Figure 4.4 Reforming of toluene with model EGR gas over Rh/CeO₂ + Ni-Fe/Mg/Al (10:90 wt% Powder mixture) catalyst without reduction (a), after reduction at 773 K (b) and 1073 K (c), Ni-Fe/Mg/Al (Ni: 12 wt%, Fe/Ni = 0.25, (Ni+Mg)/(Al+Fe) = 3) catalyst after reduction at 1073 K (d) and Rh/CeO₂ (Rh: 0.1 wt%). ● (red circle): toluene conversion, ● (gray circle): carbon balance, ▲: H₂, △: CH₄, □: CO, ■: CO₂. Reaction conditions: $W_{cat} = 100$ mg; $W/F = 0.19$ g h mol⁻¹. reaction temperature, 773 K; reaction time, 300 min. $S/C_{HC} = 1.7$ (Toluene/H₂O/N₂/CO₂ = 1.0/11.8/71.2/11.8 (molar ratio)). Feeding rate: toluene, 6 mmol h⁻¹; steam, 65 mmol h⁻¹; N₂, 382 mmol h⁻¹; CO₂, 64 mmol h⁻¹.

Table 4.3 Reforming of toluene with model EGR gas over Rh/CeO₂ + Ni-Fe/Mg/Al (10:90 wt% Powder mixture), Ni-Fe/Mg/Al (Ni: 12 wt%, Fe/Ni = 0.25, (Ni+Mg)/(Al+Fe) = 3) and Rh/CeO₂ (Rh: 0.1 wt%) catalysts.

Entry	Catalyst	Reduction temp. [K]	Toluene conv. [%]	Formation rate [mmol h ⁻¹ g _{cat} ⁻¹]					H ₂ /CO ratio [-]	Carbon balance [%]	Amount of coke deposition ^c [g _{coke} g _{cat} ⁻¹]		
				H ₂	CH ₄	CO	CO ₂	C ₆ H ₆			Inlet	Middle	Outlet
1	Rh/CeO ₂ + Ni-Fe/Mg/Al	-	76 ^a	26	0	12	-2	2	2.3	93			
			56 ^b	26	0	7	0	2	3.5	97	0.00	0.00	0.00
2	Rh/CeO ₂ + Ni-Fe/Mg/Al	773	86 ^a	39	0	11	-2	2	3.5	86			
			71 ^b	26	0	8	1	1	3.3	87	0.00	0.00	0.00
3	Rh/CeO ₂ + Ni-Fe/Mg/Al	1073	100 ^a	55	5	24	5	0	2.2	95			
			85 ^b	61	1	26	4	0	2.3	99	0.01	0.01	0.01
4	Ni-Fe/Mg/Al	1073	100 ^a	50	8	24	13	0	2.0	106			
			70 ^b	50	1	17	15	0	3.0	108	0.01	0.01	0.01
5	Rh/CeO ₂	573	74 ^a	25	0	7	6	2	3.5	96			
			54 ^b	22	0	6	-1	2	3.7	95	0.00	0.00	0.00

Reaction conditions: $W_{cat} = 100$ mg; $W/F = 0.19$ g h mol⁻¹. reaction temperature, 773 K; reaction time, 300 min.

$S/C_{HC} = 1.7$ (Toluene/H₂O/N₂/CO₂ = 1.0/11.8/71.2/11.8 (molar ratio)). Feeding rate: toluene, 6 mmol h⁻¹; steam, 65 mmol h⁻¹; N₂, 382 mmol h⁻¹; CO₂, 64 mmol h⁻¹. ^a Initial: at 10-30 min, ^b Steady state: at 280-300 min, ^c After reaction at 300 min, n.d.: no data.

4.3.4. Characterization of used or fresh catalyst of Rh/CeO₂ + Ni-Fe/Mg/Al and Rh/Ni-Fe/Mg/Al

H₂-TPR was carried out to investigate the reduction behavior (Fig. 4.5). The profile was recorded up to 1073 K which was the actual reduction temperature for the catalytic test. The reduction of Ni/Mg/Al was not completed at 1073 K, and the reduction degree after the reduction at 1073 K for 30 min was Ni: 0.65 and Fe: 0.71, respectively (Chapter 2). As reported in our previous paper [25], the profile of Ni-Fe/Mg/Al had a similar shape to that of Ni/Mg/Al, while the intensity was significantly larger, indicating that the reduction of Ni and Fe occurred simultaneously (Chapter 3).

The profile of Rh/Mg/Al catalyst had H₂ consumption peak only at 673 -773 K, which suggested the reduction of Rh. On the other hand, the profile of Rh/Ni-Fe/Mg/Al catalyst had two H₂ consumption peaks at 673-773 K and 773-1073 K. The H₂ consumption peak at 773-1073 K was assigned to the reduction of Ni and Fe. In comparison

with Ni-Fe/Mg/Al, the H₂ consumption peak by reduction of Ni and Fe was broad, and the reduction started at a lower temperature. It indicated that the reducibility of Ni-Fe/Mg/Al was improved by the addition of Rh. The profile of Rh/CeO₂ + Mg/Al (Powder mixture, 10:90 wt%) catalyst had two H₂ consumption peaks at 373 K and 573-773 K, which can be assigned to Rh and surface CeO₂, respectively. On the other hand, the profile of Rh/CeO₂ + Ni-Fe/Mg/Al (Powder mixture, 10:90 wt%) catalyst had three peaks at 373 K, 573-773 K and 773-1073 K. The H₂ consumption peak at 773-1073 K was assigned to the reduction of Ni and Fe similar to Rh/Ni-Fe/Mg/Al catalyst. In addition, the reduction peak by reduction of Ni and Fe was broad, and the reduction started at a lower temperature than Ni-Fe/Mg/Al catalyst. The addition of Rh increased the H₂ consumption for Ni or Fe reduction for both addition methods, and the addition of Rh/CeO₂ more increased the H₂ consumption than that by impregnation. The reduction temperature was also shifted to the lower range by Rh addition. These results showed the improvement of reducibility of Ni-Fe/Mg/Al.

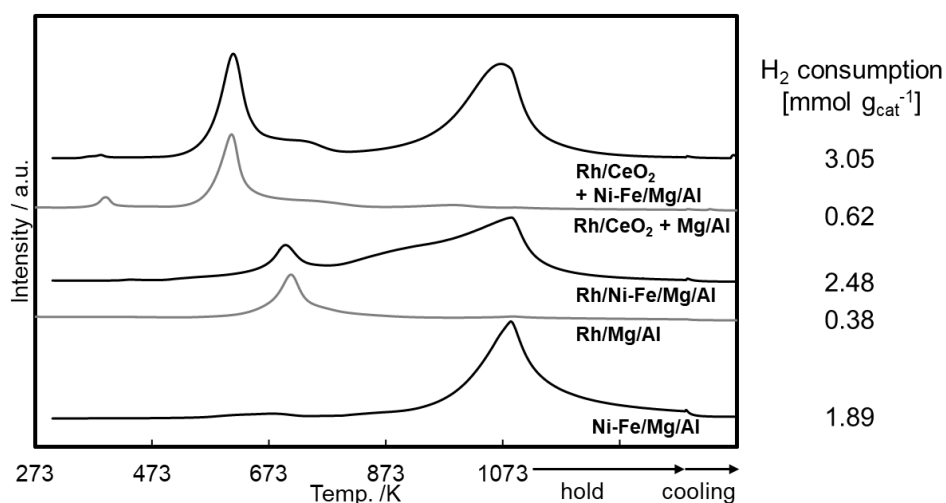


Figure 4.5 TPR profiles of Rh/CeO₂ (Rh: 1 wt%) + Ni-Fe/Mg/Al (Ni: 12 wt%, Fe/Ni = 0.25, (Ni+Mg)/(Al+Fe) = 3) catalysts (10:90 wt% Powder mixture) and Rh/Ni-Fe/Mg/Al (Rh: 0.1 wt%, Ni: 12 wt%, Fe/Ni = 0.25, (Ni+Mg)/(Al+Fe) = 3) catalysts.

Measurement conditions: 5% H₂/Ar, 30 ml min⁻¹; room temperature to 1073 K at a rate of 10 K min⁻¹, then the temperature was maintained at 1073 K for 30 min; sample, 50 mg.

The Rh/CeO₂ + Ni-Fe/Mg/Al (powder mixture, 10:90 wt%) and Rh/Ni-Fe/Mg/Al catalysts after toluene reforming with model EGR gas were characterized with XAFS, and the data are shown in **Fig. 4.6** and **Tables 4.4, 4.5 and 4.6**. In the non-reduced catalysts, the reaction temperatures were raised from 523 K to 673 (**Fig. 4.6 (1) and (4)**) and

Tables 4.4-6 Entries 1 and 4), 773 K (**Fig. 4.6 (2) and (5)**) and **Tables 4.4-6 Entries 2 and 5**) and 873 K (**Fig. 4.6 (6) and (7)**) and **Tables 4.4-6 Entries 3 and 6**), respectively. In addition, in the non-reduced Rh/CeO₂ + Ni-Fe/Mg/Al (powder mixture, 10:90 wt%) catalyst was measured, and the reaction at 773 K for 300 min (**Fig. 4.6 (7)** and **Tables 4.4-6 Entry 7**). At all absorption edges, the metal in most of the samples was in the oxidized state. Especially, from the Ni K edge spectra, the reduction of Ni hardly proceeded. From the Rh K edge spectra, the peak attributed to metallic Rh in the Rh/Ni-Fe/Mg/Al catalyst slightly increased with increasing reaction temperature. On the other hand, the Rh/CeO₂ + Ni-Fe/Mg/Al (Powder mixture, 10:90 wt%) catalyst showed the peak attributed to metallic Rh at any reaction temperature. In addition, in the Rh/CeO₂ + Ni-Fe/Mg/Al (Powder mixture, 10:90 wt%) catalyst after 300 min reaction at 773 K, the peak attributed to metallic Rh was larger than the peak attributed to Rh oxide, showing reduction of Rh. Also, those peaks attributed to metallic Rh might include Fe-Rh alloy. However, it is not possible to judge whether each metal was alloyed from the XAFS results.

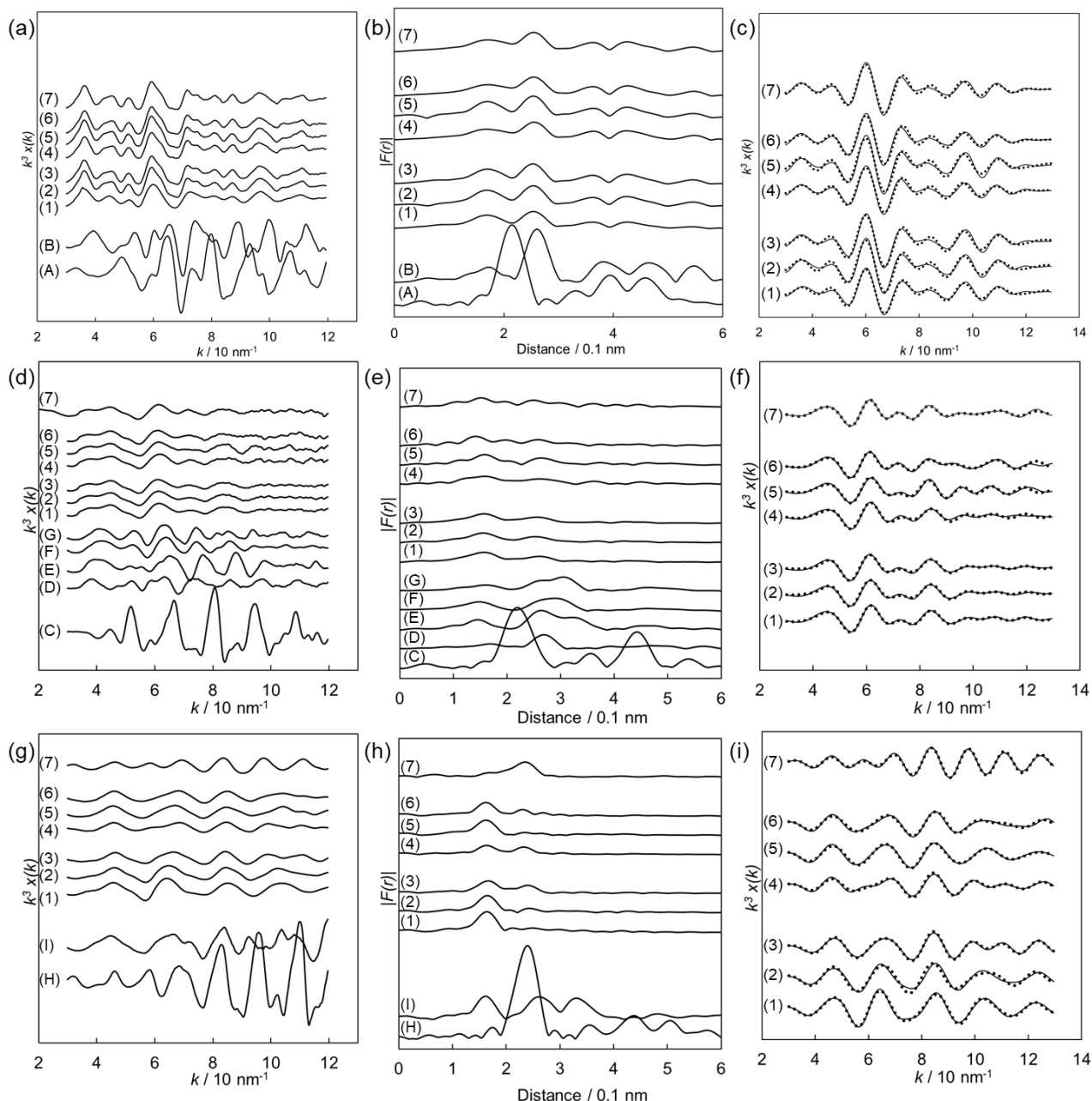


Figure 4.6 EXAFS analyses of Rh-added Ni-Fe/Mg/Al (Ni: 12 wt%, Fe/Ni = 0.25, (Ni+Mg)/(Al+Fe) = 3) catalyst and reference compounds: Rh/Ni-Fe/Mg/Al (Rh: 0.1 wt%) catalysts: (1) after reaction at 523-673 K, (2) after reaction at 523-773 K, (3) after reaction at 523-873 K, and Rh/CeO₂ (Rh: 1 wt%) + Ni-Fe/Mg/Al (Powder mixture, 10:90 wt%) catalysts: (4) reaction at 523-673 K, (5) after reaction at 523-773 K, (6) after reaction at 523-873 K, (7) after reaction at 773 K. Reference compounds: (A) Ni foil, (B) NiO, (C) Fe foil, (D) FeO, (E) α -Fe₂O₃, (F) γ -Fe₂O₃, (G) Fe₃O₄, (H) Rh foil, (I) Rh₂O₃. (a)-(c) Ni K edge, (d)-(f) Fe K edge, (g)-(i) Rh K edge. (a), (d), (g) k^3 -weighted EXAFS oscillation; (b), (e), (h) Fourier transform of k^3 -weighted EXAFS, FT range: 3-13 10 nm⁻¹; (c), (f), (i) Fourier-filtered EXAFS data (solid line) and calculated data (dotted line), Fourier filtering range: 0.1074-0.3590 nm for the Ni K edge, 0.1074-0.3590 nm for the Fe K edge, 0.1197-0.3283 nm for the Rh K edge.

*Effect of addition of noble metal to hydrotalcite-derived Ni-Fe alloy catalyst
for steam reforming of toluene using exhaust gas as reforming agent*

Table 4.4 Curve-fitting results for the Ni K-edge EXAFS of **Fig. 4.6**.

Entry	catalyst	Condition	Shells	CN ^a	R ^b [$\times 10^{-1}$ nm]	σ^c [$\times 10^{-1}$ nm]	ΔE_0^d [eV]	R _r ^e [%]
1	Rh/Ni-Fe/Mg/Al (Rh: 0.1 wt%)	reaction (~ 673 K)	Ni-Ni (or Fe)	0.3	2.38	0.600 ^f	19.37	3.85
			Ni-O	7.5	2.10	0.800 ^f	3.45	
			Ni-O-Ni	7.7	2.99	0.100 ^f	-13.09	
			Ni-Rh	-	-	-	-	
2	Rh/Ni-Fe/Mg/Al (Rh: 0.1 wt%)	reaction (~ 773 K)	Ni-Ni (or Fe)	0.2	2.64	0.060 ^f	-0.19	4.89
			Ni-O	8.4	2.08	0.080 ^f	-1.06	
			Ni-O-Ni	9.0	2.98	0.100 ^f	-14.27	
			Ni-Rh	-	-	-	-	
3	Rh/Ni-Fe/Mg/Al (Rh: 0.1 wt%)	reaction (~ 873 K)	Ni-Ni (or Fe)	0.4	2.41	0.080 ^f	24.36	4.60
			Ni-O	8.5	2.10	0.080 ^f	3.51	
			Ni-O-Ni	8.9	2.98	0.100 ^f	-13.59	
			Ni-Rh	-	-	-	-	
4	Rh/CeO ₂ +Ni-Fe/Mg/Al (Rh: 0.1 wt%)	reaction (~ 673 K)	Ni-Ni (or Fe)	0.1	2.51	0.060 ^f	-9.73	4.30
			Ni-O	9.0	2.10	0.100 ^f	2.60	
			Ni-O-Ni	8.3	3.00	0.100 ^f	-12.34	
			Ni-Rh	-	-	-	-	
5	Rh/CeO ₂ +Ni-Fe/Mg/Al (Rh: 0.1 wt%)	reaction (~ 773 K)	Ni-Ni (or Fe)	0.0	0.25	0.060	3.77	5.77
			Ni-O	8.7	2.08	0.080	-0.80	
			Ni-O-Ni	9.6	2.99	0.100	-14.04	
			Ni-Rh	-	-	-	-	
6	Rh/CeO ₂ +Ni-Fe/Mg/Al (Rh: 0.1 wt%)	reaction (~ 873 K)	Ni-Ni (or Fe)	0.2	2.54	0.680	-5.72	4.31
			Ni-O	9.4	2.11	0.100 ^f	2.69	
			Ni-O-Ni	8.7	2.99	0.100 ^f	-12.88	
			Ni-Rh	-	-	-	-	
7	Rh/CeO ₂ +Ni-Fe/Mg/Al (Rh: 0.1 wt%)	reaction (773 K, 5 h)	Ni-Ni (or Fe)	0.2	2.47	0.071	-13.23	4.59
			Ni-O	9.8	2.11	0.100 ^f	2.75	
			Ni-O-Ni	8.9	2.99	0.100 ^f	-12.89	
			Ni-Rh	-	-	-	-	
8	Ni foil		Ni-Ni	12.0	2.49	0.060	0.00	-
9	NiO		Ni-O	6.0	2.08	0.060	0.00	-
10	FEFF		Ni-Rh	-	2.59	-	0.00	-

^a Coordination number. ^b Bond length. ^c Debye–Waller factor. ^d Difference in the origin of photoelectron energy between the reference and the sample. ^e Residual factor. Fourier range: 0.1074–0.3590 nm. ^f Fixed value.

Table 4.5 Curve-fitting results for the Fe K-edge EXAFS of t Fig. 4.6.

Entry	catalyst	Condition	Shells	CN ^a	R ^b [$\times 10^{-1}$ nm]	σ^c [$\times 10^{-1}$ nm]	ΔE_0^d [eV]	R _f ^e [%]
1	Rh/Ni-Fe/Mg/Al (Rh: 0.1 wt%)	reaction (~ 673 K)	Fe-Fe (or Ni)	1.1	2.21	0.100 ^f	10.81	0.96
			Fe-O	8.4	1.99	0.100 ^f	5.50	
			Fe-O-Fe	2.5	3.02	0.087	-8.00	
			Fe-Rh	-	-	-	-	
2	Rh/Ni-Fe/Mg/Al (Rh: 0.1 wt%)	reaction (~ 773 K)	Fe-Fe (or Ni)	0.2	2.44	0.060 ^f	-16.72	2.41
			Fe-O	7.1	1.97	0.100 ^f	-0.46	
			Fe-O-Fe	3.6	2987.00	0.100 ^f	-13.81	
			Fe-Rh	-	-	-	-	
3	Rh/Ni-Fe/Mg/Al (Rh: 0.1 wt%)	reaction (~ 873 K)	Fe-Fe (or Ni)	0.3	2.48	0.060 ^f	-12.49	2.01
			Fe-O	6.6	1.98	0.100 ^f	-0.15	
			Fe-O-Fe	3.7	2.99	0.100 ^f	-13.99	
			Fe-Rh	-	-	-	-	
4	Rh/CeO ₂ +Ni-Fe/Mg/Al (Rh: 0.1 wt%)	reaction (~ 673 K)	Fe-Fe (or Ni)	0.7	2.50	0.074	-10.10	5.97
			Fe-O	6.4	1.99	0.100 ^f	2.42	
			Fe-O-Fe	2.4	3.01	0.080 ^f	-10.80	
			Fe-Rh	-	-	-	-	
5	Rh/CeO ₂ +Ni-Fe/Mg/Al (Rh: 0.1 wt%)	reaction (~ 773 K)	Fe-Fe (or Ni)	0.6	2.54	0.060 ^f	-2.62	3.88
			Fe-O	7.4	2.01	0.100 ^f	5.73	
			Fe-O-Fe	1.9	3.06	0.060 ^f	-5.10	
			Fe-Rh	0.3	2.58	0.060 ^f	-0.37	
6	Rh/CeO ₂ +Ni-Fe/Mg/Al (Rh: 0.1 wt%)	reaction (~ 873 K)	Fe-Fe (or Ni)	2.5	2.55	0.080 ^f	-4.86	4.87
			Fe-O	5.4	1.88	0.100 ^f	-13.15	
			Fe-O-Fe	2.5	3.13	0.100 ^f	2.60	
			Fe-Rh	0.9	2.55	0.060 ^f	-1.86	
7	Rh/CeO ₂ +Ni-Fe/Mg/Al (Rh: 0.1 wt%)	reaction (773 K, 5 h)	Fe-Fe (or Ni)	1.9	2.49	0.080	-14.28	1.01
			Fe-O	5.4	1.94	0.100	-2.36	
			Fe-O-Fe	2.5	3.19	0.100	13.52	
			Fe-Rh	1.3	2.55	0.080	5.34	
8	Ni foil		Fe-Fe	12.0	2.49	0.060	0.00	-
9	NiO		Fe-O	6.0	2.08	0.060	0.00	-
10	FEFF		Fe-Rh	-	-	-	0.00	-

^a Coordination number. ^b Bond length. ^c Debye–Waller factor. ^d Difference in the origin of photoelectron energy between the reference and the sample. ^e Residual factor. Fourier range: 0.1074–0.3590 nm. ^f Fixed value.

Table 4.6 Curve-fitting results for the Rh K-edge EXAFS of **Fig. 4.6**.

Entry	catalyst	Condition	Shells	CN ^a	R ^b [$\times 10^{-1}$ nm]	σ^c [$\times 10^{-1}$ nm]	ΔE_0^d [eV]	R _f ^e [%]
1	Rh/Ni-Fe/Mg/Al (Rh: 0.1 wt%)	reaction (~ 673 K)	Rh-Rh	1.3	2.88	0.080 ^f	-14.73	1.90
			Rh-O	6.6	2.07	0.071	1.65	
			Rh-Ni (or Fe)	0.9	2.62	0.080 ^f	0.29	
2	Rh/Ni-Fe/Mg/Al (Rh: 0.1 wt%)	reaction (~ 773 K)	Rh-Rh	1.0	2.67	0.080 ^f	3.00	1.10
			Rh-O	5.9	2.07	0.730	3.91	
			Rh-Ni (or Fe)	0.4	2.56	0.080 ^f	-13.06	
3	Rh/Ni-Fe/Mg/Al (Rh: 0.1 wt%)	reaction (~ 873 K)	Rh-Rh	1.8	2.66	0.080 ^f	6.07	1.11
			Rh-O	4.9	2.07	0.080 ^f	5.31	
			Rh-Ni (or Fe)	0.2	2.51	0.080 ^f	-13.22	
4	Rh/CeO ₂ + Ni-Fe/Mg/Al (Rh: 0.1 wt%)	reaction (~ 673 K)	Rh-Rh	1.4	2.61	0.080 ^f	-5.92	3.77
			Rh-O	3.5	2.07	0.080 ^f	5.07	
			Rh-Ni (or Fe)	0.3	2.90	0.080 ^f	6.15	
5	Rh/CeO ₂ + Ni-Fe/Mg/Al (Rh: 0.1 wt%)	reaction (~ 773 K)	Rh-Rh	0.3	2.63	0.080 ^f	-2.81	1.53
			Rh-O	5.4	2.05	0.078	2.22	
			Rh-Ni (or Fe)	0.2	2.96	0.060 ^f	14.68	
6	Rh/CeO ₂ + Ni-Fe/Mg/Al (Rh: 0.1 wt%)	reaction (~ 873 K)	Rh-Rh	1.0	2.59	0.080 ^f	-7.99	4.96
			Rh-O	4.7	2.05	0.079	3.99	
			Rh-Ni (or Fe)	0.1	2.23	0.080 ^f	-4.54	
7	Rh/CeO ₂ + Ni-Fe/Mg/Al (Rh: 0.1 wt%)	reaction (773 K, 5 h)	Rh-Rh	4.9	2.63	0.080 ^f	-5.92	1.37
			Rh-O	0.5	2.09	0.080 ^f	9.97	
			Rh-Ni (or Fe)	0.9	2.63	0.060 ^f	0.60	
8	Rh foil		Rh-Rh	12.0	2.49	0.060	0.00	-
9	Rh ₂ O ₃		Rh-O	6.0	2.08	0.060	0.00	-
10	FEFF		Ni-Rh	-	2.59	-	0.00	-
11	FEFF		Fe-Rh	-	-	-	0.00	-

^a Coordination number. ^b Bond length. ^c Debye–Waller factor. ^d Difference in the origin of photoelectron energy between the reference and the sample. ^e Residual factor. Fourier range: 0.1197–0.3283 nm. ^f Fixed value.

The TEM-EDX image of Rh/CeO₂ + Ni-Fe/Mg/Al (Powder mixture, 10:90 wt%) catalysts after reduction at 1073 K and after reaction at 573-773 K was shown **Fig. 4.7**. There were Rh/CeO₂-rich domains and Ni-Fe/Mg/Al domains in each granule. The EDX after reduction suggested that Rh was highly dispersed on CeO₂. The Ni-Fe alloy particles were also found to be highly dispersed on the catalyst surface. On the other hand, in the Rh/CeO₂ +

Ni-Fe/Mg/Al (Powder mixture, 10:90 wt%) catalyst after reaction at 573-773 K, no detectable metal particles were formed. These results agreed with XAFS data that only a very small amount of Ni and Fe was reduced.

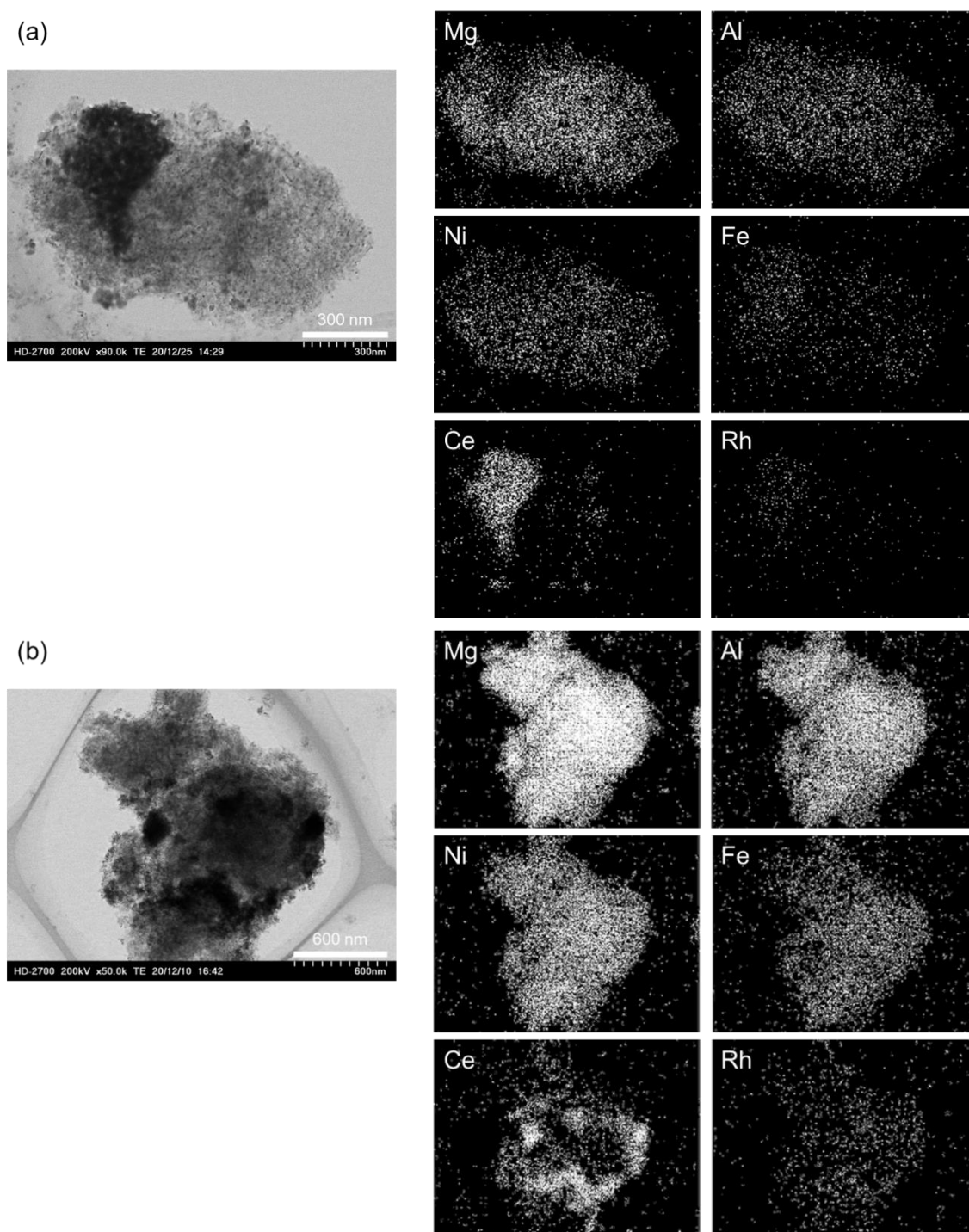
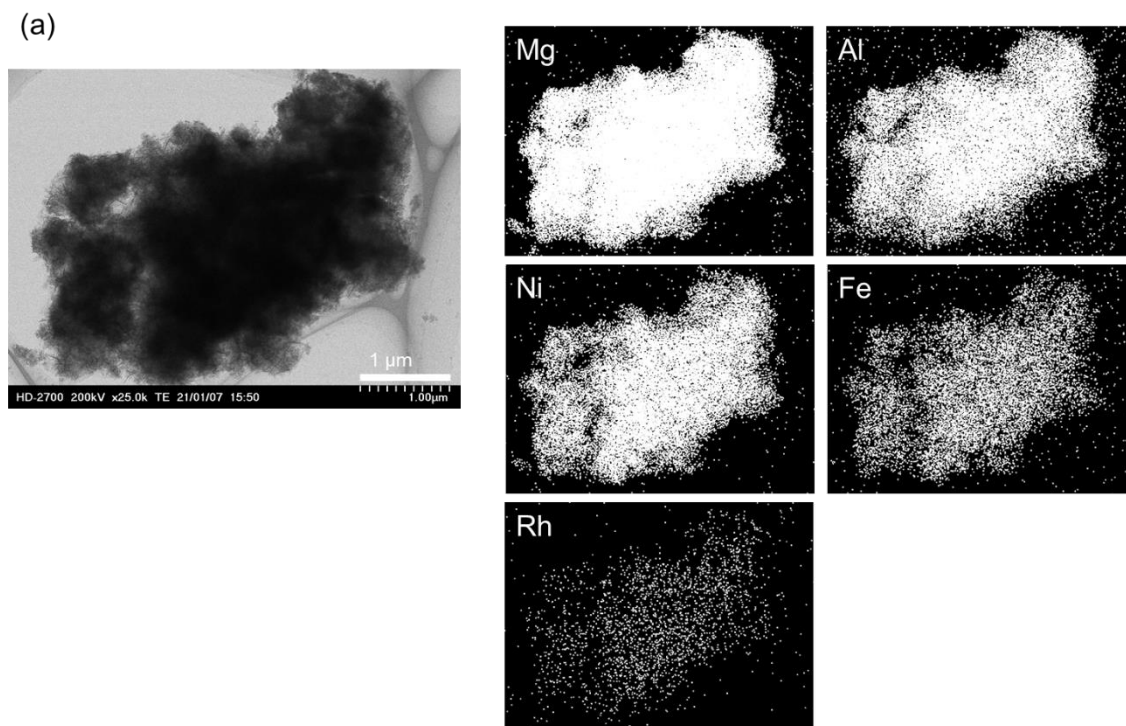


Figure 4.7 TEM images of Rh/CeO₂ (Rh: 1 wt%) + Ni-Fe/Mg/Al (Ni: 12 wt%, Fe/Ni = 0.25, (Ni+Mg)/(Al+Fe) = 3) catalysts (10:90 wt% Powder mixture) after reduction at 1073 K (a) and after reaction at 573-773 K (b). Reduction conditions: 50%/50% H₂/N₂, 773 or 1073 K, 30 min. Reaction conditions: $W_{cat} = 100$ mg; $W/F = 0.19$ g h mol⁻¹. reaction temperature, 523-773 K; reaction time, 265 min. S/C_{HC} = 1.7 (Toluene/H₂O/N₂/CO₂ = 1.0/11.8/71.2/11.8 (molar ratio)). Feeding rate: toluene, 6 mmol h⁻¹; steam, 65 mmol h⁻¹; N₂, 382 mmol h⁻¹; CO₂, 64 mmol h⁻¹.

Effect of addition of noble metal to hydrotalcite-derived Ni-Fe alloy catalyst for steam reforming of toluene using exhaust gas as reforming agent

The TEM-EDX image of Rh/Ni-Fe/Mg/Al catalysts after reduction at 1073 K and after reaction at 573-773 K was shown in **Fig. 4.8**. The EDX suggested that Rh was highly dispersed on the Ni-Fe/Mg/Al catalyst. Similar to Rh/CeO₂ + Ni-Fe/Mg/Al (powder mixture, 10:90 wt%), Ni-Fe alloy particles were observed after reduction but not after the reaction. The results suggest that only a small amount of Ni and Fe exposed on the catalyst surface was activated without growing to Ni-Fe particles.



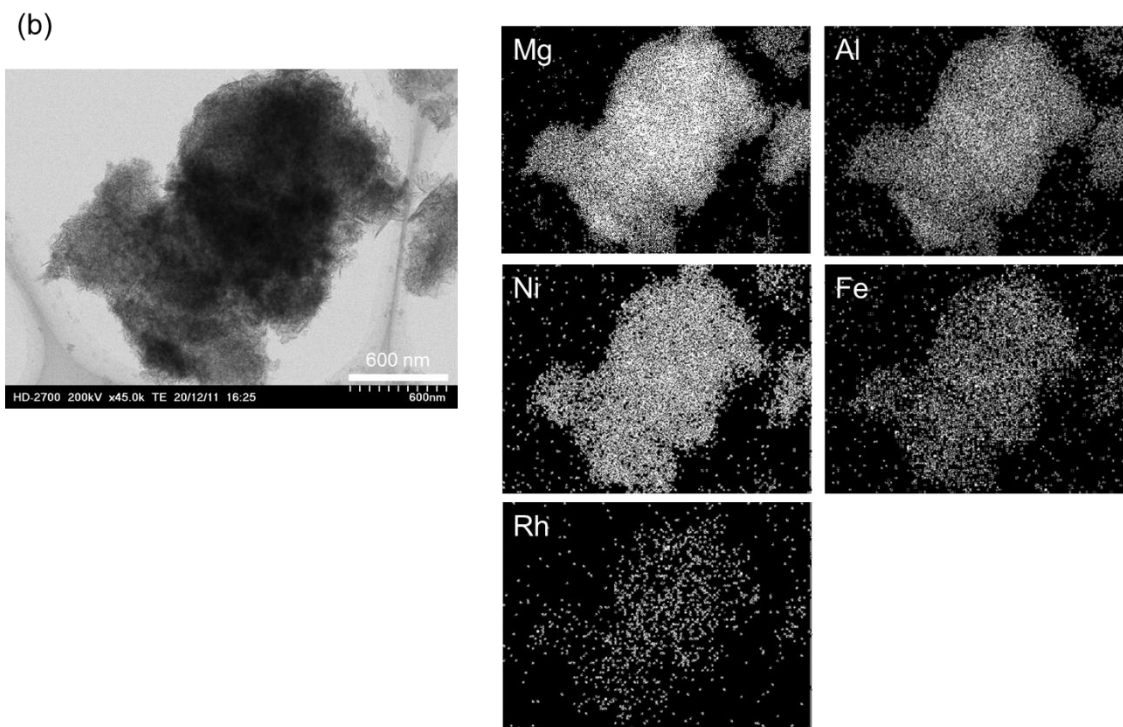


Figure 4.8 TEM images of Rh/Ni-Fe/Mg/Al (Rh: 0.1 wt%, Ni: 12 wt%, Fe/Ni = 0.25, (Ni+Mg)/(Al+Fe) = 3) catalyst after reduction at 1073 K (a) and after reaction at 573-773 K (c). Reduction conditions: 50%/50% H₂/N₂, 773 or 1073 K, 30 min. Reaction conditions: $W_{cat} = 100$ mg; $W/F = 0.19$ g h mol⁻¹. reaction temperature, 523-773 K; reaction time, 265 min. $S/C_{HC} = 1.7$ (Toluene/H₂O/N₂/CO₂ = 1.0/11.8/71.2/11.8 (molar ratio)). Feeding rate: toluene, 6 mmol h⁻¹; steam, 65 mmol h⁻¹; N₂, 382 mmol h⁻¹; CO₂, 64 mmol h⁻¹.

4.3.5. Attempt to decrease Rh amount

The reaction results of Rh/CeO₂ + Ni-Fe/Mg/Al (Powder mixture, 10:90 wt%) without pre-reduction in the previous section showed only a small increase of conversion by addition of Ni-Fe/Mg/Al. Therefore the effect, to decrease the Rh amount to obtain the same result is limited. Here, the author attempted to decrease the Rh amount in Rh/CeO₂ + Ni-Fe/Mg/Al catalyst. Two methods were tested: decreased the ratio of Rh/CeO₂ (Rh: 1 wt%) to Ni-Fe/Mg/Al and decrease of Rh loading in Rh/CeO₂. The results of the toluene reforming reaction with model EGR gas over Rh/CeO₂ (Rh: 1 wt%) + Mg/Al or Ni-Fe/Mg/Al (Powder mixture, 1:99 wt%) and Rh/CeO₂ (Rh: 0.1 wt%) + Ni-Fe/Mg/Al (Powder mixture, 10:90 wt%) catalysts are shown in **Fig. 4.9**. The Rh/CeO₂ (Rh: 1 wt%) + Ni-Fe/Mg/Al (powder mixture, 1:99 wt%) catalyst showed a slight conversion of toluene at 773 K, but there was no increase in the toluene conversion as the temperature was increased. The toluene conversion of the Rh/CeO₂ (Rh: 1 wt%) + Ni-Fe/Mg/Al (Powder mixture, 10:90 wt%) catalyst was about 1/10 of that of the Rh/CeO₂ (Rh: 1 wt%) +

Ni-Fe/Mg/Al (Powder mixture, 1:99 wt%) catalyst. The Rh/CeO₂ (Rh: 1 wt%) + Mg/Al (powder mixture, 1:99 wt%) catalyst had only a slightly higher toluene conversion than the Rh/CeO₂ (Rh: 1 wt%) + Ni-Fe/Mg/Al (powder mixture, 1:99 wt%) catalyst. The amount of CeO₂ might be too small to supply a sufficient amount of hydrogen to activate Ni and Fe, because hydrogen spillover on CeO₂ support might be involved in the transfer of activated hydrogen species on Rh to Ni-Fe/Mg/Al. Therefore, to keep the CeO₂ content as the same as the Rh/CeO₂ (Rh: 1 wt%) + Mg/Al (Powder mixture, 10:90 wt%) catalyst, Rh/CeO₂ (Rh: 0.1 wt%) was prepared and mixed with Ni-Fe/Mg/Al catalyst at 10:90 wt%. The toluene conversion behavior of Rh/CeO₂ (Rh: 0.1 wt%) + Ni-Fe/Mg/Al (powder mixture, 10:90 wt%) was still almost identical to that of Rh/CeO₂ (Rh: 1 wt%) + Ni-Fe/Mg/Al (powder mixture, 1:99 wt%) catalyst. The reason for the low startability performance of the catalysts could be simply due to the low hydrogen production over Rh for reduction of Ni and Fe because of the lower Rh amount.

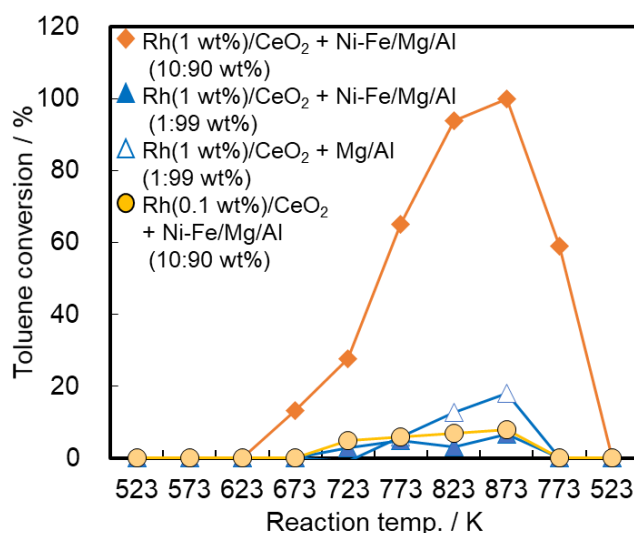


Figure 4.9 Reforming of toluene over Rh/CeO₂ (Rh: 0.1 or 1 wt%) + Ni-Fe/Mg/Al (Ni: 12 wt%, Fe/Ni = 0.25, (Ni+Mg)/(Al+Fe) = 3) catalysts (10:90 or 1:99 wt% Powder mixture). Reaction conditions: $W_{cat} = 100$ mg; $W/F = 0.19$ g h mol⁻¹. reaction temperature, 523-873 K; reaction time, 470 min. $S/C_{HC} = 1.7$ (Toluene/H₂O/N₂/CO₂ = 1.0/11.8/71.2/11.8 (molar ratio)). Feeding rate: toluene, 6 mmol h⁻¹; steam, 65 mmol h⁻¹; N₂, 382 mmol h⁻¹; CO₂, 64 mmol h⁻¹.

The H₂-TPR measurement was used to confirm if the reducibility was improved by the addition of a little amount of Rh as Rh/CeO₂. The H₂-TPR profiles of Rh/CeO₂ (Rh: 1 wt%) + Ni-Fe/Mg/Al (Powder mixture, 1:99 wt%) and Rh/CeO₂ (Rh: 0.1 wt%) + Ni-Fe/Mg/Al (Powder mixture, 10:90 wt%) catalysts were shown in **Fig. 4.10**, as well as

the those of Rh/CeO₂ (Rh: 1 wt%) + Ni-Fe/Mg/Al and Mg/Al (Powder mixture, 10:90 wt%) and Ni-Fe/Mg/Al catalysts. In the Rh/CeO₂ (Rh: 1 wt%) + Ni-Fe/Mg/Al (Powder mixture, 1:99 wt%) and Rh/CeO₂ (Rh: 0.1 wt%) + Ni-Fe/Mg/Al (Powder mixture, 10:90 wt%) catalysts, there were three H₂ consumption peaks; broad peak at 473-673 K, a small peak at 673-773 K, large peak at 773-1073 K. The peaks at 473-673 K and 673-773 K can be assigned to reduction of Rh and Ni + Fe, respectively. The peaks at 773-1073 K corresponding to the reduction of Ni and Fe of the Rh/CeO₂ (Rh: 1 wt%) + Ni-Fe/Mg/Al (Powder mixture, 1:99 wt%) and Rh/CeO₂ (Rh: 0.1 wt%) + Ni-Fe/Mg/Al (Powder mixture, 10:90 wt%) catalysts were slightly shifted to lower temperature. It was suggested that the reducible of Ni and Fe was also improved by adding a few Rh/CeO₂. However, Rh/CeO₂ (Rh: 1 wt%) + Ni-Fe/Mg/Al mixture catalyst with 1:99 ratio showed even lower reduction temperature than that with 10:90 ratio. Considering the very low reduction degree of all the used catalysts without reduction pretreatment the position of this signal may not affect the performance. The small signal at about 700 K might be related to the catalysts, which can be assigned to the reduction of part of Ni + Fe.

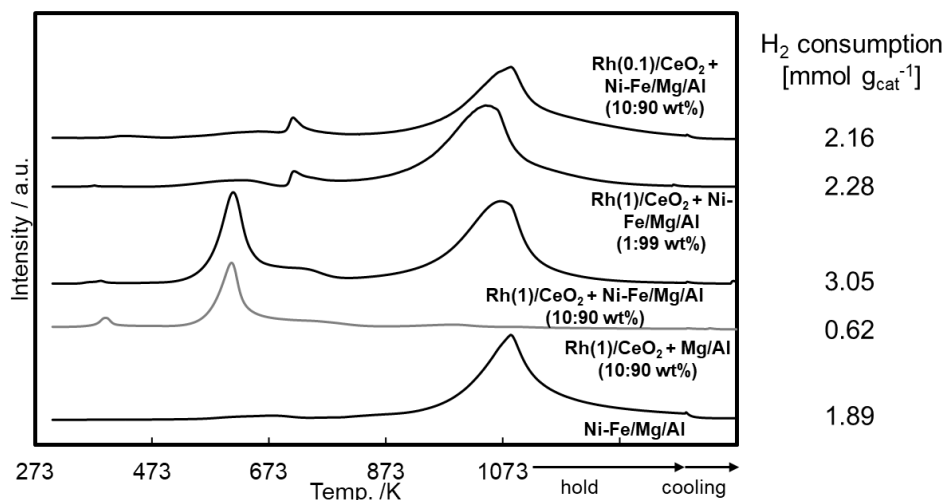


Figure 4.10 TPR profiles of Rh/CeO₂ (Rh: 0.1 wt%) + Ni-Fe/Mg/Al (Ni: 12 wt%, Fe/Ni = 0.25, (Ni+Mg)/(Al+Fe) = 3) catalysts (10:90 wt% Powder mixture) catalyst.

Measurement conditions: 5% H₂/Ar, 30 ml min⁻¹; room temperature to 1073 K at a rate of 10 K min⁻¹, then the temperature was maintained at 1073 K for 30 min; sample, 50 mg.

4.4. Conclusions

1. Among Ni-Fe/Mg/Al catalysts with the addition of Rh by various methods, the Rh/CeO₂ + Ni-Fe/Mg/Al (Powder mix, contained amount of Rh: 0.1 wt%) catalyst showed higher startability and toluene conversion at 673-873 K than the Rh/CeO₂ + Ni-Fe/Mg/Al (Separate and Granule mixture, contained amount of Rh: 0.1 wt%) and Rh/Ni-Fe/Mg/Al catalysts.
2. It was suggested that the addition of Rh activated Ni and Fe. The activation effect of Ni and Fe was similar in Rh/Ni-Fe/Mg/Al and Rh/CeO₂ + Ni-Fe/Mg/Al (Powder mix, contained amount of Rh: 0.1 wt%). This suggests that startability can be obtained if Rh, Ni and Fe are present in the same granule.
3. In the case of M/CeO₂ (M = Rh, Pt, Ir, Ru, Pd) + Ni-Fe/Mg/Al (Powder mix, contained amount of M: 0.1 wt%), Rh showed high start-up performance and high toluene conversion, although the large part of the activity was due to the activity of Rh itself. Ni and Fe were activated by the addition of all noble metals except Pd.
4. The Rh/CeO₂ + Ni-Fe/Mg/Al (Powder mix, contained amount of Rh: 0.01 wt%) was not sufficient to produce H₂, resulting in low start-up performance and low toluene conversion.
5. Rh/CeO₂ + Ni-Fe/Mg/Al (Powder mix, contained amount of Rh: 0.1 wt%) showed high activity stability and high coke deposition resistance in a 5 h reaction.

References

- [1] L. Tartakovsky, M. Sheintuch, Fuel reforming in internal combustion engines, *Prog. Energy Combust. Sci.*, 2018, 67, 88-114. <https://doi.org/10.1016/j.peccs.2018.02.003>
- [2] S. Golunski, What is the point of on-board fuel reforming?, *Energy Environ. Sci.*, 2010, 3, 1918–1923. <https://doi.org/10.1039/c0ee00252f>
- [3] V. Chintala, D. Banaerjee, P. K. Ghodke, E. Porpatham, Hydrogen rich exhaust gas recirculation (H₂EGR) for performance improvement and emissions reduction of a compression ignition engine, *Int. J. Hydrogen. Energy*, 2019, 44, 18545-18558. <https://doi.org/10.1016/j.ijhydene.2019.05.141>

- [4] S. R. Gomes, N. Bion, D. Duprez, F. Epron, Hydrogen production from hydrocarbons over Rh supported on Ce-based oxides for automotive applications, *Appl. Catal. B: Environ.*, 2016, 197, 138-145. <https://doi.org/10.1016/j.apcatb.2016.01.022>
- [5] S. Peucheret, M. Feavioir, S. Golunski, Exhaust-gas reforming using precious metal catalysts, *Appl. Catal. B: Environ.*, 2006, 65, 201-206. <https://doi.org/10.1016/j.apcatb.2006.01.009>
- [6] J. Thormann, L. Maier, P. Pfeifer, U. Kunz, O. Dautschmann, K. Schubert, Steam reforming of hexadecane over a Rh/CeO₂ catalyst in microchannels: Experimental and numerical investigation, *Int. J. Hydrogen Energy*, 2009, 34, 5108-5120. <https://doi.org/10.1016/j.ijhydene.2009.04.031>
- [7] D. Li, Y. Nakagawa, K. Tomishige, Methane reforming to synthesis gas over Ni catalysts modified with noble metals, *Appl. Catal. A: Gen.*, 2011, 408, 1-24. <https://doi.org/10.1016/j.apcata.2011.09.018>
- [8] J. Chen, M. Tamura, Y. Nakagawa, K. Okumura, K. Tomishige, Promoting effect of trace Pd on hydrotalcite-derived Ni/Mg/Al catalyst in oxidative steam reforming of biomass tar, *Appl. Catal. B: Environ.*, 2015, 179, 412-421. <https://doi.org/10.1016/j.apcatb.2015.05.042>
- [9] Y. Khani, Z. Shariatnia, F. Bahadoran, High catalytic activity and stability of ZnLaAlO₄ supported Ni, Pt and Ru nanocatalysts applied in the dry, steam and combined dry-steam reforming of methane, *Chem. Eng. J.*, 2016, 299, 353-366. <https://doi.org/10.1016/j.cej.2016.04.108>
- [10] S. Katheria, G. Deo, D. Kunzru, Rh-Ni/MgAl₂O₄ catalyst for steam reforming of methane: Effect of Rh doping, calcination temperature and its application on metal monoliths, *Appl. Catal. A: Gen.*, 2019, 570, 308-318. <https://doi.org/10.1016/j.apcata.2018.11.021>
- [11] V. K. Jaiswar, S. Katheria, G. Deo, D. Kunzru, Effect of Pt doping on activity and stability of Ni/MgAl₂O₄ catalyst for steam reforming of methane at ambient and high pressure condition, *Int. J. Hydrogen Energy*, 2017, 42, 18968-18976. <https://doi.org/10.1016/j.ijhydene.2017.06.096>
- [12] S. C. Baek, K. W. Jun, Y. J. Lee, J. D. Kim, D. Y. Park, K. Y. Lee, Ru/Ni/MgAl₂O₄ catalysts for steam reforming of methane: effects of Ru content on self-activation property, *Res Chem Intermed.*, 2012, 38, 1225-1236. <https://doi.org/10.1007/s11164-011-0462-0>

- [13] K. Takehira, "Intelligent" reforming catalysts: Trace noble metal-doped Ni/Mg(Al)O derived from hydrotalcites, *Journal of Natural Gas Chemistry*, 2009, 18, 237-259. [https://doi.org/10.1016/S1003-9953\(08\)60123-1](https://doi.org/10.1016/S1003-9953(08)60123-1)
- [14] D. Li, Y. Zhan, K. Nishida, Y. Oumi, T. Sano, T. Shishido, K. Takehira, "Green" preparation of "intelligent" Pt-doped Ni/Mg(Al)O catalysts for daily start-up and shut-down CH₄ steam reforming, *Appl. Catal. A: Gen.*, 2009, 363, 169-179. <https://doi.org/10.1016/j.apcata.2009.05.0>
- [15] D. Li, K. Nishida, Y. Zhan, T. Shishido, Y. Oumi, T. Sano, K. Takehira, Sustainable Ru-doped Ni catalyst derived from hydrotalcite in propane reforming, *Appl. Clay Sci.*, 2009, 43, 49-56. <https://doi.org/10.1016/j.clay.2008.07.014>
- [16] D. Li, K. Nishida, Y. Zhan, T. Shishido, Y. Oumi, T. Sano, K. Takehira, Superior catalytic behavior of trace Pt-doped Ni/Mg(Al)O in methane reforming under daily start-up and shut-down operation, *Appl. Catal. A: Gen.*, 2008, 350, 225-236. <https://doi.org/10.1016/j.apcata.2008.08.017>
- [17] D. Li, T. Shishido, Y. Oumi, T. Sano, K. Takehira, Self-activation and self-regenerative activity of trace Rh-doped Ni/Mg(Al)O catalysts in steam reforming of methane, *Appl. Catal. A: Gen.*, 2007, 332, 98-109. <https://doi.org/10.1016/j.apcata.2007.08.008>
- [18] D. Li, I. Atake, T. Shishido, Y. Oumi, T. Sano, K. Takehira, Self-regenerative activity of Ni/Mg(Al)O catalysts with trace Ru during daily start-up and shut-down operation of CH₄ steam reforming, *J. Catal.*, 2007, 250, 299-312. <https://doi.org/10.1016/j.jcat.2007.06.002>
- [19] T. Miyata, D. Li, M. Shiraga, T. Shishido, Y. Oumi, T. Sano, K. Takehira, Promoting effect of Rh, Pd and Pt noble metals to the Ni/Mg(Al)O catalysts for the DSS-like operation in CH₄ steam reforming, *Appl. Catal. A: Gen.*, 2006, 310, 97-104. <https://doi.org/10.1016/j.apcata.2006.05.022>
- [20] M. Koike, D. Li, Y. Nakagawa, and K. Tomishige, A Highly Active and Coke-Resistant Steam Reforming Catalyst Comprising Uniform Nickel-Iron Alloy Nanoparticles, *ChemSusChem*, 2012, 5, 2312-2314. <https://doi.org/10.1002/cssc.201200507>
- [21] D. Li, L. Wang, M. Koike, Y. Nakagawa, K. Tomishige, Steam reforming of tar from pyrolysis of biomass over Ni/Mg/Al catalysts prepared from hydrotalcite-like precursors, *Appl. Catal. B: Environ.*, 2011, 102, 528-538. <https://doi.org/10.1016/j.apcatb.2010.12.035>

- [22] M. Betchaku, Y. Nakagawa, M. Tamura, K. Tomishige, Reforming of toluene with simulated automobile exhaust gas over hydrotalcite-like-compound-derived Ni catalyst, *Fuel Process. Technol.*, 2020, 209, 106545. <https://doi.org/10.1016/j.fuproc.2020.106545>
- [23] H. Chen, H. Yu, Y. Tang, M. Pan, G. Yang, F. Peng, H. Wang, J. Yang, Hydrogen production via autothermal reforming of ethanol over noble metal catalysts supported on oxides, *J. Nat. Gas Chem.*, 2009, 18, 191-198. [https://doi.org/10.1016/S1003-9953\(08\)60106-1](https://doi.org/10.1016/S1003-9953(08)60106-1)
- [24] D. Duprez, Selective steam reforming of aromatic compounds on metal catalysts, *Appl. Catal. A: Gen.*, 1992, 82, 111-157. [https://doi.org/10.1016/0926-860X\(92\)85001-R](https://doi.org/10.1016/0926-860X(92)85001-R)
- [25] D. Li, M. Koike, L. Wang, Y. Nakagawa, Y. Xu, K. Tomishige, Regenerability of Hydrotalcite-Derived Nickel-Iron Alloy Nanoparticles for Syngas Production from Biomass Tar, *ChemSusChem*, 2014, 7, 510-522. <https://doi.org/10.1002/cssc.201300855>

Chapter 5

Summary

In this thesis, the author investigated the performance of hydrotalcite-like-compounds-derived Ni-based catalysts for reforming of toluene with model EGR gas ($\text{H}_2\text{O}/\text{N}_2/\text{CO}_2 = 11.8/71.2/11.8$). The performance was evaluated in views of activity, coke deposition resistance, stability and startability. The results are summarized as described below.

In Chapter 2, Ni/Mg/Al catalyst prepared from the calcination and reduction of hydrotalcite-like compounds containing Ni, Mg and Al, which has been reported to be active in simple steam reforming, was applied to the reforming of toluene with model exhaust gas. The Ni/Mg/Al catalyst showed higher performance than Ni/ α - Al_2O_3 catalyst in terms of activity, stability and coke deposition resistance. The activity of Ni/Mg/Al after the initial deactivation was about 1/200 of Rh/CeO₂ based on the weight of active metal (Ni or Rh), and the difference was much smaller than that of price between Ni and Rh. The amount of coke deposition on Ni/Mg/Al catalyst was increased with increases of W/F or partial pressure of toluene, especially at the outlet of the catalyst bed, where the coke formation is mainly due to CO disproportionation. The deactivation was also severer in larger partial pressure of toluene when the toluene feed was changed while partial pressure of H₂O, N₂ and CO₂ was set constant to the model EGR gas. Large steady state H₂ formation and high conversion were obtained at conditions with low partial pressure of toluene, similarly to the case of simple steam reforming, the Ni/Mg/Al catalyst after reaction can be regenerated by the combination of oxidation (at 773 K) and reduction (at 1073 K) treatments. The effect of feed ratio of H₂O:N₂:CO₂ showed that low partial pressure of steam in model EGR gas in comparison with standard feed gas for steam reforming is the main reason for low toluene conversion and coke deposition resistance. On the other hand, the presence of CO₂ did not affect the conversion and the coke deposition behavior so significantly.

In Chapter 3, catalysts with the addition of a second metal (Fe, Co, Cu) to a Ni/Mg/Al catalyst were prepared and their effect on alloy formation was investigated. The Ni-Fe/Mg/Al (Fe/Ni = 0.25) catalyst prepared from hydrotalcite-like precursor compound showed higher performance than Ni/Mg/Al, Ni-M/Mg/Al (M/Ni = 0.25, M = Co, Cu) and

Ni-Fe/ α -Al₂O₃ (Fe/Ni = 0.25) catalysts in terms of activity, stability and coke deposition resistance. The optimum Fe/Ni molar ratio of Ni-Fe/Mg/Al catalysts was 0.25 from the toluene conversion and the suppression of benzene formation. The Ni-Fe/Mg/Al (Fe/Ni = 0.25) catalyst showed high coke deposition resistance at both inlet and outlet positions of the catalyst bed, indicating that both substrate decomposition to coke and CO disproportionation were suppressed. The coke amount hardly increased even under low reaction temperature or higher concentration of toluene; however, the activity gradually decreased under such conditions. The regeneration of deactivated catalyst under higher toluene conversion was tested with several methods. The activity was recovered to a similar level as the fresh catalyst by treatment with N₂ flow at 873 K, catalytic use at 973 K, or re-reduction.

In Chapter 4, the addition of trace amounts of noble metals (Rh, Pt, Ir, Pd, Ru) to Ni-Fe/Mg/Al catalyst was investigated to impart startability. In the no reduction, the startability was provided to Ni-Fe/Mg/Al catalyst by noble metal except Pd. In addition, the Rh/CeO₂ (Rh: 1 wt%) + Ni-Fe/Mg/Al (Powder mixture, 10:90 wt%) catalyst was showed higher startability than Rh/CeO₂ (Rh: 1 wt%) + Ni-Fe/Mg/Al (Separate and Granule mixture, 10:90 wt%), Rh/Ni-Fe/Mg/Al and M/CeO₂ (M = Pt, Ir, Pd, Ru, M: 1 wt%) + Ni-Fe/Mg/Al (Powder mixture, 10:90 wt%) catalysts. Then, in the add Rh catalysts, it was suggested that the startability was provided since the reducibility of catalyst was improved by Rh. However, the toluene conversion at 773 K of Rh/CeO₂ (Rh: 1 wt%) + Ni-Fe/Mg/Al (Powder mixture, 10:90 wt%) catalyst significantly lower than toluene conversion of Ni-Fe/Mg/Al catalyst after reduction at 1073 K. In addition, the startability of catalyst, was decreased to 1/10 of the Rh addition amount, was very little. On the other hand, after reduction at 1073 K, the Rh/CeO₂ (Rh: 1 wt%) + Ni-Fe/Mg/Al (Powder mixture, 10:90 wt%) catalyst suppressed the decrease in toluene conversion more than the Ni-Fe/Mg/Al catalyst.

In this thesis, the author found that Ni-Fe/Mg/Al catalyst has activity in reforming of toluene which is a typical source of coke among gasoline compounds without coking, and this catalyst is reusable by calcination as regeneration. Although it is difficult to reduce this catalyst with toluene, mixing with Rh/CeO₂ which is a typical catalyst for Reformed EGR can partially reduce Ni-Fe/Mg/Al to show activity to some extent. These findings will be useful for decreased of the amount of precious metals in reformed EGR catalysts and for developing reforming catalysts for other challenging conditions.

Acknowledgements

First of all, the author is deeply grateful to Prof. Keiichi Tomishige (School of Engineering, Tohoku University) for his kind encouragement, support and guidance to this forward-looking and important research field of catalytic reforming reaction with model EGR gas. Thanks to his invaluable instructions, many fruitful comments, advice, and suggestion, the author accomplished this work.

The author also expresses gratitude to Prof. Atsushi Muramatsu (School of Engineering, Tohoku University), Prof. Toshiaki Yoshioka (School of Engineering, Tohoku University) and Prof. Yasuhiro Fukushima (School of Engineering, Tohoku University) for their participation in the degree committee.

Earnest thanks are offered to Prof. Yoshinao Nakagawa (School of Engineering, Tohoku University) for many helpful suggestions, and kind instruction and assistance in this work; Prof. Masazumi Tamura (Research Center for Artificial Photosynthesis, Osaka City University) for his fruitful comments and suggestions; and Prof. Mizuho Yabushita (School of Engineering, Tohoku University) for notable discussion and advice.

The author is in acknowledge to Mr. Shinya Iida (Mazda Motor Corporation), Mr. Yasutomo Miura (Cosmo Oil Co., Ltd.) and Mr. Nobuyasu Ohshio (Cosmo Oil Co., Ltd.) for collaborative research.

A part of this research was supported by the project of Next generation Energies for Tohoku Recovery the JSPS KAKENHI “Grant in Aid for Scientific Research (S)” 18H05247.

A part of this work was approved by the Japan Synchrotron Radiation Research Institute (JASRI; Proposal Nos. 2019A1827, 2019B1906, and 2020A1841).

Special thanks are owed to Mr. Mitsuru Koike, Mr. Susumu Ishikawa, Mr. Teruhisa Oshino, Mr. Kensuke Tokuma, Mr. Yu Gu, Mr. Keitaro Matsuda, Mr. Shin Yanatake, Mr. Cong cong Li, and Mr. Lujie Liu for their support. This thesis could not have been completed without their cooperation. The author also thanks all other members of the Tomishige Laboratory at the Tohoku University past 5 years for lending valuable advice and encouragement, for helpful discussions, and for providing great experience during the research and in the laboratory.

The author is indebted to Mr. Masataka Nakauchi and Mr. Yuya Ishizaki for enriched my university life.

Acknowledgements

Finally, the author wish to express my deepest gratitude to her family and her friends, and appreciate for their heartfelt encouragement and support.

January 2021

School of Engineering

Tohoku University

Mii Betchaku

List of Publications

1. Mii Betchaku, Yoshinao Nakagawa, Masazumi Tamura, Keiichi Tomishige
Reforming of toluene with simulated automobile exhaust gas over hydrotalcite-like-compound-derived Ni catalyst, *Fuel Proc. Technol.*, 2020, 209, 106545.
2. Mii Betchaku, Yoshinao Nakagawa, Masazumi Tamura, Keiichi Tomishige
Catalytic performance of hydrotalcite-like-compound-derived Ni-metal alloy catalyst for reforming reaction of toluene with gasoline engine exhaust model gas as reforming agent (in preparation)
3. Masazumi Tamura, Susumu Ishikawa, Mii Betchaku, Yoshinao Nakagawa, Keiichi Tomishige
Selective hydrogenation of amides to alcohols in water solvent over a heterogeneous CeO₂-supported Ru catalyst, *Chem. Commun.*, 2018, 54, 7503-7506.
4. Shin Yanatake, Yosuke Nakaji, Mii Betchaku, Yoshinao Nakagawa, Masazumi Tamura, Keiichi Tomishige
Selective C-C Hydrogenolysis of Alkylbenzenes to Methylbenzenes with Suppression of Ring Hydrogenation, *ChemCatChem*, 2018, 10, 4172-4181.